



Considerations of Nano-alumina-based Polyethylene and Polypropylene Composites for HVDC Insulation

Thesis presented for the degree of

Doctor of Philosophy

in the

Department of Electronic and Electrical Engineering

University of Strathclyde

2023

Xuhui Duan, BEng (Hons)

Department of Electronic and Electrical Engineering

University of Strathclyde

Glasgow, UK

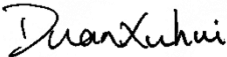
Copyright

DECLARATION OF AUTHENTICITY AND AUTHOR'S RIGHTS

This thesis is the result of the author's original research. It has been composed by the author and has not been previously submitted for examination which has led to the award of a degree.

The copyright of this thesis belongs to the author under the terms of the United Kingdom Copyright Acts as qualified by University of Strathclyde Regulation 3.50.

Due acknowledgement must always be made of the use of any material contained in, or derived from, this thesis.

Signed: 

Date: 2023/05/04

Acknowledgement

I would like to express my first thanks to my supervisors Professor W.H. Siew in Department of Electronic and Electrical Engineering, Dr Martin J. Given in Department of Electronic and Electrical Engineering and Professor John Liggat in Department of Pure and Applied Chemistry for their continuous support, supervision and guidance throughout this project. Thanks to Professor Siew for providing me with this opportunity to pursue a PhD degree at the University of Strathclyde and for his patience in supervision. Thanks to Professor Liggat for his invaluable advice on the fundamentals of polymer and composite processing.

I would also like to thank my host supervisor, Professor Jinliang He, in Tsinghua University. Thanks for his kindness in accepting me as a visiting researcher to carry out part of my research experiments (providing the relevant equipment and supervision during my visit) in the High Voltage Laboratory. He and his research group helped a lot in the nanocomposite test-samples preparation and characterization. Special thanks to Dr Yao Zhou, Dr Yang Yang, Dr Chao Yuan, Dr Xiaolei Zhao and other colleagues in Tsinghua University for their technical assistance and help in life during the period of my visit.

Many thanks to all colleagues in the High Voltage Technologies Group, University of Strathclyde, for their efforts to make a relaxing and pleasant working environment for me during my study. Special thanks to Dr Jijia Liu and Dr Qingjiang Xue, my

comrades, for their discussions and advice in terms of the writing up work. Thanks to all my friends in Glasgow for their help and care in my daily life. Thanks to all my teammates in Scottish Oriental Awesome Players (S.O.A.P.) football team and Glasgow United football team for bring me the joy and happiness on the pitch every weekend.

A special thanks to Scottish Power Energy Networks for the partial financial support through a Network Innovation Allowance (NIA) Grant.

Finally and most importantly, I would like to give my thanks to my family, Mr. Hongwei Duan, Mrs. Aiqing Li and Miss Yingqian Liang, for their unconditional and endless encouragement, support and love.

The journey of pursuing a PhD is not an easy one. It is full of challenges, self-doubt, surprises and sense of accomplishment. All good things must come to an end. Good-bye, the battlefield, Room 375B, Royal College Building, Department of Electronic and Electrical Engineering, University of Strathclyde, Glasgow, Scotland, UK.

Abstract

Extruded polymeric insulation material has been widely used in high voltage alternating current (HVAC) power transmission system for a long time. Recent years, with the advent of renewable energy around world, more large energy capacity, long distance high voltage direct current (HVDC) transmission projects were developed. The quality of insulation materials of HVDC cables has become the most critical issue that restricts the development of HVDC transmission. Cross-linked polyethylene (XLPE) has shown superior electrical, thermal and mechanical properties due to its special cross-linked structure and has become the default material for HVDC cable insulation in the last few decades. But today, with the increasing concern of environmental protection and sustainable development, traditional XLPE cables are no longer the default for future HVDC applications due to its limited operating temperature, non-recyclable nature and high energy consumption in complex production process. Therefore, new thermoplastic polymeric insulation materials are being developed, which are recyclable and can be operated under higher temperature. However, these materials still have weak points like space charge accumulation. The incorporation of nanoparticles has been proven to be an effective method to overcome these drawbacks.

In this study, thermoplastic polymers, polyethylene (PE) and polypropylene (PP), were selected as the potential matrix materials to study. Nano-alumina particles with and without surface modification were introduced into polymers at different filling contents

to make nanocomposites. This thesis reports the comprehensive study on PE/nano-alumina composite systems and PP/nano-alumina composite systems. The surface chemistry of nano-alumina with and without surface modification was characterized by thermal-gravimetric analysis and Fourier-transform infrared spectroscopy. The morphological structure of nanocomposite systems was analyzed by using polarized optical microscopy and scanning electron microscopy. Electrical properties such as DC breakdown strength, DC conductivity, and space charge were investigated to evaluate the feasibility of the proposed nanocomposite materials as future HVDC cable insulation. A deep understanding of the effect of nanoparticles on the dielectric properties of polymeric nanocomposites was achieved. After comparing the performance of PE nanocomposites and PP nanocomposites, PP nanocomposites exhibit superior electrical properties and can be considered as the future alternative to XLPE.

In conclusion, the experimental results and discussion presented in this project can contribute to the design and manufacture of recyclable polymeric nanocomposite materials for future HVDC applications.

List of Acronyms

DSC	Differential Scanning Calorimetry
EPDM	Ethylene-propylene-diene Monomer
EPR	Ethylene Propylene Rubber
FEP	Fluorinated Ethylene Propylene Copolymer
FTIR	Fourier-transform Infrared Spectroscopy
HDPE	High-density Polyethylene
HV	High Voltage
HVAC	High Voltage Alternating Current
HVDC	High Voltage Direct Current
LDPE	Low-density Polyethylene
LIMM	Laser Intensity Modulation Method
LIPP	Laser-induced Pressure Pulse Method
LLDPE	Linear Low-density Polyethylene
MIND	Mass-impregnated Non-draining
OF	Oil-filled
PE	Polyethylene
PEA	Pulsed Electro-acoustic
PET	Polyethylene Terephthalate
PHR	Per Hundred Resin
PI	Polyimide
POE	Polyolefin Elastomer
POM	Polarized Optical Microscopy

PPL	Polypropylene Paper Laminated
PPLP	Polypropylene Laminated Paper
PVDF	Polyvinylidene Fluoride
PVF	Polyvinyl Fluoride
PWP	Pressure Wave Pulse Method
SCLC	Space-charge-limited Conduction
SCOF	Self-contained Oil-filled
SEBS	Styrene-ethylene-butylene-styrene
SEM	Scanning Electron Microscopy
TGA	Thermogravimetric Analysis
TP	Thermal Pulse Method
TSC	Thermally Stimulated Current
TSDC	Thermally Stimulated Depolarization Current
TSM	Thermal Step Method
TSPC	Thermally Stimulated Polarization Current
XLPE	Cross-linked Polyethylene

List of Figures

Figure 2.1 Molecular formula of polyethylene.40

Figure 2.2 Molecular structure of (a) LDPE, (b) LLDPE and (c) HDPE.41

Figure 2.3 Molecular structure of polypropylene.42

Figure 2.4 Molecular structure of polypropylenes: (a) isotactic polypropylene; (b) syndiotactic polypropylene; (c) atactic polypropylene.44

Figure 2.5 Nanocomposite relevant publication activities.....47

Figure 2.6 Constituents of polymer nanocomposites.....48

Figure 2.7 The interface ab between two phases A and B defined by the intensity I_α of a chosen property α as it changes in passage across it [65].51

Figure 2.8 Interfacial intensities: (a) electron concentration at a metal-vacuum interface; (b) oxygen concentration at the silicon-air interface; (c) electric field distribution at a metal-n-type semi-conductor contact.....53

Figure 2.9 The Interphase volume model of nanocomposites (a) without overlap, (b) with overlap [67].....55

Figure 2.10 Interphase content according to the Interphase Volume Model for a silicone matrix with SiO_2 particles and interphase thicknesses i : (a) for a particle diameter $d = 20$ nm, (b) for a particle diameter $d = 30$ nm, (c) for a particle diameter $d = 40$ nm [67].56

Figure 2.11 Electrical double layer model produced by a positively charge nanoparticle (a) the charge distribution, (b) the resulting electrical potential distribution.58

Figure 2.12 Multi-core model of nanocomposite (adapted from [69]).	59
Figure 2.13 Sketches of the relationship between breakdown strength and time-to-breakdown for different breakdown mechanisms in solid insulation (adapted from [75]).	63
Figure 3.1 Chemical structure of KH570 silane coupling agent.	73
Figure 3.2 Procedures of nanocomposite sample preparation.	74
Figure 3.3 Nanoparticle powders with and without surface modification.	75
Figure 3.4 Schematic of the reactions between the KH570 silane coupling agent and the nano-alumina particle.	76
Figure 3.5 Design of three-layer thin film mould.	77
Figure 3.6 Thin film samples produced by using a press machine.	78
Figure 3.7 Speed setting for torque rheometer.	79
Figure 3.8 The thin film nanocomposite samples produced using the melt-blending method.	81
Figure 3.9 Procedures of DSC test for PE and PP.	84
Figure 3.10 Samples for POM test.	85
Figure 3.11 Procedures of POM observation of PP nanocomposite sample.	86
Figure 3.12 Schematics of the dielectric spectroscopy system.	87
Figure 3.13 Structure of the sample holder for dielectric spectroscopy.	88
Figure 3.14 Schematics of the DC breakdown test system.	89
Figure 3.15 Schematics of the leakage current measurement system.	90

Figure 3.16 Schematics of TSDC measurement system.....	91
Figure 3.17 Procedures of TSDC test for PE nanocomposites	91
Figure 3.18 Design of the PEA measurement system.....	93
Figure 3.19 Dumbbell sheet sample for tensile test.....	94
Figure 4.1 TGA Results	97
Figure 4.2 FTIR results	99
Figure 4.3 The typical formation and growth of nuclei in the polymer.....	100
Figure 4.4 POM results of (a) virgin PE and (b) virgin PP.....	100
Figure 4.5 POM images of PE nanocomposites containing untreated nano-alumina of (a) 1phr, (c) 2phr, (e) 5phr and PE nanocomposites containing KH570-treated nano-alumina of (b) 1phr, (d) 2phr, (f) 5phr.....	102
Figure 4.6 POM image and the spherulite statistics of virgin PP.....	103
Figure 4.7 POM images and the spherulite statistics of PP nanocomposites containing untreated nano-alumina of (a) 1phr, (b) 2phr, (c) 5phr.....	104
Figure 4.8 POM images and the spherulite statistics of PP nanocomposites containing KH570-treated nano-alumina of (a) 1phr, (b) 2phr, (c) 5phr.....	105
Figure 4.9 SEM images of (a) virgin PE and (b) virgin PP.....	107
Figure 4.10 SEM images of PE nanocomposites containing untreated nano-alumina of (a) 0.5phr, (c) 1phr, (e) 5phr and PE nanocomposites containing KH570-treated nano-alumina of (b) 0.5phr, (d) 1phr, (f) 5phr.....	109
Figure 4.11 SEM images and the particle statistics of PE nanocomposites containing (a)	

5 phr untreated nano-alumina, (b) 5 phr KH570-treated nano-alumina.	110
Figure 4.12 SEM images of PP nanocomposites containing untreated nano-alumina of (a) 0.5phr, (c) 1phr, (e) 5phr and PP nanocomposites containing untreated nano-alumina of (b) 0.5phr, (d) 1phr, (f) 5phr.	112
Figure 4.13 SEM images and the particle statistics of PP nanocomposites containing (a) 5 phr untreated nano-alumina, (b) 5 phr KH570-treated nano-alumina.	113
Figure 4.14 DSC melting traces of PE nanocomposite samples containing (a) untreated alumina and (b) KH570-treated alumina.	117
Figure 4.15 DSC melting traces of PP nanocomposite samples containing (a) untreated alumina and (b) KH570-treated alumina.	118
Figure 4.16 Typical strain-stress curves of polymers	121
Figure 4.17 Strain- stress curves of PE nanocomposites.	123
Figure 4.18 Strain- stress curves of PP nanocomposites	124
Figure 4.19 Elongation at break of PE nanocomposites containing (a) untreated alumina, (b) KH570-treated alumina.	125
Figure 4.20 Tensile strength of PE nanocomposites containing (a) untreated alumina, (b) KH570-treated alumina.	126
Figure 4.21 Elongation at break of PP nanocomposites containing (a) untreated alumina, (b)KH570-treated alumina.	128
Figure 4.22 Tensile strength of PP nanocomposites containing (a) untreated alumina, (b) KH570-treated alumina.	129

Figure 5.1 The relationship between frequency and complex permittivity with different polarization types (adapted from [128]).	133
Figure 5.2 Thin film samples for dielectric spectroscopy.....	135
Figure 5.3 Dielectric constant of PE untreated-alumina nanocomposite.....	136
Figure 5.4 Dielectric loss tangent of PE untreated-alumina nanocomposite.	137
Figure 5.5 Dielectric constant of PE KH570-alumina nanocomposite.....	138
Figure 5.6 Dielectric loss tangent of PE KH570-alumina nanocomposite.	139
Figure 5.7 Dielectric constant of PP untreated-alumina nanocomposite.	140
Figure 5.8 Dielectric loss tangent of PP untreated-alumina nanocomposite.	140
Figure 5.9 Dielectric constant of PP KH570-alumina nanocomposite.	141
Figure 5.10 Dielectric loss tangent of PP KH570-alumina nanocomposite.	142
Figure 6.1 Example plot of Weibull distribution.	148
Figure 6.2 Weibull plots of DC breakdown strength of PE untreated-alumina nanocomposites.....	150
Figure 6.3 Weibull plots of DC breakdown strength of PE/KH570-alumina nanocomposites.....	151
Figure 6.4 Weibull plots of DC breakdown strength of PP untreated-alumina nanocomposites.....	153
Figure 6.5 Weibull plots of DC breakdown strength of PE/KH570-alumina nanocomposites.....	154
Figure 6.6 Comparison of DC breakdown strength among different nanocomposite	

systems.....	156
Figure 7.1 Development of space charge in dielectric material under an electric field due to (a) dipole orientation, (b) migration of ions, (c) charge injection at interfaces between dielectric and electrodes.	165
Figure 7.2 Space charge behavior of unfilled PE (a) under 20 kV/mm DC electric field at 30 °C, (b) under 40 kV/mm DC electric field at 30 °C.....	170
Figure 7.3 Space charge behavior of PE nanocomposites containing (a) 0 phr (b) 0.5 phr (c) 1 phr (d) 2 phr (e) 5 phr of untreated nano-alumina stressed at 40 kV/mm DC electric field at 30 °C.	175
Figure 7.4 Space charge decay process of PE nanocomposites containing (a) 0 phr (b) 0.5 phr (c) 1 phr (d) 2 phr (e) 5 phr of untreated nano-alumina stressed at 40 kV/mm DC electric field at 30°C.....	176
Figure 7.5 Total charge amount during the polarization process in the PE nanocomposites samples containing untreated nano-alumina under the DC electric field of 40 kV/mm at 30 °C.....	177
Figure 7.6 Space charge behavior of PE nanocomposites containing (a) 0 phr (b) 0.5 phr (c) 1 phr (d) 2 phr (e) 5 phr of KH570-treated nano-alumina stressed at 40 kV/mm DC electric field at 30 °C.....	181
Figure 7.7 Space charge decay process of PE nanocomposites containing (a) 0 phr (b) 0.5 phr (c) 1 phr (d) 2 phr (e) 5 phr of KH570-treated nano-alumina stressed at 40 kV/mm DC electric field at 30 °C.	182

Figure 7.8 Total charge amount during the polarization process in the PE nanocomposites samples containing KH570-treated nano-alumina under the DC electric field of 40 kV/mm at 30 °C..... 183

Figure 7.9 Space charge behavior of unfilled PP under a 20 kV/mm DC electric field at 30 °C. 186

Figure 7.10 Space charge behavior of unfilled PP under a 40 kV/mm DC electric field at 30 °C. 187

Figure 7.11 Space charge dynamics of PP nanocomposites containing (a) 0 phr (b) 0.5 phr (c) 1 phr (d) 2 phr (e) 5 phr of untreated nano-alumina stressed at 40 kV/mm DC electric field at 30 °C. 190

Figure 7.12 Space charge decay process of PP nanocomposites containing (a) 0 phr (b) 0.5 phr (c) 1 phr (d) 2 phr (e) 5 phr of untreated nano-alumina stressed at 40 kV/mm DC electric field at 30°C..... 191

Figure 7.13 Total charge during the polarization process in the PP nanocomposites samples containing KH570-treated nano-alumina under the DC electric field of 40 kV/mm at 30 °C. 192

Figure 7.14 Space charge dynamics of PP nanocomposites containing (a) 0 phr (b) 0.5 phr (c) 1 phr (d) 2 phr (e) 5 phr of KH570-treated nano-alumina stressed at 40 kV/mm DC electric field at 30 °C..... 196

Figure 7.15 Space charge decay process of PP nanocomposites containing (a) 0 phr (b) 0.5 phr (c) 1 phr (d) 2 phr (e) 5 phr of untreated nano-alumina stressed at 40 kV/mm

DC electric field at 30°C.....	197
Figure 7.16 Total charge amount during the polarization process in the PP nanocomposites samples containing KH570-treated nano-alumina under the DC electric field of 40 kV/mm at 30 °C.....	198
Figure 7.17 Temperature dependent space charge behavior of (a) unfilled PP, (b) PP/nano-Al ₂ O ₃ -KH570@5 phr nanocomposite.....	201
Figure 7.18 Temperature dependent charge decay behavior of (a) unfilled, (b) PP/nano-Al ₂ O ₃ -KH570@5 phr nanocomposite.....	202
Figure 7.19 Energy band diagrams for the polymer-electrode system (a) before the polymer is in contact with the electrodes; (b) when the polymer is attached to the electrodes; (c) when an external electric field is applied.....	205
Figure 7.20 Schematic representation of trap distribution in the energy band of a polymer.	209
Figure 7.21 TSC current (left) and calculated trap distribution (right) of virgin PE.	213
Figure 7.22 Trap distribution of PE nanocomposites containing KH570-alumina....	213
Figure 7.23 Trap distribution of PP nanocomposites containing KH570-alumina.	218
Figure 8.1 Typical time variation of the leakage current in a dielectric material.	222
Figure 8.2 The measured leakage current curves of (a) PE/ untreated nano-alumina samples and (b) PE/KH570-treated nano-alumina samples at 30 kV/mm and 30 °C.	224
Figure 8.3 The DC conductivity of PE and its nanocomposites under a 30 kV/mm DC	

electric field at 30 °C.	225
Figure 8.4 The measured leakage current curves of (a) PP/untreated nano-alumina samples and (b) PP/KH570-treated nano-alumina samples at 30 kV/mm and 30 °C.	226
Figure 8.5 The DC conductivity of PP and its nanocomposites under a 30 kV/mm DC electric field at 30 °C.	227
Figure 8.6 The J-E characteristic curve of space-charge-limited conduction current.	229
Figure 8.7 Carriers distribution in the dielectric film with space-charge-limited conduction theory.	230
Figure 8.8 The J-E curve of PE/alumina nanocomposites.	234
Figure 8.9 The J-E curve of PP/alumina nanocomposites.	234
Figure 8.10 Current density versus electric field of (a) PE and (b) PE/Al ₂ O ₃ -KH570@2phr nanocomposite.	237
Figure 8.11 Current density versus electric field of (a) PP and (b) PP/Al ₂ O ₃ -KH570@2phr nanocomposite.	238

List of Tables

Table 2.1 General properties of PP	42
Table 3.1 Nanocomposite samples.....	80
Table 4.1 Thermal parameters of PE and PP.....	115
Table 4.2 The melting temperature, crystallization enthalpy and crystallinity of PE nanocomposites.....	116
Table 4.3 The melting temperature, crystallization enthalpy and crystallinity of PP nanocomposites.....	120
Table 6.1 Parameters of Weibull plots of PE nanocomposites.....	152
Table 6.2 Parameters of Weibull plots of PP nanocomposites.....	155
Table 8.1 Carrier transport rate in PE nanocomposites and PP nanocomposites.....	233
Table 8.2 The electrical ageing threshold for PE and its nanocomposite.....	239
Table 8.3 The obtained electrical ageing threshold for PP and its nanocomposite....	239

List of Publications

Journal paper

Xuhui Duan, Wah Hoon Siew, Martin Given, John Liggat, Jinliang He, “*Effect of different surface treatment agents on the physical chemistry and electrical properties of polyethylene nano-alumina nanocomposites,*” High Volt., vol. 5.no 4, pp.397-402, Aug.2020.

Conference

“*Partial Discharge Detection and Location for HVDC Cables,*” Poster, 2016, 9th UHVnet, Cardiff, UK.

Xuhui Duan, WH Siew, Martin Given, John Liggat, Mark Wilson, Jinliang He, “*Study of Polyethylene and Polypropylene Nanocomposites for HVDC Insulation,*” IEEE Conference on Electrical Insulation and Dielectric Phenomenon (CEIDP), Richland, WA, USA, Oct 2019 (Not presented for presentation due to late approval of US visa).

Contents

Chapter 1 Introduction	26
1.1 Project Background.....	26
1.2 Research aim and objectives.....	30
1.3 Main contributions	32
1.4 The structure of this thesis	35
Chapter 2 Literature Review	37
2.1 Introduction.....	37
2.2 Polymeric Insulating Materials	38
2.2.1 Polyethylene.....	38
2.2.2 Polypropylene	41
2.3 Nanocomposite Dielectrics	45
2.4 Nanocomposite Models	50
2.4.1 Intensity Model	50
2.4.2 Interphase Volume Model	54
2.4.3 Electrical Double Layer Model.....	57
2.4.4 Multi-core Model	59
2.5 Breakdown of Solid Dielectrics	61

2.6 Space Charge	66
2.6.1 Overview of Space Charge	66
2.6.2 Space Charge Measuring Techniques	68
2.7 Summary	70
 Chapter 3 Material and Experimental Techniques	
3.1 Introduction.....	71
3.2 Materials	72
3.2.1 Materials for this study	72
3.2.2 Surface Treatment of Nano-alumina	74
3.2.3 Mixing and casting of nanocomposites.....	76
3.3 Experimental Techniques	82
3.3.1 Thermal-gravimetric Analysis	82
3.3.2 Fourier-transform Infrared Spectroscopy	82
3.3.3 Differential Scanning Calorimetry.....	83
3.3.4 Polarized Optical Microscopy.....	84
3.3.5 Scanning Electron Microscopy	86
3.3.6 Dielectric spectroscopy	87
3.3.7 Electrical Breakdown Test	88

3.3.8 DC Electrical conductivity Measurement	89
3.3.9 Thermally Stimulated Current Measurement.....	90
3.3.10 Space charge Measurement.....	91
3.3.11 Mechanical Strength Test	93
Chapter 4 Physical Chemistry Characterization	
4.1 Introduction.....	95
4.2 Results and Discussion	96
4.2.1 Thermal-gravimetric Analysis	96
4.2.2 Fourier-transform Infrared Spectroscopy	97
4.2.3 Polarized Optical Microscopy.....	99
4.2.4 Scanning Electron Microscopy	105
4.2.5 Differential Scanning Calorimetry.....	113
4.2.6 Tensile test.....	120
4.3 Summary	129
Chapter 5 Dielectric Spectroscopy.....	
5.1 Introduction.....	132
5.2 Results and discussion	135
5.2.1 Measurement for PE Nanocomposites Containing Untreated Nano-alumina	

.....	135
5.2.2 Measurement for PE Nanocomposites Containing KH570-treated Nano- alumina.....	137
5.2.3 Measurement for PP Nanocomposites Containing Untreated Nano-alumina	139
5.2.4 Measurement for PP Nanocomposites Containing KH570-treated Nano- alumina.....	141
5.2.5 Discussion.....	142
5.3 Summary.....	144
Chapter 6 DC Breakdown Strength	145
6.1 Introduction.....	145
6.2 Results and Discussion	149
6.2.1 Results of PE and PE Nanocomposites.....	149
6.2.2 Results of PP and PP Nanocomposites	152
6.2.3 Discussion.....	155
6.3 Summary.....	161
Chapter 7 Space Charge Measurement and Trap Characterization.....	163
7.1 Introduction.....	163

7.2 Space Charge Formation and PEA System	164
7.3 Results and Discussion for PE and PE nanocomposites	168
7.3.1 Measurements for Unfilled PE.....	168
7.3.2 Measurements for PE Nanocomposites containing Untreated Nano-alumina	171
7.3.3 Measurements for PE Nanocomposites containing KH570-treated Nano- alumina.....	177
7.3.4 Discussion	183
7.4 Results and discussion for PP and PP nanocomposites	185
7.4.1 Measurements for Unfilled PP Sample.....	185
7.4.2 Measurements for PP Nanocomposites containing Untreated Nano-alumina	187
7.4.3 Measurements for PP Nanocomposites containing KH570-treated Nano- alumina.....	192
7.4.4 Measurements for Unfilled PP and PP Nanocomposite under Temperature Gradient.....	198
7.4.5 Discussion	203
7.5 Trap Characterization.....	207
7.5.1 Introduction.....	207

7.5.2 Results and discussion for PE Nanocomposites	213
7.5.3 Results and discussion for PP Nanocomposites.....	216
7.6 Summary.....	219
Chapter 8 DC conductivity	221
8.1 Introduction.....	221
8.2 Results and Discussion	223
8.2.1 Measurements for PE nanocomposites	223
8.2.2 Measurements for PP Nanocomposites.....	225
8.2.3 Discussion	227
8.3 Summary.....	239
Chapter 9 Conclusions and Future Work	241
9.1 Summary of Findings.....	241
9.2 Conclusions.....	244
9.3 Future Work	245
References.....	248

Chapter 1 Introduction

1.1 Project Background

With the booming development of modern economy around the world, the demand of electricity is also increasing. According to the International Energy Agency, world electricity consumption increased from 22,310 TWh in 2000 to 26,500 TWh in 2010, and to 27,880 TWh in 2018. This represents an increase of 18.4% between 2000 and 2010, and a further increase of 5.2% between 2010 and 2018. The power generation plants are often located in remote areas and the electricity needs to be transmitted to substations over long-distance before distributed to the customers. To reduce the power losses during power transmission, transmission systems with higher voltage are required. The high voltage alternating current (HVAC) and high voltage direct current (HVDC) transmission systems are developed to realize long-distance power transmission. With further development of power electronics, HVDC transmission systems have shown various advantages over HVAC transmission systems. First of all, the investment cost of the HVDC transmission system is cheaper when the transmission distance is over 600 km for the overhead line and 50 km for the submarine line [1]. This is because the conductor size of DC lines is much smaller compared with AC lines at the same current level. Secondly, there is no skin effect and reactive power loss for HVDC lines. The power losses of HVDC system are considerably lower when compared with HVAC system. Additionally, the HVDC could provide better

controllability. The voltage regulation is easy to achieve as there is no inductance in DC transmission system. Lastly, the corona effect, electromagnetic interference and acoustic noise are lower for HVDC lines [2]. On all accounts, the HVDC transmission system becomes more prevalent in long-distance power transmission. Polymeric insulation materials have been widely used for extruded HVDC cables as underground power transmission for decades due to their light weight, excellent electrical and mechanical properties, and low cost. Compared with the traditional oil-filled (OF) and Mass Impregnated Non-draining (MIND) HVDC cables, the extruded polymeric HVDC cable systems have the following advantages [3]–[6]:

- a) The conductor temperature can be raised, which make the extruded HVDC cable more compact under the same power rating.
- b) They are more environmentally friendly without the risk of oil leakage.
- c) Joints between cables are much simpler and more accessible.
- d) Reduced maintenance fees.

The popular polymeric materials for HVDC cables are mainly low-density polyethylene (LDPE), high-density polyethylene (HDPE) and cross-linked polyethylene (XLPE). However, LDPE is not suitable for larger capacity power cables as the maximum operation temperature is limited to 70 °C. To overcome this issue, XLPE, which is manufacturing by crosslinking LDPE, is designed to raise the operation temperature to about 90 °C. At present, XLPE has been the most widely used as high voltage cable

insulation. With the increasing concerns of environmental issues and sustainable development, the concept of recyclable polymeric insulation material has been proposed [3], [4], [7]–[9]. Although XLPE owns excellent insulating properties, the unique cross-linked structure makes them difficult to be recycled. The cross-linking and degassing process of XLPE also increases energy consumption and exacerbates the harmful effects of environmental contamination. Hence, the use of thermoplastic polymers such as polyethylene (PE) and polypropylene (PP) as new HVDC cable insulation has become a hot topic both in research and industry due to their low price, simple manufacturing process and recyclable nature.

However, the extruded HVDC polymeric insulation materials still have drawbacks due to the space charge accumulation [21]. The origin of space charge in the bulk of the polymeric insulation material is from the electrode injection or the ionization of the impurities in the dielectric. These accumulated space charge would distort the local electric field and accelerate insulation ageing [4], [6], [9], [10]. To improve these issues, inorganic nanoparticles such as graphene and zinc oxide are used to manufacture polymeric nanocomposite insulation materials [11], [12] and they have become promising insulating materials for future HVDC cables in research.

To further improve the mechanical, thermal and electrical properties of polymeric cable insulation, selected nanoparticles are introduced into polymeric material to make polymer nanocomposite insulating material. Previous studies have shown that the

addition of inorganic nanoparticles such as SiO₂ [3], [24], [25], MgO [13], [19], [25]–[28] and Al₂O₃ [15], [18], [29]–[33] in LDPE can increase the breakdown strength and reduce the electrical conductivity, thermal resistivity and space charge accumulation. Zhou *et al.* reported the effect of different nanoparticles on tuning the electrical properties of polypropylene [18],[34]. After adding a small quantity of surfaced-treated MgO into PP, the space charge accumulation was dramatically suppressed and the DC breakdown strength was greatly enhanced. Although plenty of works have been done in this area, the understanding of underlying mechanisms of polymer nanocomposite insulating materials is still not clear yet. A better understanding of these mechanisms would help to design future recyclable HVDC cable insulation. In addition, although the addition of nanoparticles in polymeric insulation material provides an approach of enhancing the dielectric properties of the insulation, special attention still needs to be paid on the drawbacks by the presence of nanoparticles. After studying several nanocomposite examples based on experimental work, there is a few inconsistencies in the measured results. In many cases, this is likely due to poor quality control during the preparation of new class of material. Hence, this project was proposed to design proper nanocomposite sample preparation method in the lab and investigate the effect of the addition of nano alumina particles on the physical chemistry properties and DC electrical properties of PE and PP based nanocomposites. Nano alumina is a popular nanoparticle in nanodielectric due to its high dielectric constant, high thermal stability and high mechanical strength.

1.2 Research aim and objectives.

The aim of this project is to evaluate the feasibility of using polyethylene/ nano-alumina and polypropylene/ nano-alumina as recyclable HVDC cable insulation. The evaluation of the proposed nanocomposites is in many ways such as physical chemistry properties, mechanical properties and DC electrical properties.

To achieve this aim, the main objectives and scope of this research are as following:

- To propose new thermoplastic polymer nanocomposites for future HVDC cable insulation and verify the validity of nanocomposite sample preparation method. Previous research mainly investigated the use of pure polymeric material as HVDC cable insulation. It has been proved the introduction of nanoparticles can effectively improve the electrical properties of polymeric insulating materials, which might be due to the chemical and morphological changes in nanocomposites. In this study, PE and PP were used as the matrix polymer. Nano-alumina particles with different filling contents were employed as nanofiller to manufacture PE nanocomposites and PP nanocomposites. Moreover, the silane coupling agent was used to modify the surface chemistry of nanoparticles. The structural changes of nanoparticles were identified with thermogravimetric analysis (TGA) and Fourier-transform infrared spectroscopy (FTIR) methods. The effect of interfacial chemistry was then studied by comparing the differential scanning calorimetry (DSC), scanning electron

microscopy (SEM) and polarized optical microscopy (POM) results of nanocomposites.

- To investigate the effect of nanoparticles on the electrical properties of polymer nanocomposites.

A large and growing body of literature has investigated that the addition of nanoparticles can change the electrical properties of polymer nanocomposites due to the special nano-structuration. Generally, the nanocomposites showed enhanced breakdown strength than the matrix polymer. However, reduced breakdown strength was also presented in many nanocomposite studies. The mechanism of the breakdown in nanocomposite is very complicated and not clear yet. In this study, the effect of nano-alumina with and without surface treatment on DC breakdown behaviour of polyethylene nanocomposites and polypropylene nanocomposites was respectively examined to explain the possible breakdown mechanism of the nanocomposite system. Additionally, DC volume conductivity and space charge behaviour of nanocomposites were also characterised to study the effect of different surface chemistry and filling content on the electrical properties. This study offers some critical insights into the relationship between electrical performance and the interfacial changes of nanocomposite materials.

- To explore the potential relationship between the microstructure and dielectric performance of polymer nanocomposite material.

There is a large volume of published studies describing the role of the interface in governing the dielectric performance of nanocomposites by proposing different interface models. These models were reviewed and discussed in chapter two. In this study, polyethylene/ nano-alumina and polypropylene/ nano-alumina samples were prepared as potential recyclable HVDC cable insulation material. The morphological and dielectric behaviour of polymer nanocomposites containing untreated and treated nano-alumina at different filling content were extensively studied. The effect of surface modification and filling content on the microstructure of nanocomposite was discussed. Moreover, attempts were made to explore the underlying relationship between the interfacial characteristics and the DC dielectric properties in this project.

1.3 Main contributions

The main achievements of this research are listed as following:

- The nanoparticle surface modification method and the nanocomposite sample preparation method were successfully developed, which guarantees the accuracy and validity of the measured experimental data.
- The influence of surface modification of nanoparticles on the electrical

performance of polymer nanocomposites was studied. The surface modification of nano alumina particles by using silane coupling agent has been proven an effective method in improving the dispersion and distribution of nanoparticles in matrix polymers, which results in better dielectric performance.

- The characterisations of the morphological and structural changes of nanocomposites were successfully designed and conducted to study the interfacial effect of nanocomposites. The introduction of nanoparticles enhances the nucleation effect in nanocomposites, resulting in reduced spherulite size and increased spherulite density. But it has limited influence on crystallinity of polymer nanocomposites.
- The investigation of the effect of nanoparticles on the dielectric permittivity of proposed polymer nanocomposite systems was conducted. The addition of nano-alumina particles showed a limited influence on the dielectric response of polymer nanocomposites.
- The study of the DC electrical breakdown properties of polymeric nanocomposite materials was performed. The results have been analysed and compared with pure polymer materials. Moreover, the effect of surface treatment and the impact of filling the content of nanoparticles on the DC breakdown strengths of nanocomposite samples were carefully studied. The probability of DC breakdown in polymer nanocomposites was successfully calculated with the help of Weibull statistical analysis. Sample PE/Al₂O₃-

KH570 @0.5phr has 16.2% higher DC breakdown strength than unfilled PE, 394.6 kV/mm for PE/Al₂O₃-KH570 @0.5phr and 339.7 kV/mm for unfilled PE. Sample PP/ Al₂O₃-KH570 @1phr has 14.4% higher DC breakdown strength than unfilled PP, 491.0 kV/mm for PP/ Al₂O₃-KH570 @1phr and 429.1 kV/mm for unfilled PP. Furthermore, PP/alumina nanocomposite shows higher breakdown strength than PE/alumina nanocomposite when they are filled with the equivalent amount of nano-alumina.

- The space charge accumulation of PE/ nano-alumina nanocomposites and PP/ nano-alumina nanocomposites were captured by using the PEA (pulsed electro-acoustic) method. Only homocharge accumulation was identified for all the nanocomposite samples. The total charge amount for PE nanocomposites is reduced with the filling content no more than 2 phr. While for PP nanocomposites, the total charge amount continuously decreases as the filling content is increased. The modified thermally stimulated current method was used to characterise the trap distribution of nanocomposites, which affects the space charge accumulation and development.
- The investigations of DC conductivity of PE nanocomposites and PP nanocomposites were completed. The introduction of nano-alumina particles can reduce the DC conductivity in all the nanocomposite systems compared with pure polymer system. PP/ Al₂O₃-KH570@1 phr sample has the lowest DC conductivity, which is about 14 times smaller than that of unfilled PP.

Furthermore, the carrier mobility and electrical ageing threshold of pure polymer and polymer nanocomposites were calculated based on space-charge-limited conduction theory. It has been shown that the introduction of nano-alumina can improve the electrical ageing threshold for nanocomposites.

- A comparison between PE nanocomposites and PP nanocomposites was made throughout the entire research. Results showed that PP and its composites have superior electrical properties over PE and its composites.

1.4 The structure of this thesis

The overall structure of this thesis takes the form of ten themed chapters.

Chapter 1 provides the background of this research, aims and objectives of this research, main contributions and the structure of this thesis.

Chapter 2 reviews the current literature associated with this research and it could be divided into six sections:

- Section 2.1 is an introductory section of this chapter.
- Section 2.2 introduces the fundamentals of polymeric materials and the basic properties of polyethylene and polypropylene polymers.
- Section 2.3 begins with a brief overview of nanocomposites and then goes to the advantages of nanocomposite material.
- Section 2.4 introduces four popular nanocomposite models.

- Section 2.5 is the reviews mainly about the breakdown in the solid insulation.
- Section 2.6 reviews the fundamentals of space charge and its measurement techniques.

Chapter 3 describes the preparation of nanocomposite samples for this study and introduces the experimental techniques involved in this study.

Chapter 4 reports the physical chemistry characterizations of all proposed nanocomposite systems, which includes the surface chemistry study of nanoparticles by using TGA and FTIR, morphological observations by using POM and SEM, thermal analysis by using DSC and mechanical properties by using the tensile test.

From Chapter 5 to Chapter 8, a comparison is made among four nanocomposites systems, i.e., PE/untreated nano-alumina, PE/KH570-treated nano-alumina, PP/untreated nano-alumina and PP/KH570-treated nano-alumina in the following aspects:

- Dielectric spectroscopy in Chapter 5
- DC breakdown strength in Chapter 6
- Space charge behaviours in Chapter 7
- DC conductivity in Chapter 8

Chapter 9 summarizes the main findings and conclusions in this project and provides the suggestion for future work.

Chapter 2 Literature Review

2.1 Introduction

Polymers have been widely used in many areas such as packaging, pipes, components for chemical industry and electrical insulation. With the widespread usage of polymeric materials in the electrical insulation field, many researchers and research institutions have raised environmental concerns. Cross-linked polyethylene is the most popular and widely used polymeric insulation material for HVAC and HVDC cables due to its excellent mechanical, thermal and electrical properties. Although it has been served as cable insulating material for around 60 years [6], XLPE cannot meet the requirements of sustainable development due to its complicated manufacturing process and hard-to-recycle property. To address this concern, thermoplastic polymers, which can be easily recycled, become more popular than thermoset polymers [13]. Moreover, nanoparticles are introduced into polymeric material to modify its physical chemistry and electrical performance.

In this chapter, the relevant chemistry and engineering background of polymer nanocomposite insulation materials are introduced and discussed, which helps to establish a basic understanding of the nanocomposite insulating material.

2.2 Polymeric Insulating Materials

Based on their chemical properties, polymers can be divided into three different types: thermoplastic polymer, thermosetting polymer, and elastomers. Their molecular structure determines the chemical properties of them. The most commonly used polymer for electrical cables is thermoplastic and thermosetting materials due to their excellent insulating properties, lightweight and easy manufacture.

Thermosetting polymers can keep their infusible state formed through a series of chemical reactions, including heating, ultraviolet illuminating, and catalyzing. It cannot be modified once cured due to the formed cross-linking bonds. On the contrary, thermoplastic polymers can be melted or softened by heating up to their melting point and solidified by dropping the temperature repeatedly. Thermoplastic materials will change state among crystalline, semi-crystalline and amorphous states when the temperature is too high or flow under high pressure. This feature makes thermoplastic materials suitable to be used as environmentally-friendly cable insulation. To meet the requirements of future recyclable HVDC cable insulation, thermoplastic polymers such as polyethylene and polypropylene are popular polyolefins both in research and industry. In 2015, Prysmian Group developed their prototype of 320 kV polypropylene recyclable HVDC cable.

2.2.1 Polyethylene

Polyethylene is one of the most popular polymer materials for electrical insulation

nowadays because of its low water absorption, excellent flexibility, good toughness and high chemical resistance [10]. Polyethylene is a semicrystalline thermoplastic polymer formed by the polymerization of ethene and has long linear chains in three dimensions without cross-links. Figure 2.1 shows its basic formula. With different manufacturing processes, the physical and chemical properties of polyethylene polymers are different. The degree of crystallinity and molecular weight of polyethylene play an essential role in determining material properties. The crystallinity of polyethylene is influenced by the size of the side chains due to its branched structure. For example, with the increasing degree of crystallinity, the toughness decreases. The most widely-used polyethylene polymers are low-density polyethylene (LDPE) with a large number of short and long branches, linear low-density polyethylene (LLDPE) with a considerable number of short branches and high-density polyethylene (HDPE) with a small number of branches, as shown in Figure 2.2. However, HDPE is not a common material for cable insulation as it is too rigid due to its high crystallinity. Compared with HDPE, LDPE has relatively lower crystallinity because the side branches impede the development of crystalline structures. It is replacing the oil-impregnated paper as cable insulation due to its higher electrical strength. The LLDPE has similar properties as LDPE but with higher melting temperature and better flexibility. It has been noticed that LLDPE is replacing LDPE as HV (high voltage) cable insulation in the power cable industry due to its better flexibility and higher resistance to environmental stress cracking [14], [15].

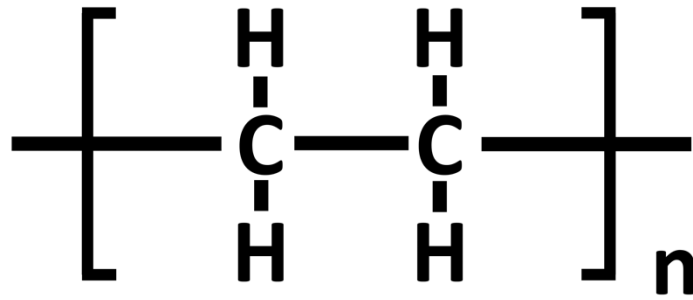


Figure 2.1 Molecular formula of polyethylene.

However, polyethylene-based power cables are not suitable for large capacity transmission systems as they can only work below 70 °C [16], [17]. To meet the temperature requirements for HVDC applications, cross-linked polyethylene (XLPE) has been developed and proved to be a reliable choice in commercial applications. It is normally synthesized by using LDPE and organic peroxide (typically dicumyl peroxide) [4], [18]. The long-time operation temperature of XLPE is up to 90 °C. To date, cable manufacturers such as ABB and Prysmian have successfully invented the 500 kV XLPE HVDC cables. However, XLPE is a kind of thermoset material, which means it hard to be recycled to meet the requirement of sustainable development of modern society. Furthermore, by-products such as methane, acetophenone and cumyl alcohol are generated during the cross-linking process and they would result in the degradation of electrical properties. Additional degassing processes are required to reduce the by-products during the manufacturing process. These processes are very complicated,

resulting in a long production time which is about at least five times longer than that of thermoplastic materials [10], [19], [20]. Hence, the polypropylene based polymeric insulation material has been proposed and studied in recent years.

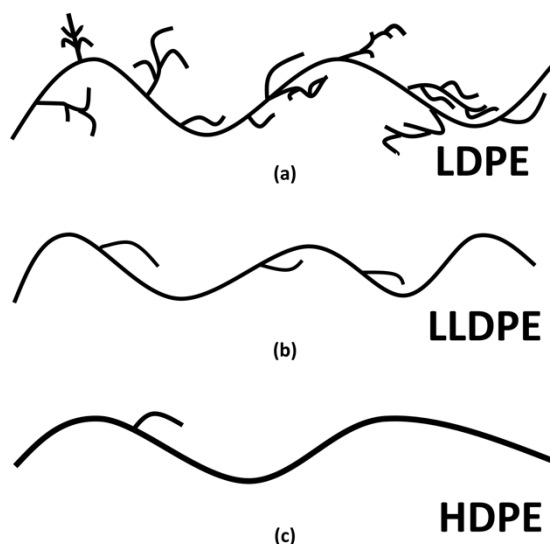


Figure 2.2 Molecular structure of (a) LDPE, (b) LLDPE and (c) HDPE.

2.2.2 Polypropylene

Polypropylene is the lightest plastic material with a high softening point and lower shrinkage, which is made by the polymerization of propylene monomer. The basic structure of polypropylene is shown in Figure 2.3. The general properties of polypropylene are listed in Table 2.1. The density of polypropylene is usually in the range of $0.89 - 0.91 \text{ g/cm}^3$. The melting temperature of polypropylene is around $160 \text{ }^\circ\text{C}$, which shows better thermostability when comparing with polyethylene polymers. It also has good physical and mechanical properties, such as good abrasion resistance and high surface hardness. Compared with polyethylene, polypropylene has high chemical

resistance as it can resist many organic, alkaline and acid solvent. Furthermore, polypropylene owns good insulating properties.

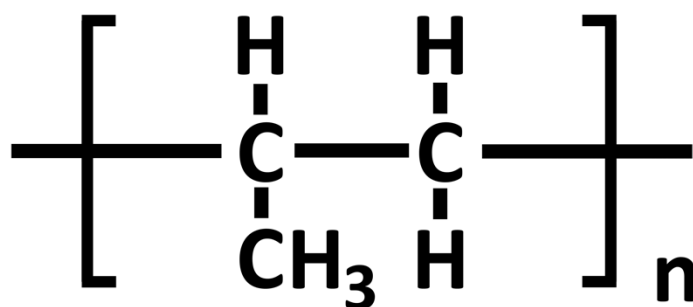


Figure 2.3 Molecular structure of polypropylene.

Table 2.1 General properties of PP

Thermo-physical properties	
Melting point, °C	160-163
Density, g/cm ³	0.89-0.91
Thermal conductivity, W/mK	0.17-0.23
Rockwell hardness	R65-R100
PP melt flow, g/10min	4-12
Electrical properties	
Dielectric strength, kV/mm	23-25
Volume resistivity, ohm·m	>10 ¹⁴
Dielectric constant @ 1 MHz	2.1-2.6
Mechanical properties @23 °C	
Tensile strength, MPa	31-45
Elongation, %	11-12
Elongation at break	50 - 145
Flexural modulus, MPa	1400-1800
Notched Impact Strength, J/m	35-60
Other properties	
Processing temperature, °C	200-280
Water Absorption (24 hr. Immersion), %	0.01-0.03
Continuous working temperature	90-120

Polypropylene could be categorized as isotactic polypropylene, syndiotactic polypropylene and atactic polypropylene according to the various locations of methyl groups in the polypropylene chain, as illustrated in Figure 2.4. The methyl groups of isotactic polypropylene are all located on the same side of the polypropylene backbone. The methyl groups of syndiotactic polypropylene are alternatively located on both sides of the polypropylene backbone. For atactic polypropylene, the methyl groups are randomly located on both sides of the polypropylene backbone. Yoshino, K et al. have studied the possibility of using syndiotactic polypropylene as recyclable cable insulation material [21]. Although it has shown excellent DC volume resistivity, thermal and mechanical properties, the prohibitively high cost is a crucial problem for its industrialization. Previous studies have proven that the melting point of isotactic polypropylene is about 160 °C and can work at 100 °C for long time operation [22]. It also has outstanding thermal stability and breakdown strength. However, the modulus of isotactic polypropylene is relatively high when the temperature is low [23].

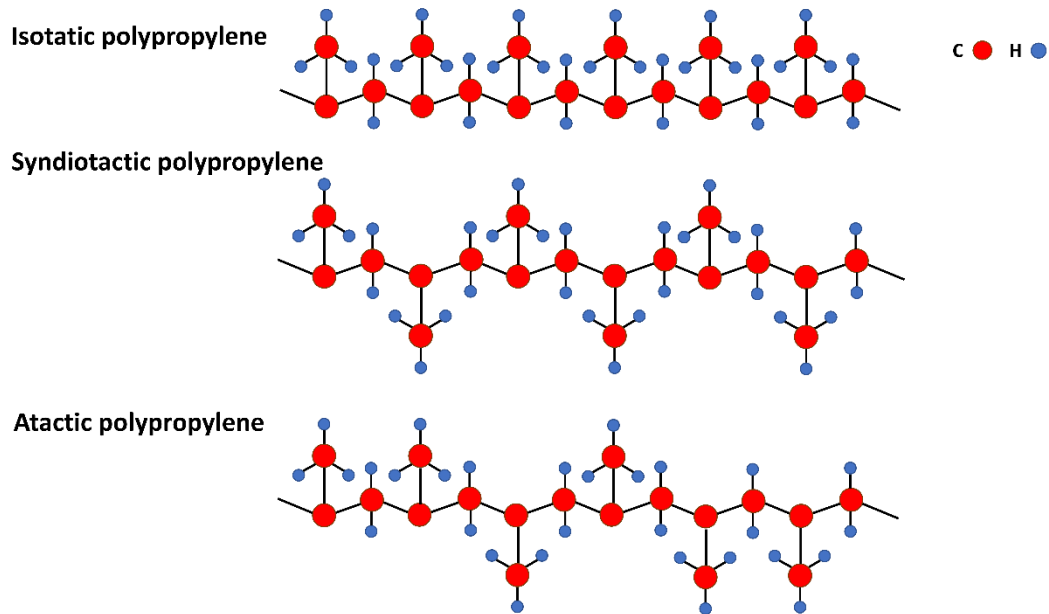


Figure 2.4 Molecular structure of polypropylenes: (a) isotactic polypropylene; (b) syndiotactic polypropylene; (c) atactic polypropylene.

However, the poor mechanical properties like the inherent rigidity impede the development and application of PP as high capacity HVDC cable insulation. Numerous studies have attempted to improve the mechanical properties of PP and the most reliable and effective method is to make polypropylene blend with other thermoplastic elastomers. The most commonly used polymers include ethylene propylene rubber (EPR), styrene-ethylene-butylene-styrene (SEBS), ethylene-propylene-diene monomer (EPDM) and polyolefin elastomer (POE). Hosier *et al.* published a paper in which they used propylene-ethylene copolymer and their blends as potential HVDC cable insulation. While all the proposed materials showed one or more desired properties, none of them possesses all the requirements of an ideal thermoplastic insulation system such as low temperature flexibility, high breakdown strength and high temperature

integrity [24]. Ma et al. investigated the PP/ ethylene octene copolymer blends and results show that improved notched impact toughness and the decreased rigidity and tensile strength [25]. Green *et al.* developed a propylene homopolymer/ propylene-ethylene copolymer blend as thermoplastic insulation material. It has optimized electrical and mechanical properties when the blend is composed of 50% iPP and 50% copolymer [26]. Zhou *et al.* studied PP/POE blend as recyclable HVDC cable insulation. Results show the PP/POE blend can improve mechanical flexibility, good thermal properties and enhanced electrical properties [27]. In [28], they introduced MgO nanoparticles into the PP/POE blend to further improve the electrical properties, especially the space charge accumulation.

2.3 Nanocomposite Dielectrics

Nanotechnology was formally introduced to polymer in 1988 when a US patent was issued to Johnston and Markovitz [29]. They had shown that the micaceous system used for ground-wall insulation was improved by adding filler particles into the polymer. In 1994, Lewis published a theoretical paper about nanodielectrics, which has been considered as the foundation of nanodielectric research until today [30]. He pointed out that the introduction of nanoparticles enhanced the electrical performance of insulation materials. In 1999, Henk et al. found that silica nanoparticles could enhance the voltage endurance of polymer insulation. They also figured that the smaller the size of the

nanoparticle, the higher the voltage it could withstand [31]. Then, Nelson et al., a US/UK team, had done the experimental trials of epoxy/ titanium oxide composites and published in 2002 [32]. After this, nanodielectric has become a popular and worldwide topic in the insulation research area. Until now, the functional requirements of insulation material are in high demand due to the ever-increasing voltage level of electricity transmission. Figure 2.5 indicates that the time-based publication activities, acquired from CompendexTM database, regarding terms ‘dielectric nanocomposite’ and ‘nanodielectrics’ since 1990. It reveals that there is an explosive growth of nanodielectric research activities after 2002. By the end of 2022, the number of dielectric nanocomposite relevant publication activities is over 11200, which reflects the continued interest and potential for these materials in various fields of research and application.

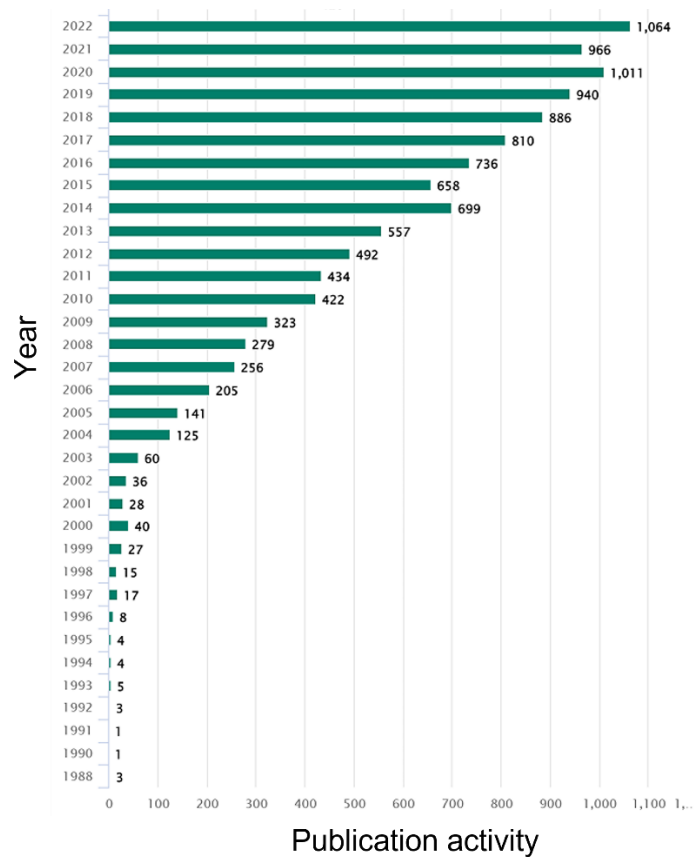


Figure 2.5 Nanocomposite relevant publication activities.

Nanocomposite materials are made by adding nano-scale particles into the insulating polymer material. The average size of nano fillers is within 100 nm. When the binary system of composites consists of nano-scale fillers and polymer, it is called nanocomposites. But the properties are not simply the sum of each composition. In general, polymer nanocomposite consists of three parts, the polymer matrix, the nanofillers and the interaction area between the matrix and the nanoparticles, as illustrated in Figure 2.6. T.J Lewis first described the relationship between the interface effect and special properties of nanocomposite in his published papers [30].

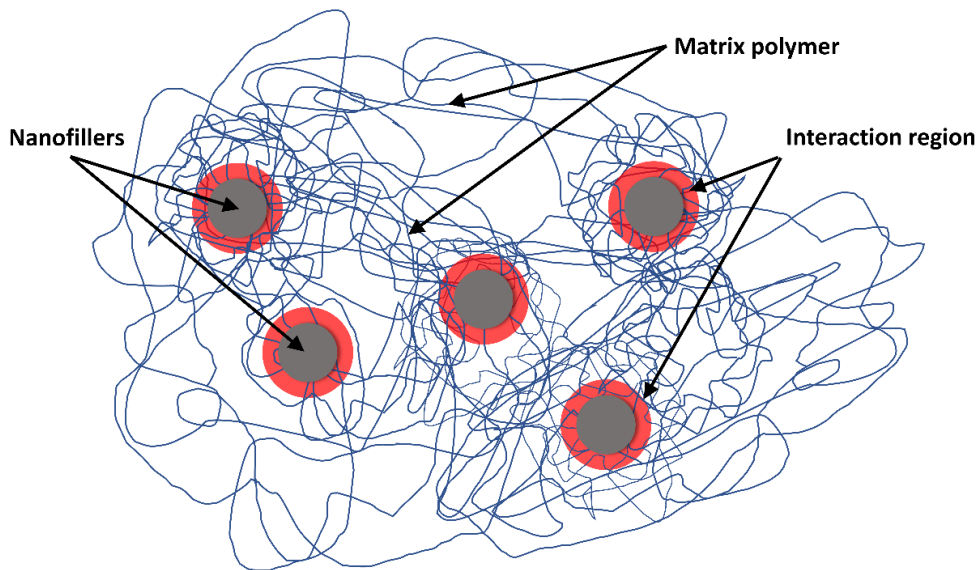


Figure 2.6 Constituents of polymer nanocomposites.

The polymer nanocomposites show great advantages in increasing thermal endurance, improving electrical properties and extending lifetime of composite materials. The first commercial polymer nanocomposite was manufactured by Toyota in 1990, which was used in timing belt covers to enhance its thermal and mechanical performance [33]. Later, many published papers have proved that polymer nanocomposites have great potentials both in research and commercial use [15], [18], [34]–[42]. There are some factors that influence the dielectric performance of nanodielectric materials:

- Particle size
- Particle type
- Particle concentration
- Matrix material
- Surface functionalization of filler

In general, the particle size, type and concentration play the most vital role in influencing the dielectric properties of nanocomposites. The surface functionalization and the matrix material are considered to have a secondary role and they affect the stability and compatibility of the nanoparticles within nanocomposite material. In the electrical insulation field, nanocomposite is defined as a homogeneous blend of insulation materials and filler particles. And the particles are always in size of a few to a few tens nanometers. In most published books and papers, nanocomposite and nanodielectric refer to polymer/ nanoparticle composite. The range of nano-scale fillers varies from few nanometers to several hundred nanometers. Based on different shapes, nanoparticles can be classified into whiskers, rod particles, spherical particles, and platelet particles. Nano clays, carbon nanotubes, metal oxides and metal oxides are the most common types of synthesis nanodielectric. Compared with microparticles, nanoparticles have a larger specific surface area, quantum size effect and unique interface between the polymer matrix and the nanoparticles, which all contribute to the enhancement of electrical and chemical performance [43]. Carbon black, zinc oxide, magnesium oxide and alumina particles have been widely employed in research to improve and functionalize insulation materials [11], [44]–[48].

Previous studies have shown the nanoparticle agglomeration has a negative impact on the electrical performance of polymer nanocomposite materials [48]–[56]. It has been reported that the agglomeration of nanoparticles resulted in the reduced breakdown strength and increased conductivity of polymer nanocomposites [39], [56]. Moreover,

the poor adhesion between the polymer matrix and the nanoparticles would cause the debonding of nanoparticles from the polymer matrix under mechanical stress. A large number of cavities could then be generated, resulting in the degradation of electrical properties [40], [41]. To reduce the possibility of early electrical breakdown, it is necessary to achieve uniform dispersion of nanoparticles within the polymer matrix and decrease the particle agglomeration [57]. Surface modification of nanoparticles based on silane chemistry has been proved to be a practical way to improve the interfacial adhesion and minimize nanoparticle agglomeration [11], [54], [58], [59]. Recently investigators have examined the effect of surface modification on the breakdown strength, conductivity and space charge accumulation of polymer nanocomposites strength [44], [47], [55], [60]–[63].

2.4 Nanocomposite Models

There are many different models proposed to explain the structure of nanocomposite. The existence of the interface, which is between the matrix material and the nanoparticles, is mentioned by all the models. The interface is believed to have a dominant impact in determining the properties of the nanocomposite. This might give us the reasons why the characteristics of nanocomposite change when adding nanoparticles. Four popular models are introduced in the following part.

2.4.1 Intensity Model

The intensity model of nanocomposite was proposed by Lewis in 2004 [64]. The main

idea of this model is that the intensity I_α for a specific material property α changes gradually across the interface area (usually a few nanometers). The interaction effect exists between atoms and molecules and their surroundings [65]. The property α would be either a physical or chemical property of the nanocomposite material. Figure 2.7 shows the changing intensity over the interface ab . The most straightforward situation would be a concentration of a constituent in a specific system. The constituent could be an ion, an atomic, or an electron[66].

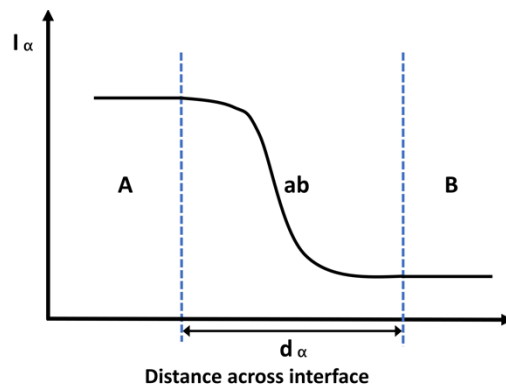


Figure 2.7 The interface ab between two phases A and B defined by the intensity I_α of a chosen property α as it changes in passage across it [65].

Three examples are provided in Figure 2.8 to understand the intensity model. Figure 2.8(a) describes the electron concentration at a metal-vacuum interface. Figure 2.8(b) shows the oxygen concentration at the surface of silicon. Figure 2.8(c) shows the normal electric field distribution at a metal-n-type semiconductor contact. Based on the examples, it can be concluded that the intensity of an appointed property will not be

only between the phase A and B. The intensity of the property on the interface could be smaller or even larger than A or B. In nanocomposites, the A phase is a nanoparticle surrounded by the B phase, the matrix material. The interface ab will increase when the size of the nanoparticle is decreased. The disadvantage of this model is that it does not illustrate the physical processes or changes of the interact area. However, it offers the visualized change of the interface property in nanocomposite system.

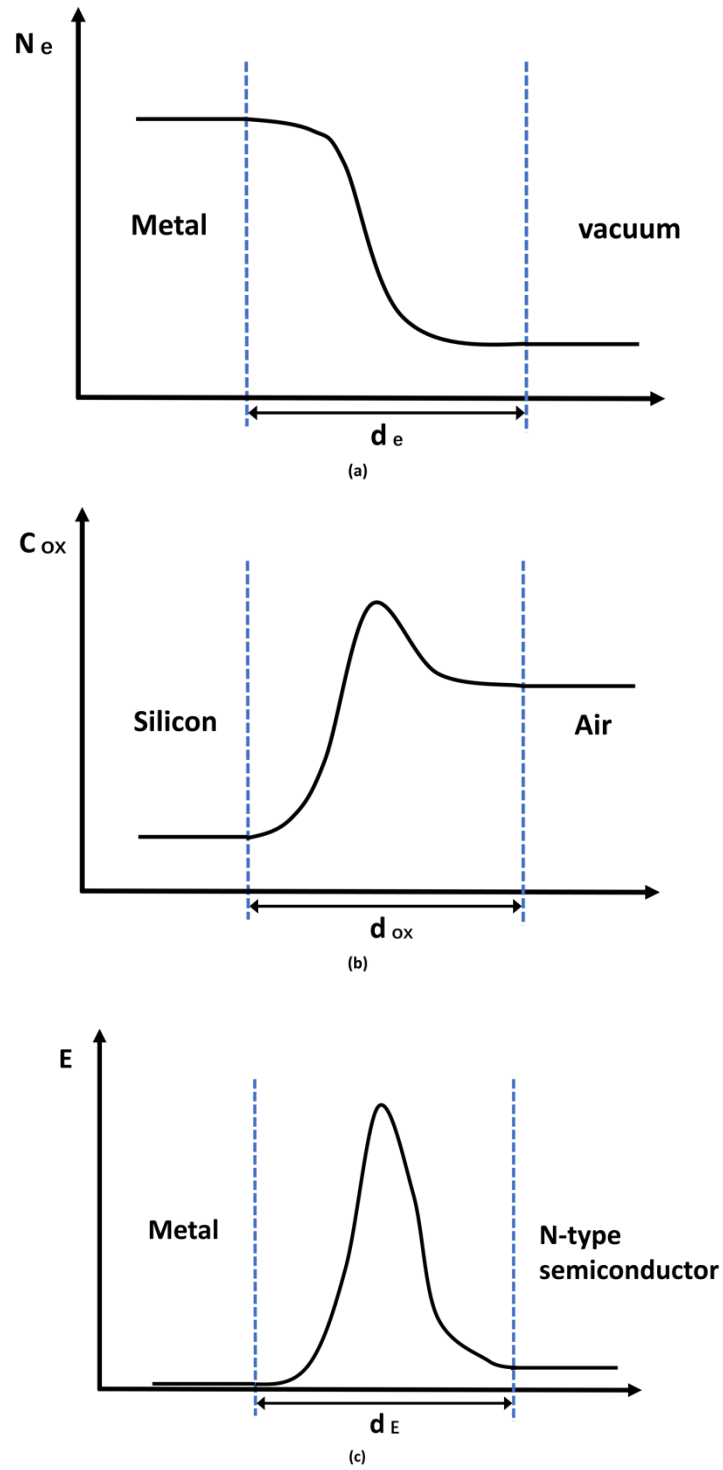


Figure 2.8 Interfacial intensities: (a) electron concentration at a metal-vacuum interface; (b) oxygen concentration at the silicon-air interface; (c) electric field distribution at a metal-n-type semi-conductor contact.

2.4.2 Interphase Volume Model

Ratzke proposed the interphase volume model to explain the influence of nanoparticles on the improved material properties of nanocomposite for high voltage insulation [67]. It is based on the assumption that the interfacial region between matrix polymer and nanoparticles has a strong impact on the properties of nanocomposites. This model further explains the relationship between the interphase and the increased resistance of nanocomposite to the electrical discharge activities. Such electrical activities include electrical treeing, partial discharge and high voltage arcing. The following assumptions are made for the interphase volume model [67]:

- a) all the nanoparticles are spherical and have the same diameter d .
- b) all the nanoparticles are homogeneously dispersed in the matrix polymer.
- c) all the nanoparticles are enclosed in interphase with the thickness of i .
- d) the properties of the interphase are different from those of the uninfluenced polymer.

Figure 2.9 shows the possible distribution of nanoparticles in the nanocomposite based on the interphase volume model. The interphase volume content could be calculated based on the filling content of nano-fillers and the thickness of the interphase. The calculation is driven from a mathematical model based on a body-centered crystal lattice unit cell and the thickness of the interfacial area is i [67]. Figure 2.10 shows the results of calculated interphase volume in a silicone/ silica nanocomposite. It can be concluded that the maximum volume fraction of interphase exists for high interphase

thickness of 20 nm and 30nm and is determined by both the size of the nanofiller and the interphase thickness. But, when the interphase thickness is 10 nm and the diameter of the particle is 30 nm and 40nm, the interphase volume continuously increases as the filling content is increased and no maximum value occurs even up to 10 wt%. The highest enhancement of the resistance to high voltage arcing and the resistance to tracking and erosion is also in agreement with the high interphase volume. In this model, the effect of the nanoparticle size on the properties of nanocomposite is well explained. Moreover, the saturation effect on material properties observed in nanocomposite can also be well presented. However, the study of the properties of the interfaces is very limited in this model.

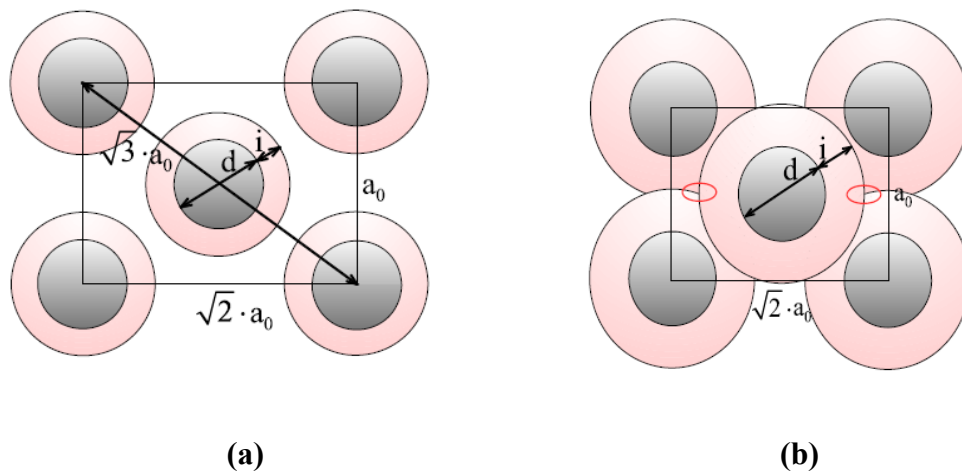


Figure 2.9 The Interphase volume model of nanocomposites (a) without overlap, (b) with overlap [67].

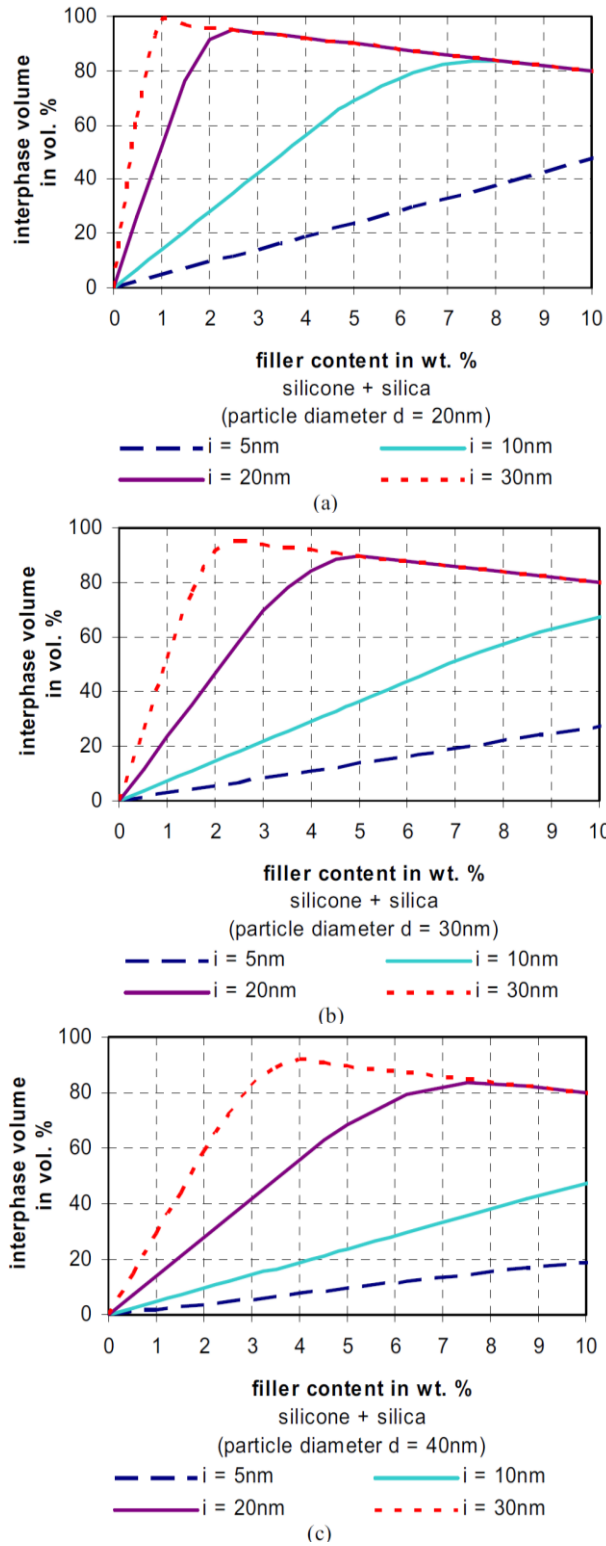


Figure 2.10 Interphase content according to the Interphase Volume Model for a silicone matrix with SiO₂ particles and interphase thicknesses i : (a) for a particle diameter $d = 20\text{ nm}$, (b) for a particle diameter $d = 30\text{ nm}$, (c) for a particle diameter $d = 40\text{ nm}$ [67].

2.4.3 Electrical Double Layer Model

Helmholtz proposed the electrical double layer model to describe the layers formed between a solid phase and a liquid phase. In his model, one phase must be mobile. In nanocomposite, the chains of the polymer can move slightly. Thereafter, the electrical double layer model for nanocomposite was then developed by T.J. Lewis [30], [64], which could be used to understand the interphase structure between the nanoparticles and the matrix polymer. When the nanoparticles are attached with the matrix material, the nanoparticle will be charged due to the absorption of the ions from the matrix material or the ionization of the surface groups. Then, an opposite charge atmosphere will be formed in the matrix material to shield the charged nanoparticles. This model involves two layers, a Stern layer (inner layer) and a diffuse Gouy-Chapman layer (outer layer). The Stern layer is the inner region where ions are strongly bound. The diffuse Gouy-Chapman layer is a diffuse region where the ions have higher mobility.

Figure 2.11 illustrates charge distribution in the diffuse electrical double layer when the nanoparticles are positively charged. The Stern layer consists of dipoles or adsorbed ions of opposite polarity and is of molecular thickness (about 1nm). It is closely attached to the nanoparticles due to the extremely strong electrostatic force produced by positively charged nanoparticles, as shown in

Figure 2.11 (a). In the diffuse layer, both positive charges and negative charges coexist and they are loosely distributed in this region. The thickness of the diffuse layer is

inversely proportional to the conductivity of the matrix material. If the polymer is weakly conductive, the thickness of the diffuse layer may be 10 nm or more [68]. The distribution of the resulting electrical potential across the interphase is shown in

Figure 2.11(b). The Stern potential is defined by the ions attached by the surface potential of the nanoparticles and has the same polarity as the Stern layer. It should be noted that the extremely high charge density in Stern layer results in a sharp drop of the electric potential. The electrical double layer model can be used as a part of the multi-core model, which is usually superimposed over the nanoparticles.

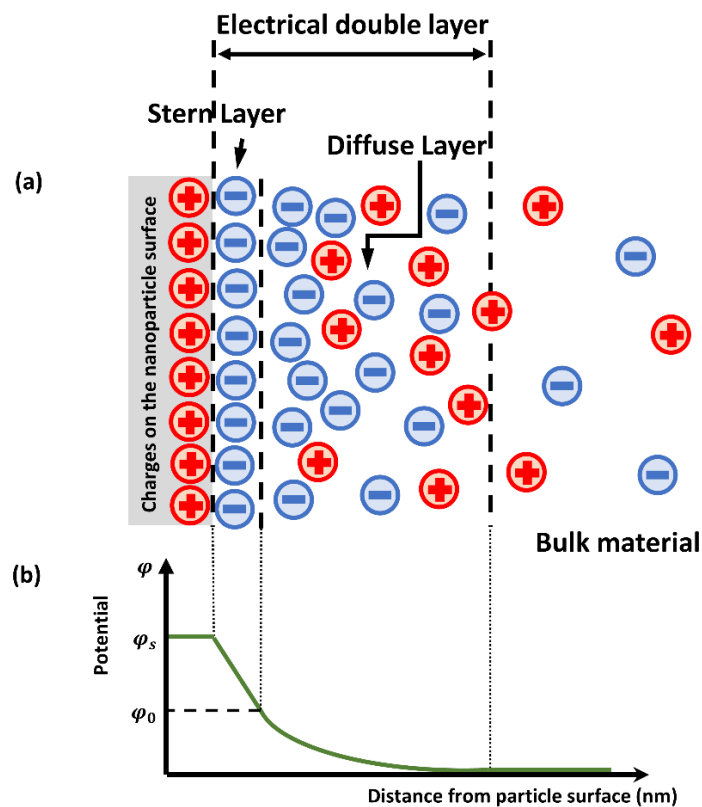


Figure 2.11 Electrical double layer model produced by a positively charge nanoparticle (a) the charge distribution, (b) the resulting electrical potential distribution.

2.4.4 Multi-core Model

The multi-core model, which is a simplified term of the multi-layered core model, is the one of most popular and recognized nanodielectric models. It was firstly proposed by T. Tanaka et al. to understand the various properties that the polymer nanocomposites display as electric insulation in 2005 [69]. Figure 2.12 shows the multi-core model for the specific case that a spherical inorganic nanoparticle is embedded into a matrix polymer. It consists of the following layers:

- 1) a bonded layer (first layer).
- 2) a bound layer (second layer).
- 3) a loose layer (third layer).
- 4) an electric double layer overlapping the above three layers.

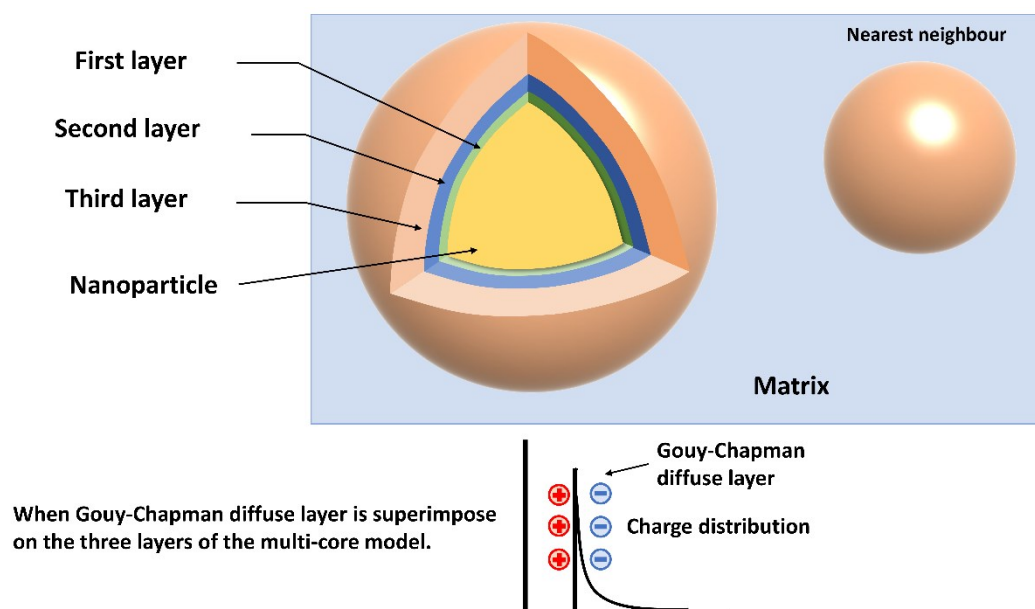


Figure 2.12 Multi-core model of nanocomposite (adapted from [69]).

The matrix material in this area is not influenced by the other layers and remains the same properties as the virgin matrix. The first layer is a transition layer tightly bonded to both the inorganic nanoparticle and the matrix polymer through chemical interaction such as covalent bond, ionic bond and hydrogen bond. The surface modification of nanoparticle by coupling agents such as silane is in this layer. The presumable thickness of the first layer is around 1 nm. The second layer is a bound layer consisting of a layer of polymer chains strongly bonded and/or interacted to the bonded layer and the nanoparticle. Hence, there is less freedom movement of polymer chains in this layer. The polymer chains or part of the chains are aligning perpendicular to the surface of the inorganic nanoparticle. The thickness of the second layer depends on the intensity of interaction between nanoparticle and matrix polymer and is between 2 and 9 nm. The third layer is a loose layer, which is loosely coupling and interacting with the bound layer due to its long distance to the nanoparticle and other layers. The chain mobility, chain formation, free volume and crystallinity of this layer are different from the polymer matrix. The thickness of the third layer can be several tens of nanometers. The multi-core model provides a basic physical explanation of the phenomena in nanocomposite, but it is too vague to predict the changes of macroscopic properties of nanocomposite.

Additional coulombic interaction is superimposed when the dielectric and electric insulation properties are examined. When a polymer matrix has mobile charge carriers, the nanoparticle is charged positively or negatively. The mobile charger carriers are

distributed in the interface in such a way that the counter charge carriers with opposite polarity are diffused outward from the contact surface to the Debye shielding length. [69], [70]. This is the formation process of the Gouy-Chapman diffused layer. The charge decays exponentially with distance according to the Born approximation. Debye shielding length is calculated as 30 nm for example. At this moment, the model of nanocomposite can be regarded as a superposition of both a multi-core model and an electrical double layer model. It is worth noting that the Gouy-Chapman diffuse layer may extend over the loose layer. When it happens, a far-field effect will lead to collaborative effect among neighboring nanoparticles. In multi-core model with the far-field effect, the macroscopic properties differ for materials with different thickness and interaction strength.

2.5 Breakdown of Solid Dielectrics

Solid insulation materials have been widely used in high voltage applications. Such materials include ceramic, insulating papers, polymeric materials and polymer nanocomposites. However, solid insulation material will lose its insulating properties if breakdown happens. The solid breakdown occurs when the applied electric field is sufficiently high enough that the acquired energy by the free charge carriers cannot entirely be dissipated by phonon-photon emission [71], [72]. The charge carrier emission at an electric field of varying intensity is normally through the field electron emission (Fowler and Nordheim emission) [71] and the field-enhanced thermionic

emission (Schottky emission) [72]. When the applied electric field is high enough, the concentration of free charge carriers increases rapidly due to electron avalanche, in which the charge carriers collide with and ionize nearby molecules. It results in a rapid increase in the electrical conductivity [73]. The possibility of streamer forming and propagating towards the breakdown point will be increased [74]. Once the breakdown channel is formed and filled with gas with low relative permittivity, the local electric field will be increased.

Several mechanisms have been proposed to explain the mechanism of solid breakdown activities. Such breakdown mechanisms include intrinsic breakdown, electro-mechanical, thermal breakdown, breakdown due to discharges and electro-chemical breakdown [75]–[77]. The breakdown of solid insulating materials is usually caused by the combination of multiple mechanisms rather than singly voltage application. Figure 2.13 shows the relationship between the breakdown mechanisms and the voltage-on time [75]. The breakdown of solid insulation can be divided into short-time breakdown and long-time breakdown based on the developing time of breakdown. The short-time breakdown strength, representing the strength of a material, is usually obtained within a short period of time (usually less than 10^{-3} s) when a testing voltage across the material is rising at a constant rate or in steps. The long-time breakdown reflects the partial discharge properties and the ageing resistance properties of a material and can be determined through partial discharge tests and treeing tests. The measured breakdown strength of long-time could be evidentially lower than the intrinsic breakdown.

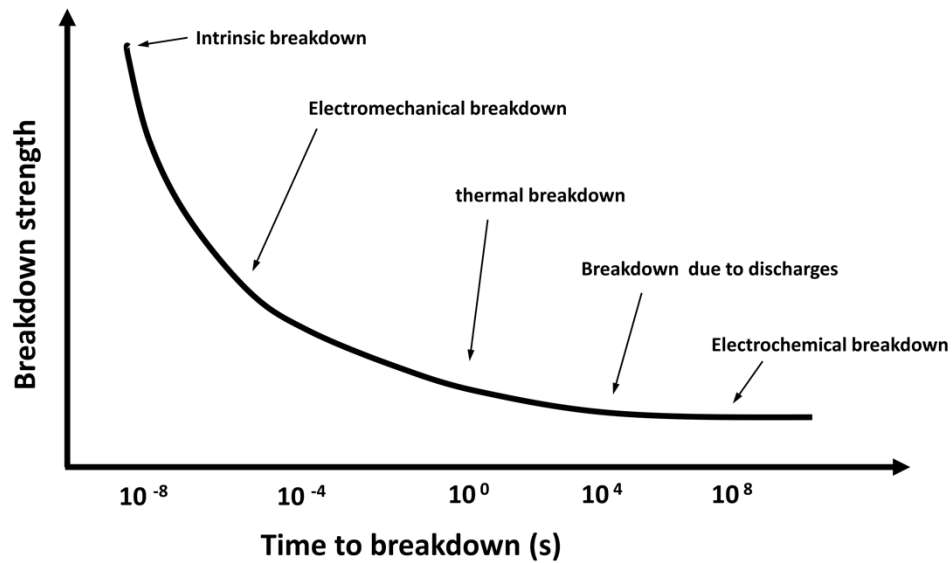


Figure 2.13 Sketches of the relationship between breakdown strength and time-to-breakdown for different breakdown mechanisms in solid insulation (adapted from [75]).

The intrinsic breakdown, also named the electronic breakdown, defines the maximum breakdown strength of solid insulation material. It is only determined by the material property and can occur without other breakdown mechanisms [78]. The intrinsic breakdown theory for solid is developed based on the knowledge of avalanche processes in gases. Under a high electric field, the inherent electrons inside the insulating material acquire energy through collisions, causing the electronic or avalanche breakdown. However, the strength of this type of breakdown is hard to measure as a consequence of the non-homogeneous nature of solid insulating material and the imperfect testing environment. Experimentally, the intrinsic breakdown

strength can only be obtained under the best experimental conditions.

Electromechanical breakdown occurs when the electrostatic compressive force of insulating material at an electric field of high intensity becomes higher than its mechanical compressive strength. As reported by Stark and Garton [79], the equilibrium between the electrostatic compressive forces and the mechanical compressive strength before the electromechanical breakdown appears could be described by:

$$\frac{\varepsilon_0 \varepsilon_r V^2}{2d^2} = Y \ln(d_0 / d) \quad (2.1)$$

Where ε_0 is the vacuum permittivity, ε_r is the relative permittivity of the insulating material, Y is the Young modulus, d_0 is the initial thickness of the material and d is the thickness after voltage V is applied across the material. It should be noted that the calculated breakdown strength based on this model is higher than the real breakdown strength of the solid material.

Thermal breakdown often occurs when the cumulative joule heating in a material cannot be effectively dissipated at a high electric field. As a result, the rapidly increased temperature of the material increases the conductivity of the material, resulting in thermal instability and breakdown. For example, the thermal breakdown temperature of polyethylene is around 250-350°C, while for polypropylene it is around 340-400°C.

The discharges in the solids may appear internally or externally of material in short-term and long-term electric tests. Internal discharges are localized discharges that occur

within the bulk of a solid insulation at the defects, such as voids and impurities. The partial discharge would then result in the accumulation of space charge and the development of electrical treeing, leading to the eventual breakdown. In the case of external discharges, the breakdown may occur outside the boundary of electrodes as the discharges occur in the surrounding medium of the insulating material [75]. The previous research has indicated that the partial discharges and space charge plays an important role in the long-term electrical degradation and breakdown [43], [80]–[84].

Electrochemical breakdown of solid insulating material occurs when chemical changes such as oxidation, hydrolysis and other chemical actions are developed under continuous electric field. These chemical deteriorations increase as the temperature rises. Therefore, the operation of solids at high temperature should be avoided.

The breakdown strength is one of the most vital parameters to evaluate the insulating properties of a material. The breakdown processes often occur in combination rather than singly on solid insulation. A number of studies have examined the breakdown performance of polymer nanocomposites [43] [55], [85], [86], but the breakdown mechanism of nanocomposites is still not fully clear now.

2.6 Space Charge

2.6.1 Overview of Space Charge

Space charge refers to the net charges accumulated in the bulk of insulating material at some point in time and is mainly from the electrode injection and ionization of impurities in insulating material. The developed charges would then migrate in the bulk of the material over time [87], [88]. The charge injection are mainly affected by the work function of the electrode material and the interface between the electrode and the testing sample [77]. Details on this will be further explained in Chapter 8. When the applied electric field is higher than the charge injection threshold, homo charges from the electrodes will be injected into the material through the interfaces. According to [89], [90], the space charge injection threshold for polyethylene-based materials is usually between 10 kV/mm and 20 kV/mm. The ionization of impurities is attributed to the ionization of polar groups such as additives, impurities and cross-linking byproducts introduced during the manufacturing process, resulting in the development of space charges.

Early papers about space charge were published by Child [91] and Langmuir [92] at the beginning of the 20th century. Space charge plays a valuable role in affecting the electrical properties and lifetime of polymeric insulation, which limits the development of polymeric HVDC cable insulation. Such electrical properties include the breakdown, conduction and ageing performance [3], [93]–[96]. The phenomenon of space charge

packet has been firstly reported in polymeric insulation by Hozumi et al. in 1994 [97]. Then, it has been proved that the space charge packet effect can seriously distort the local electrical field, resulting in the early failure of insulation material [12], [99], [92]. In recent years, many attempts have been made to suppress the space charge accumulation in polymeric insulation from two aspects: modification of the property of the electrode-polymer interfaces and modification of bulk polymer material. To suppress the charges injected from the electrode, an additional layer such as polyvinyl fluoride (PVF) [100] polyethylene terephthalate (PET) [101] or fluorinated ethylene propylene copolymer (FEP) [102], is placed between the electrode and the polymeric material. This is due to the high electronegativity and high dielectric constant of these material. Moreover, there are two main methods to modify bulk polymer material. One way to alter the properties of the bulk polymer is to introduce organic and inorganic additives or fillers into polymer [11], [103]. Another way is to blend polymer with another polymer [104], [105]. Among all these methods, polymer nanocomposite with the addition of inorganic nanoparticles has been proved to be an effective way in space charge suppression. It is believed that the space charge accumulation and transportation at the interfaces such as polymer/ nanoparticles interface and nanocomposite/ electrode interface affect the electrical properties and lifetime of polymer insulation. However, the mechanism of the interface effect on the space charge formation and accumulation in nanocomposite is still not clear yet.

2.6.2 Space Charge Measuring Techniques

As stated above, space charge has a significant influence on the electrical properties of polymeric HVDC cable insulation. It is of great importance to accurately measure the injection, migration and dissipation processes of space charge. In the early 1970s, the distribution of space charge in polymers was identified by using destructive methods such as the dust figure method and the field probe method, which were used to study the space charge in the thick samples and cable sections [106], [107]. However, the execution and interpretation of destructive methods are very complicated. From the late 1970s, many nondestructive methods for characterizing the space charge in dielectric materials were developed. These methods have been detailed reviewed and summarize by Ahmed and Srinivas [108]. Another important review published by Khalil [109] found that only some of the methods mentioned in [108] would be suitable for characterizing space charge in polymeric material used as HVDC cable insulation. They are the thermal pulse method (TP), the thermal step method (TSM), the laser intensity modulation method (LIMM), the pressure wave pulse method (PWP), the laser-induced pressure pulse method (LIPP), and the pulsed electroacoustic method (PEA). The TP, TSM and LIMM are categorized as thermal methods. The PWP, LIPP and PEA are categorized as wave propagation methods. The space charge distribution in dielectric samples is obtained by analyzing the current or voltage signals caused by thermal, mechanical or electrical disturbances.

The thermal pulse method was firstly developed by Collins [110]. A thermal pulse is applied on the metal electrode of the polymeric dielectric and the heat is then transferred and diffused in the sample, resulting in the small movement of space charge. The generated electric response is recorded as a function of time to analysis the space charge distribution through necessary deconvolution calculation. TP method can be used to capture the space charge characteristics in thin film samples and cables.

The PWP method was proposed by Anderson and Kurtz [111]. It is based on the propagation of a pressure wave inside the sample. When the pressure wave travels to the space charges, the charges move and lead to the change of surface charge on the electrodes. The displacement current is then measured to acquire the charge distribution in the sample.

The PEA method proposed by T. Takada [112] has become the most widely used method for space charge measurement in solid insulation materials as it is believed to be the most reliable nondestructive method for the samples at high electric fields. An external electrical pulse is applied to the dielectric sample, perturbing the space charge within the sample. The movement of the charges generates an acoustic wave, which could be detected by a piezoelectric transducer attached to the electrode. The acoustic signal is then converted into the voltage signal containing the space charge information. After appropriate signal processing, the space charge distribution within the sample can be restored. More details about the PEA technique will be described in Chapter 3 and 7.

2.7 Summary

In this chapter, the general chemical structure and properties of polyethylene and polypropylene has been introduced. In addition, the history and fundamentals of nanocomposites insulation materials are also briefly reviewed and four popular theoretical nanocomposite models are reviewed and discussed. Based on this, it is concluded that the large interfacial region between nanoparticles and the base material plays a significant role in determining the changes of dielectric properties in nanocomposites. Therefore, when designing new nanocomposite insulation systems, it is essential to consider the dispersion of nanoparticles and how to reduce their agglomeration. The chapter also reviews the fundamentals of breakdown in solid dielectrics and space charge measurement methods, with the PEA method being a popular choice. Despite the advancements in improving the dielectric properties of nanocomposite materials, it is still unclear whether this improvement is induced by the nature of the nanoparticle or the surface treatment of nanoparticles. The literature review presented in this chapter has shown a potential link between space charge injection and electrical strength of nanocomposite. In this project, PE and PP nanocomposites with different surface conditions and filling content were prepared and investigated to evaluate the DC electrical performance of proposed nanocomposite insulation.

Chapter 3 Material and Experimental Techniques

3.1 Introduction

Polymeric composite materials are widely used in the aviation industry, packaging industry and power industry. With the emphasis on environmental problems, more attention has been drawn to recyclable polymers. Thermoset polymer is gradually losing ground to the thermoplastic polymer in cable insulation as they are more difficult to recycle than thermoplastics due to their cross-linked molecular structure [9] [14] [99].

In this chapter, materials employed for this study are introduced. Moreover, the surface modification method for nanoparticles and sample manufacturing method is described.

To ensure the quality and reproducibility of the testing results, how the samples are prepared should be well controlled. The quality of the sample might be affected by many factors such as moulding pressure, mixing time and mixing temperature. As there is no standard method in the literature, some trials have been made. The challenges that occurred during the sample preparation are also discussed. The manufacture of nanocomposite samples is introduced. Also, the surface modification of nanoparticles is described. The nanocomposite material is prepared using the melt-blending method and then the thin film samples used for testing are made by the hot pressing method. In the end, chemical, mechanical and electrical testing set-ups for nanocomposite material characterization are introduced.

3.2 Materials

3.2.1 Materials for this study

The polymers employed as the base material in this study were polyethylene and polypropylene. The additive-free linear low-density polyethylene (LLDPELL4004EL) pellets, with a melt flow of 3.6 g/10 min, a density of 0.924 g/cm³ and a melting point of 122 °C, were purchased from ExxonMobil, referred to as PE in this study. The polypropylene (PP5722E1) pellets, with a melt flow of 4 g/10min and a density of 0.900 g/cm³, were also obtained from ExxonMobil, referred to as PP in this study.

The nano alumina particles owns high dielectric constant, high thermal stability and high mechanical strength, which make it a popular nanoparticle material in nanodielectric applications. In addition, it can also achieve good dispersion within polymer matrices, which results in improved electrical and mechanical properties of the resulting nanocomposites[113]. The use of nano-alumina as filler to improve the electrical properties in nanodielectric has been reported by many researchers in recent years [11], [46], [50], [114]–[117]. The nanoparticle used in this study is alumina (Al₂O₃) nanopowder (A119402), obtained from Aladdin Industrial Inc., China with a quoted average diameter of 30 ±10 nm. The size distribution was not measured in the lab before this study. It is referred to as unmodified/untreated nano-alumina in this study.

To conduct surface treatment for nanoparticles, γ -methacryloxypropyltrimethoxysilane (KH570), purchased from Sinopharm Chemical Reagent Co. Ltd, was used to modify

the surface of nano-alumina particles. The methoxy groups of the KH570 hydrolyse to hydroxyl groups (silanol) that can condense with the hydroxyl groups on the surface of nano-alumina particles to form covalent bonds. Then the KH570 coupling agent wraps up the nano-alumina particles and a monomolecular layer is formed outside the surface of the nanoparticles. The chemical structure of KH570 is shown in Figure 3.1(a). The nanofiller is referred to as pure nano- Al_2O_3 . The nanoparticles with surface modification are referred to as KH570- Al_2O_3 in this thesis. The xylene solution in chemically pure grade was also purchased from Aladdin Industrial Inc. The procedures of nanocomposite thin film preparation are shown in Figure 3.2 and the details of each step are described in the following sections.

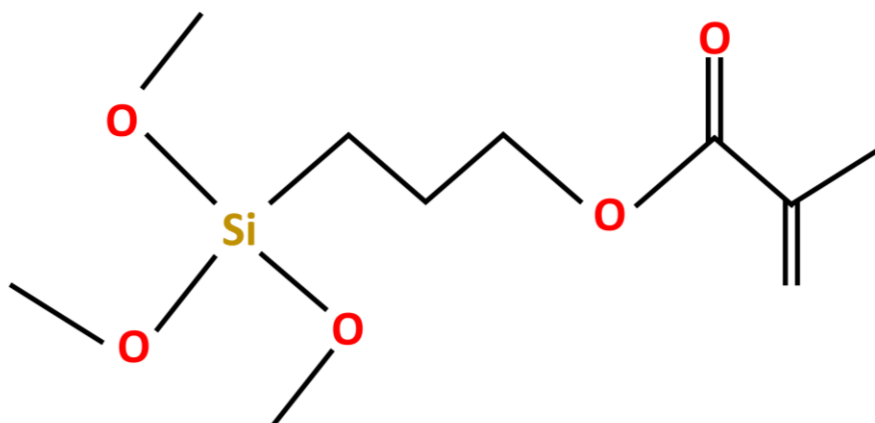


Figure 3.1 Chemical structure of KH570 silane coupling agent.

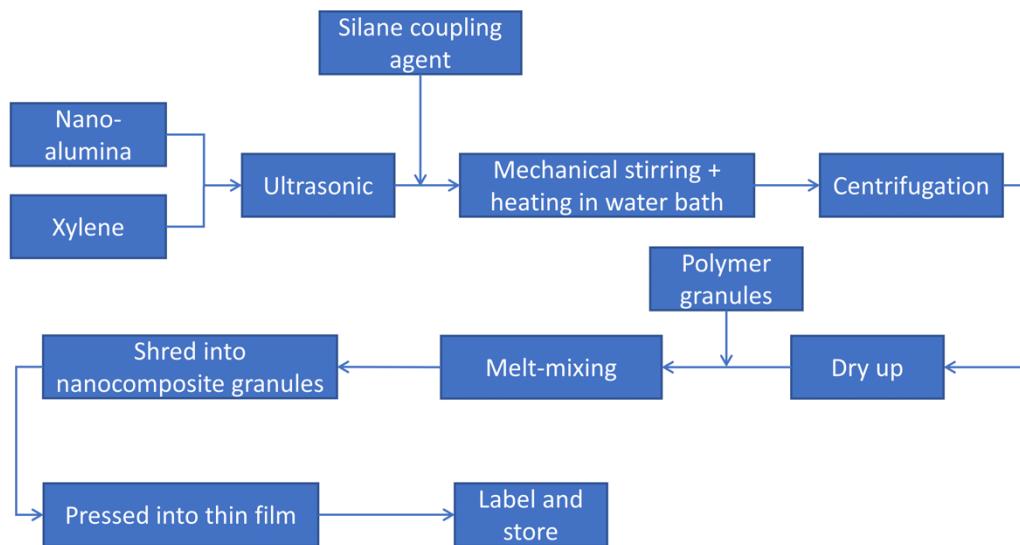


Figure 3.2 Procedures of nanocomposite sample preparation.

3.2.2 Surface Treatment of Nano-alumina

The surface treatment of nano- Al_2O_3 particles was completed with the help of silane coupling agents. After a few trials in the laboratory and reference to published works [41], [47], [59], [62], the formula and production procedures of nanocomposites used in this project are determined. The procedures of nanocomposite thin film preparation are shown in Figure 3.2 and Figure 3.4 shows the reactions between KH570 silane coupling agent and nano-alumina particle. 10 g of nano-alumina particles was firstly weighed by using an electronic scale and then was dried in a vacuum oven at 100 °C for 24 hours. Then the nanoparticles were put into a beaker and 100 ml xylene solution was added as well. The next step was stirring the mixture by ultrasonic mixing for 60 minutes to disperse the nanoparticles in the solution evenly. After that, the mixture was

transferred into a three-neck flask, which was connected with a mechanical stirrer and a condenser, before 10 ml of KH570 coupling agent was added. A condenser was connected with water cooling equipment to cool the evaporated mixture. Then another 150 ml xylene and weighted coupling agent were slowly added into the flask. The mixture was refluxed in an oil bath at 80 °C for 12 hours with the mechanical stirrer was set at 60 rpm. Prior to centrifugation at 6000 rpm for 6 min, the resulting mixture was equally divided into 13-14 test tubes. After removing the supernatant, each test tube was filled with pure xylene to conduct double centrifugation to remove the extra coupling agent. Lastly, precipitation was collected and placed in the vacuum oven at 80 °C until dried. The dry modified nanoparticle powder was then ground, labeled and stored in new test tubes. Figure 3.3 shows the resultant nanoparticle powders.



Figure 3.3 Nanoparticle powders with and without surface modification.

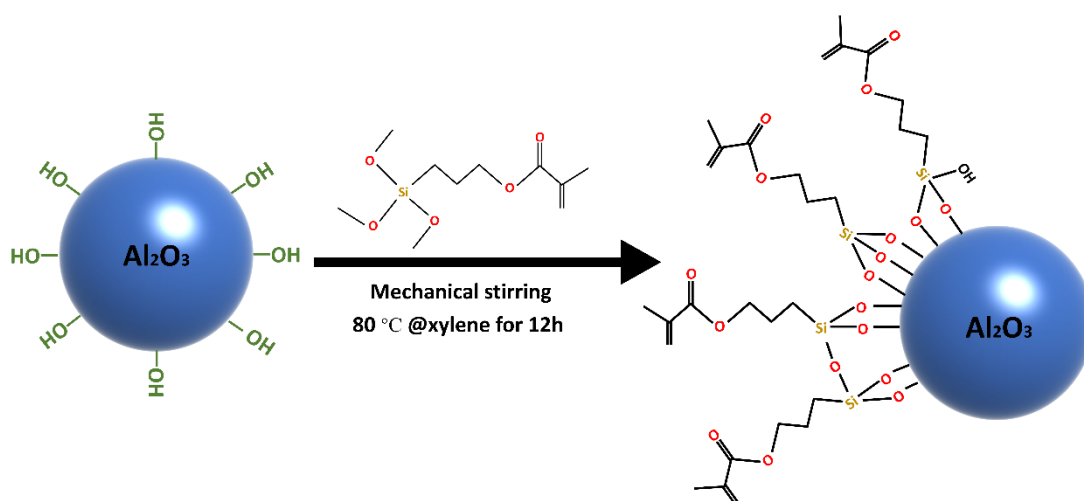


Figure 3.4 Schematic of the reactions between the KH570 silane coupling agent and the nano-alumina particle.

3.2.3 Mixing and casting of nanocomposites.

In this study, both PE and PP nanocomposite samples were manufactured by using the melt-blending method. At the very beginning of the experimental work, a PRISM extruder from the Pure & Applied Chemistry Department, University of Strathclyde, was employed to make the composite in the form of an extruded lace. The amount of the coupling agent to be added is expressed in parts per hundred resin/rubber (phr). Phr provides the quality of additives per 100 units of the matrix polymer. In this study, 1 phr means 1 unit of nano-alumina particles is added into 100 units of the matrix polymer. For example, to make PE/ nano- Al_2O_3 @1phr composite 100 g PE powder/granules and 1 g nano-alumina powder were gradually added into the extruder chamber. The virgin PE was in powder as we thought the nanoparticles could achieve a better distribution

in powder rather than in granules.

The next step was to cut the composite wires into small granules and press the granules into thin film samples using a hot-pressing machine. To control the thickness of thin film samples, which is different for different tests, a 10 cm × 10 cm three-layer stainless steel mould set, shown in Figure 3.5, was made by the departmental mechanical workshop. Middle layers with varying thicknesses were used to control nanocomposite film samples with required specifications.

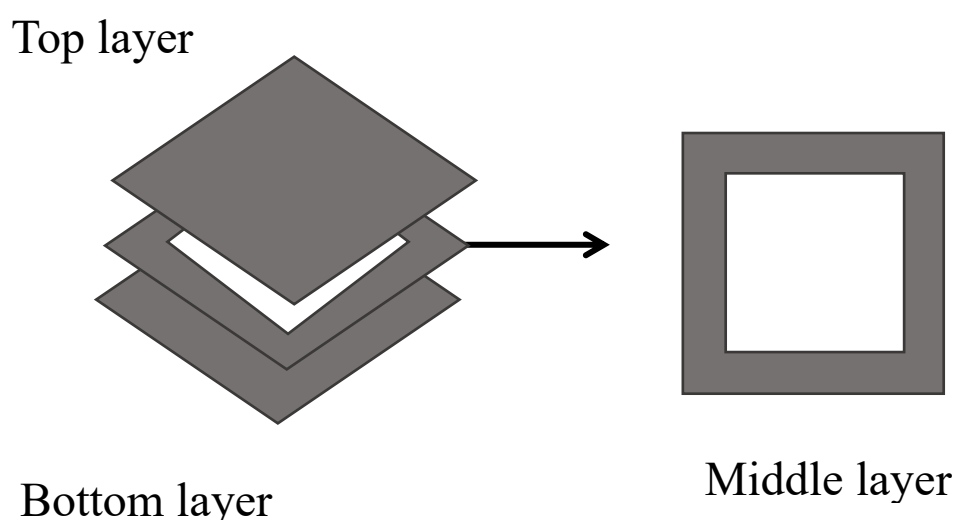


Figure 3.5 Design of three-layer thin film mould.

To prevent the sample from sticking to the mould, two thin foil films were placed on both sides of the middle layer. The final products are shown in Figure 3.6. Unfortunately, the quality of the first few batches of samples was proven to be poor. There were few problems raised under the current laboratory condition. Firstly, it was hard to separate

the foil film from the sample surface area, which will make the sample partly conductive. Secondly, the hot press machine in this laboratory was a manual-controlled one which was hard to maintain the pressure added on the mould and degassing the sample. Thirdly, as the extruder was lack of maintenance, the high operating temperature would result in an extra burden for the whole extruding system and often led to the breakdown of the extrusion machine. Lastly, the dispersion state of nanoparticles within the base material was poor. The agglomeration can be found macroscopically.



Figure 3.6 Thin film samples produced by using a press machine.

To improve the quality of the testing samples, a visiting researcher arrangement was made with Professor Jinliang He of the High Voltage Laboratory, Tsinghua University, Beijing, China, to continue the experimental investigation there. Unlike the previous situation, a HAPRO RM-200C torque rheometer was used to mix the composites. The speed ratio of two rollers in the mixing chamber was set as 1: 1.25, as shown in Figure

3.7. Prior to the melt-blending, virgin PE granules, untreated nano-alumina and surfaced-treated nano-alumina were dried in a vacuum oven at 100 °C for 12 hours. The rotation speed of the RM-200C torque rheometer was set at 60 rpm. The melt-blending for PE nanocomposites was conducted at 170 °C. All different kinds of samples were listed in Table 3.1 below. As for PP and its composites, the melt-blending temperature was set at 190 °C [118]. Pure PE granules were processed at the same condition without any additive as the reference batch.

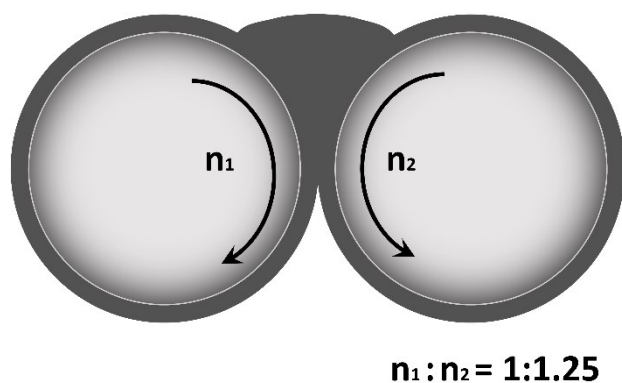


Figure 3.7 Speed setting for torque rheometer.

Table 3.1 Nanocomposite samples.

Name	Matrix (g)	Nano-Al ₂ O ₃ (g)	Silane Coupling Agent
PE	50	0	None
PE/Al ₂ O ₃ -Pure@0.5phr	50	0.25	None
PE /Al ₂ O ₃ -Pure@1phr	50	0.5	None
PE /Al ₂ O ₃ -Pure@2phr	50	1	None
PE /Al ₂ O ₃ -Pure@5phr	50	2.5	None
PE/Al ₂ O ₃ -KH570@0.5phr	50	0.25	KH570
PE/Al ₂ O ₃ -KH570@1phr	50	0.5	KH570
PE/Al ₂ O ₃ -KH570@2phr	50	1	KH570
PE/Al ₂ O ₃ -KH570@5phr	50	2.5	KH570
PP	50	0	None
PP /Al ₂ O ₃ -Pure@0.5phr	50	2.5	None
PP /Al ₂ O ₃ -Pure@1phr	50	0.15	None
PP /Al ₂ O ₃ -Pure@2phr	50	0.25	None
PP /Al ₂ O ₃ -Pure@5phr	50	0.35	None
PP /Al ₂ O ₃ -KH570@0.5phr	50	0.25	KH570
PP /Al ₂ O ₃ -KH570@1phr	50	0.5	KH570
PP /Al ₂ O ₃ -KH570@2phr	50	1	KH570
PP /Al ₂ O ₃ -KH570@5phr	50	2.5	KH570

The next step was to press the composite granules into thin film samples with a thickness of 100 μm , 200 μm , 500 μm and 1 mm by compression moulding under 15 MPa at 200 °C. Polyimide (PI) film was used instead of foil film between the middle layer and the other layers in the three-layered mould due to its high temperature

resistance. The films were then annealed to room temperature by circulating water while the compression mould was still maintained at a pressure of 15 MPa. Finally, all the samples were labeled and stored in a dry and clean place. Before each test, the film samples were put in a vacuum oven at 100 °C for 12 hours to remove the moisture from the sample surface. The final products were displayed in Figure 3.8. Reference samples and PP/nano-alumina composite samples were manufactured in the same way as PE composite sample. The morphology and physical chemistry study of nanocomposite samples will be discussed in Chapter 4.

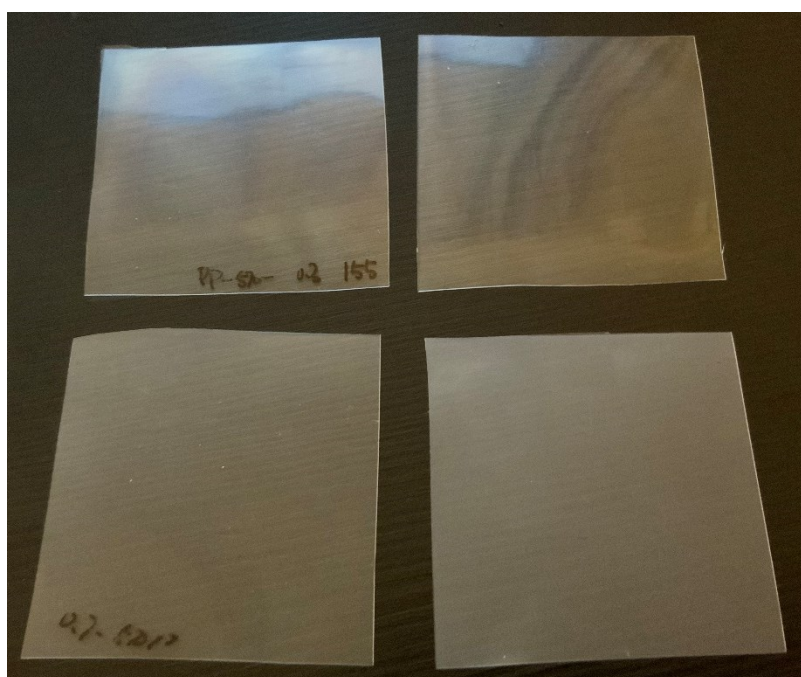


Figure 3.8 The thin film nanocomposite samples produced using the melt-blending method.

3.3 Experimental Techniques

3.3.1 Thermal-gravimetric Analysis

TGA is employed to measure the mass changes of samples during heating by using a TA Q500 instrument, TA Instruments, USA. The nanoparticle samples are pretreated in a vacuum oven at 100 °C for 12 h to remove the moisture content before test. 5 mg of nano-powder is placed in a weighting plate and then is heated with a heating rate of 10 °C/min until 800 °C under the atmosphere of nitrogen. The change of mass is recorded along with time. In this study, untreated nano-Al₂O₃ and KH570-treated nano-Al₂O₃ are tested separately to study the effect of surface modification on nano-alumina.

3.3.2 Fourier-transform Infrared Spectroscopy

Until today, infrared spectroscopy is still a popular technique in polymer science. When infrared radiation is injected into a sample, some of the radiation that corresponds to its vibration frequency will be absorbed by the tested sample, while the others will be transmitted. As a result, the relationship between infrared radiation absorption and the frequency of infrared photons is acquired by the infrared spectrometer, which can produce an infrared spectrum. Usually, the whole spectrum covers a range between 10 cm⁻¹ and 12820 cm⁻¹. It could be divided into three regions according to their relationship with visible spectrum: near-, mid- and far-infrared, which is covering about 14000–4000 cm⁻¹, 4000–400 cm⁻¹ and 400–10 cm⁻¹ respectively. From the obtained spectrum, molecules in the tested sample will be identified by matching the absorption

frequency/wavelength to those already known in the database.

In order to study the effect of surface treatment on the chemical structure of nano-alumina particles, FTIR technique is used to study the vibrational response of molecules. In this research, the testing equipment is Thermo Fisher Nicolet iS10, USA. The sample used in this research is nanoparticle powders. Spectrum data of pure nano- Al_2O_3 and KH570-treated nano- Al_2O_3 powder are obtained over the range from 400 cm^{-1} to 4000 cm^{-1} with a resolution of 2 cm^{-1} .

3.3.3 Differential Scanning Calorimetry

Differential scanning calorimetry test is conducted by a TA Q2000 instrument to identify the thermal behavior of the samples through measure the difference of heat flow between reference sample and testing sample over time. Then, the change of enthalpy can be calculated based on the measurement.

For each individual test, a 4-5 mg weighted nanocomposite sample is prepared and enclosed in a set of aluminum pan. The device should be warmed up at least 40 min prior to any test and the whole test should be done under a nitrogen atmosphere. The non-isothermal melt-crystallization testing procedures of polymer are shown in Figure 3.9. The purpose of removing thermal history is to eliminate the ordered structure of the sample and minimize the effect of the external environment on its melting and crystallization behavior. After the test, crystallinity and melting enthalpy are calculated based on the recorded curves. Both PE and PP are semicrystalline polymers, so they

have a combination of crystalline region and amorphous region. The crystalline characteristic of polymers may affect their mechanical properties, space charge dynamics and breakdown behavior.

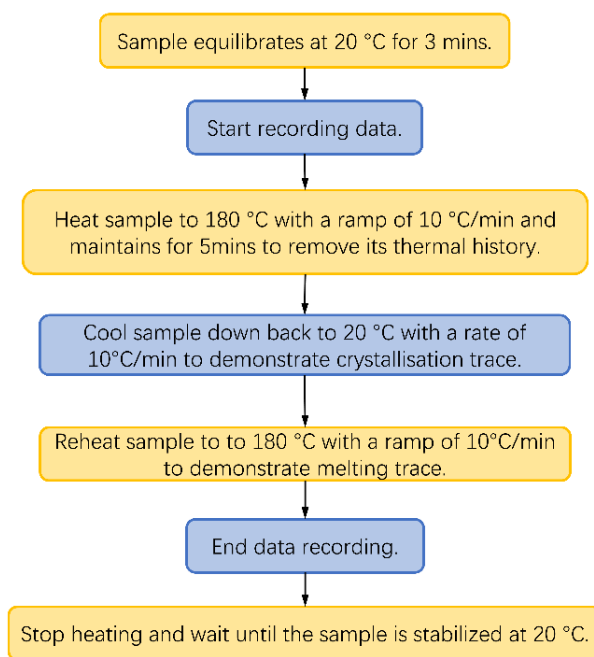


Figure 3.9 Procedures of DSC test for PE and PP.

3.3.4 Polarized Optical Microscopy

Polarized optical microscopy is widely selected in investigating the crystal morphology of the material. In this study, a Nikon Eclipse LV100 NPOL microscope equipped with a Linkam LTS420 hot stage is used. In the beginning, the light is injected through the polarizer and it becomes plane polarized light. Then it reaches the sample and generates two wave components at a right angle to each other. On the other side of the sample, when an analyzer with constructive and destructive interference receives these two waves with different phases, extinction occurs and the unique black cross pattern of

spherulites, called Maltase cross, appears. The hot stage is employed to complete the isothermal crystallization of the polymeric sample. The sample preparation method for the POM test is shown in Figure 3.10. The experimental procedures for PP nanocomposites are detailed in Figure 3.11. For PE nanocomposite samples, the procedures are the same except the crystallization temperature was set at 110 °C.



Figure 3.10 Samples for POM test.

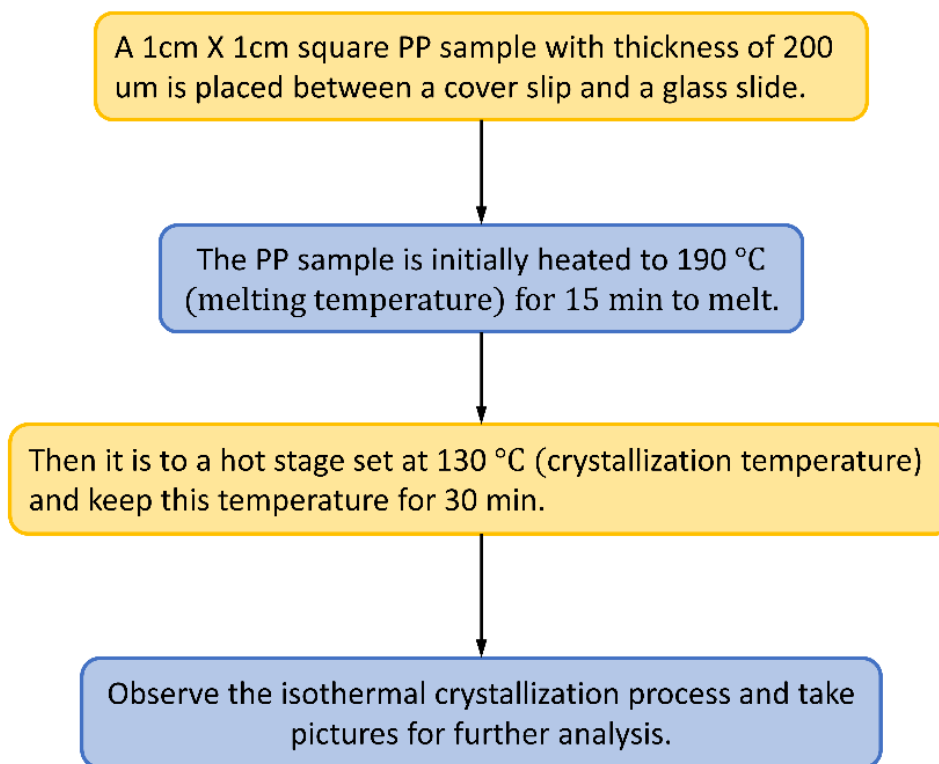


Figure 3.11 Procedures of POM observation of PP nanocomposite sample.

3.3.5 Scanning Electron Microscopy

To study the morphology of the sample and distribution of nanoparticles within base material, a Hitachi SU8010 scanning electron microscopy instrument was employed. A 10 kV accelerated voltage was used. Before observation, the sample with 1 mm thickness was put in liquid nitrogen before broke off. Then the fractured cross-sections were sputtered with gold to avoid charge accumulation under high voltage. To conducting the gold coating, an ETD-2000M coating machine connected with a vacuum pump was used. The coating process lasted for 60 seconds at 40 mA for each sample.

3.3.6 Dielectric spectroscopy

The dielectric performance was evaluated by using a Novolcontrol GmbH Concept 40 broadband dielectric system equipped with an Alpha-A high-performance frequency analyser, Germany. Figure 3.12 shows a simplified circuit schematic for dielectric spectroscopy measurement and the structure of the sample holder is shown in Figure 3.13. The sample with a thickness of $100 \pm 10 \mu\text{m}$ is cut into $5 \text{ cm} \times 5 \text{ cm}$ square sheet. Before testing, round gold electrodes with a diameter of 2 cm are sputtered on both sides of the film sample to guarantee good conduction between the sample and electrodes. The sample is then placed between a pair of 20 mm electrodes and applied with a 1 V AC voltage. The measurement is made over a wide frequency range from 10^{-1} Hz to 10^6 Hz at $30 \text{ }^\circ\text{C}$. For each kind of sample, tests are repeated three times to calculate its permittivity and loss tangent.

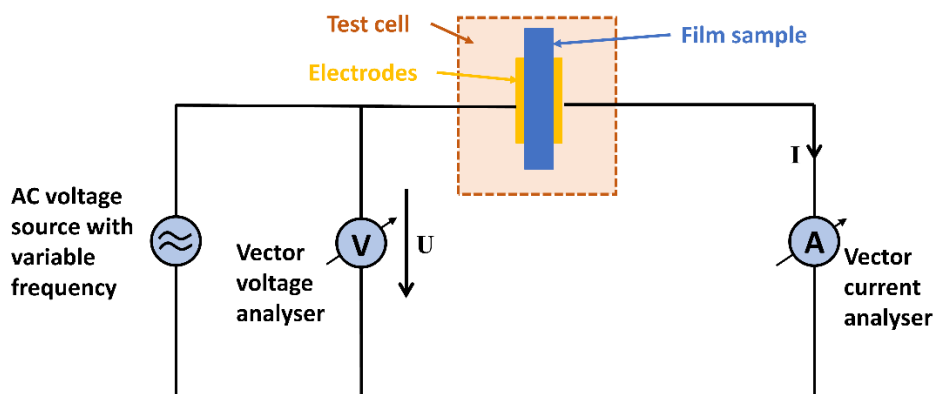


Figure 3.12 Schematics of the dielectric spectroscopy system.

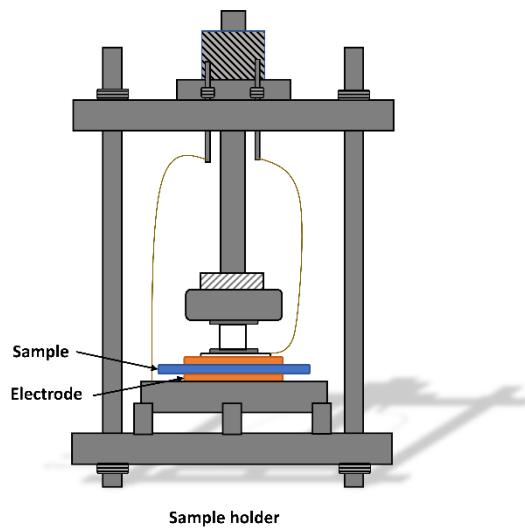


Figure 3.13 Structure of the sample holder for dielectric spectroscopy.

3.3.7 Electrical Breakdown Test

In this study, only DC breakdown strength is carried out for all the nanocomposites. The samples are synthesis using the same method that was detailed for the dielectric spectroscopy test. The whole test is designed according to IEC 60243 and the schematic setup of DC breakdown test is shown in Figure 3.14. A dielectric strength tester (Z-VI, Suzhou Industrial Park HaiWo Technology Co., LTD. China) is used as DC power supply and a pair of 10 mm stainless steel balls is employed as electrodes. The film sample is placed between electrodes and immersed in silicone oil to avoid flashover. The whole test is conducted at room temperature and the testing voltage is raising with a rate of 1 kV/s. For each sample, 20 points are examined and data are recorded for further analysis.

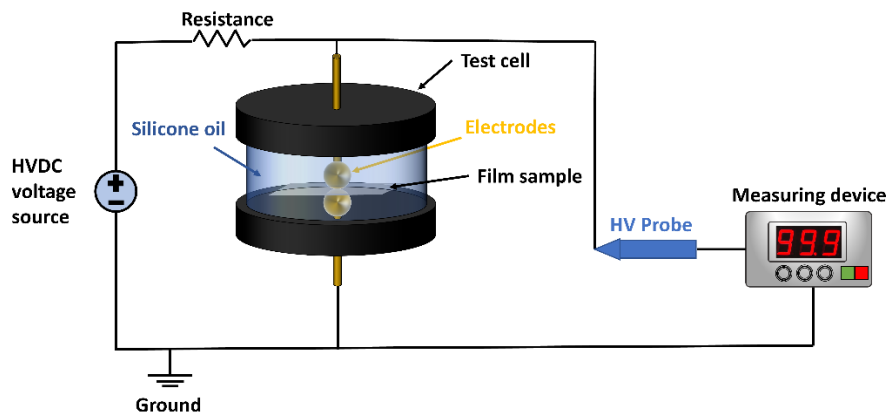


Figure 3.14 Schematics of the DC breakdown test system.

3.3.8 DC Electrical conductivity Measurement

The leakage current of samples is measured by a Keithley 2635B electrometer with a standard three-electrode system, as shown in Figure 3.15. The guard electrode is used to keep the surface current from passing through the measuring instrument and to make the electric field under the measuring electrode evenly distributed. The thickness of the thin film testing sample is about 100 μm and both sides of the sample are sputtered with gold for conduction. Before each test, the sample is short-circuited in the vacuum oven at 80 $^{\circ}\text{C}$ for 24 hr to remove internal charges and absorbed moisture. The electrodes are fixed in an oven so that the testing temperature is precisely controlled within ± 1 $^{\circ}\text{C}$. The DC voltage is supplied by a Keithley 2290-10 power source to provide a stepped electric field from 5 kV/mm to 60 kV/mm with a step of 5 kV/mm. At each electric field, the current is measured as a function of time. For each kind of

sample, three specimens are tested and only one typical result from each group of samples was selected for conductivity calculation.

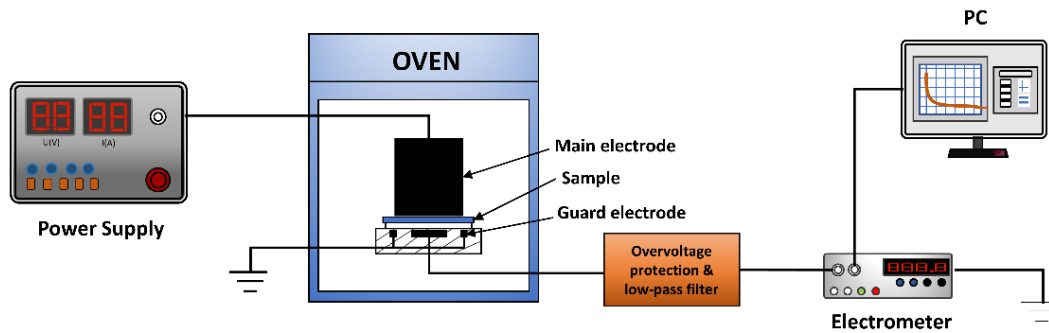


Figure 3.15 Schematics of the leakage current measurement system.

3.3.9 Thermally Stimulated Current Measurement

To study the trap information of nanocomposites, thermally stimulated depolarization current (TSDC) method [119] is employed. The schematics of the TSDC measurement system are shown in Figure 3.16. The temperature control system of this test is realised by using the Novocontrol Concept 40 system and the current measurement is conducted by using a Keithley 6517B electrometer. The requirement for samples used for the TSDC test is the same as dielectric spectroscopy. The process of the whole TSDC test is shown in Figure 3.17. The test temperature range for PE nanocomposites is from -80 °C to 80 °C and it is from -80 °C to 100 °C for PP nanocomposites.

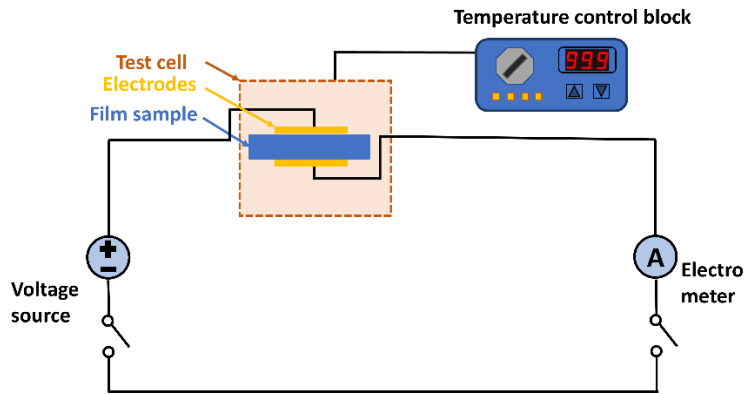


Figure 3.16 Schematics of TSDC measurement system.

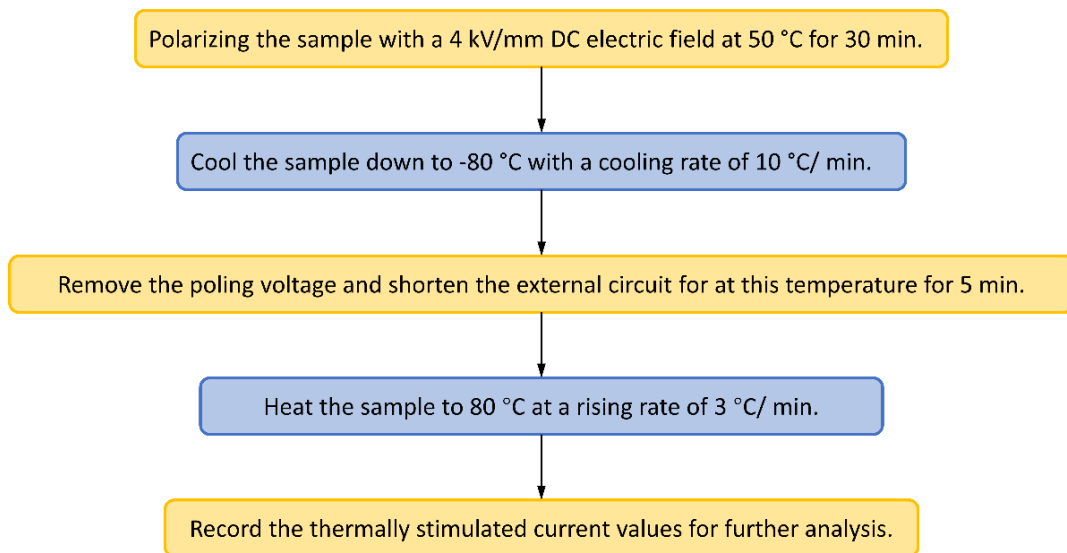


Figure 3.17 Procedures of TSDC test for PE nanocomposites

3.3.10 Space charge Measurement

The space charge behaviour is studied by using the pulsed electro-acoustic method.

Figure 3.18 schematically displays the PEA system, which includes a PEA test unit, a

PC unit, a temperature controller, a voltage amplifier, a waveform generator, an impulse

generator and an oscilloscope. A 500-pF capacitor sealed by epoxy resin with high temperature resistance is used as part of the upper electrode of the PEA unit and it can withstand 30 kV voltage at 150 °C. The waveform generator is Tektronix 3000C. The impulse generator is AVTECH AVG-4B-C, Canada. An 800 V impulse signal with 6 ns width and 10 kHz frequency is generated and then transmitted to the sample. The oscilloscope is Lecroy WaveRunner 610Zi with a 1 GHz bandwidth and 2.5 GHz sampling rate. The transducer in this test is a 9 μm Polyvinylidene fluoride (PVDF) piezoelectric film connected with a Metiq 1291 signal amplifier. Ahead of each test, film samples are electrically short-circuited at 100 °C for 12 h. Then film sample is placed between HV electrodes and silicone oil is added between the electrodes and the sample to guarantee good acoustic conduction. The sample is polarized under a DC electric field of 40 kV/mm for 30 mins at 30 °C to collect the space charge accumulation data. The external voltage is then removed to achieve short-circuits state for 10 mins to measure the charge decay dynamics during depolarization. The recorded data is then processed by calibration and deconvolution techniques in LabView to obtain the original space charge signal.

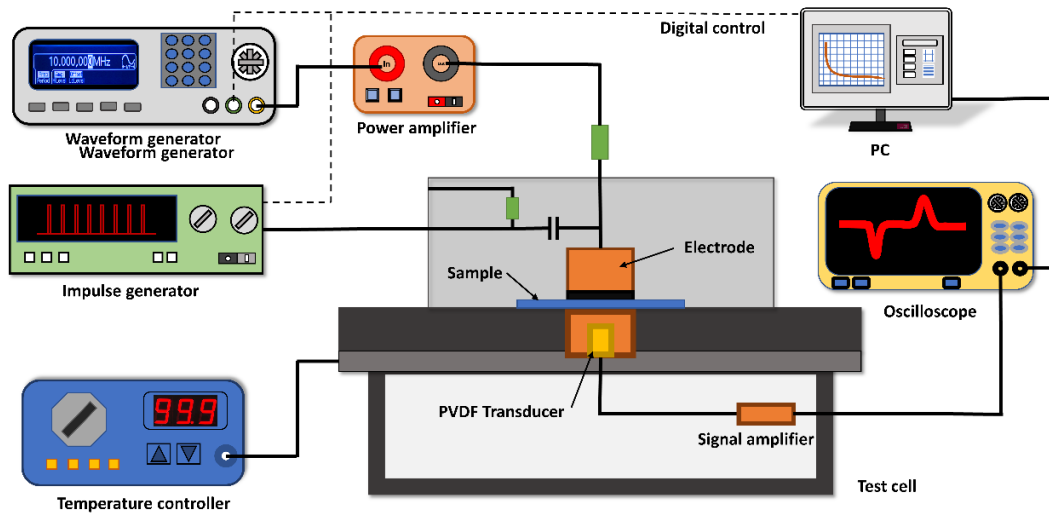


Figure 3.18 Design of the PEA measurement system.

3.3.11 Mechanical Strength Test

The tensile experiment is performed by using a CMT4000 universal testing machine made by MTS Systems Co., Ltd. The dumbbell shape samples with 1 mm thickness are prepared, as shown in Figure 3.19. A fixed stretching speed of 150 mm/min at room temperature is applied to each samples to acquire the stress-strain curve according to ASTM D638. Three tests are repeated for each kind of nanocomposite system to obtain the average value of elongation at break and tensile modulus.

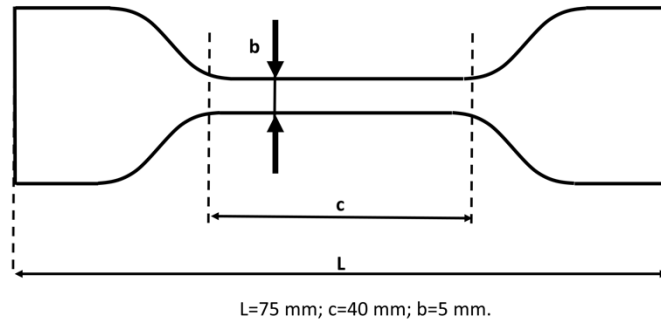


Figure 3.19 Dumbbell sheet sample for tensile test.

Chapter 4 Physical Chemistry

Characterization

4.1 Introduction

In the last chapter, nano- Al_2O_3 particles with an average size of 30 nm were added into PE and PP respectively by the melt-blending method. KH570 silane coupling agent was employed to conduct the surface modification for nanoparticles to improve the compatibility between the inorganic fillers and matrix material. The filling content of nano-alumina in nanocomposites was up to 5 phr. Morphology and chemical structure play important roles in influencing the properties of polymers such as optical, mechanical and electrical properties. It is determined by the compatibility between particles and matrix material. The nanoparticles have high surface free energy and they are usually present as agglomerated clusters rather than monodispersed particles in composite systems as reported by [120], [121]. To improve the compatibility between nanoparticles and matrix material, nano-alumina particles were modified with silane coupling agents before mixing with the PE or PP.

In this chapter, validation of surface modification of nanoparticles is characterized by using TGA and FTIR spectroscopy. The thermal analysis of polymer nanocomposites is conducted by using DSC. To illustrate the structural and morphological of nanocomposites, POM is used to reveal the isothermal crystallization process and SEM is employed to observe the morphology of nanocomposites. At the end of this chapter,

the mechanical properties of nanocomposites are profiled.

4.2 Results and Discussion

4.2.1 Thermal-gravimetric Analysis

The aim of the TGA test is to determine the thermal degradation behavior of both unmodified and KH570-modified nano-alumina particles. The measurement was completed by the TA Q500 thermal-gravimetric analyzer and the testing procedure was presented in Chapter 3. The TGA curves are shown in Figure 4.1 and they confirm the KH570 silane coupling agent is successfully grafted onto the surface of nano-alumina particles. The solid lines (TGA curves) provide the mass changes varying with temperature and the dash lines (Derivative-TGA curves) describe the rate of sample mass changes upon heating. Compared with the virgin alumina sample, there is a higher mass loss for the KH570-treated sample. For the as-received nano- Al_2O_3 sample, the total mass loss is about 2 %, which mainly occurs below 160 °C. It is believed to be the evaporation of absorbed moisture. But for the KH570-modified sample, below 160 °C, the mass loss of it is less than 1 %. This is credited to the KH570 coupling agent, which makes the surface of the nanoparticle hydrophobic. A new 6% mass loss peak is shown between 160 °C and 600 °C, which is caused by the pyrolysis of KH570 coupling agents. In addition, for both samples, the weight loss between 200 °C and 350 °C is likely to be the decomposition of some unwanted impurities. It can be considered to be negligible as the total amount of mass loss is limited. According to the TGA results, the mass of

introduced KH570 is about 6% of total KH570 treated nano alumina sample. The molar mass of alumina is approximately 101.96 g/mol and the molar mass of KH570 is approximately 292.44 g/mol. With calculation for the number of moles, the ratio of number of moles between alumina and KH570 is about 4, which suggests the nano alumina particles might agglomerate together rather than singly dispersed. In conclusion, TGA results demonstrate the KH570 was successfully attached to the nano-alumina particles.

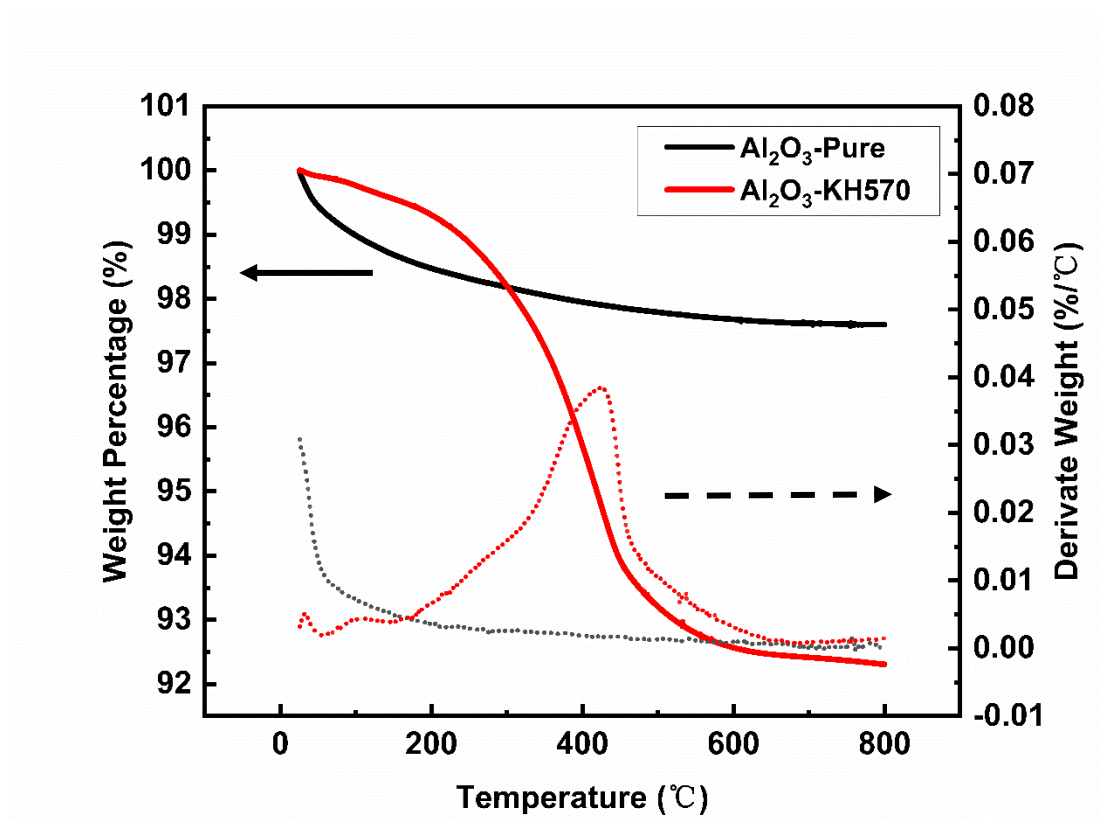


Figure 4.1 TGA Results

4.2.2 Fourier-transform Infrared Spectroscopy

FTIR spectroscopy is used to identify the chemical structural change of Al₂O₃

nanoparticles before and after the surface modification by KH570. The obtained typical spectra in the range between 400 cm^{-1} and 4000 cm^{-1} are shown in Figure 4.2. These traces have been vertically offset for clarity of presentation. Many new absorption peaks are found on the spectrum of KH570-modified nano-alumina as compared with untreated nano-alumina particles. The new absorption peak at 2950 cm^{-1} represents the carbon-hydrogen, C-H, bonds. The peaks at 2920 cm^{-1} and 2850 cm^{-1} are the distinctive stretching and bending bonds of the $-\text{CH}_2-$ bond. Another characteristic is the C=O stretching peak of the KH570 silane coupling agent that is located at 1718 cm^{-1} . The peak at 1640 cm^{-1} is assigned to the nonconjugated C=C stretching vibrations of the KH570 structure. The peaks found at 1443 cm^{-1} , 1390 cm^{-1} and 1080 cm^{-1} imply that the existence of the Si-O- CH_2CH_3 bond. In addition, for both spectra, the peaks at about 920 cm^{-1} are the typical stretching vibrations of the Al-O bond and the broad absorption band at 3500 cm^{-1} is attributed to the stretching vibrations of the -OH group on the surface of nano-alumina particles. All the new peaks identified on the KH570- Al_2O_3 spectrum indicate that the success of surface modification for nano- Al_2O_3 particles by the KH570 coupling agent.

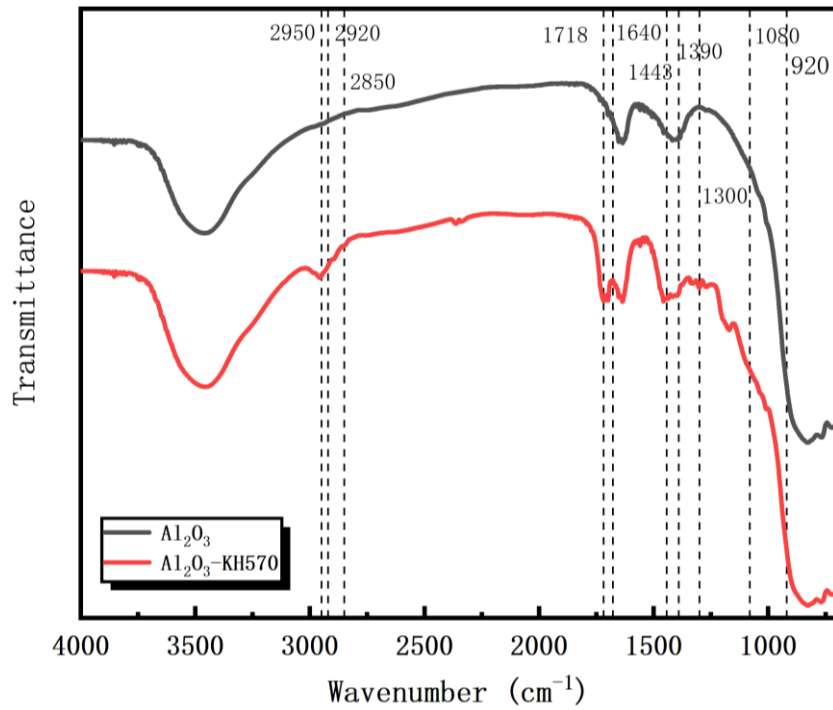


Figure 4.2 FTIR results

4.2.3 Polarized Optical Microscopy

The typical evolution of spherulites is illustrated in Figure 4.3. In the beginning, the nuclei firstly appear at multiple locations and then they grow up at a constant rate in space under the isothermally crystallized process. The process stops when spherulites impinge on each other and then take up the whole space. POM is used to study the crystalline morphology of polymer composite material.

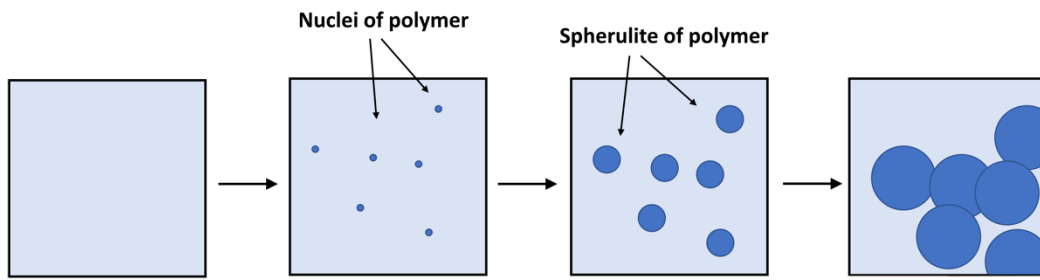


Figure 4.3 The typical formation and growth of nuclei in the polymer.

The POM images of virgin PE and Virgin PP are shown in Figure 4.4. As the spherulite size of PE is smaller than the resolution of the optical microscope, the boundaries of spherulites are blurry. The size of PE spherulite is less than 10 μm . For crystalline polymer material, the break often starts from the interphase area of lamellar crystals. Compared with PE, PP has a larger spherulite size, which makes it easy to crack.

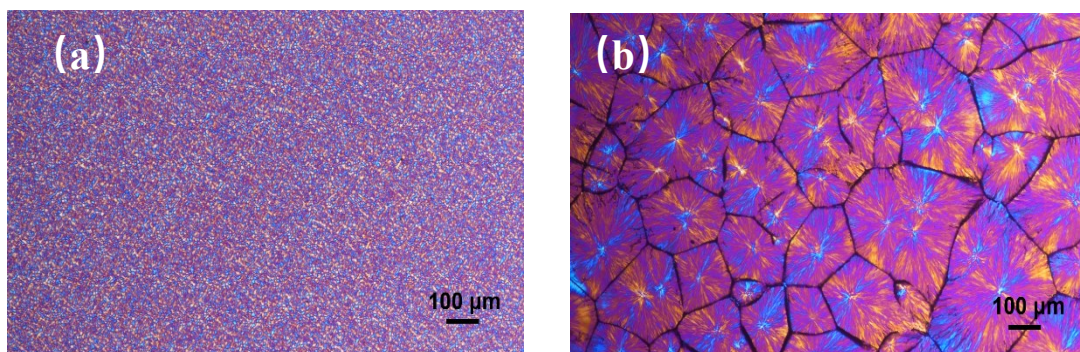


Figure 4.4 POM results of (a) virgin PE and (b) virgin PP.

Previous studies have proven that nanoparticles often work as nucleating agents within the composite system during crystallization [55]. The POM image of the virgin PE sample is showed in Figure 4.4(a). It is hard to identify a single PE spherulite as its spherulite size is smaller than the resolution of the used optical microscopy. The POM images of PE nanocomposite are shown in Figure 4.5. It is hard to observe the spherulite structure and the results are assured by qualitative observation. The crystallization region is spotted as the blue and yellow regions. The morphology of the crystallised systems are perturbed by the introduction of nano-alumina particles. This is evident in Figure 4.5(a) and Figure 4.5(b), which illustrates the PE nanocomposite system containing 1 phr of untreated nano-alumina and PE nanocomposite system containing 1 phr of KH570-treated nano-alumina, respectively. The addition of both untreated and KH570-treated nano-alumina particles results in similar morphologies Compared with virgin PE, introduction of nano-alumina in PE nanocomposites results in the increment of the total number of spherulites and the reduction of spherulite size, as shown in Figure 4.5. By comparing the PE nanocomposites containing 1 phr, 2 phr and 5 phr of KH570-treated nano-alumina in Figure 4.5, the sample containing 1 phr nano-alumina has larger spherulite size and no obvious distinction can be made between the samples containing 2 phr and 5phr nano-alumina due to the limitation of optical microscopy.

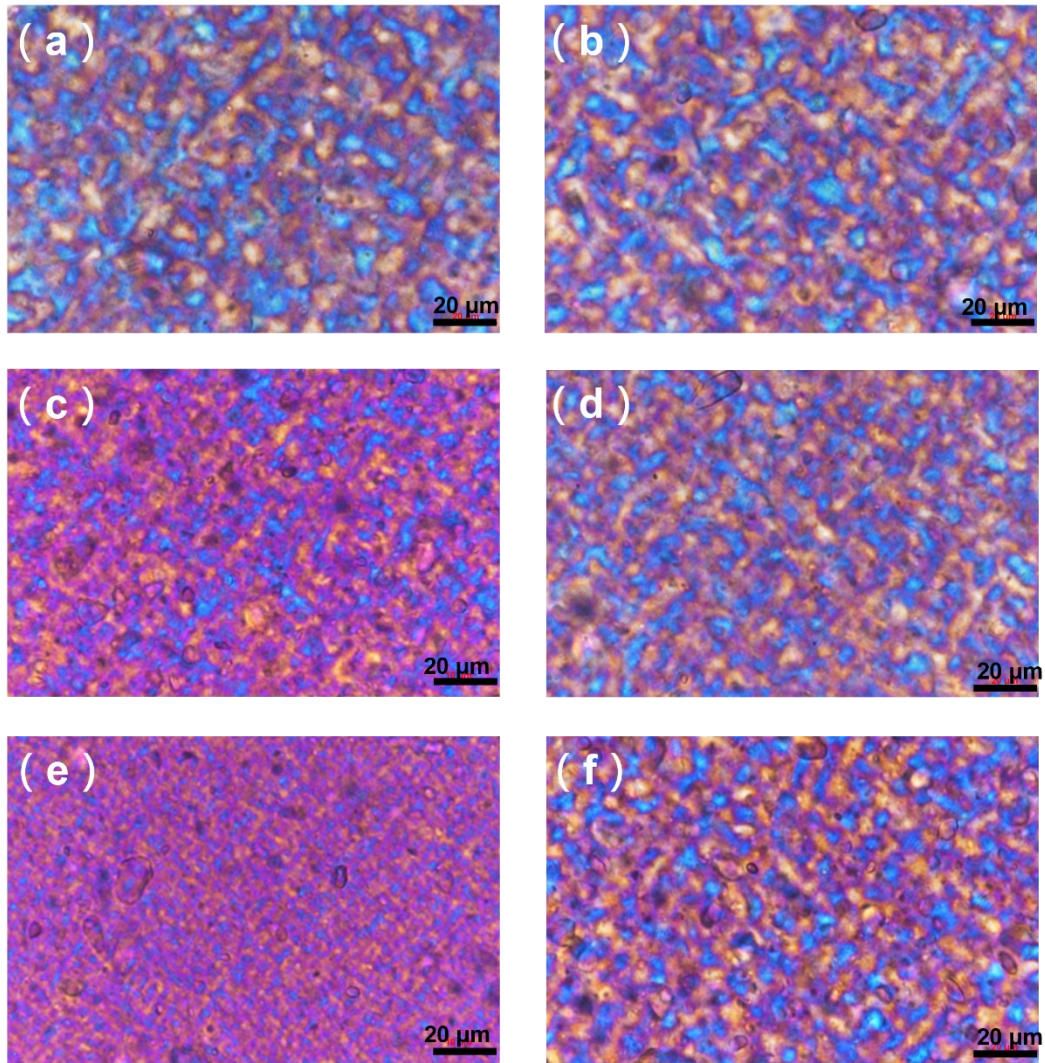


Figure 4.5 POM images of PE nanocomposites containing untreated nano-alumina of (a) 1phr, (c) 2phr, (e) 5phr and PE nanocomposites containing KH570-treated nano-alumina of (b) 1phr, (d) 2phr, (f) 5phr.

The polarized optical images of virgin PP, PP nanocomposites containing untreated nano-alumina, and PP nanocomposites containing KH570-treated nano-alumina are shown in Figure 4.6, Figure 4.7 and Figure 4.8, respectively. All the tested samples show typical spherulite structure and their spherulite size is calculated by using Nano Measure software. The spherulites of virgin PP have clear boundaries and the average size is about 220.1 μm . After introducing the nano- Al_2O_3 particles, the spherulite size

significantly decreases and the spherulite number increases for all the PP composite samples. This phenomenon can be attributed to the hindrance effect of nucleation when nano-alumina particles are introduced. The average spherulite size of PP/ Al₂O₃-Pure@1phr, PP/ Al₂O₃-Pure@2phr and PP/ Al₂O₃-Pure@5phr is 126.0, 140.0 and 118.0 μm, respectively. There is not much difference between these results. It is probably because the poor distribution of nanoparticles at high filling content weakens the nucleating effect during the crystallization process. But for nanocomposite samples containing KH570-treated nano-alumina particles, the average spherulite size of PP/ Al₂O₃-KH570@1phr, PP/ Al₂O₃-KH570@2phr and PP/ Al₂O₃-KH570@5phr is 90.0, 70.7 and 39.7 μm respectively. The average size of spherulite further decreases and the total spherulite number increases when more surfaced-modified nanoparticles are added. Meanwhile, the boundaries between spherulites become blurry. Similar results are reported in [42], [118]. It is believed that the change of crystallinity characteristics plays an important role in influencing the trap distribution of nanocomposite material, which will be discussed in the other chapter.

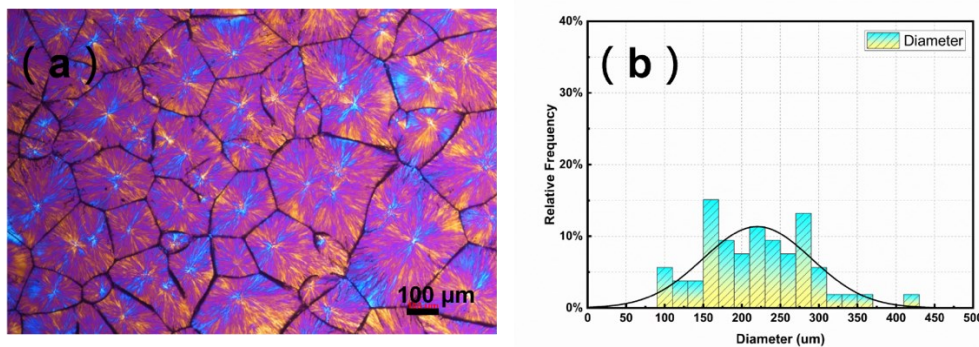


Figure 4.6 POM image and the spherulite statistics of virgin PP.

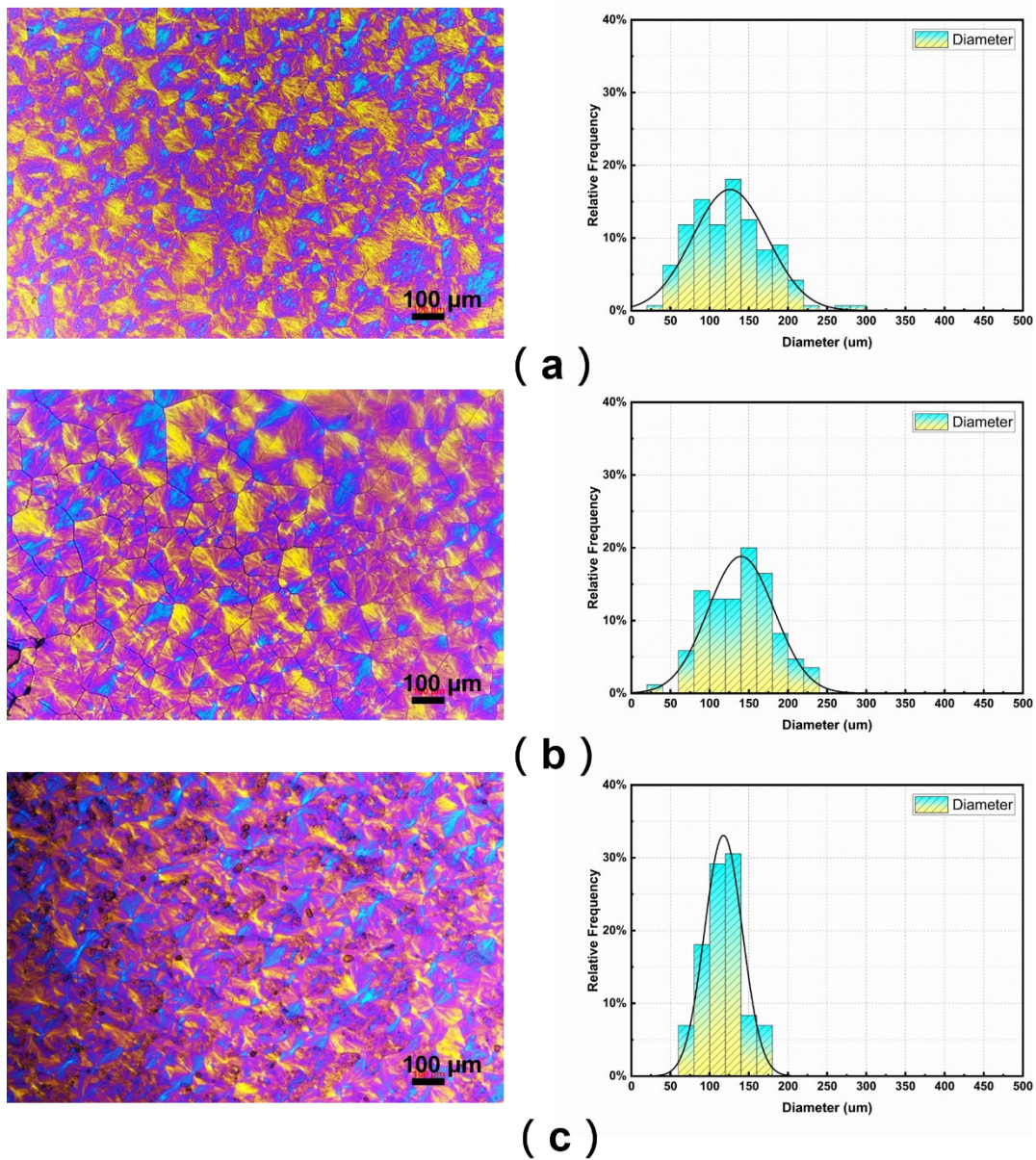


Figure 4.7 POM images and the spherulite statistics of PP nanocomposites containing untreated nano-alumina of (a) 1phr, (b) 2phr, (c) 5phr.

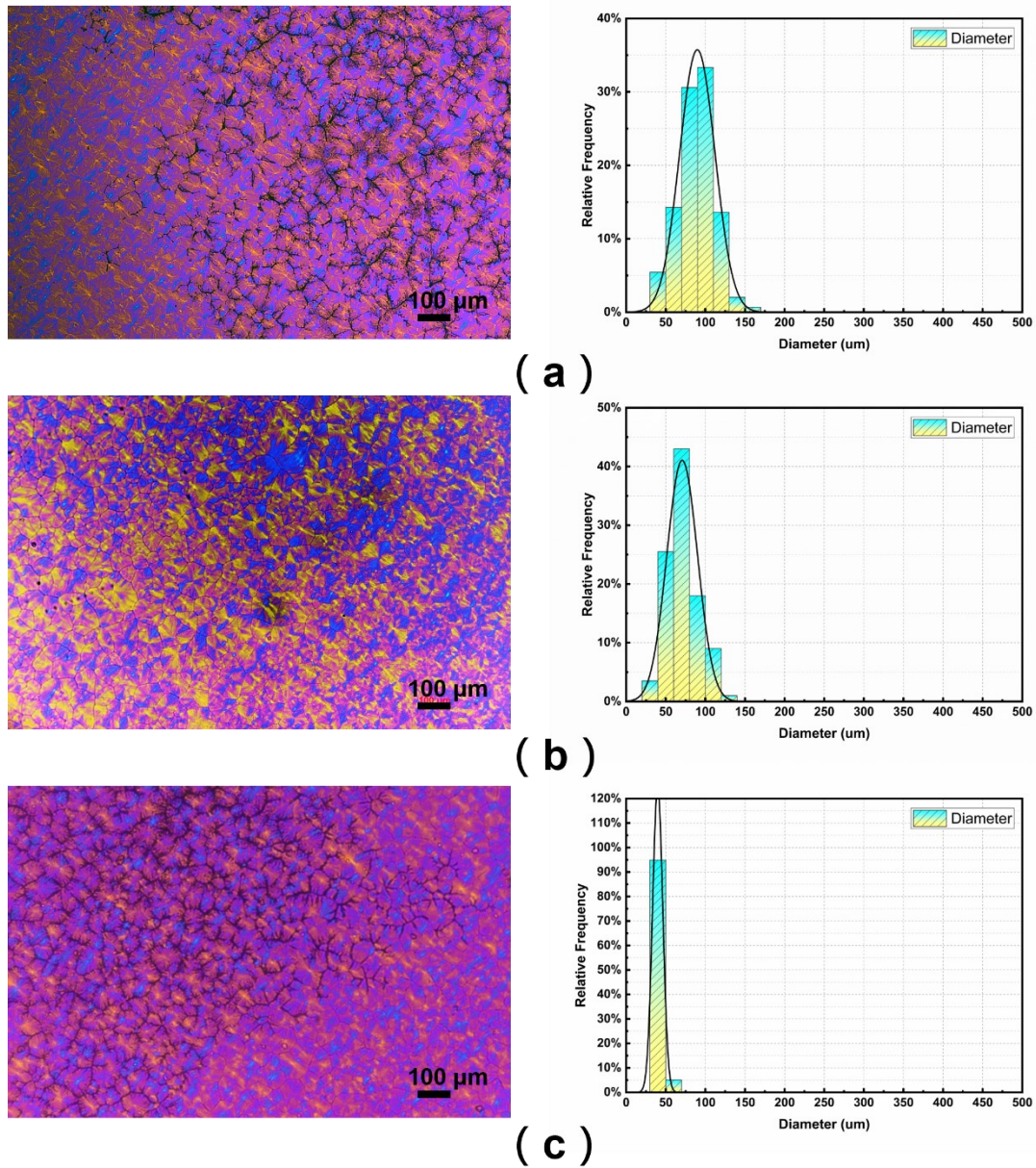


Figure 4.8 POM images and the spherulite statistics of PP nanocomposites containing KH570-treated nano-alumina of (a) 1 phr, (b) 2 phr, (c) 5 phr.

4.2.4 Scanning Electron Microscopy

Before discussing the physical and chemical properties of nanocomposite material, some work should be done to identify their microstructure, which includes the particle

size, particle dispersion and distribution within matrix polymer material. With the help of SEM, it is possible to take high-resolution images of a sample surface. For conventional optical microscopy, it is impossible to observe any object smaller than 300 nm as the wavelength of visual light is in the range of 300 nm and 800 nm. However, for electron microscopy, the wavelength of the electron beam could reach around 0.1 nm when an accelerating voltage is used, so it is widely used to study the nano-scale object. The dispersion and distribution of nanoparticle in the PE and PP matrix is investigated by employing SEM.

Within the composite material, the filler is either in the monodispersed state or agglomerated state. Poor dispersion and distribution of nanoparticles often lead to the reduction of electrical strength. Therefore, it is important to study the distribution and dispersion state of nano-alumina particles within matrix polymer material. Previous studies [120], [121] have stated that the existence of nanoparticles with the composite system is usually in the aggregated state rather than the monodispersed state. The morphological observations of virgin PE and PP are shown in Figure 4.9. For virgin PP, it has a clear layered structure. While for virgin PE, the fractured surface has many filament-like structures, which means it has lesser rigidity and hardness than PP. The white dot in Figure 4.9(a) refers to the break points of PE.

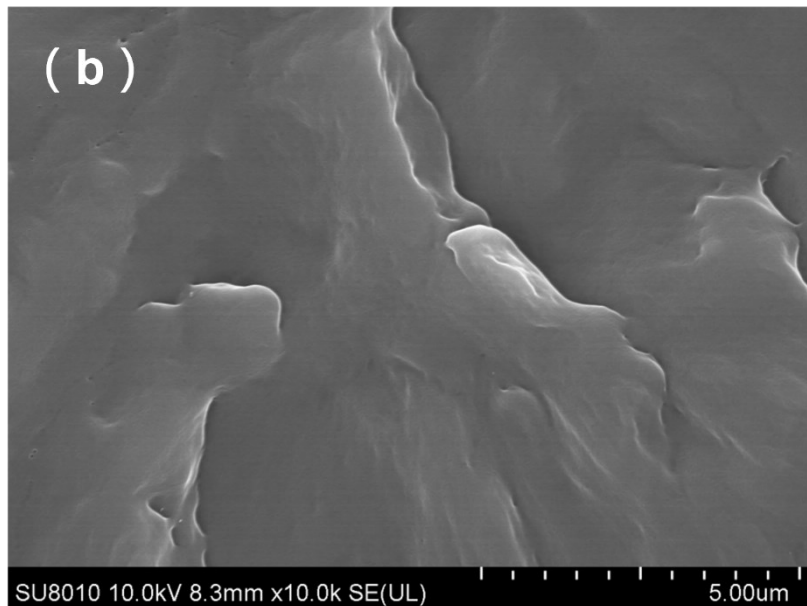
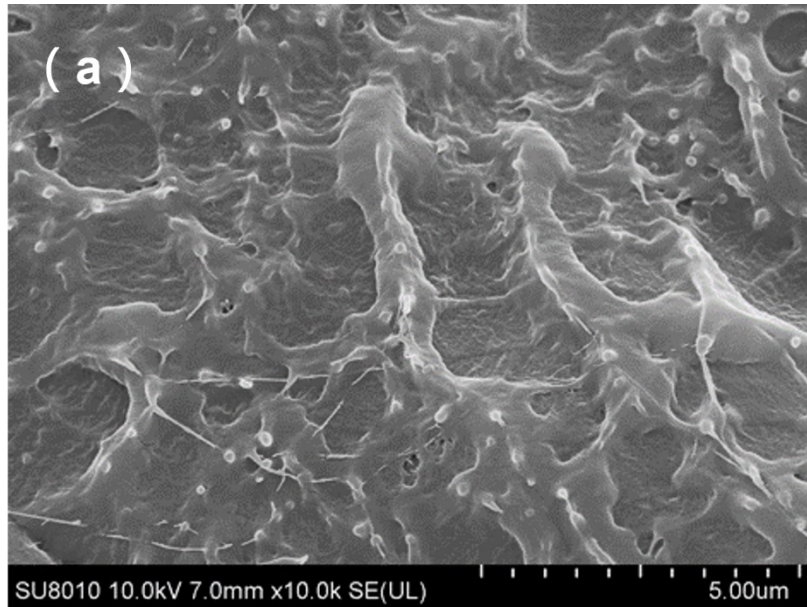


Figure 4.9 SEM images of (a) virgin PE and (b) virgin PP.

Figure 4.10 displays the SEM images of PE nanocomposites filled with untreated and KH570-treated nano-alumina particles with different loading content. Compared with virgin PE in Figure 4.9(a), the morphology of PE nanocomposite is different and the microstructure around nanoparticles changes. For PE containing untreated nano- Al_2O_3

samples with 0.5 phr loading, nano-alumina clusters with more than 2 μm in diameter are found as showed in Figure 4.10 (a). With surface modification, no prominent cluster is observed at this loading level. When the filling content increases, the agglomeration of unmodified nano-alumina becomes more serious. Although the agglomeration seems to be inevitable, the KH570-modified nano-alumina particles achieve better dispersion. In addition, for samples with 5 phr filling content, the size of captured nano-alumina particles is counted and depicted in Figure 4.11. Both untreated and treated particles tend to cluster together. The size of the unmodified nano-alumina clusters is distributed in a wide range and the biggest clusters are up to 1.5 μm . However, most of the clusters of KH570-treated nano-alumina particles are under 300 nm in size and they have a uniform size distribution. All the results suggest that the surface modification by KH570 helps nano-alumina particles with their dispersion and distribution in PE matrix material.

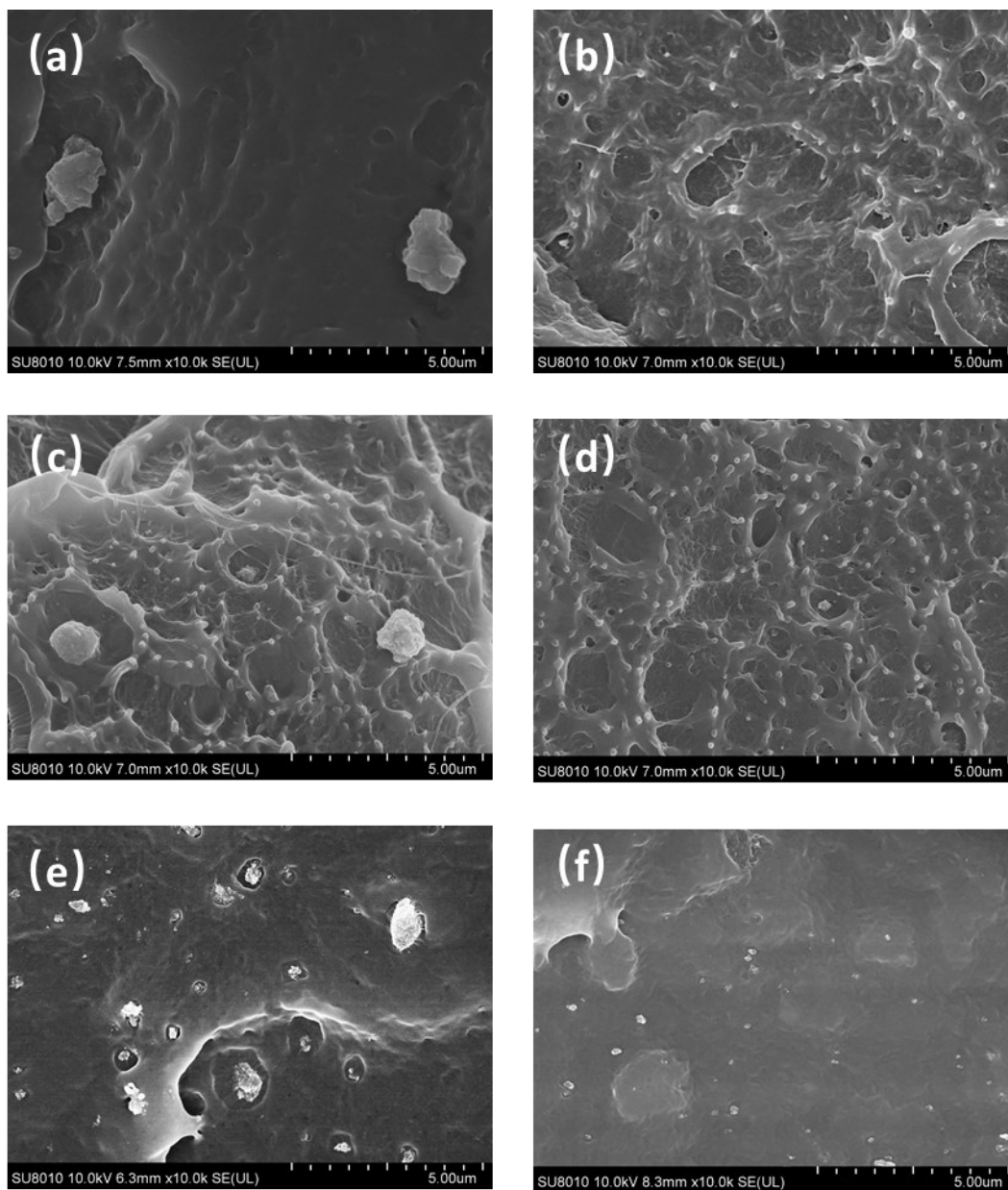


Figure 4.10 SEM images of PE nanocomposites containing untreated nano-alumina of (a) 0.5phr, (c) 1phr, (e) 5phr and PE nanocomposites containing KH570-treated nano-alumina of (b) 0.5phr, (d) 1phr, (f) 5phr.

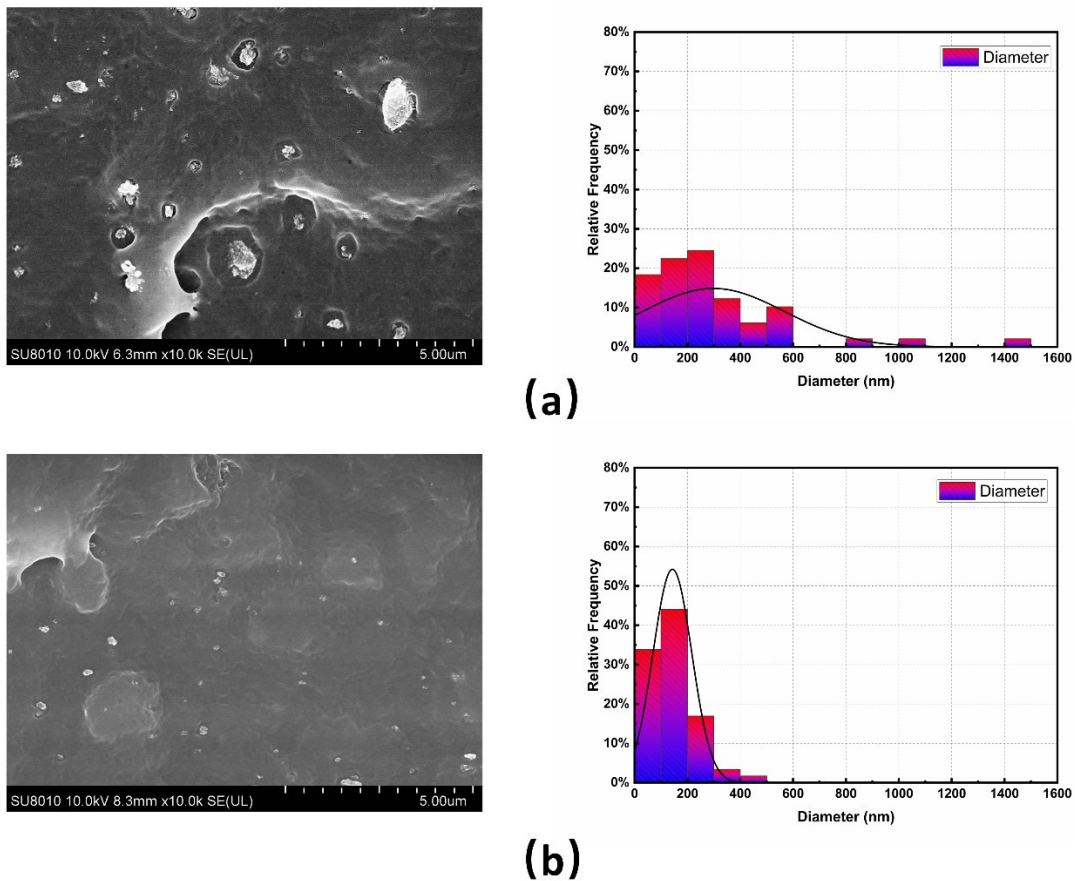


Figure 4.11 SEM images and the particle statistics of PE nanocomposites containing (a) 5 phr untreated nano-alumina, (b) 5 phr KH570-treated nano-alumina.

The fractured surfaces of PP nano-alumina composites are shown in Figure 4.12. Serious agglomeration is found for all the samples filled with unmodified nano-alumina particles. The agglomerated clusters become more significant with the increasing filling content and they are in micrometer size. It can be concluded that the agglomeration of nano-alumina cannot be fully avoided and it usually appears as clusters rather than as every single particle in composites [120], [121]. According to the statistical results in Figure 4.13, the cluster size in PP nanocomposite sample containing 5 phr KH570-

modified nano-alumina is less than 400 nm and it shows a narrow size distribution around 200 nm. The small clusters are well distribution within the PP matrix. It suggests that the use of KH570 reduces the interaction between interfaces, thus improves the compatibility between matrix material and nanofillers. In conclusion, the use of KH570 for surface modification improves the dispersion and distribution of nano-alumina particles in the PP composite system.

The agglomeration of nanoparticles is due to the strong van der Waals forces between particles. The magnitude of the force is inversely proportional to the distance between adjacent particles. The average distance between nanoparticles could be calculated based on:

$$l = \left[\left(\frac{4\pi}{3v} \right)^{1/3} - 2 \right] \times r \quad (4.1)$$

where v is the volume percentage of fillers and r is the radius of filler. When the filling content is low, the average distance is relatively long, so that the van der Waals force is weak. After increasing the filling content, the distance between particles dramatically decreases. The force then sharply increases, which leads to serious agglomeration. Furthermore, for virgin nano-alumina particles, there are many hydroxyl groups on the surface of nanoparticles and then the hydrogen bonds are generated between different nanoparticles, which also results in agglomeration. After conducting the surface treatment by using KH570, some of the hydroxyl groups are consumed during the coupling reaction with KH570 and the grafted coupling agents also have strong steric

hindrance effect on the surface of nano-alumina. Consequently, no serious agglomerations are spotted from the samples filled with treated nanoparticles and better particle distribution is identified within the composite systems.

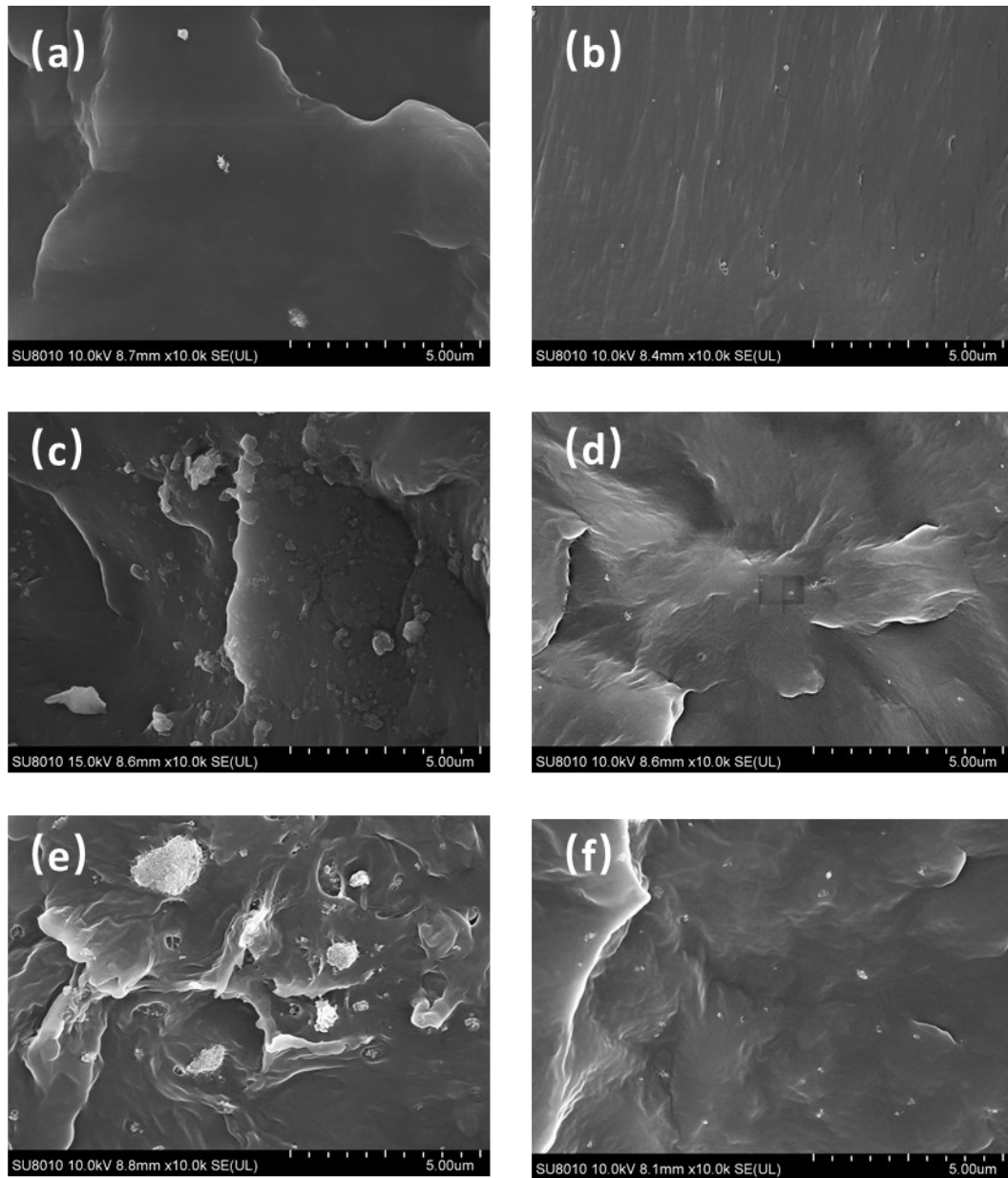


Figure 4.12 SEM images of PP nanocomposites containing untreated nano-alumina of (a) 0.5phr, (c) 1phr, (e) 5phr and PP nanocomposites containing untreated nano-alumina of (b) 0.5phr, (d) 1phr, (f) 5phr.

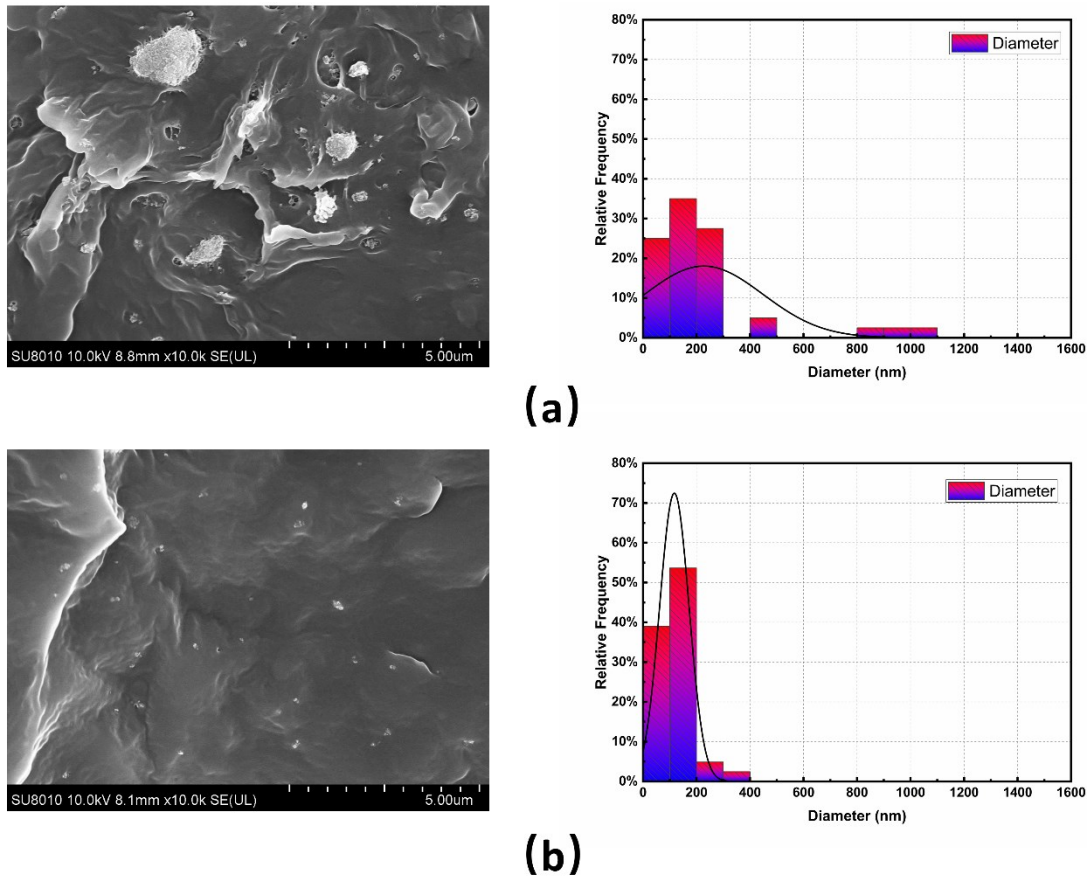


Figure 4.13 SEM images and the particle statistics of PP nanocomposites containing (a) 5 phr untreated nano-alumina, (b) 5 phr KH570-treated nano-alumina.

4.2.5 Differential Scanning Calorimetry

Both PE and PP are semi-crystalline polymers. It is believed that the crystallinity of composite is of great significance in determining its mechanical properties and charge transportation. From previous studies [118], [122], adding nanoparticles into polymer material could result in the reduction of both spherulite size and amorphous area. Moreover, the crystal structure tends to be more organized and well-stacked. This is because the possibility of heterogeneous nucleation increases when nanoparticles are

introduced. Generally, homogeneous nucleation is the primary crystallization type for most polymers and leads to large spherulite sizes. When nanoparticles are added to PE and PP, they work as heterogeneous nucleating agents and transfer the homogeneous nucleation into heterogeneous nucleation. Hence, more spherulites are formed in different crystallization types.

The DSC analysis is used to study the relationship between crystalline characteristics and properties in mechanical and electrical aspects of polymer nanocomposite material. The melting temperature, enthalpy of melting and crystallinity are obtained from the crystallization curves. The degree of crystallinity of each tested sample is calculated by:

$$X_c = \frac{\Delta H_m}{\Delta H_{100}} \times 100\% \quad (4.2)$$

ΔH is the melting enthalpy of the nanocomposite sample and ΔH_{100} is the enthalpy of 100% crystallized PE and PP sample. The typical value of ΔH_{100} of PE is 293.0 J/g [123], [124] and it is 209.0 J/g for PP [125], [126]. The crystal thickness of the polymeric sample, L_c , is calculated according to the Thomson-Gibbs equation:

$$L_c = \frac{2\sigma_e T_m^0}{(T_m^0 - T_m) \times \Delta H_{100} \times \rho_c} \quad (4.3)$$

where σ_e is the fold surface free energy, ΔH_{100} is the melting enthalpy of 100% crystallized polymer, T_m^0 is the equilibrium melting point of the test sample, T_m is the

melting temperature, and ρ_c is the density of the polymeric sample. Table 4.1 summarizes all the parameters used to determine the crystal thickness of PE and PP samples [123]–[126].

Table 4.1 Thermal parameters of PE and PP.

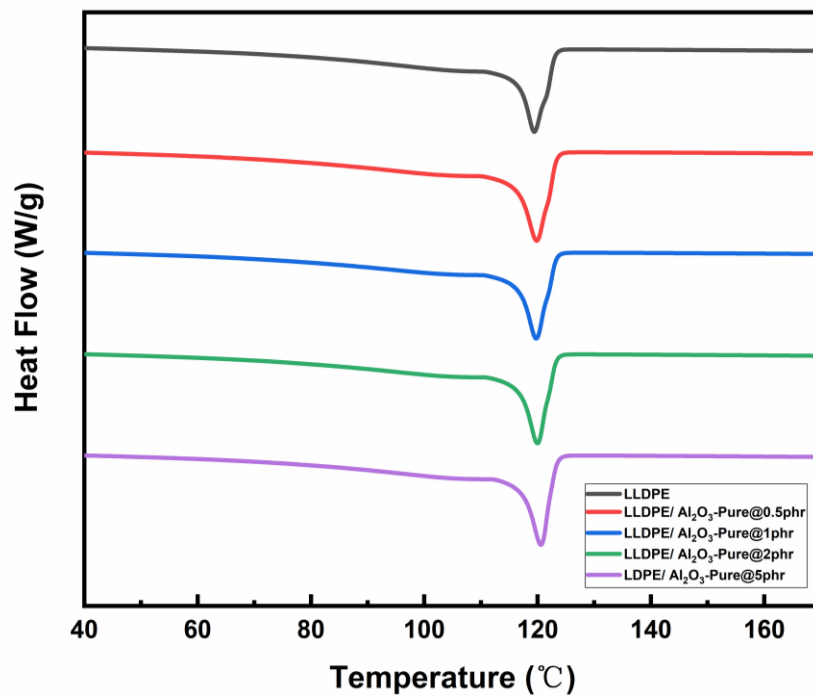
	σ_e (mJ/m ²)	ΔH_{100} (J/g)	T_m^0 (K)	ρ_c (g/cm ³)
PE	93	293	410	0.924
PP	123	209	459	0.900

The DSC tests were conducted for all PE and PP nano-alumina composite samples with and without surface modification. Figure 4.14 represents the DSC melting curves of PE and PE nano-alumina composites. During the melting process, there is only one endothermic peak for PE and its nanocomposite samples. From Figure 4.14, all the PE-based samples have almost the same melting temperature. These samples filled with unmodified and KH570-modified alumina particles have melting peaks similar to virgin PE. The melting temperature, melting enthalpy and crystallinity are summarized in Table 4.2. T_m is the melting temperature, ΔH is the melting enthalpy and X_c is the calculated crystallinity. Both the melting temperature and the melting enthalpy were taken as integral values due to the precision of the measurement system. Based on the results, all the nanocomposites did not show significant difference in the melting

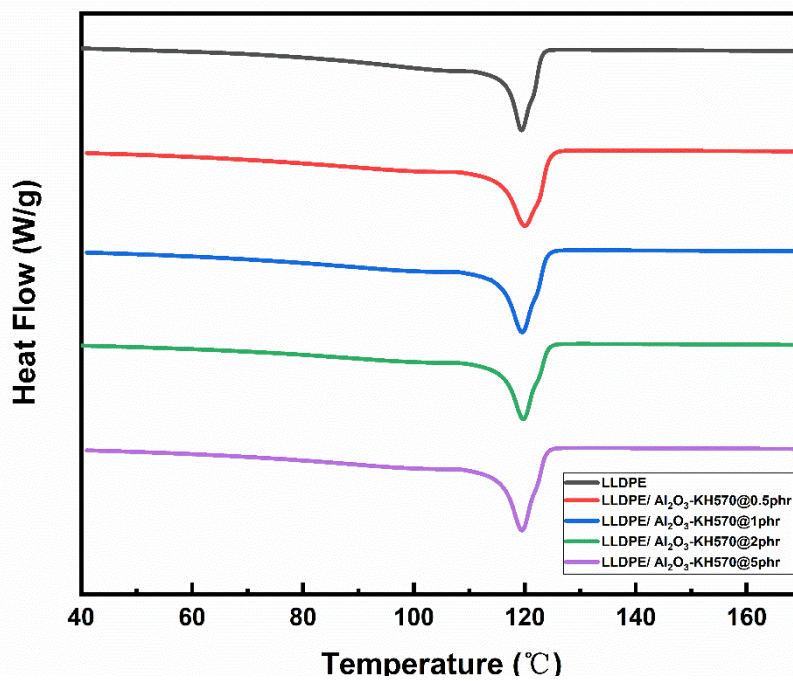
temperature and the percentage of crystallinity as compared with the unfilled PE sample when taking into account the random experimental uncertainties. With the increasing filling content, both the melting peak temperature and the crystallinity of PE composite samples containing the untreated nano-alumina increases, indicating that nanoparticles enhance the formation of the nucleus [59], [127]. However, the addition of 0.5 phr and 1 phr of untreated nano-alumina slightly reduces the crystallinity. This might be because the poor distribution of nanoparticles disturbs the crystallization process of the nanocomposite. Upon the surface treatment of nanoparticles, the crystallinity of PE nanocomposites containing the KH570-treated nano-alumina are increasing and they are all larger than unfilled PE, suggesting that the well-dispersed KH570-modified alumina particles act as heterogeneous nucleating agents and improve the crystallinity of nanocomposite. The melting temperature of PE nanocomposites does not show significant change.

Table 4.2 The melting temperature, crystallization enthalpy and crystallinity of PE nanocomposites.

Sample	T_m (°C)	ΔH (J/g)	X_c (%)	L_c (nm)
PE	115.82	83.31	28.73	13.39
PE/Al ₂ O ₃ -Pure@0.5 phr	116.11	78.33	27.01	13.58
PE/Al ₂ O ₃ -Pure@1 phr	116.37	79.09	27.27	13.75
PE/Al ₂ O ₃ -Pure@2 phr	116.58	83.58	28.82	13.90
PE/Al ₂ O ₃ -Pure@5 phr	116.97	87.21	30.07	14.17
PE/Al ₂ O ₃ -KH570@0.5 phr	116.21	84.35	29.09	13.65
PE/Al ₂ O ₃ -KH570@1 phr	116.40	86.68	29.89	13.77
PE/Al ₂ O ₃ -KH570@2 phr	116.53	89.53	30.87	13.86
PE/Al ₂ O ₃ -KH570@5 phr	116.75	96.33	33.22	14.01

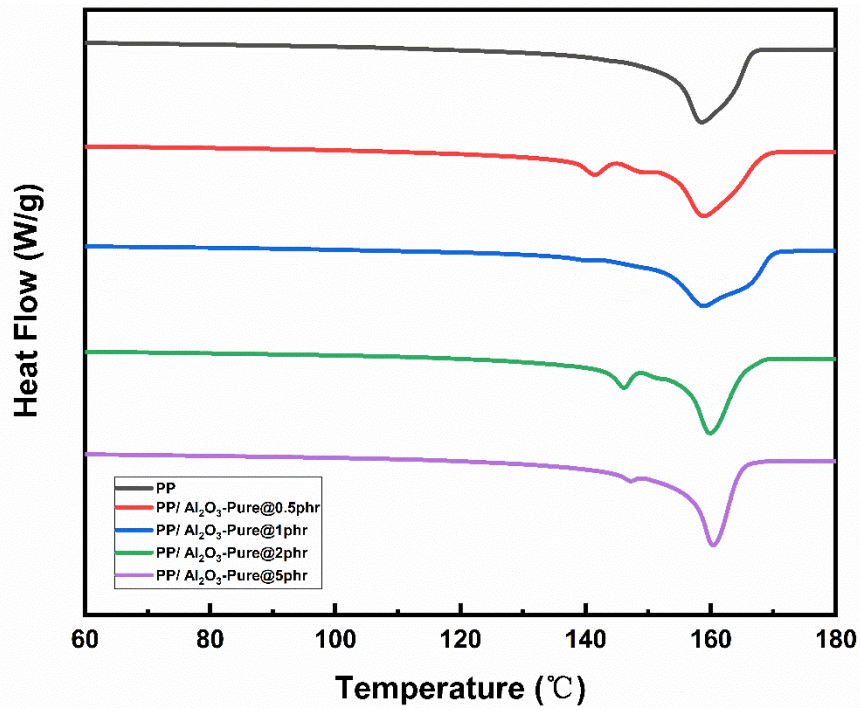


(a)

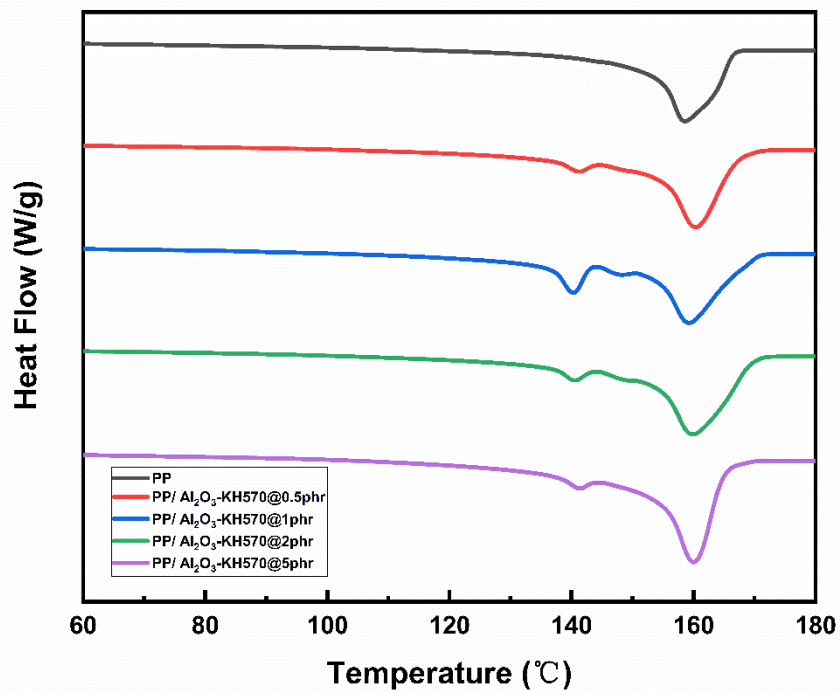


(b)

Figure 4.14 DSC melting traces of PE nanocomposite samples containing (a) untreated alumina and (b) KH570-treated alumina.



(a)



(b)

Figure 4.15 DSC melting traces of PP nanocomposite samples containing (a) untreated alumina and (b) KH570-treated alumina.

Figure 4.15 displays the DSC melting traces of virgin polyethylene and PP/nano-alumina composites with and without surface treatment. It is noteworthy that there is only one peak for virgin PP, but there are two peaks for almost all nanocomposite samples. The appearance of a new peak at around 145 °C is the typical melting peak of β phase crystal of PP nanocomposite, which is caused by the addition of nano-alumina particles. The addition of nanoparticles acts like heterogeneous nucleating agent and results in the new melting peak of β phase crystal. The calculated melting enthalpy, crystallinity and crystal thickness are summarized in Table 4.3. Both α and β peaks are included to calculate the crystallinity of PP nanocomposite. The melting temperature of all PP composite samples does not exhibit significant difference upon the introduction of nano-alumina particles, although some nanocomposite systems show a small change up to 3 °C. Compared with PE nanocomposites with a melting temperature of about 115 °C, PP and its alumina nanocomposites have higher melting peak temperature thus can work under higher temperatures. With the addition of KH570-treated nano-alumina, the crystallinity of PP/ nano-alumina composites slightly increases as the filling content increases. The crystallinity of all the PP composite samples is between 40% and 43%, indicating that adding nano-alumina can reduce the spherulite size but has a limited influence on the melting point and crystallinity of nanocomposite systems.

Table 4.3 The melting temperature, crystallization enthalpy and crystallinity of PP nanocomposites.

Sample	T _m (°C)	ΔH (J/g)	X _c (%)	L _c (nm)
PP	153.41	85.76	41.03	18.50
PP/Al ₂ O ₃ -Pure@0.5 phr	154.00	89.62	42.88	18.85
PP/Al ₂ O ₃ -Pure@1 phr	152.21	84.37	40.37	17.84
PP/Al ₂ O ₃ -Pure@2 phr	155.39	85.08	40.71	19.71
PP/Al ₂ O ₃ -Pure@5 phr	156.34	85.41	40.48	20.34
PP/Al ₂ O ₃ -KH570@0.5 phr	155.34	84.97	40.66	19.68
PP/Al ₂ O ₃ -KH570@1 phr	154.96	85.50	40.91	19.43
PP/Al ₂ O ₃ -KH570@2 phr	154.31	87.45	41.84	19.03
PP/Al ₂ O ₃ -KH570@5 phr	156.26	88.84	42.51	20.28

4.2.6 Tensile test

The stress-strain curve obtained from the tensile test is widely used to describe the ability of a material to absorb energy and resist possible deformation. The mechanical properties of polymers are determined by factors such as the molecular chain, intermolecular forces and flexibility of the molecule. The test results are affected by the environment humidity, testing temperature and elongation rate. Figure 4.16 describes the typical stress-strain curve of polymers. Curve (a) shows the stress-strain curve of brittle material like epoxy resin. Curve (b) belongs to quasi-brittle material. Curve (c) represents the ductility material like most polymeric material and curve (d) represents the rubber material. Under tensile stress, a material with high ductility can withstand the high strain.

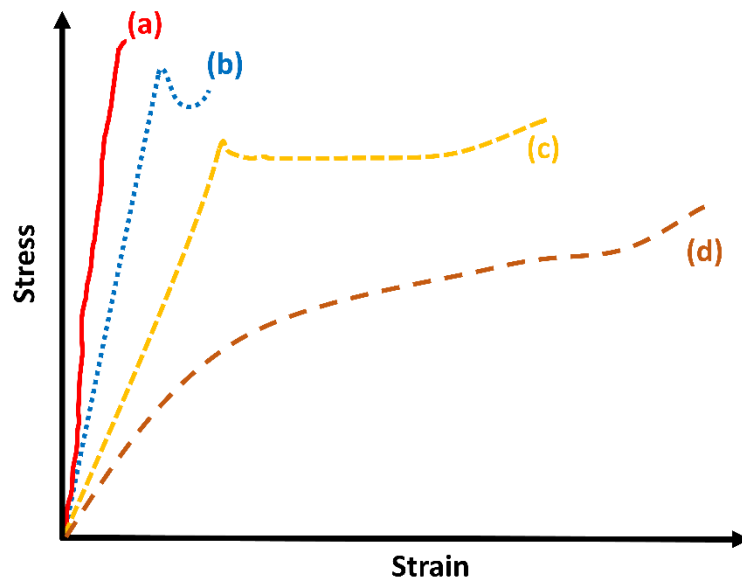


Figure 4.16 Typical strain-stress curves of polymers

To compare the mechanical property of different samples, tensile strength and elongation at break of nanocomposite material are studied according to Standard ASTM D638. Tensile strength shows the maximum tensile stress that could be sustained on a sample and elongation at break is the percentage increase in length that material will be before breaking. The tensile strength is calculated according to Equation (4.4)

$$s = P / a \quad (4.4)$$

where s is the tensile strength, P is the force applied on the material when breaking and a is the original area of the cross section. The elongation at break is calculated based on Equation (4.5):

$$\varepsilon = \frac{L_1 - L_0}{L_0} \times 100\% \quad (4.5)$$

where L_0 is the original length of the tested sample and L_1 is the measured length at breaking.

To study the effect of surface modification and filling content on the mechanical performance of composite materials, the strain-stress curves of PE nanocomposites and PP nanocomposites are measured and the representative curves are displayed in Figure 4.17 and Figure 4.18 respectively. All the samples show the typical strain-stress curve of ductility material.

For the strain-stress curves of PE/ nano-alumina composite samples, they all follow the similar trend. All the samples shows reversible deformation initially and the strain hardening is identified until the break takes place. The tensile strength and elongation at break of PE composites are calculated and reported in Figure 4.19 and Figure 4.20 respectively. When composite samples are filled with unmodified nano-alumina particles, the elongation at break decreases along with the increased filling load. It is about an approximate 21% drop for PE/ Al_2O_3 -Pure@5 phr sample when compared to that of virgin PE sample. This should be attributed to the aggregation of the nano-alumina particles at high filling content, leading to local stress concentration at the interfaces between PE matrix and nanoparticles when external force is applied. However, in each filling content, the PE/ Al_2O_3 -KH570 nanocomposites show enhanced the elongation at break when compared with PE / Al_2O_3 -Pure nanocomposites. This might be because the surface modification of nanoparticle improves the dispersion

of nanoparticles and enhances the physical interaction between polymer and nanoparticles. As for the tensile strength, the introduction of nano-alumina particles has limited impact on the tensile strength of PE nanocomposites. All the samples containing the untreated and KH570-treated alumina have roughly the same level of tensile strength around 25 MPa except PE/ Al_2O_3 -Pure@5 phr with about 15% reduction. The introduction of nanoparticles and the surface modification of nanoparticle show insignificant impact on the tensile strength of the PE nanocomposites.

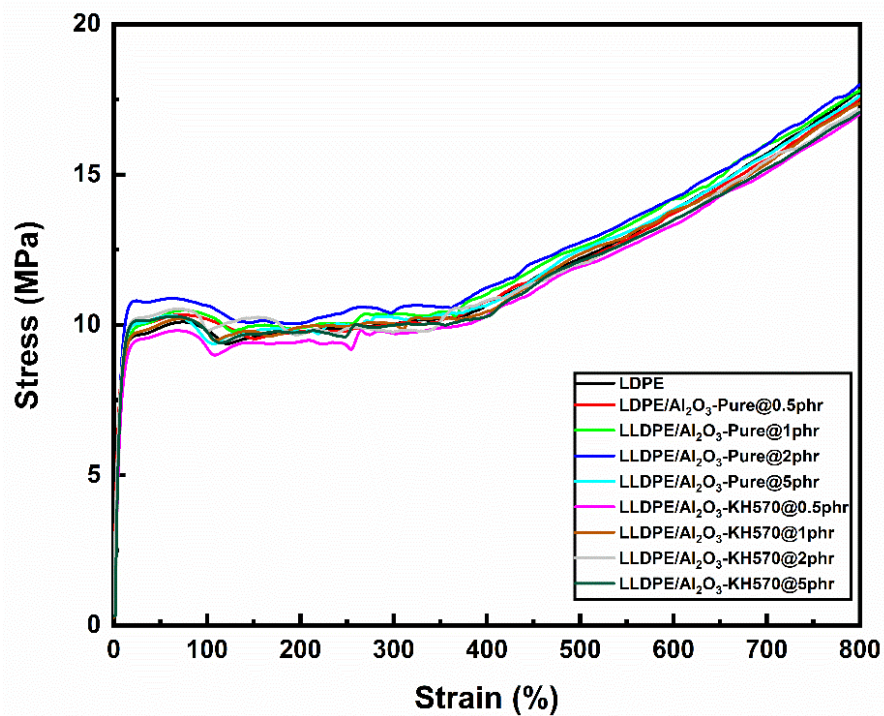


Figure 4.17 Strain- stress curves of PE nanocomposites.

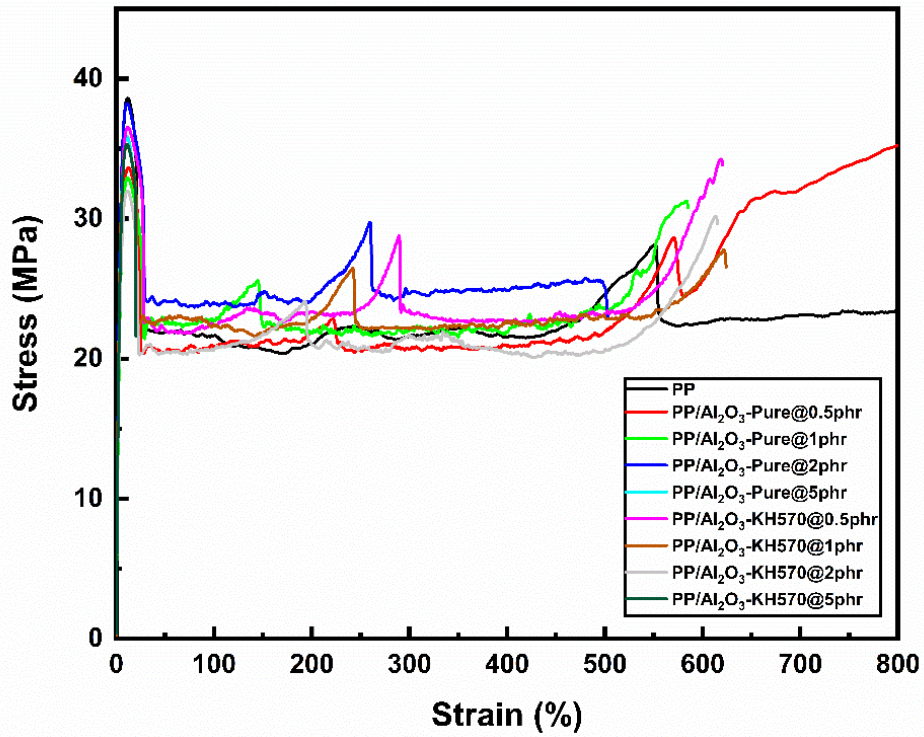
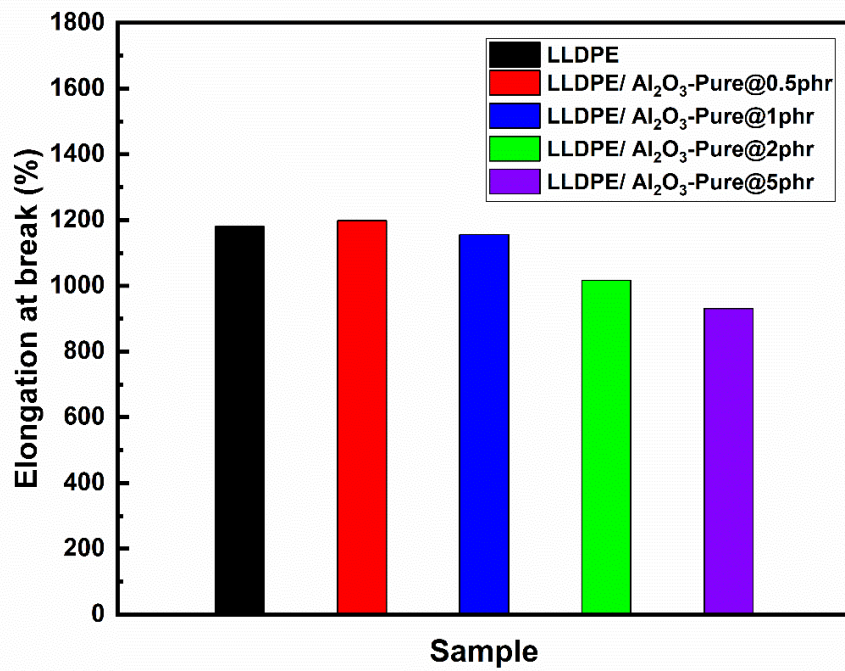
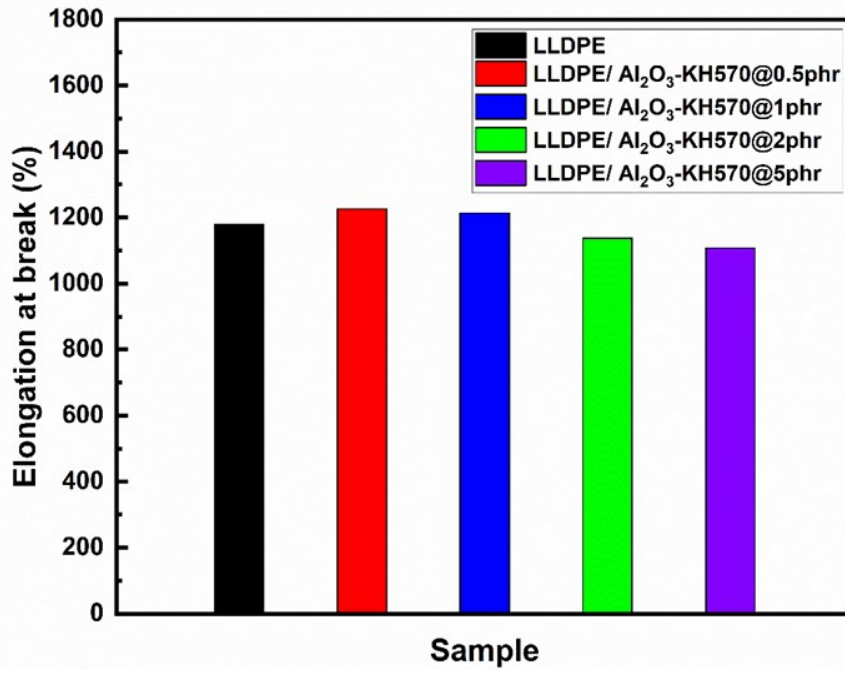


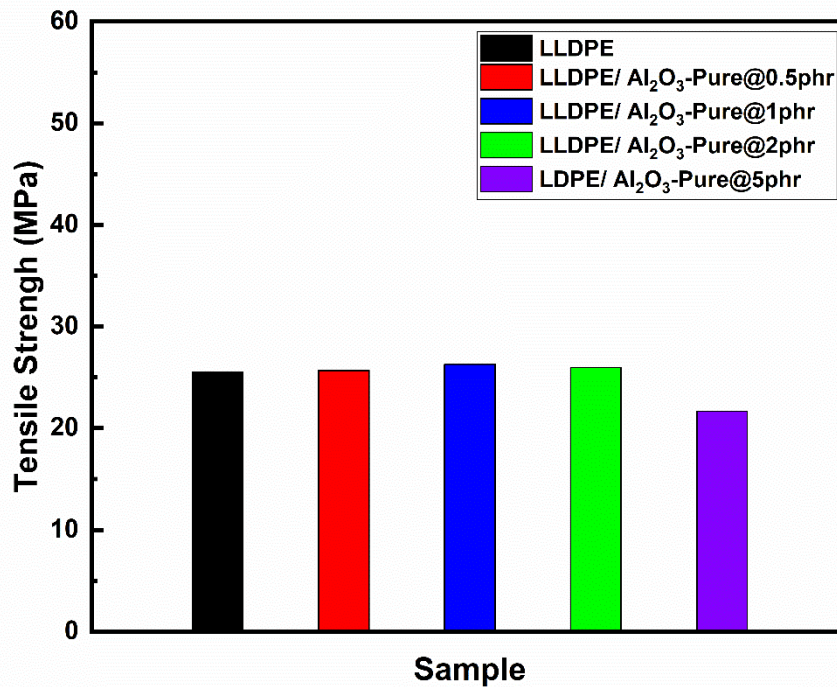
Figure 4.18 Strain- stress curves of PP nanocomposites



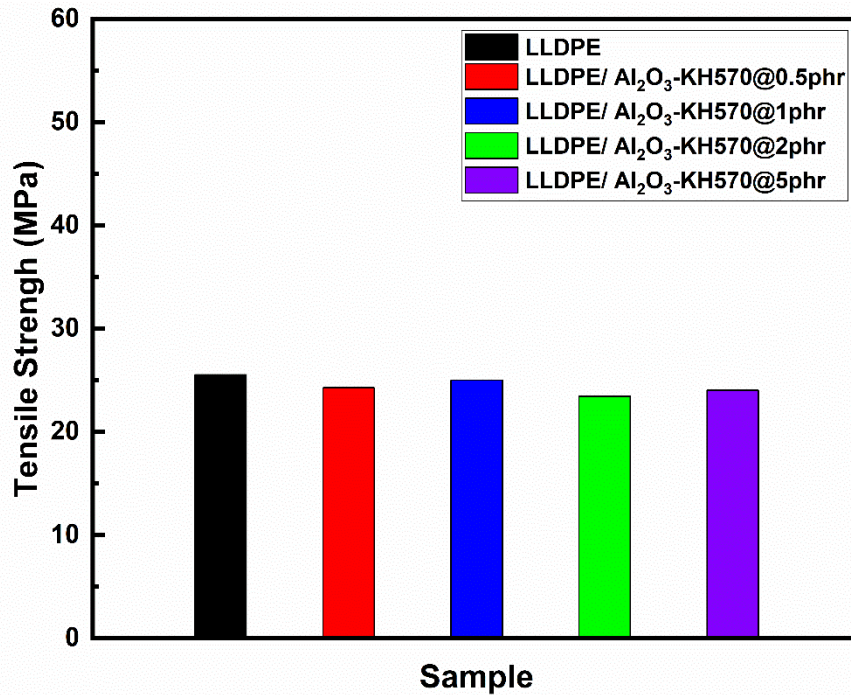


(b)

Figure 4.19 Elongation at break of PE nanocomposites containing (a) untreated alumina, (b) KH570-treated alumina.



(a)

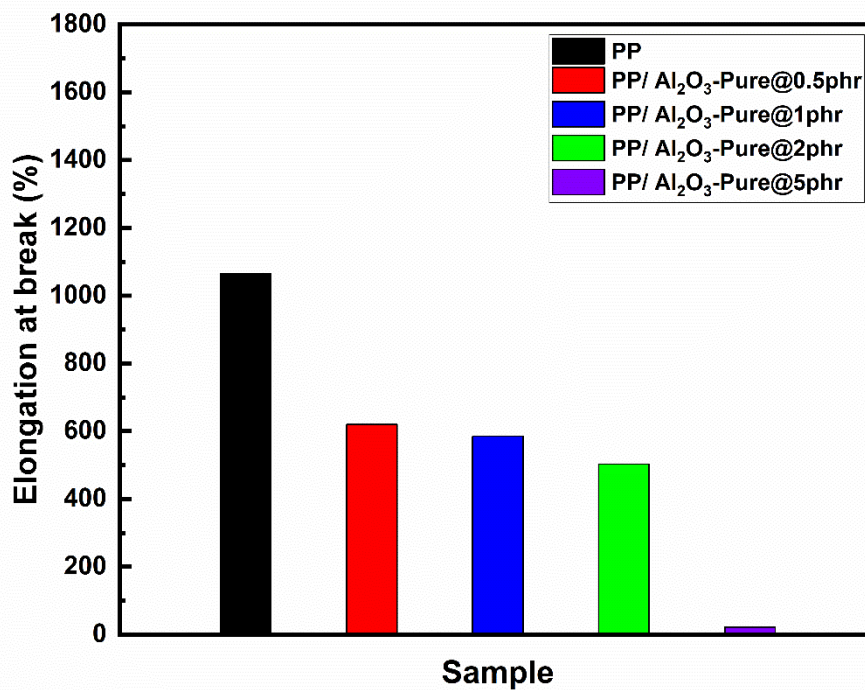


(b)

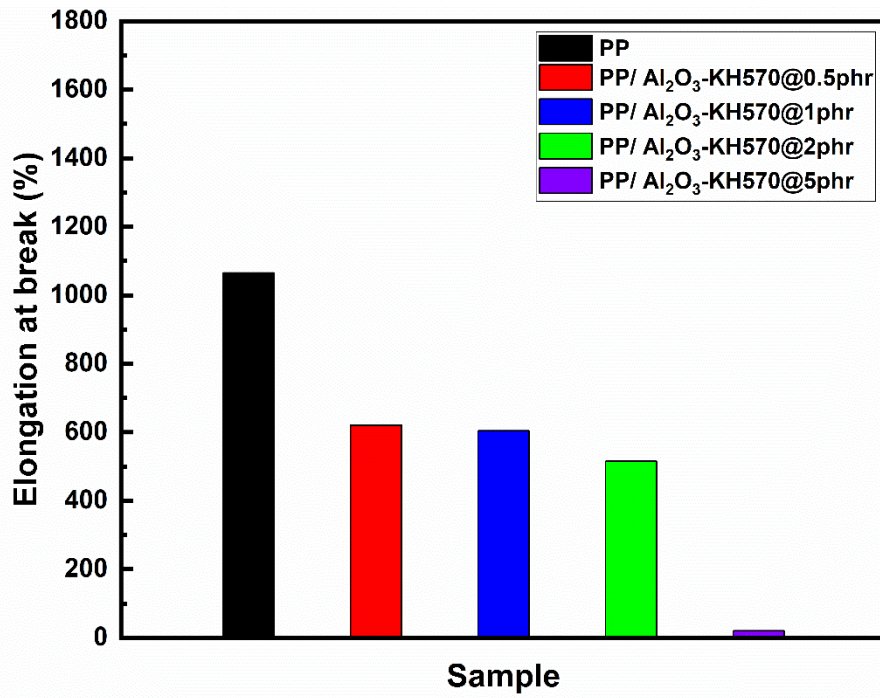
Figure 4.20 Tensile strength of PE nanocomposites containing (a) untreated alumina, (b) KH570-treated alumina.

The strain-stress curves of virgin PP and PP nano-Al₂O₃ composites are shown in Figure 4.18. All the PP samples show typical stress-strain of semi-crystalline polymers. The reversible deformation is found at small deformation for each sample and a sharp yield point is identified before the stable neck occurs. Then, another yield point takes place followed with the strain hardening and break. The effect of surface modification and filling content of nanoparticles on mechanical properties of composites is studied and obtained elongation at break and tensile strength are shown in Figure 4.21 and Figure 4.22. The elongation at break significantly reduces after introducing nanoparticles and it decreases as the filling content increases for both PP/Al₂O₃-Pure and PP/Al₂O₃-KH570 samples. The elongation at break is only about 20% for PP/Al₂O₃-KH570@5phr.

The degeneration of the elongation at break is due to the aggregation of nano-alumina particles with the filling content is increased, which results in the defects and local stress concentration in the interface between polymer and nanoparticles. Compared with the tensile strength of 42.9 MPa for virgin PP, the introduction of KH570-modified alumina nanoparticles in PP nanocomposites results in a slightly decreased tensile strength of about 35.3 MPa. A possible explanation for these results might be the introduction of nanoparticles disrupts the regularity of the original molecular arrangement and the nanoparticles act as defects during the tensile process, resulting in the decrease of the tensile strength. Compared with PE nanocomposites, PP nanocomposites have poor elongation at break but comparative tensile strength.

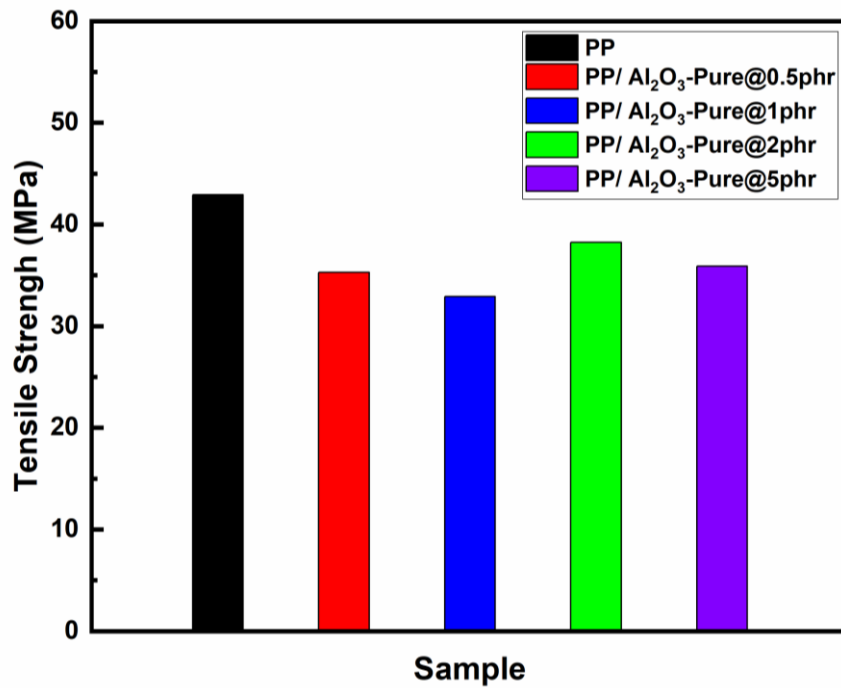


(a)

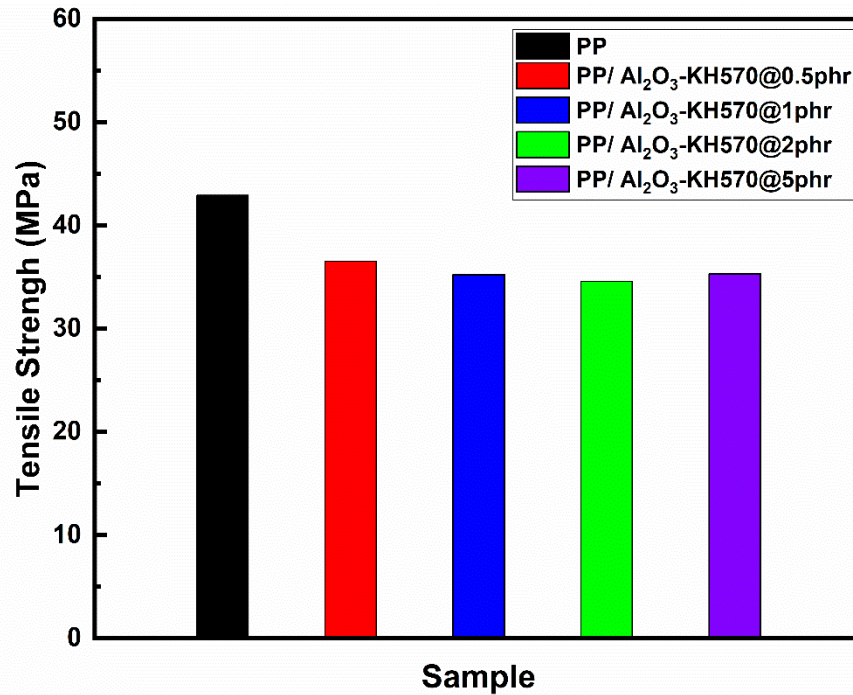


(b)

Figure 4.21 Elongation at break of PP nanocomposites containing (a) untreated alumina, (b)KH570-treated alumina.



(a)



(b)

Figure 4.22 Tensile strength of PP nanocomposites containing (a) untreated alumina, (b) KH570-treated alumina.

4.3 Summary

The weight changes upon the temperature of untreated and treated nano-alumina particles were characterized by using TGA and the additional weight loss at higher temperature of KH570-modified alumina suggested the loss of the organic groups introduced by the surface treatment. The change of chemical structure of the KH570-treated nano-alumina was also evaluated by FTIR spectroscopy. The presence of the C=O bond and the Si-O-CH₂CH₃ bond suggests that the addition of KH570 on the surface of alumina nanoparticles. Together with the TGA results, nano-alumina particles and KH570 coupling agents were successfully grafted on the surface of the

nano-alumina particles.

The size of spherulites of polymer and polymer nanocomposites was observed through polarized optical microscopy. Compared with virgin PE, PE nanocomposites show smaller spherulite size, but this conclusion is obtained based on qualitative analysis. For PP nanocomposites, the development of spherulites was significantly affected by the addition of nanoparticles. With the increasing filling content, the number of spherulites in PP nanocomposites increases and the size of the spherulite decreases. Upon surface modification, the size of the spherulite further decreases. The dispersion and the distribution of the nanoparticles in the nanocomposites was assessed by the analysis of SEM images. Without the surface modification, the size of the nanoparticles spanned a wide range. The size of the KH570-treated nanoparticles becomes smaller and the nano-alumina are well-distribution in nanocomposites. The surface modification can effectively reduce nanoparticle agglomeration.

Thermal properties such as melting point and crystallinity of nanocomposites were explored by using the DSC technique. For nanocomposites, the KH570-modified alumina particles can slightly increase the crystallinity of nanocomposites as the filling content increases. The melting point and the thickness of lamellae are similar for all the PE nanocomposites. As for PP nanocomposites, the introduction of nano-alumina slightly affects crystallization.

The addition of both untreated and KH570-treated nano-alumina does not have a

significant influence on the mechanical properties of PE nanocomposites. For PP nanocomposites, the inclusion of nano-alumina into polypropylene results in obvious degradation of the elongation at break and this phenomenon becomes more pronounced with the increasing filling content. To make it suitable for practical HVDC applications soon, more work on improving the mechanical properties of PP nanocomposites should be considered in the future.

Chapter 5 Dielectric Spectroscopy

5.1 Introduction

Dielectric spectroscopy is a useful tool to study the dielectric processes of new material.

When an external electric field is applied, the dielectric displacement of the material can be recorded as a function of frequency. Although the dielectric response is not a key parameter in designing DC cable insulation material, it can reveal the molecular change of the tested material.

When a dielectric material is applied with external electric field, the dielectric displacement will appear, resulting in the polarisation of the dielectric material. There are three most common mechanisms of dielectric polarisation: electronic polarisation, dipolar polarization, and ionic polarisation. Electronic polarization is caused by the movement of electrons around the atomic cores under an electric field in a material. It will lead to a dipole moment. The time to achieve a new equilibrium is named relaxation time. The characteristic time of electronic polarization is about 10^{-15} s. Dipolar polarization often occurs when a permanent dipole moment exists. The dipoles will be aligned by rearranging the position of molecules when an external electric field is applied, thus resulting in the polarization of the material. This polarisation usually takes about 10^{-2} to 10^{-10} s. As for ionic polarisation, it usually arises in ionic crystal elements. When there is an external electric field, the ions are displaced and the induced polarisation occurs. It often takes place at low frequency and contributes to the relative

permittivity of the material. It also has a quick relaxation time, which is about 10^{-13} s. When it comes to composite material with multiphase, the interfacial polarization, also known as space charge polarization, should be considered for polarisation analysis. It occurs when charge carriers accumulate around the interface such as the inner dielectric boundary and electrodes under an external electric field. The charges within the material are then separated in distance and lead to the dielectric loss tangent. This effect is also called Maxwell-Wagner-Sillars polarisation. The relationship between complex permittivity associated with different polarization types and the frequency is shown in Figure 5.1 [128].

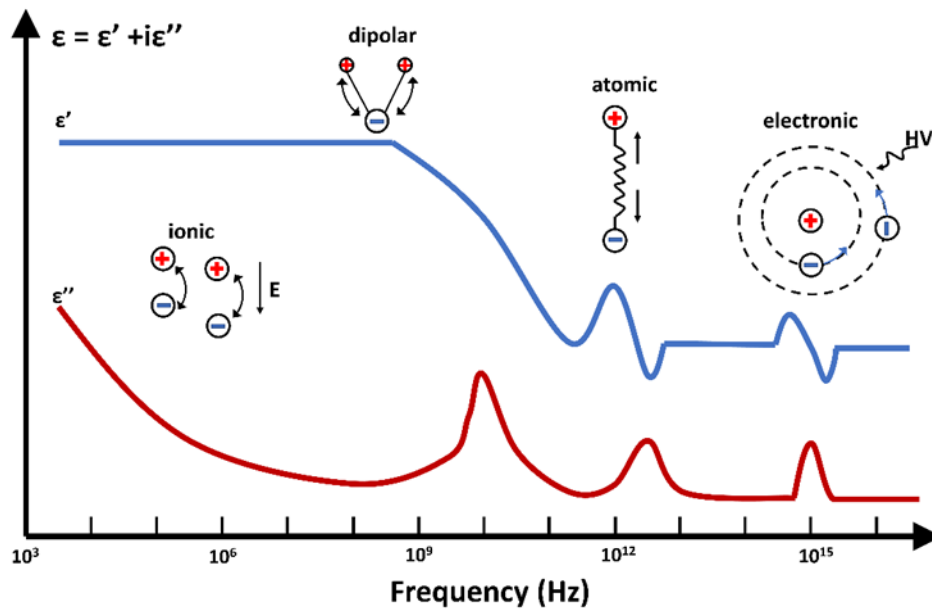


Figure 5.1 The relationship between frequency and complex permittivity with different polarization types (adapted from [128]).

The complex permittivity ϵ_c can be derived from Maxwell's equations as shown in Equations (5.1) and (5.2):

$$J = \sigma E \quad (5.1)$$

$$\nabla \times H = J + j\omega\epsilon E = (\sigma + j\omega\epsilon)E = j\omega(\epsilon - j\frac{\sigma}{\omega})E \quad (5.2)$$

where J is the current density, σ is the AC conductivity of the material, E is the electric field strength, H is the magnetic field strength, ω is the angular frequency of the electromagnetic wave and ϵ is the permittivity of the material. The complex permittivity then can be expressed as Equation (5.3):

$$\epsilon_c = \epsilon - j\frac{\sigma}{\omega} \equiv \epsilon' - j\epsilon'' \quad (5.3)$$

The real part of the complex permittivity is written as ϵ' , which describe the relationship between electric field E , and the electric flux density D of the material, shown as Equation(5.4):

$$D = \epsilon' E = \epsilon_0 \epsilon_r E \quad (5.4)$$

where ϵ_0 is the vacuum permittivity of 8.854×10^{-12} F/m and ϵ_r is the relative permittivity of the material, also known as the dielectric constant. The imaginary part of complex permittivity is written as ϵ'' and is relevant to the energy loss caused by dipole relaxation.

The dielectric loss tangent, $\tan \delta$, can be written as Equation (5.5):

$$\tan \delta = \frac{\epsilon''}{\epsilon'} \quad (5.5)$$

The testing frequency is set between 0.1 Hz and 1 MHz at room temperatures. Three samples of each kind of nanocomposites are tested and the average value is calculated as the result of dielectric permittivity. An example of the test samples is shown in Figure 5.2. The testing setup was introduced in Chapter 3. The effect of nanoparticles on nanocomposite material and the effect of surface modification on dielectric permittivity of nanocomposite are investigated and discussed in this chapter.

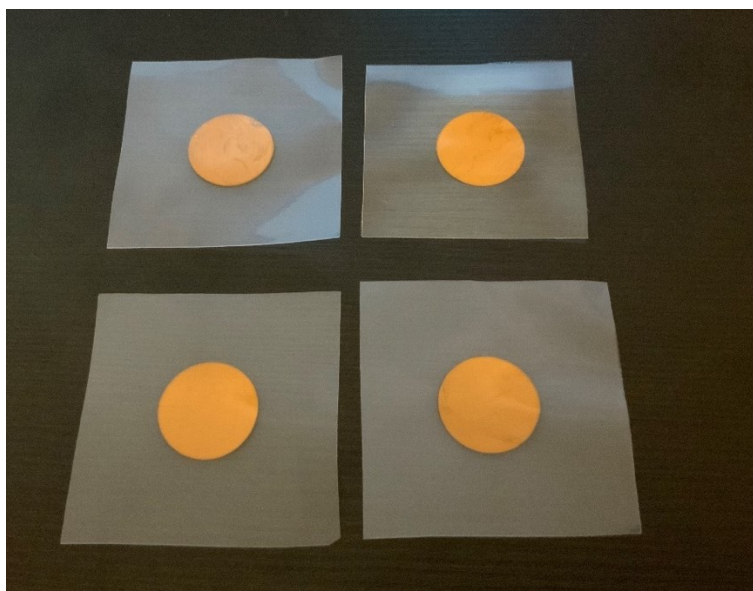


Figure 5.2 Thin film samples for dielectric spectroscopy.

5.2 Results and discussion

5.2.1 Measurement for PE Nanocomposites Containing Untreated Nano-alumina

For all composite samples, the dielectric constant and dielectric loss are dependent on the frequency and filling content of the nanoparticle. Figure 5.3 shows the dielectric constant of the permittivity for PE and PE/ untreated-alumina composites. The unfilled

PE has dielectric constant of 2.53 with a measured frequency from 0.1 Hz to 1 MHz. The difference between these results should be attributed to the poor dispersion and distribution of untreated nano alumina in PE nanocomposites, which has been shown in SEM results. The dielectric loss tangent of PE nanocomposites is shown in Figure 5.4. The dielectric loss tangent of unfilled PE is below 0.001 throughout the measured frequency range. The difference among unfilled PE, 0.5 phr and 1 phr nanocomposites is not significant. For 2 phr and 5 phr PE/ Al₂O₃-Pure samples, the dielectric loss increases as the frequency decreases with this behaviour being pronounced for PE/Al₂O₃-Pure@5phr sample. The phenomenon of the high dielectric loss at low frequency could be affected by the interfacial polarisation [129]–[132], which could be attributed to the charge build-up at the interfaces within the nanocomposite system.

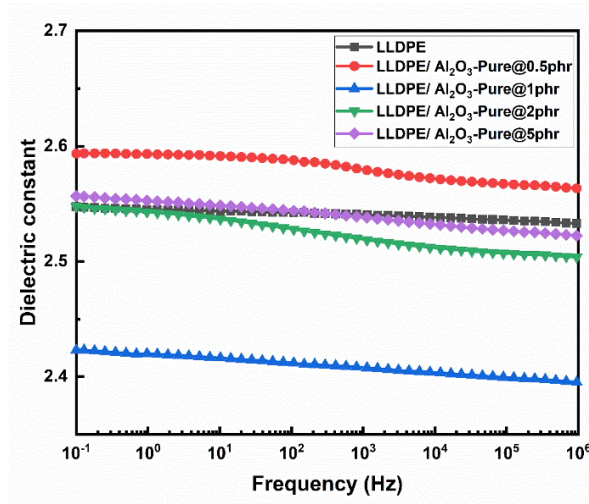


Figure 5.3 Dielectric constant of PE untreated-alumina nanocomposite.

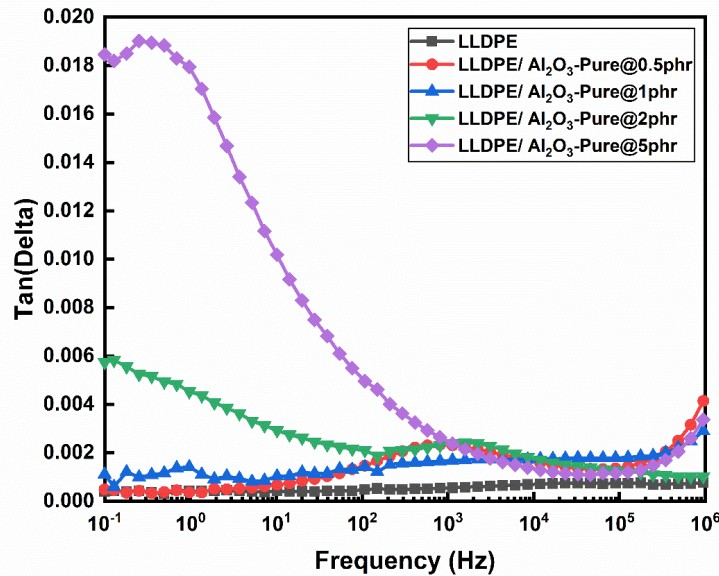


Figure 5.4 Dielectric loss tangent of PE untreated-alumina nanocomposite.

5.2.2 Measurement for PE Nanocomposites Containing KH570-treated Nano-alumina

The dielectric constant and dielectric loss of LDEP/ Al₂O₃-KH570 samples are shown in Figure 5.5 and Figure 5.6, respectively. The dielectric permittivity and dielectric loss of these samples are dependent both on the frequency and the filling percentage of nanoparticles. The dielectric constant of all samples slightly decreases with the increase of frequency and LDEP/ Al₂O₃-KH570@0.5 phr has the lowest value of dielectric constant. A slightly increase of dielectric constant is found as the amount of KH570-treated nano-Al₂O₃ increases. In Figure 5.6, the dielectric loss of PE samples containing KH570-treated nano-alumina shows similar trends throughout the measured frequency range. The dielectric loss of samples containing KH570-treated nano-alumina becomes less sensitive to the filling content compared with that of samples containing untreated

nano-alumina. This may be due to the modified surface state of nano-alumina particles. The surface of the untreated nano-alumina is principally characterised by the hydroxyl groups while the surface of the KH570-treated nano-alumina is principally characterized by the methacrylate groups. Compared with methacrylate groups, the hydroxyl groups and any bound water on the surface of nano-alumina are more sensitive to the external electric field.

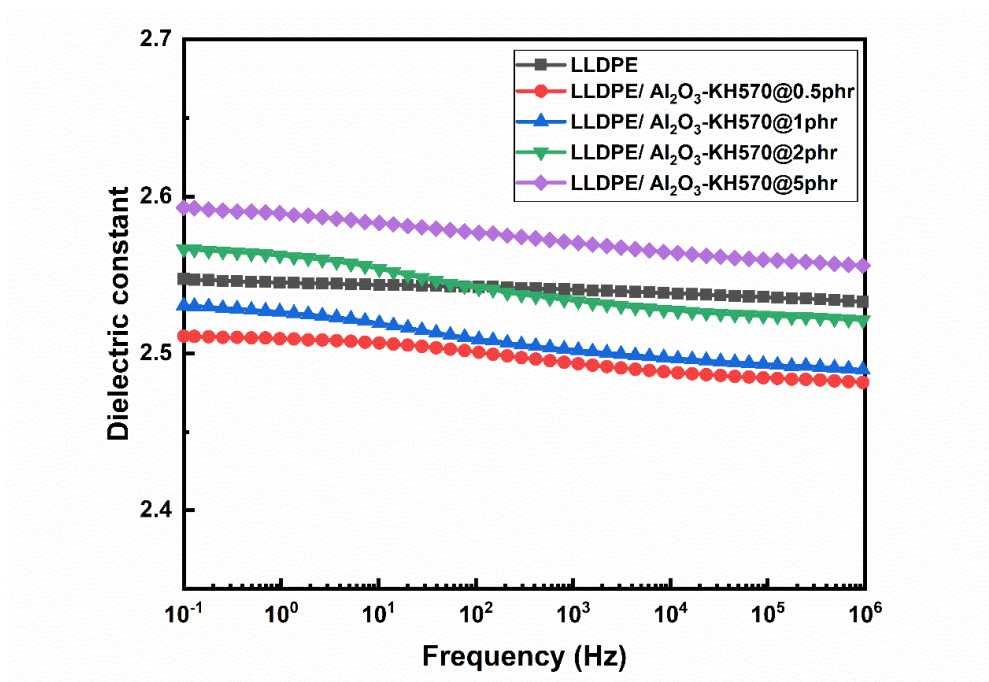


Figure 5.5 Dielectric constant of PE KH570-alumina nanocomposite.

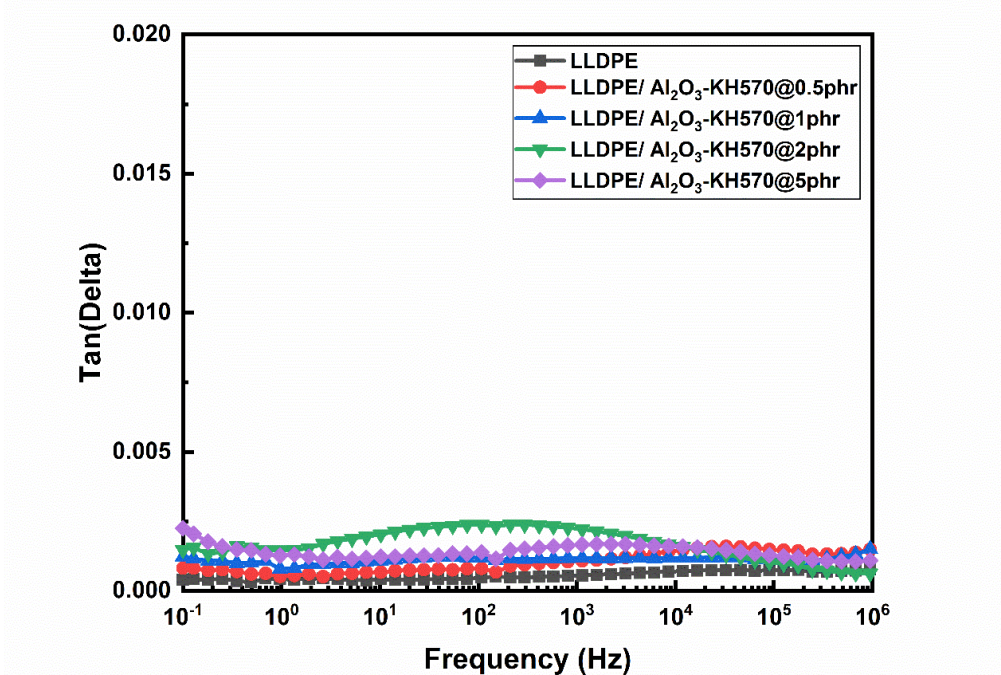


Figure 5.6 Dielectric loss tangent of PE KH570-alumina nanocomposite.

5.2.3 Measurement for PP Nanocomposites Containing Untreated Nano-alumina

Figure 5.7 shows the relationship between the dielectric constant of PP/Al₂O₃-Pure nanocomposites and the frequency. The dielectric constant of nanocomposites is slightly decreasing when the measurement frequency increases. There is no obvious difference between composite samples with no more than 2phr loading. The dielectric loss tangent of PP/untreated-alumina nanocomposites increases with the increase of filling content of nano-alumina, as displayed in Figure 5.8. All samples have approximately the same dielectric loss except the sample with 5 phr of nanoparticles. All the samples have a peak at the low frequency around 10 Hz and it should be caused by the interfacial polarization as discussed before.

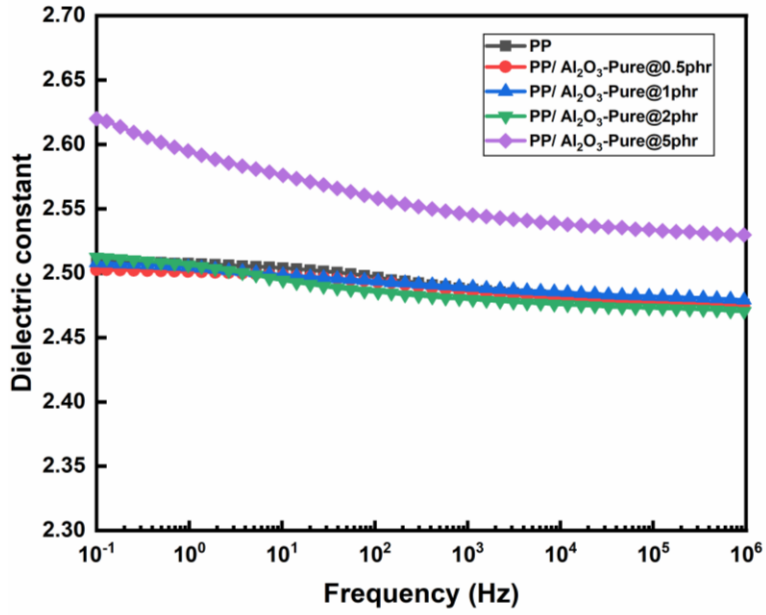


Figure 5.7 Dielectric constant of PP untreated-alumina nanocomposite.

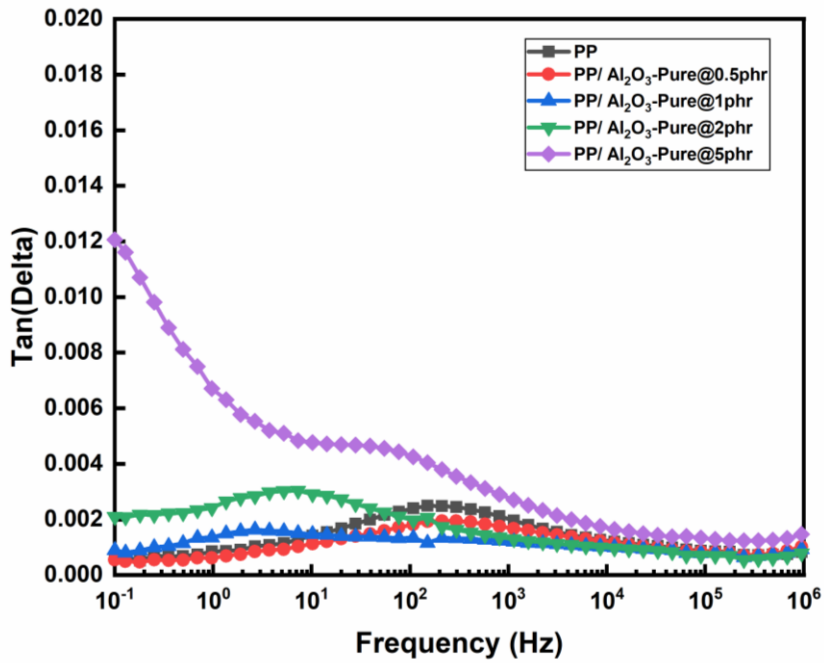


Figure 5.8 Dielectric loss tangent of PP untreated-alumina nanocomposite.

5.2.4 Measurement for PP Nanocomposites Containing KH570-treated Nano-alumina

The dielectric constant and dielectric loss tangent of PP nanocomposites containing KH570-treated alumina are shown in Figure 5.9 and Figure 5.10, respectively. For PP/Al₂O₃-KH570 samples, the dielectric constant does not appear to change with the increase of the filling content. It is noted that the changes are relatively small. The reason might be because the well-distributed nano-alumina particles within matrix PP impede the movement of the molecular chains, resulting in the limited influence on the dielectric constant. The loss tangent of PP/Al₂O₃-KH570 at different filling content stay at a stable level and a similar peak is found at low frequency level as the result of interfacial polarization.

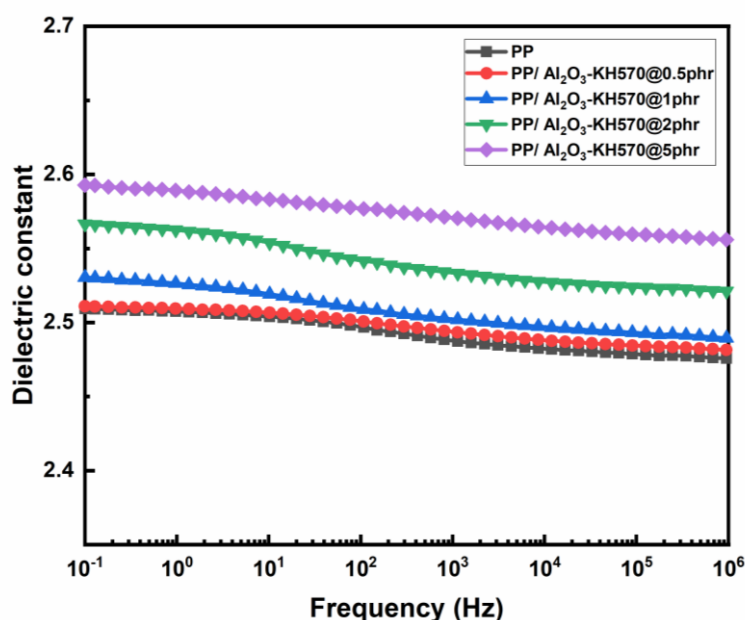


Figure 5.9 Dielectric constant of PP KH570-alumina nanocomposite.

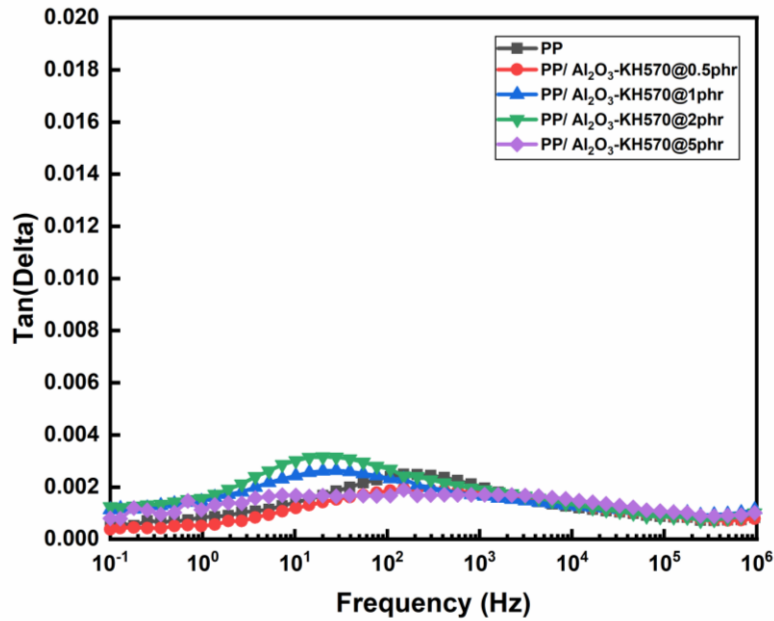


Figure 5.10 Dielectric loss tangent of PP KH570-alumina nanocomposite.

5.2.5 Discussion

The presented results summarize the dielectric response for PE and PP nanocomposites containing varying filling content of alumina and different surface conditions. For nanocomposite material, the change of dielectric response is affected by the interfacial relaxation, which is relevant to the interfacial polarization and the character of interfaces between the matrix polymer and nanoparticles. As discussed before, the interfacial polarization might occur at the interfacial region, resulting in the slight increment of the dielectric constant. However, the interaction between matrix polymer and nanoparticles could limit the movement of molecular chains thus suppress the polarisation. When the filling content increases, the agglomeration of nanoparticles becomes serious and the properties of the interface are then changed. It facilitates the

interfacial polarisation process, which will result in slightly higher dielectric loss and a wider span of the loss peak. The result is consistent with previous studies [55], [132], [133]. The dielectric response should be determined by recognizing the dominant factor. From the obtained results, the interfacial polarisation becomes predominant when the filling content is increasing.

Surface treatment of nanoparticles also plays an important role in determining the dielectric response of both PE and PP nanocomposites. It is believed that the functional groups on the surface of modified nano-alumina limit the movement of charges within nanocomposites, which then increase the permittivity [134], [135]. Unlike the composite samples containing the untreated nano-alumina particles, samples containing KH570-treated nano-alumina particles show different dielectric performances. The samples filled with KH570-treated nano-alumina have smaller variation in dielectric constant and reduced dielectric loss when comparing with nanocomposite filled with untreated alumina. The surface treatment of nanoparticle offset the polarisation caused by high filling content to some extent. The results show that it is possible to control the dielectric constant and dielectric loss of nanocomposites if the nanoparticles are with well surface modification. Besides, with surface treatment, the nanocomposites are less dependent on the frequency, which might be widely used in the electronics industry in the future.

5.3 Summary

In this chapter, the dielectric permittivity was firstly introduced. The dielectric response of PE/ alumina nanocomposites and PP/ alumina nanocomposites was presented. The effect of nanoparticles on dielectric spectroscopy was also discussed. For unfilled PE and PP, there is barely any change for their dielectric constant and loss. For PE composites containing untreated nano-alumina, the dielectric constant and dielectric loss are strongly affected by the filling content of the nanoparticles and testing frequency. However, this has changed after the nano-alumina particles were treated by silane coupling agent KH570. The dielectric loss remains at a low level throughout the frequency range. This could be attributed to the improved dispersion of nanoparticles. The dielectric constant of PP nanocomposites with varying filling content showed small variation throughout the tested frequency. But obvious loss peaks were observed for them. Surface treatment of nanoparticles weakened the effect of filling content on dielectric loss. Despite the differences in dielectric response of PE and PP nanocomposites, they are the result of a combination of the enhanced permittivity and the weakened polarisation around nanoparticles within nanocomposites. However, it is still not possible to fully explain the obtained results and the mechanism of the effect of nanoparticles on the dielectric response is still no consensus.

Chapter 6 DC Breakdown Strength

6.1 Introduction

In the design of insulating material for HVDC power cable insulation, DC breakdown strength is an important parameter to evaluate the dielectric properties of insulation material. Dielectric breakdown strength is the potential gradient at which breakdown occurs. It describes the ability of insulating material in resisting decomposition under electrical stress and is usually stated as voltage per unit thickness.

A number of researchers have proposed many theories to explain breakdown mechanisms from electrical, thermal, chemical and electrical aspects [75]. But now, it is still hard to determine the exact breakdown mechanism. Theoretically, the intrinsic breakdown strength is obtained for a perfect sample under ideal conditions. In other words, it is determined only by the physical characteristics of the material. However, it is very difficult to have a perfect sample in the laboratory as they are always with chemical impurities or defects at a microscopic level. Notably, the film samples with thinner thickness are still with fewer imperfections and samples with a thickness of around 100 μm are used to obtain the breakdown strength in this project.

In practice, the breakdown strength of insulating material is determined not only by its intrinsic properties but also extrinsic factors such as electrode type, voltage rate and environmental condition [136]. Therefore, the test method and electrode configuration must be carefully selected. There are two popular approaches to measure the breakdown

voltage. One is the constant-stress testing. A constant electric voltage is applied across the testing sample and the time required to cause breakdown is measured. Another one is progressive-stress testing. The testing voltage applied across the sample is a function of time. The magnitude of voltage is recorded when the breakdown happens. Surveys such as that conducted by Stone et al. and Dissado et al. [137] show that the variation of the results of progressive-stress testing is smaller than that of constant-stress testing. Additionally, the constant-stress testing always requires an extended period of time due to the critical field control while the progressive-stress testing can be completed within a reasonably short time. Consequently, the progressive-stress testing is preferred in this project and the testing setup was introduced in Chapter 3. The DC voltage applied across the sample is increased continuously at a uniform rate of 1 kV/s according to IEC Standard 60243 [136]. In the matter of electrode configuration, the electrodes used in this test is a pair of stainless-steel ball electrodes with the diameter of 20 mm. As the radius of curvature of the ball electrodes is much greater than the thickness of the testing sample, it is believed to produce a uniform stress between electrodes. Commonly, the breakdown strength analysis of solid insulation material can be achieved by using two-parameter Weibull distribution method according to IEEE Standard 930-2004. It is a kind of extreme value distribution in which the system fails when the weakest link fails. The function of the cumulative probability to failure for the two-parameter Weibull is in Equation (6.1):

$$F(E) = 1 - \exp\left[-\left(\frac{E}{\alpha}\right)^\beta\right] \quad (6.1)$$

where E is the measured DC breakdown strength; $F(E)$ is the probability of failure under breakdown strength E ; α is the scale parameter, describing the characteristic breakdown strength which has 63.2% probability to breakdown; β is the shape parameter, describing the discreteness of the breakdown data. The approximation for the most likely probability of failure is calculated according to the method reported by Ross[138], shown as Equation (6.2):

$$F(E) = \frac{i - 0.44}{n + 0.25} \times 100\% \quad (6.2)$$

where i is the i -th of breakdown strength when the breakdown strength results are ordered in ascending order and n is the total number of breakdown tests, 20 times is believed to deliver a reliable breakdown strength result. In this study, $n=20$. In Minitab software, all the obtained breakdown data are listed in ascending order and the corresponding cumulative probability is assigned to each result. A fitted line is calculated based on the Maximum Likelihood Estimation theory with 95% confidence interval. The α and β parameters are also provided for further analysis.

Figure 6.1 shows the example plot of the Weibull distribution. The Equation (6.1) can be transformed in to Equation (6.3) given by :

$$\log\left[-\ln(1 - F(E))\right] = \beta \log E - \beta \log \alpha \quad (6.3)$$

It is an equation of a straight line. The slope β of the line is a measurement of the spread

of the Weibull distribution. The larger the value of β , the smaller is the variation of the experimental DC breakdown strength data. The vertical scale $\log[-\ln(1-F(E))]$ is a non-linear function of the probability of occurrence of the breakdown. The horizontal scale $\log E$ is the logarithm of the measured breakdown strength. The intercept $-\beta \log \alpha$ can be used to identify the characteristic breakdown strength at which point that 62.3% of the sample fails. The plot based on the Equation(6.3) is completed by using Origin software.

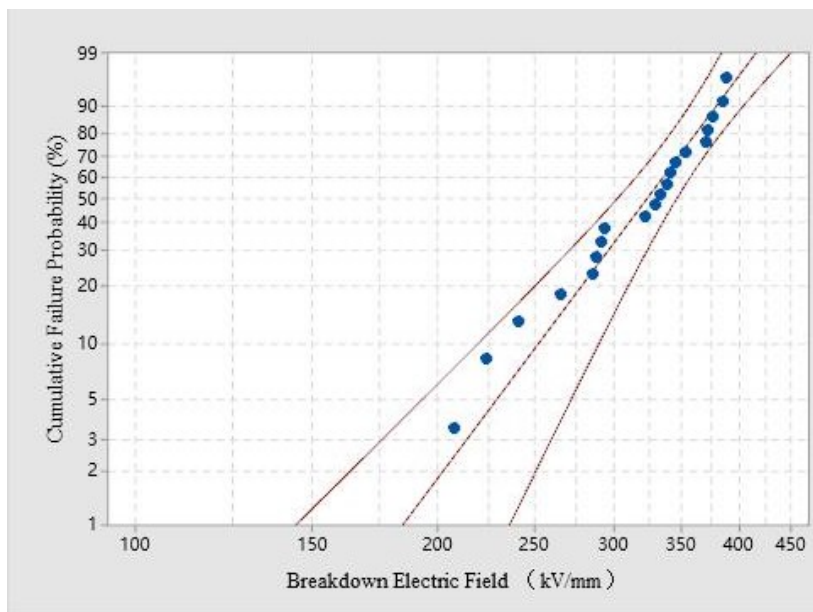


Figure 6.1 Example plot of Weibull distribution.

In this chapter, the electric strength of PE nanocomposites and PP nanocomposites are presented and discussed. Sample preparation and test setup have already been introduced in Chapter 3. Previous studies [139]–[142] have shown that polymer nanocomposites show higher dielectric breakdown strength than virgin polymer.

However, some opposite results have also been reported in [143]–[146]. The main objective of this chapter is to study the effect of filling content and surface treatment of nano-alumina on the breakdown strength of PE and PP nanocomposites and analyze the possible breakdown mechanisms of polymer nanocomposite.

6.2 Results and Discussion

6.2.1 Results of PE and PE Nanocomposites

The DC breakdown results of unfilled PE and PE composites containing untreated nano-alumina with varying filling content are shown in Figure 6.2. The critical parameters of the Weibull distribution of these samples are summarized in Table 6.1. The DC breakdown strength of unfilled PE is about 339.7 kV/mm. Only the PE nanocomposite sample with 0.5 phr of untreated alumina has shown improved dielectric strength, 352.6 kV/m, which is about 3.7% higher than that of unfilled PE. However, the slight enhancement of DC breakdown is within the uncertainty of Weibull distribution. The sample with the addition of untreated nano-alumina of 1 phr has comparable DC breakdown strength as the unfilled PE. With further growth of the filling content, the DC breakdown strength continuously decreases. Especially when 5 phr untreated nano-alumina is added into PE, a marked decline of 43.8 kV/mm in DC breakdown strength is noticed, which is about 12.9% lower than that of unfilled PE.

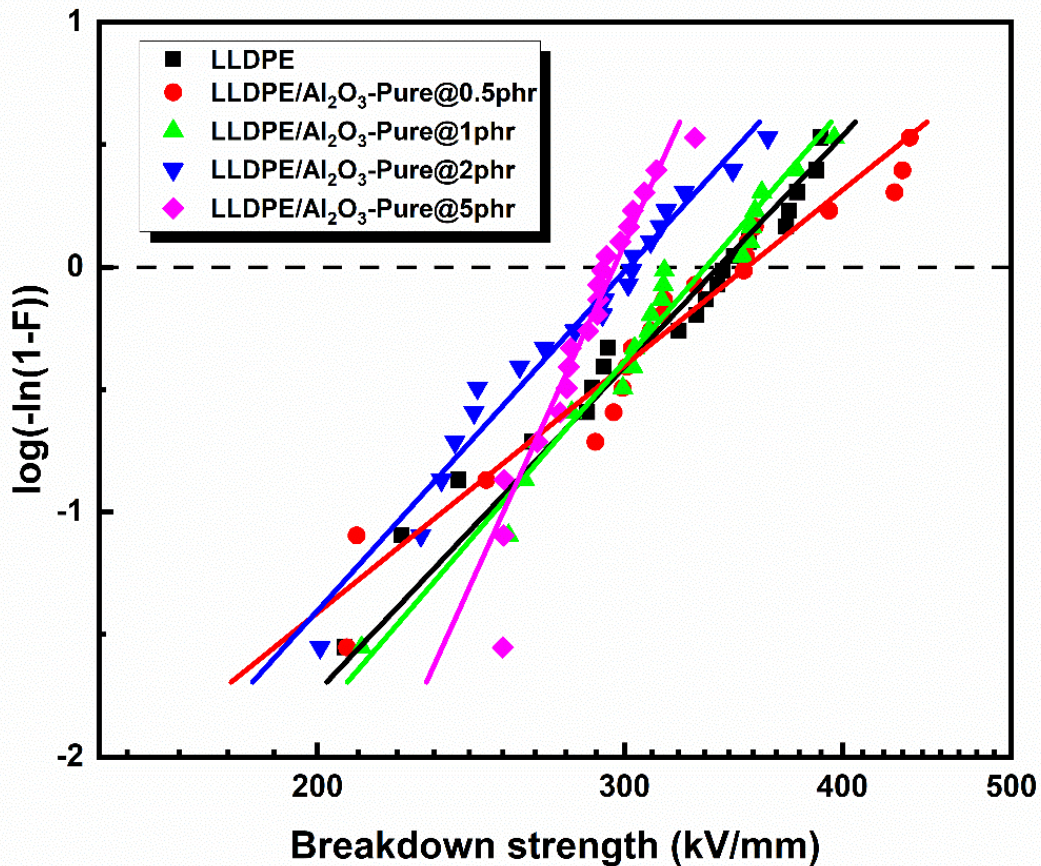


Figure 6.2 Weibull plots of DC breakdown strength of PE untreated-alumina nanocomposites.

After conducting the surface treatment of nano-Al₂O₃, the DC breakdown strength of PE nanocomposites containing the KH570-treated nano-Al₂O₃ is higher than that of unfilled PE, as shown in Figure 6.3. The characteristic DC breakdown strength and the shape parameter are listed in Table 6.2. PE composite containing 0.5 phr of KH570-treated nano- alumina shows the maximum DC breakdown strength of 394.6 kV/mm, which is 16.2% higher than that of unfilled PE. But as the filling content continuously increases up to 5 phr, the DC breakdown strength is gradually decreasing. Remarkably, the PE composite sample with 5 phr of KH570-treated nano-alumina has almost the

same DC breakdown strength of unfilled PE. Additionally, the shape parameter of samples with surface-modified nanoparticles is larger than that of the samples with untreated nanoparticles. As mentioned before, a larger shape parameter means, the smaller variation across the data set. This can also be observed in Figure 6.2 and Figure 6.3. Taken together, surface treatment of nano-alumina has improved the DC breakdown strength of PE nanocomposites.

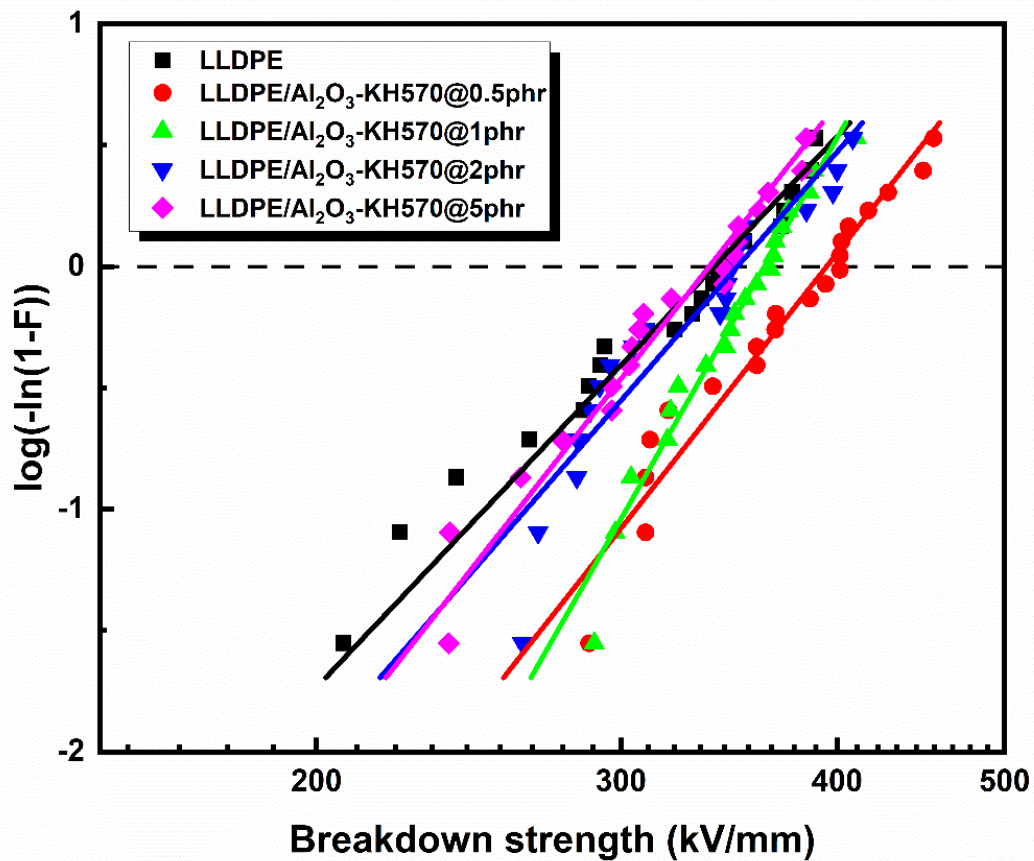


Figure 6.3 Weibull plots of DC breakdown strength of PE/KH570-alumina nanocomposites.

Table 6.1 Parameters of Weibull plots of PE nanocomposites.

Sample	α (kV/mm)	β
PE	339.7	7.54
PE/ Al ₂ O ₃ -Pure @0.5phr	352.6	5.73
PE/ Al ₂ O ₃ -Pure @1phr	334.1	8.24
PE/ Al ₂ O ₃ -Pure @2phr	301.5	7.87
PE/ Al ₂ O ₃ -Pure @5phr	295.9	9.74
PE/Al ₂ O ₃ -KH570 @0.5phr	394.6	9.07
PE/ Al ₂ O ₃ -KH570 @1phr	363.1	12.57
PE/ Al ₂ O ₃ -KH570 @2phr	350.3	8.20
PE/ Al ₂ O ₃ -KH570 @5phr	337.4	9.96

6.2.2 Results of PP and PP Nanocomposites

The DC breakdown results of unfilled PP and PP composites containing untreated nano-alumina with 0.5 phr, 1 phr, 2 phr and 5 phr filling content are showed in Figure 6.4. The obtained critical parameters of the Weibull distribution are also presented in Table 6.2. The DC breakdown strength of unfilled PP is 429.1 kV/mm. After introducing the untreated nano-alumina, the DC breakdown strength of PP composites reduces. The breakdown strength of PP/untreated nano-alumina with 0.5 phr loading is comparable with that of unfilled PP but with poor distribution. The addition of 1 phr of untreated nano-alumina reduces the DC breakdown strength to 406.9 kV/mm, which is 5.2% lower than unfilled PP. The minimum DC breakdown strength is 295.9 kV/mm when 5 phr of untreated nano-alumina is added into PP. It is 31.8% lower than that of the unfilled PP sample. Generally, the shape parameter also becomes smaller as the filling content increases.

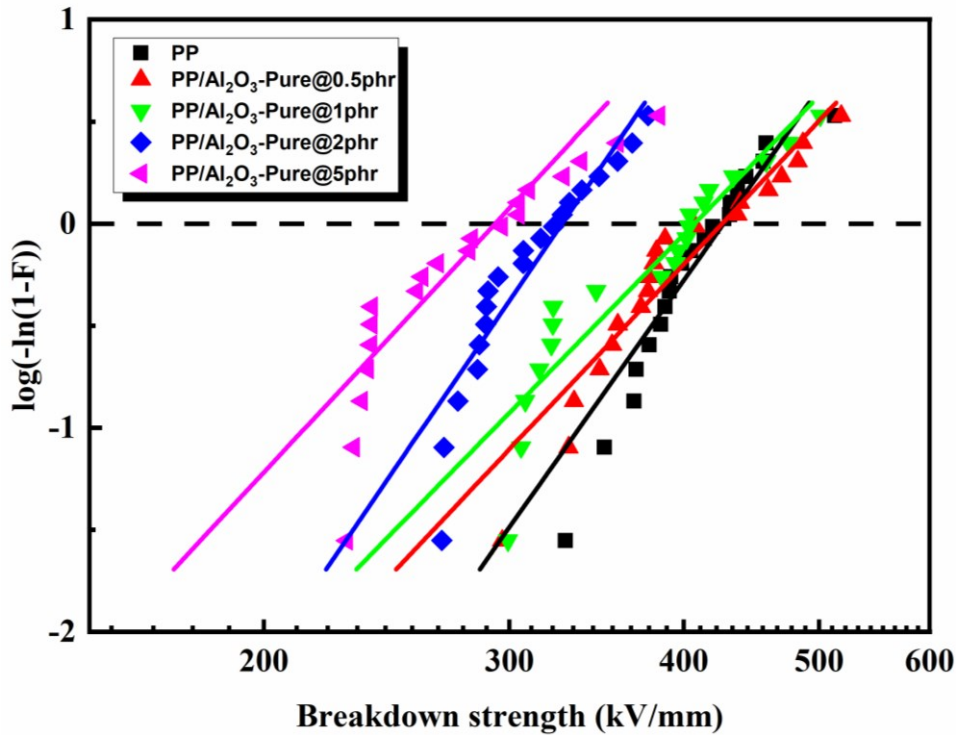


Figure 6.4 Weibull plots of DC breakdown strength of PP untreated-alumina nanocomposites.

When speaking about the PP nanocomposites filled with KH570-treated nano-alumina, the DC breakdown strength is significantly improved compared with the PP nanocomposites filled with untreated nano-alumina. The distribution plots are illustrated in Figure 6.5 and the key parameters are listed in Table 6.2. The DC breakdown strength increases along with the increasing filling content when it is no more than 1 phr. The DC breakdown strength reaches its maximum value of 491.0 kV/mm, which is 14.4% higher than that of unfilled PP. With further increase of KH570-treated nano-alumina up to 5 phr, the DC breakdown strength of PP nanocomposite starts to decrease. The DC breakdown strength of the PP composite

sample containing 5 phr of KH570-treated nano-alumina is 392.4 kV/mm, 8.6% smaller than that of unfilled PP. Despite the changing breakdown strength, the shape parameter for all the samples are higher, suggesting that surface treatment of nano-alumina has a significant effect in enhancing the DC breakdown strength of PP nanocomposites.

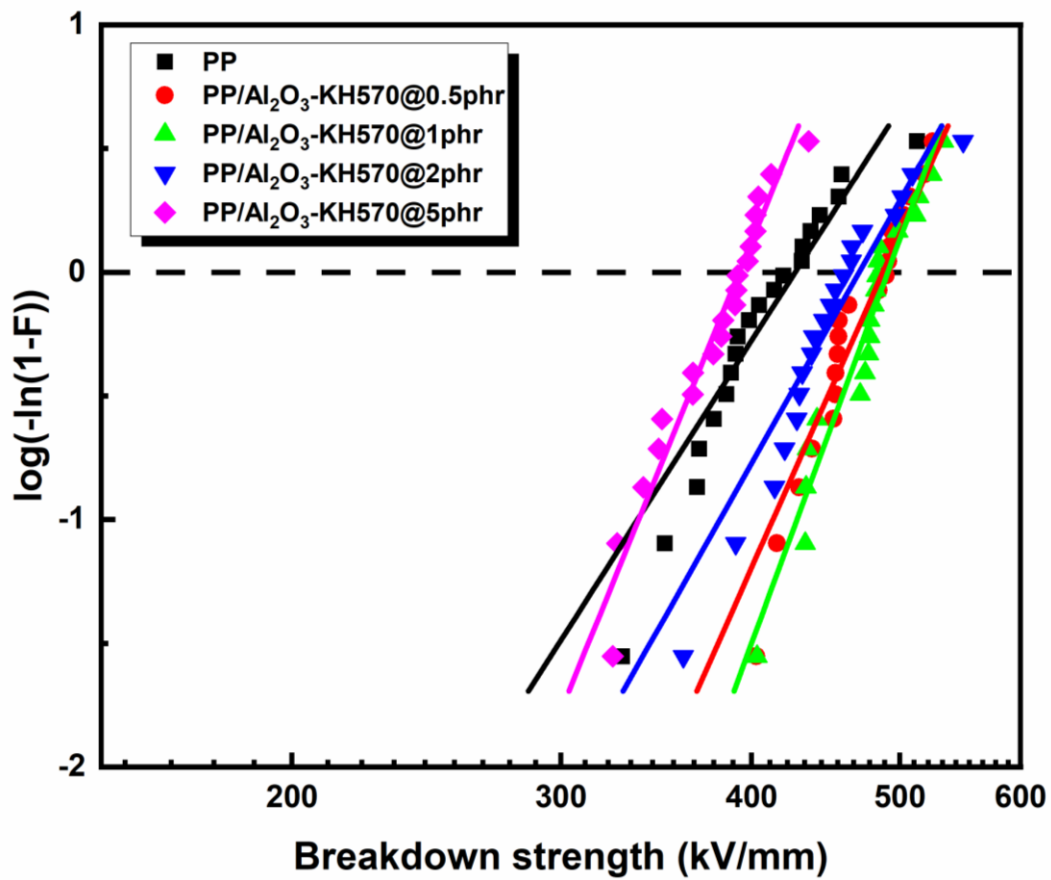


Figure 6.5 Weibull plots of DC breakdown strength of PE/KH570-alumina nanocomposites.

Table 6.2 Parameters of Weibull plots of PP nanocomposites.

Sample	α (kV/mm)	β
PP	429.1	9.90
PP/ Al ₂ O ₃ -Pure @0.5phr	426.0	7.25
PP/ Al ₂ O ₃ -Pure @1phr	406.9	6.99
PP/ Al ₂ O ₃ -Pure @2phr	327.1	10.01
PP/ Al ₂ O ₃ -Pure @5phr	292.9	7.35
PP/ Al ₂ O ₃ -KH570 @0.5phr	484.4	16.16
PP/ Al ₂ O ₃ -KH570 @1phr	491.0	16.81
PP/ Al ₂ O ₃ -KH570 @2phr	470.4	10.95
PP/ Al ₂ O ₃ -KH570 @5phr	392.4	15.19

6.2.3 Discussion

From the presented results, the introduction of nano-alumina has noticeable effect on improving the DC breakdown performance for both PE and PP nanocomposite. The comparison between nano-alumina composites against filling content is shown in Figure 6.6. According to the results, the DC breakdown strength of nanocomposites is strongly affected by the filling content and nanoparticle surface treatment.

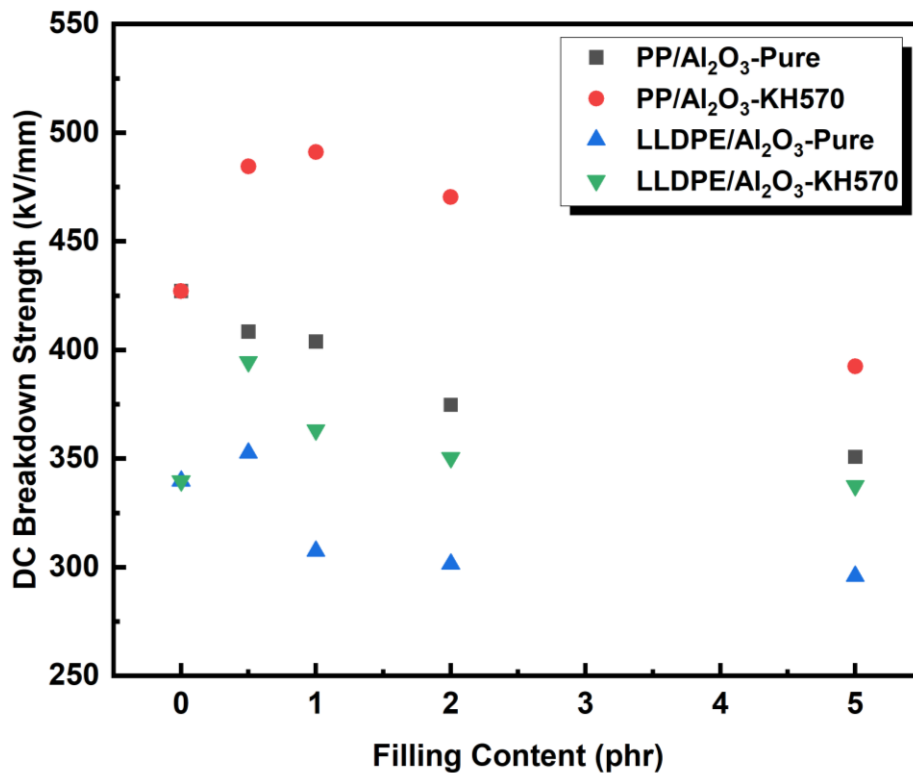


Figure 6.6 Comparison of DC breakdown strength among different nanocomposite systems.

From the literature review, it is commonly believed that an electronic process usually occurs in short time electrical breakdown. The density of free electrons and the energy they can gain are the main factors in this process [43], [77]. The electrons are from the impurity emission and electrode injection. When an external electric field is applied, the free electrons can gain energy from the electric field and be accelerated, resulting in the ionization of macromolecules and the initiation of electron avalanche. Then, the local discharge takes place in the material and leads to formation of the conducting channels and the final breakdown. But for polymeric material, the electron avalanches are unlikely to happen as the free path length of electron is short in polymer and the

injected electron from the electrons are easily trapped in the traps. So, the formation of breakdown in polymers are attributed to voids or low density region. The large voids can be formed during manufacture by impurities and additives' decomposition, or by evaporation of decomposition products in different chemical reactions induced by hot electrons and electron and hole recombination, or by the interface defect at the large spherulite boundary, etc.. In other words, the electrical breakdown would benefit from the decrement of the free electron density, carrier mobility and voids and defects [147].

PE nanocomposites containing untreated alumina and PE nanocomposites containing KH570-treated alumina have shown a similar trend of DC breakdown strength when the filling content is increasing. Generally, introduction of nanoparticles creates more interfacial areas between nanoparticles and base material due to the large specific surface area of the nanoparticles. The interface can introduce large amount of the charge traps within the composite [95], [118], [147], [148]. At a low filling level, the homocharges are likely to be trapped in the vicinity of the electrode by nano-alumina particles under a high electric field. Thus, further charge injection from the electrodes is then reduced, resulting in an increase in DC breakdown strength [82], [149], [150]. Moreover, the nanoparticles suppress the conduction current by reducing the local field of electrodes. Therefore, the breakdown is probably difficult to happen. The electrical breakdown strength is then improved. Therefore, the interaction area between matrix material and nanoparticles is critical. A novel barrier model is proposed by S.T. Li et al. [43], [151], [152] to explain the relationship between DC breakdown strength and

filling content. When the filling content is low, nanoparticles are well-distributed within composite and the interfacial regions are isolated from each other. At the same time, charge carriers collide with the traps generated by the nanoparticles and consume the energy gained from the applied electric field. Hence, a higher electric field is required to accelerate the electrons to cause a breakdown. But with the increasing filling content, the interfacial regions start overlapping. A possible conductive path is formed for charge carrier transportation. The charge carrier mobility under the DC electric field is then increased, which decreases the DC breakdown strength.

The breakdown strength of PE nanocomposites containing KH570-treated alumina is always higher than that of PE nanocomposites containing the same amount of untreated alumina. This also evidently shows the importance of nanoparticle surface treatment on the enhancement of DC breakdown strength. The reason might be the untreated nano alumina particles show relatively poor distribution in the polymer matrix and large agglomerations of nanoparticles is found in Figure 4.10. In addition, the weak adhesion between the untreated nano-alumina and the PE matrix results in the formation of voids on the fracture of the nanocomposites. When external electric field is applied, these agglomerations and voids act as defects and that lead to distortion of electric field. Local partial discharge take places around the defects and the premature electrical breakdown occurs.

The agglomeration of nanoparticles might be the main reason for reduced breakdown

strength when the filling content is increased. These nanoparticles can be treated as impurities and defects for matrix polymer. The imperfections of structure could result in the charge accumulation within nanocomposite. Previous studies have revealed this is a potential link between space charge accumulation and DC breakdown strength [154], [155]. The poor distribution of nanoparticles in nanocomposite can lead to more free volume to develop space charge under high DC field. For this reason, the DC breakdown strength of nanocomposites is reduced. From the SEM images shown in Chapter 4, it is clear that the untreated nano-alumina nanoparticles exhibit poor distribution in matrix PE with large clusters. Additionally, the poor adhesion between PE and untreated nano-alumina particles is also confirmed by the observation of the voids on the fracture surface. These clusters and voids are weak points and act as defects under the electric field, which has a negative impact on the DC breakdown strength [153], [154]. Clusters and voids have weaker bonding between their atoms or molecules, which make them prone to deformation and failure under electrical stress. When an electric field is applied to the material, the molecules in the clusters and voids experience a stronger stress than the rest of the material due to their weaker bonding. This causes these weak points to break down more easily, leading to the formation of defects such as microcracks, which can in turn lead to partial discharge or even electrical breakdown. After conducting surface treatment by using KH570, particles within PE are well distributed in a smaller size and the agglomeration is barely observed. As a result, the DC breakdown strength of PE nanocomposite containing KH570-

treated nano-alumina is higher than that of PE nanocomposite containing untreated nano-alumina with the same filling content. Moreover, all nanocomposites containing less than 5 phr KH570-treated nano-alumina have higher DC breakdown strength than unfilled PE. Similar results are also found for PP nanocomposites, as showed in Figure 6.6. Such reason is also adequate in explaining the DC breakdown strength improvement of PP composites containing surfaced-treated nanoparticles. Similar results are also reported in [35], [144], [152], [153].

The morphology of nanocomposites seems to affect the DC breakdown strength. The POM results have confirmed that the spherulite size reduces as the filling content of nano-alumina increases for both PE and PP nanocomposites. The total length of the channel the breakdown must form is one of the determining factors influencing DC breakdown strength. The conducting channel for DC breakdown follows the interface between rather than through the nanoparticles. When nanoparticles are surface-treated and the filling content is appropriate, the agglomeration barely exists, indicating the alumina nanoparticles are well distributed within the matrix polymer. Before the intrinsic breakdown happens, a local breakdown may exist between each individual particle and base polymer. However, due to the small size of nanoparticles and reduced spherulite size, the total length of the breakdown path increases, which enhances the breakdown strength of the composite system [155], [156]. However, this may not be the dominant factor in deciding the DC breakdown strength.

In summary, the addition of surfaced-treated nano-alumina improves the DC breakdown strength of PE nanocomposites and PP nanocomposites. But the exact mechanisms are still not fully clear yet and some possible explanations are discussed as above.

6.3 Summary

In this chapter, the DC breakdown strength of PE/ alumina nanocomposites and PP/ alumina nanocomposites was investigated. Compared with the unfilled PE, unfilled PP has higher DC breakdown strength. In addition, PP/alumina nanocomposite shows higher breakdown strength than PE/alumina nanocomposite when they have the equivalent amount of nano-alumina.

The effect of nano-alumina filling content on DC breakdown strength was also studied. For each type of polymer nanocomposite, DC breakdown strength firstly increase and then decreases when the filling content is rising. In addition, surface treatment of nanoparticles and the filling concentration play an important role in the DC breakdown performance of nanocomposites. All optimal results of DC breakdown strength in various nanocomposites were all found at a low filling level. Sample PE/Al₂O₃-KH570 @0.5phr has 16.2% higher DC breakdown strength than unfilled PE. Sample PP/ Al₂O₃-KH570 @1phr has 14.4% higher DC breakdown strength than unfilled PP. This is mainly due to the good dispersion and distribution of nano-alumina within the base polymer at low filling content, which is achieved by nanoparticle surface treatment.

High filling content may lead to agglomeration of nanoparticles and it is the source of the structural imperfections of the nanocomposite material.

For a nanocomposite system with the same matrix polymer, the nanocomposite sample filled with KH570-treated alumina consistently exhibits higher DC breakdown strength compared with the nanocomposite sample filled with untreated alumina when the filling level is the same. Such observation is related to the effect of surface treatment on improving the dispersion of nanoparticles and amending the interphase area between matrix polymer and nano-alumina particles. Less agglomeration of nanoparticles and improved adhesion between matrix and nanoparticle are observed in Chapter 4. There are fewer defects and free volume to allow space charge development. Thus, a higher DC breakdown strength is measured when the sample is filled with modified nanoparticles. However, it is still hard to identify the exact DC breakdown mechanism in nanocomposite system as it might be a complex result of thermal, chemical and electrical mechanisms.

Chapter 7 Space Charge Measurement and Trap Characterization

7.1 Introduction

Space charge has become the most critical factor in constraining the development of HVDC polymeric power cables. It results in the severe distortion of the electric field within the insulation material, which then could lead to local enhancement of the electric field. The consequent result would be the degradation and premature breakdown of the electrical insulation. Previous studies have revealed that the incorporation of nanoparticles can suppress space charge accumulation and electric field distortion of polymeric insulation material [60]. It is believed the traps generated in nanocomposites are tightly linked with these changes [149], [157]–[159]. But the exact mechanism of how the nanoparticle suppresses the space charge is still not clear. In this chapter, the space charge profiles of LDPE nanocomposite and PP nanocomposite are investigated. As the space charge is tightly linked with the charge transportation in the polymeric material, the trap information of nanocomposite is characterized. The effect of nanoparticles on the trap distribution in nanocomposites are also discussed.

7.2 Space Charge Formation and PEA System

The space charge is formed when there is a difference between the charge injection rate and the charge dissipation rate under the electric field. Over the past decades, many studies have been carried out on the characterization and the suppression of space charge. According to Lewiner [160], there are three major space charge accumulation scenarios, as displayed in Figure 7.1.

Under the first scenario, the dipoles are oriented under electric field and space charge occurs around both electrodes.

Under the second scenario, heterocharge is formed due to the migration of ions under an electric field. The positive charges move to the negative electrode and the negative charges to the positive electrode inside the insulation. The mobility of different charges is different. As a result, a global positive space charge peak near the negative electrode and a global negative space charge peak near the positive electrode is observed.

Under the third scenario, the homocharges are formed near the electrodes. When the mobility of charge is low, the charges injected from the electrodes will accumulate around the electrode with the same polarity. In other words, positive charges accumulate near the positive electrode and negative charges accumulate near the negative electrode.

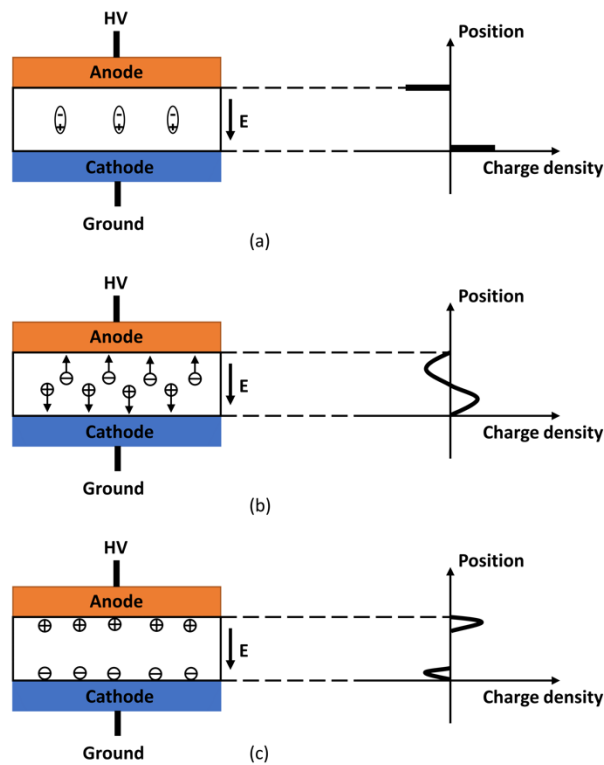


Figure 7.1 Development of space charge in dielectric material under an electric field due to (a) dipole orientation, (b) migration of ions, (c) charge injection at interfaces between dielectric and electrodes.

Many works have been done to suppress the space charge accumulation in polymeric insulating material. The space charge at the interface is usually suppressed by inserting a functional interlayer, such as PVF [100], PET [101] and FEP [102], between polymer and electrodes. As for the bulk space charge accumulation, it could be suppressed by adding organic fillers, inorganic fillers or other polymers into matrix polymer according to [11], [98], [161].

The space charge measurement can provide the charge distribution and electric field distribution inside the insulation material, which could be further used to study its ageing state. There are many detection techniques to measure the space charge of solid

dielectric materials as introduced in Chapter 2 Section 2.6. The pulsed electro-acoustic method, a non-destructive measuring method firstly proposed by T. Takada [162], is most widely used to characterize the charge distribution of solid insulating material at present. The principle of this method is that the acoustic pulses are generated by the displacement of the charges inside the sample when an electrical pulse is applied to the sample. The generated acoustic wave is then detected by the piezoelectric transducer connected to the ground electrode. The transducer converts the acoustic signal into an electrical voltage signal. The electrical signal is then amplified before sent to an oscilloscope for further analysis. Despite the fact that the PEA has been used by different researchers in the characterization of dielectric material, the results from different institutes are different due to the system resolution and testing procedure [120]. In 2012, a standard was provided by IEC to guide the measurement procedure [163]. The detail of the employed PEA measurement system have been described in Chapter 3 Section 3.3.10. This system is designed and built by the High voltage Laboratory, Tsinghua University. The specific testing procedures are as following:

- a) The desired testing temperature is set through the temperature controller and keeps temperature for 1 hour. The pressure between the transducer and lower electrode is adjusted by using the nut to eliminate the effect of thermal expansion and contraction on the transducer.
- b) Apply the silicone oil between the electrodes and sample to ensure good acoustic coupling between the sample and the electrodes. The upper electrode

is connected to high voltage input and the lower electrode is grounded. A semiconducting layer is placed between the upper electrode and sample to match acoustic impedance and contact close with sample.

- c) Maintain this temperature for another 1 hour to stabilize the whole system before applying the high electric field.
- d) The polarization process is conducted under the DC electric field of 40 kV/mm for 30 mins. To reduce the error from the white noise, the sampling rate of the oscilloscope is set to 5000 Hz.
- e) The external electric field is then removed and the circuit is short-circuited, while acoustic signal is monitored during the depolarization process.
- f) The recorded data is processed by a deconvolution program in LabVIEW to obtain the space charge distribution and electric field distribution results.

To quantify the development of space charge inside the nanocomposite sample, it is necessary to calculate the total amount of space charge accumulation at different times.

The calculation is based on a subtraction method proposed by Liu et al. in [164], which is used to remove the capacitive charges from the electrode. The charge density of the injected charges in the sample and its induced image charge at the electrodes can be obtained by Equation(7.1), expressed as

$$\rho_{acc}(x) = \rho_{app}(x) - \frac{V_{app}}{V_{ref}} \rho_{ref}(x) \quad (7.1)$$

where V_{ref} is the reference voltage, V_{app} is the applied voltage, $\rho_{acc}(x)$ is the space charge

density after subtraction, $\rho_{app}(x)$ is the charge density at applied voltage and $\rho_{ref}(x)$ is the charge density at the reference voltage. In this study, the reference voltage is equal to the applied voltage. Therefore, the total charge amount in the sample bulk during the polarization process, Q_p , could be calculated by

$$Q_p(t) = \left(\int_{x_c}^{x_a} |\rho(x,t)| dx - \int_{x_c}^{x_a} |\rho(x,t_0)| dx \right) \times S \quad (7.2)$$

Where $\rho(x,t)$ is the charge density at position x and time t , x_a is the anode position on the space charge spectrum, x_c is the cathode position on the space charge spectrum, t_0 is the time of selected reference waveform and S is the area of electrode in the PEA system. In this study, the charge density at 1st second is taken as reference. The charge amount in the sample bulk during the depolarization process, Q_d , could be calculated by

$$Q_d(t) = \int_{x_c}^{x_a} |\rho(x,t)| dx \times S \quad (7.3)$$

where $\rho(x,t)$ is the charge density at position x and time t , x_a is the anode position on the space charge spectrum, x_c is the cathode position on the space charge spectrum and S is the area of electrode in the PEA system.

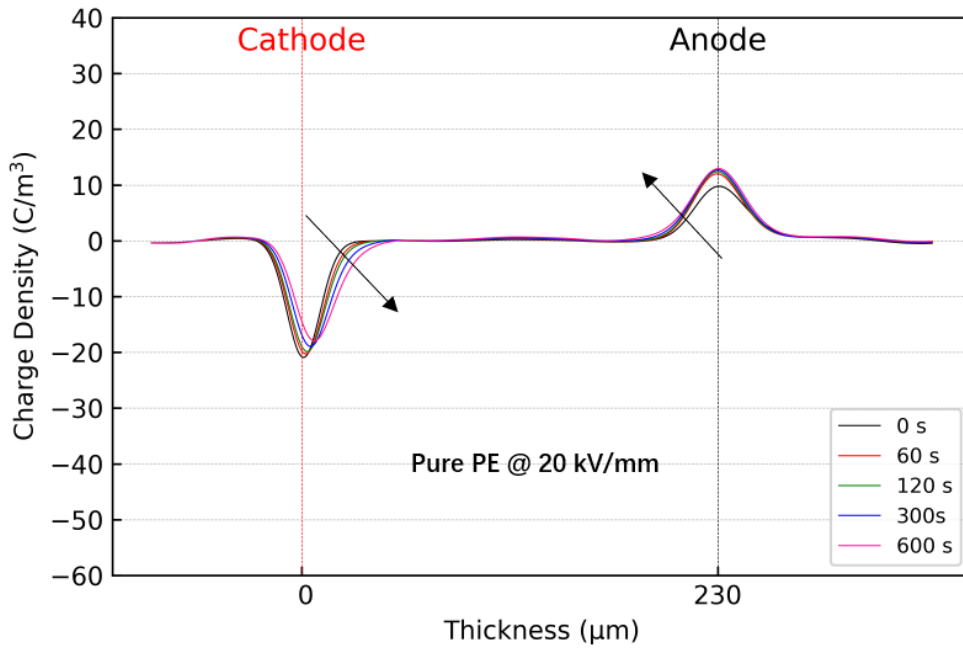
7.3 Results and Discussion for PE and PE nanocomposites

7.3.1 Measurements for Unfilled PE

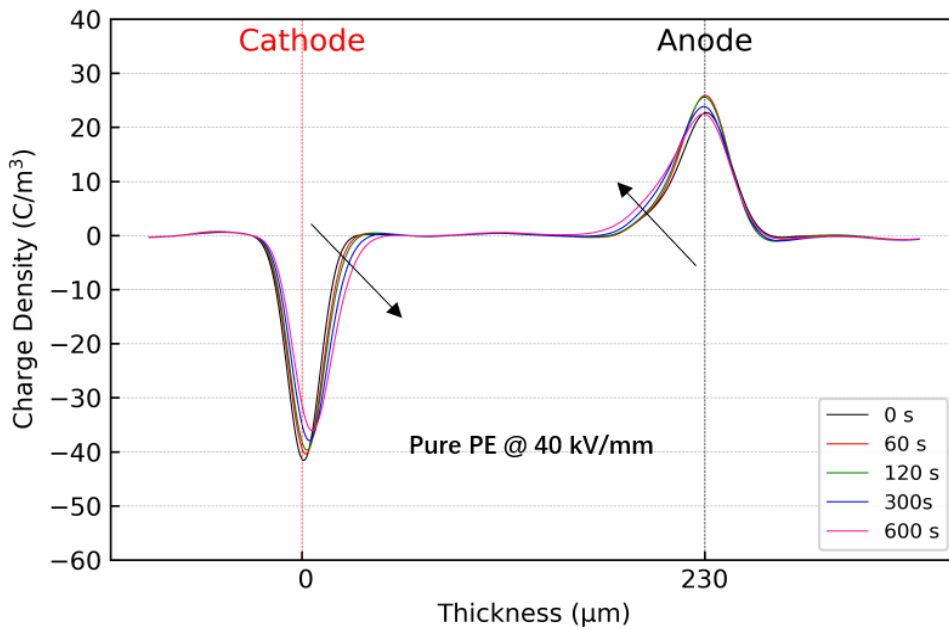
Figure 7.2(a) shows the space charge behavior of the unfilled PE sample stressed at 20

kV/mm DC electric field for 600s. The horizontal axis of the graph represents the thickness of the sample and the vertical axis of the graph represents the volume density of the space charge inside the sample. The position of the cathode electrode, which is made of aluminum, is shown as the red dotted line. The position of the anode electrode, which is made by a semiconducting material, is shown as the black dotted line. The arrow in the graph indicates the increase in time. Homocharge injection is observed near both electrodes. A small amount of space charge is found near the cathode and it moves towards the bulk of the insulating material along with time. There is barely any space charge development near the anode. The peak of the charge distribution is becoming higher with time and this is because of the increases of the induced charges near the anode when more charges are injected near the cathode.

To study the effect of the electric field strength on the space charge development, another higher DC electric field is then employed. Figure 7.2(b) displays the space charge behavior of the unfilled PE under DC electric field of 40 kV/mm. The homocharge development is identified again around both electrodes. The charge density is increased with the increase of the electric field strength. At the anode side, the amount of space charge is increased as compared with the observations for the case of 20 kV/mm electric field. The injected space charge at both electrodes moves towards the bulk of the unfilled PE with time.



(a)



(b)

Figure 7.2 Space charge behavior of unfilled PE (a) under 20 kV/mm DC electric field at 30 °C, (b) under 40 kV/mm DC electric field at 30 °C.

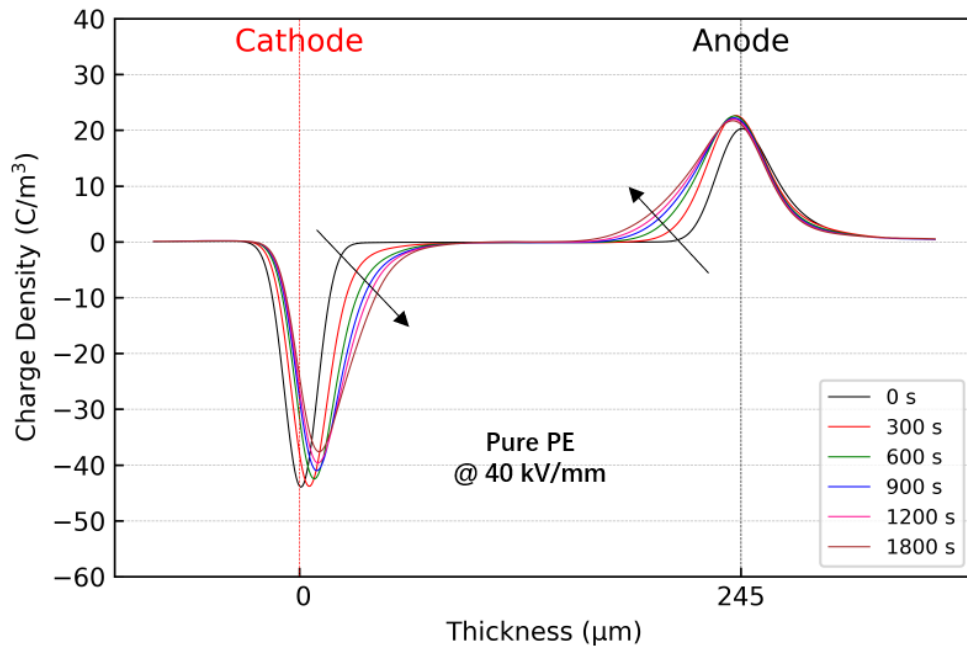
7.3.2 Measurements for PE Nanocomposites containing Untreated Nano-alumina

The space charge dynamics of PE/ untreated nano-alumina nanocomposites with 0 phr (unfilled PE), 0.5 phr, 1 phr, 2 phr and 5 phr filling content stressed under a 40 kV/mm DC electric field for 30 minutes at 30 °C are presented in Figure 7.3. All the tested samples suffered from homocharge accumulation and many space charge packets are found inside the film samples. The formed homocharges move towards the bulk of the insulation. In addition, no heterocharge is found for these samples. For the unfilled PE, the homocharge is mainly developed in the vicinity of the cathode. With the addition of 0.5phr and 1phr untreated alumina, obvious injection of homocharge is observed around both electrodes, as shown in Figure 7.3(b) and (c). The movement of homo space charge near the anode is not obvious in PE nanocomposite sample containing 2 phr of untreated alumina. Overall, the depth and the charge density of the homocharge is increasing as the filling content increases.

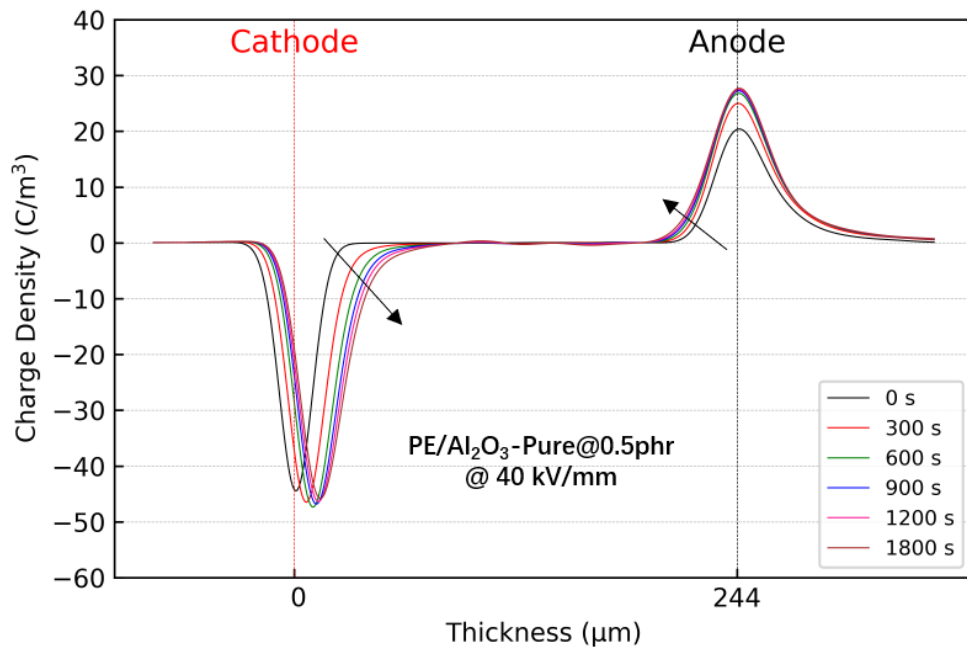
Figure 7.4 shows the space charge decay process of PE/ untreated alumina nanocomposites when the measurement circuit is short-circuited. The space charge decay process in a dielectric material involves the redistribution of charges inside the material, leading to a decrease in the net charge density over time. As these charge carriers move, they can neutralize some of the trapped charges, reducing the overall space charge density in the material. Compared with the polarization process, the effect

of induced charges around the electrodes could be eliminated when the applied voltage is removed, by which it shows the charge distribution inside the sample. The peaks observed between the dotted lines are caused by the accumulated charges in the sample bulk and the peaks near the two dotted lines are caused by the induced charges around the electrodes. From Figure 7.4, the charge accumulation in the PE/untreated alumina nanocomposites is homocharge injection. The accumulated charge decays rapidly with time after the DC electric field is removed. In addition, the PE nanocomposite sample containing 2 phr of untreated alumina has the least amount of space charge when compared with other nanocomposite samples with different filling content.

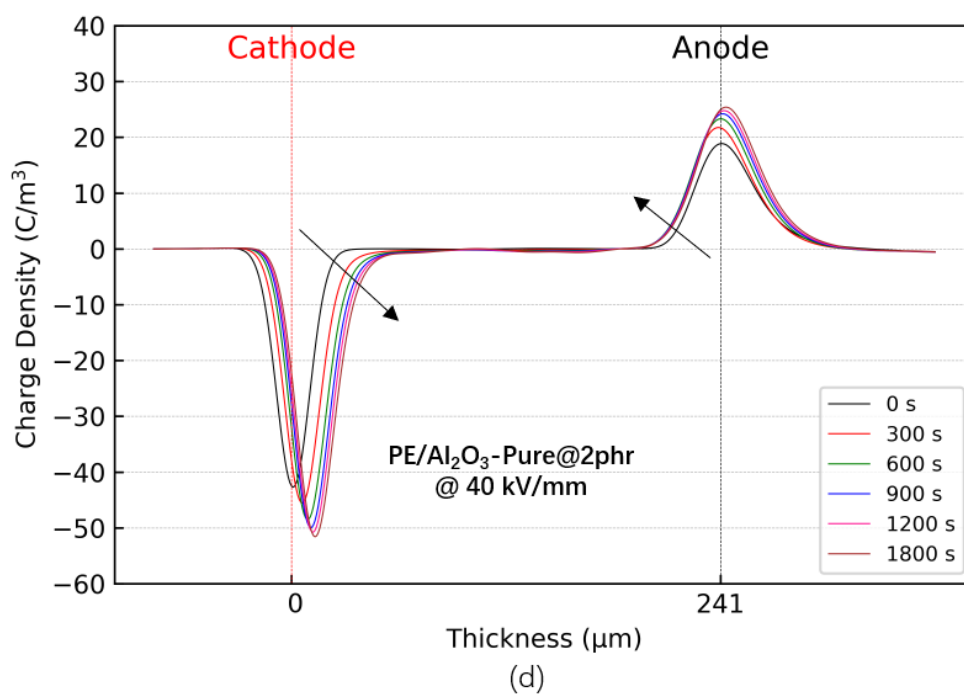
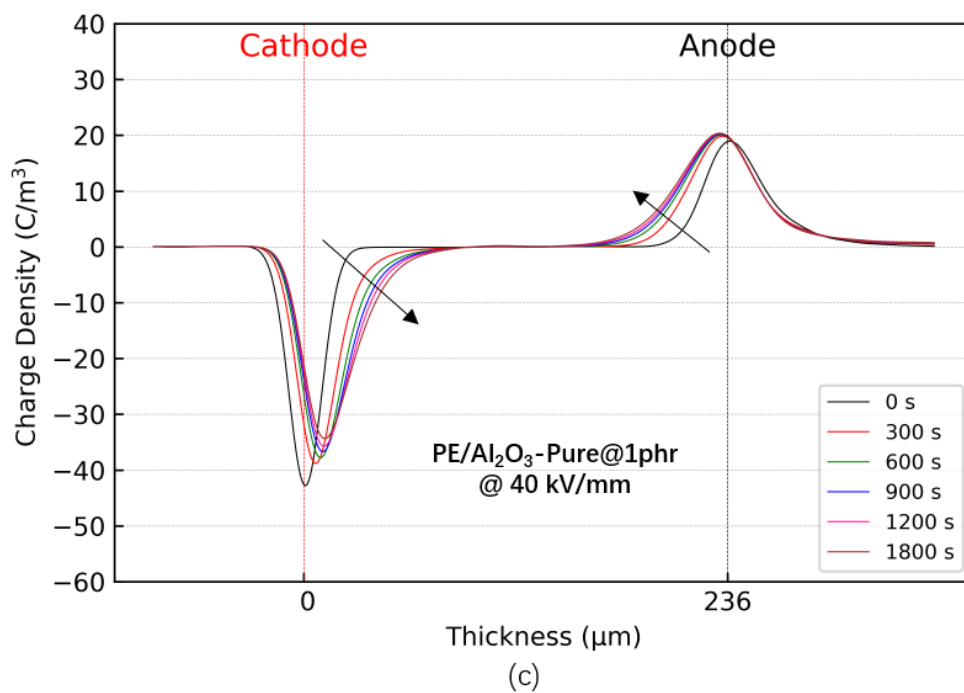
The change of total charge of PE/ untreated alumina nanocomposites as a function of time is shown in Figure 7.5. At the end of 1800s polarization, the total charge amount of the unfilled PE is about 184.2 nC. The total amount of space charge of all tested samples gradually increases and turns to be stable over time. Moreover, it should be noticed that the total amount of space charge firstly decreases and then increases with the increasing filling content. The PE nanocomposite sample containing 2 phr of untreated nano-alumina particles exhibits the best performance in space charge suppression. When the filling content is high (5 phr in this case), the total amount of injected space charge is even higher than that of unfilled PE.



(a)



(b)



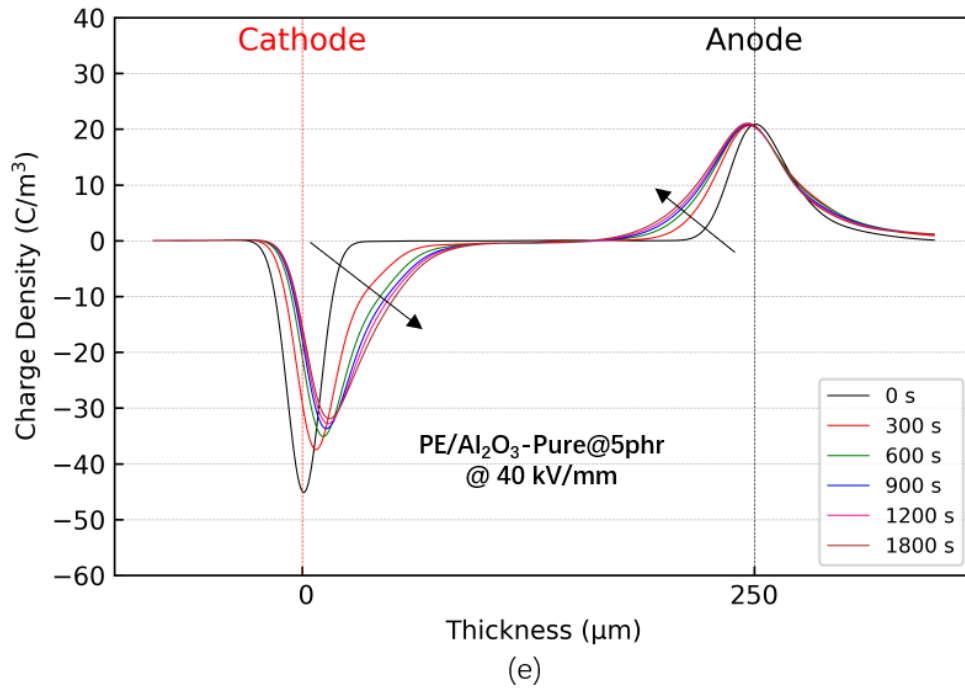


Figure 7.3 Space charge behavior of PE nanocomposites containing (a) 0 phr (b) 0.5 phr (c) 1 phr (d) 2 phr (e) 5 phr of untreated nano-alumina stressed at 40 kV/mm DC electric field at 30 °C.

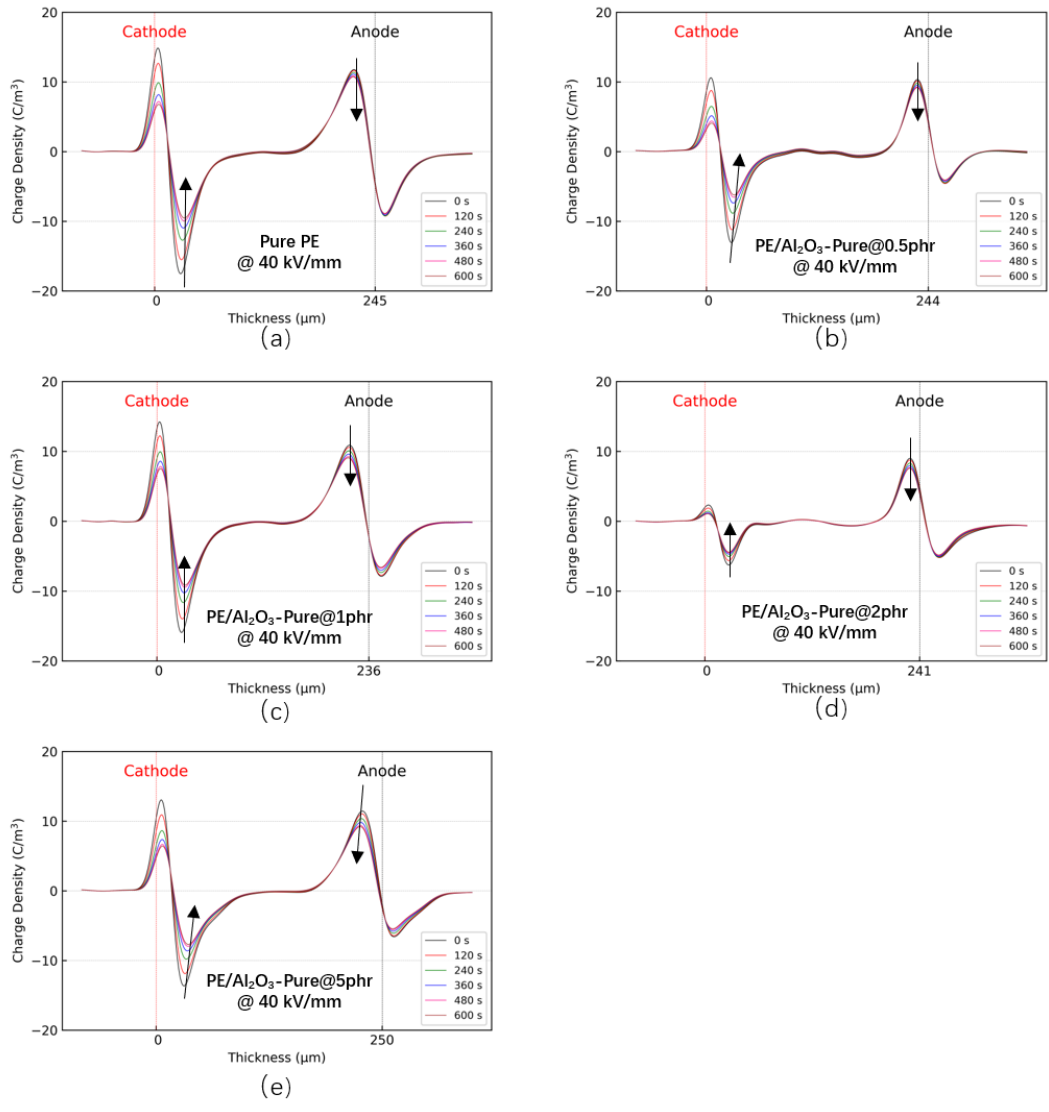


Figure 7.4 Space charge decay process of PE nanocomposites containing (a) 0 phr (b) 0.5 phr (c) 1 phr (d) 2 phr (e) 5 phr of untreated nano-alumina stressed at 40 kV/mm DC electric field at 30°C.

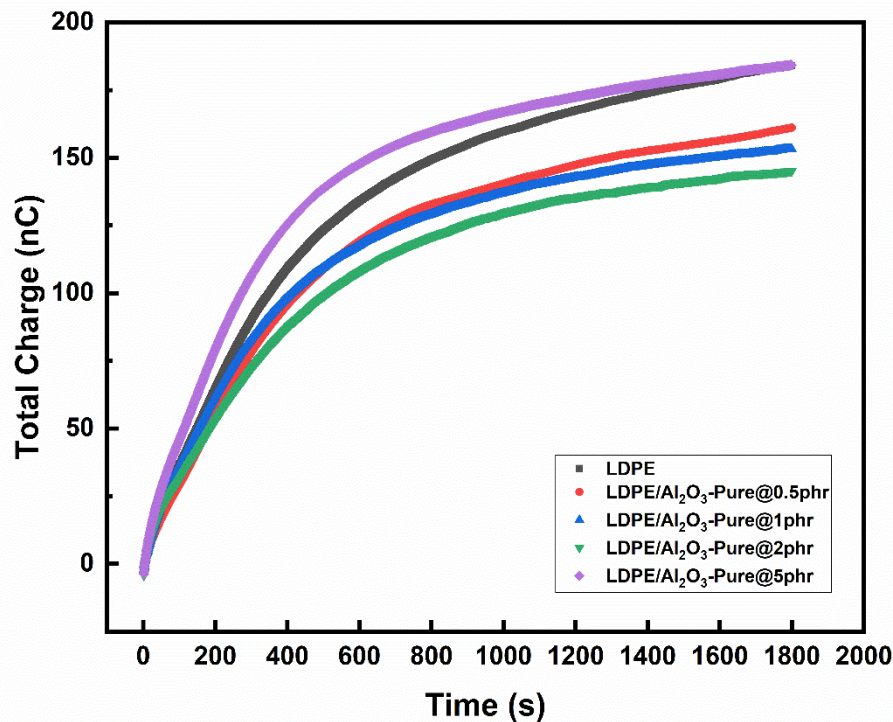


Figure 7.5 Total charge amount during the polarization process in the PE nanocomposites samples containing untreated nano-alumina under the DC electric field of 40 kV/mm at 30 °C.

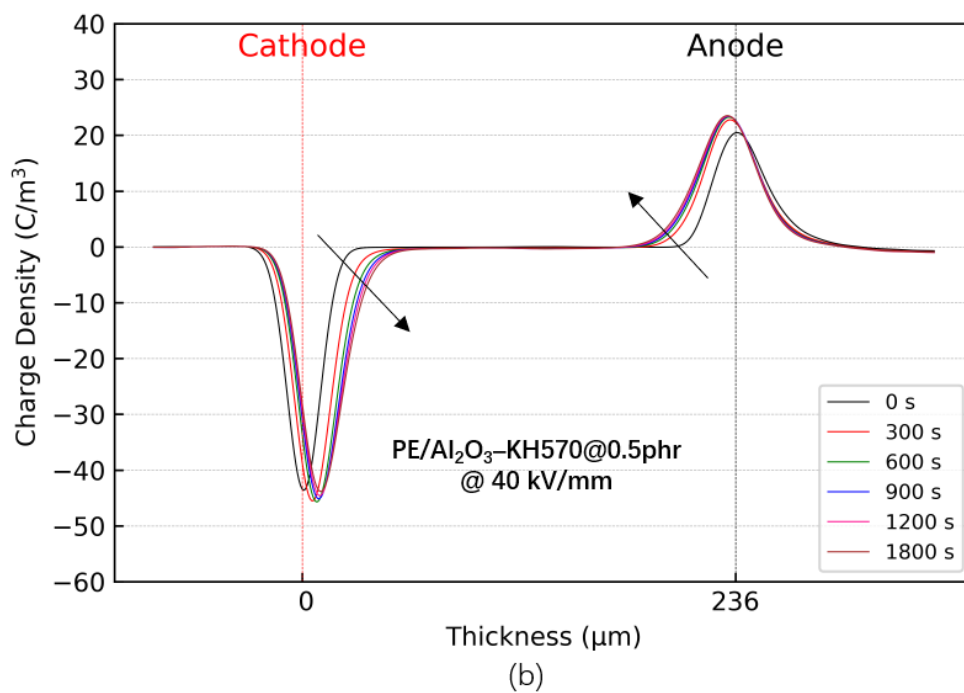
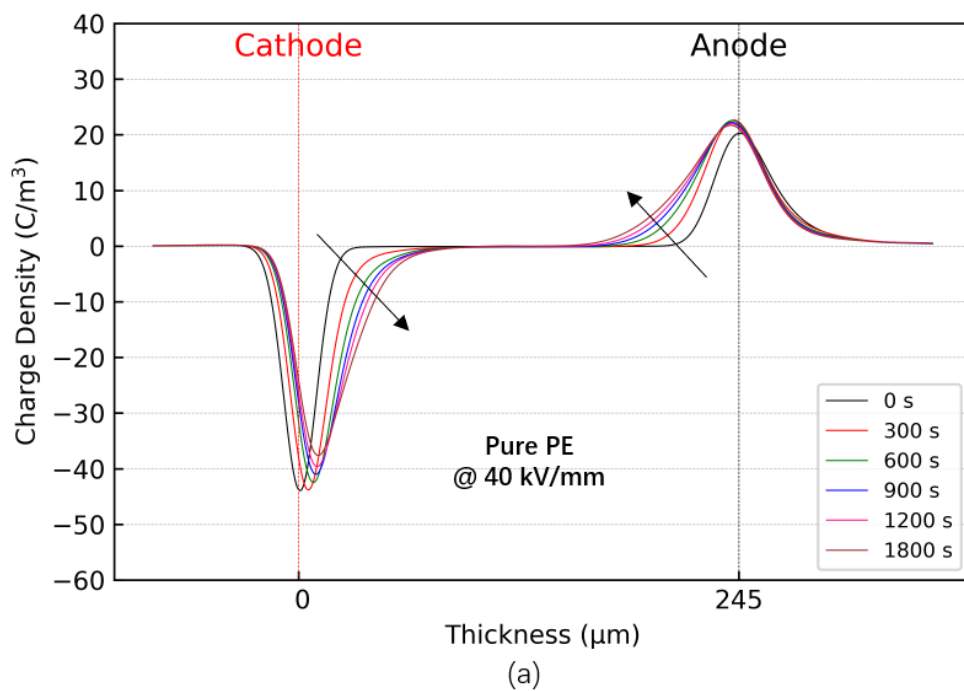
7.3.3 Measurements for PE Nanocomposites containing KH570-treated Nano-alumina

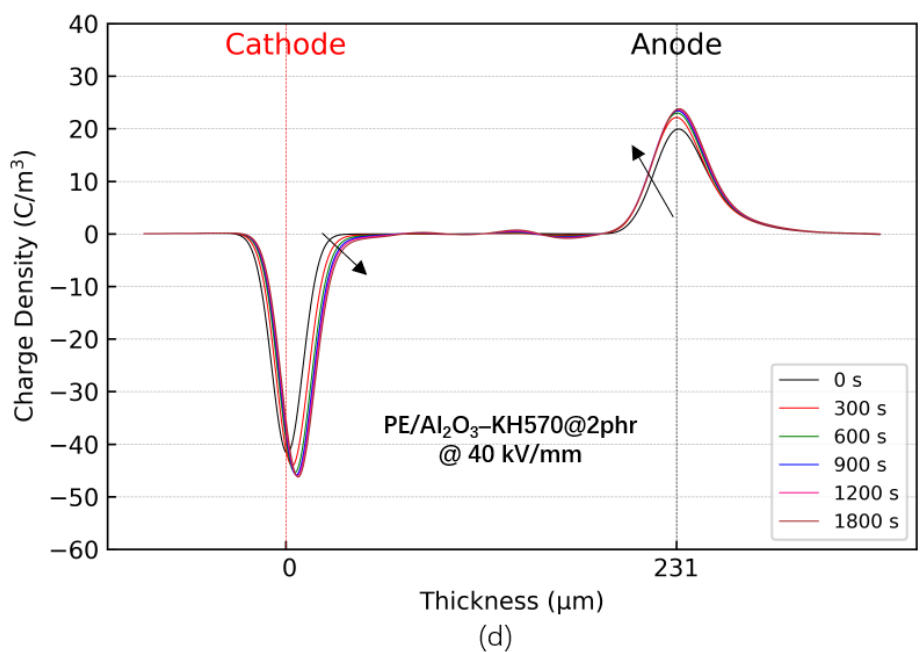
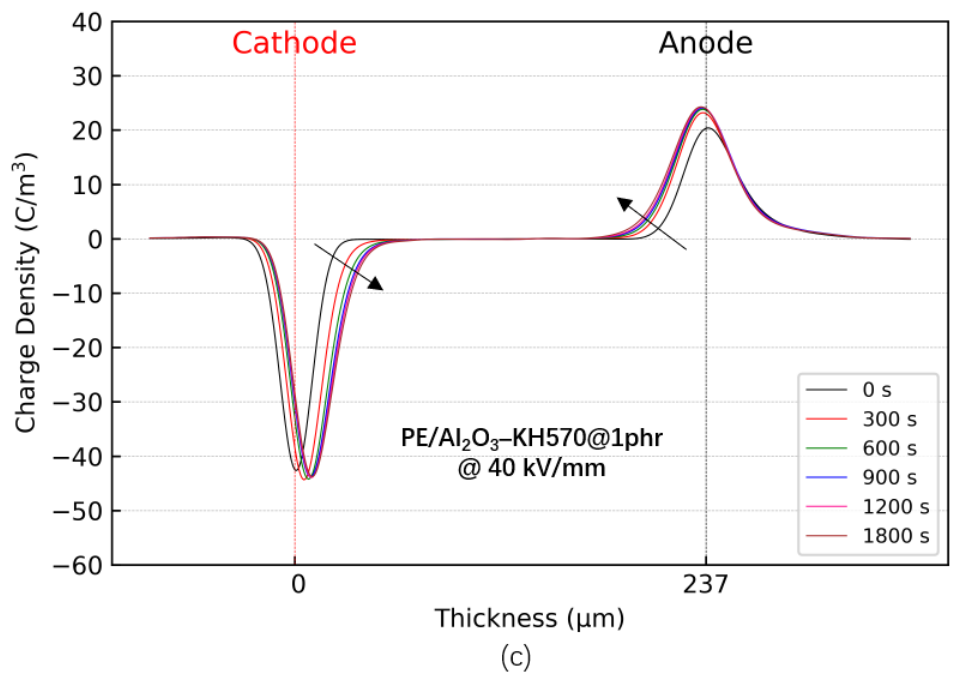
The space charge dynamics of PE nanocomposite samples containing 0.5 phr, 1 phr, 2 phr and 5 phr of KH570-treated nano-alumina under DC electric field of 40 kV/mm at 30 °C are presented in Figure 7.6. Similar to the unfilled PE sample, the only homocharge is observed near both electrodes for all the tested samples. As compared with the nanocomposite samples filled with the same amount of unfilled nano-alumina, the space charge development of the samples filled with treated nano-alumina is

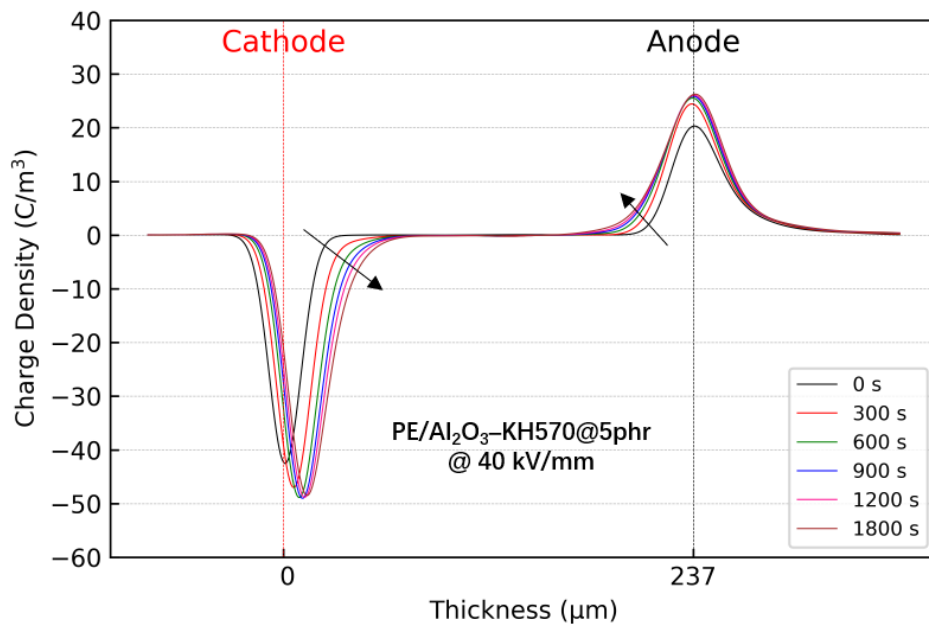
suppressed. The homocharge accumulation near the anode remains low, and the charge migration is rare after 300s. The charge density trades narrowly with the varying filling content. However, the movement of space charge towards the bulk of the sample is reduced as the filling content increases up to 2 phr. The density and depth of the space charge seem to become higher again for PE/ Al₂O₃-KH570@5 phr sample.

The charge decay behavior of PE nanocomposites filled with surface treated alumina is shown in Figure 7.7. It has proved that the homocharge is actually injected at both electrodes. The accumulated space charge gradually decreases after removing the applied voltage, as previously reported. It should be noticed that the homocharge density of PE nanocomposite samples with KH570-treated alumina at 0s is smaller than that of PE nanocomposite samples with untreated alumina when the filling content is the same. Additionally, the accumulated space charges cannot completely dissipate without the help of an electric field with reverse polarity.

Figure 7.8 shows the total charge dynamics of PE/ KH570-treated alumina nanocomposites. At 30 °C and 40 kV/mm, all the composite samples have less space charge injection than unfilled PE over the polarization period. For each sample, the amount of the injected homocharge increases with time. The total charge amount firstly decreases and then increases as the filling content of treated alumina increases. At the end of the measurement, samples containing 2 phr of KH570-treated alumina have the smallest amount of space charge, which is 84.2 nC.







(e)

Figure 7.6 Space charge behavior of PE nanocomposites containing (a) 0 phr (b) 0.5 phr (c) 1 phr (d) 2 phr (e) 5 phr of KH570-treated nano-alumina stressed at 40 kV/mm DC electric field at 30 °C.

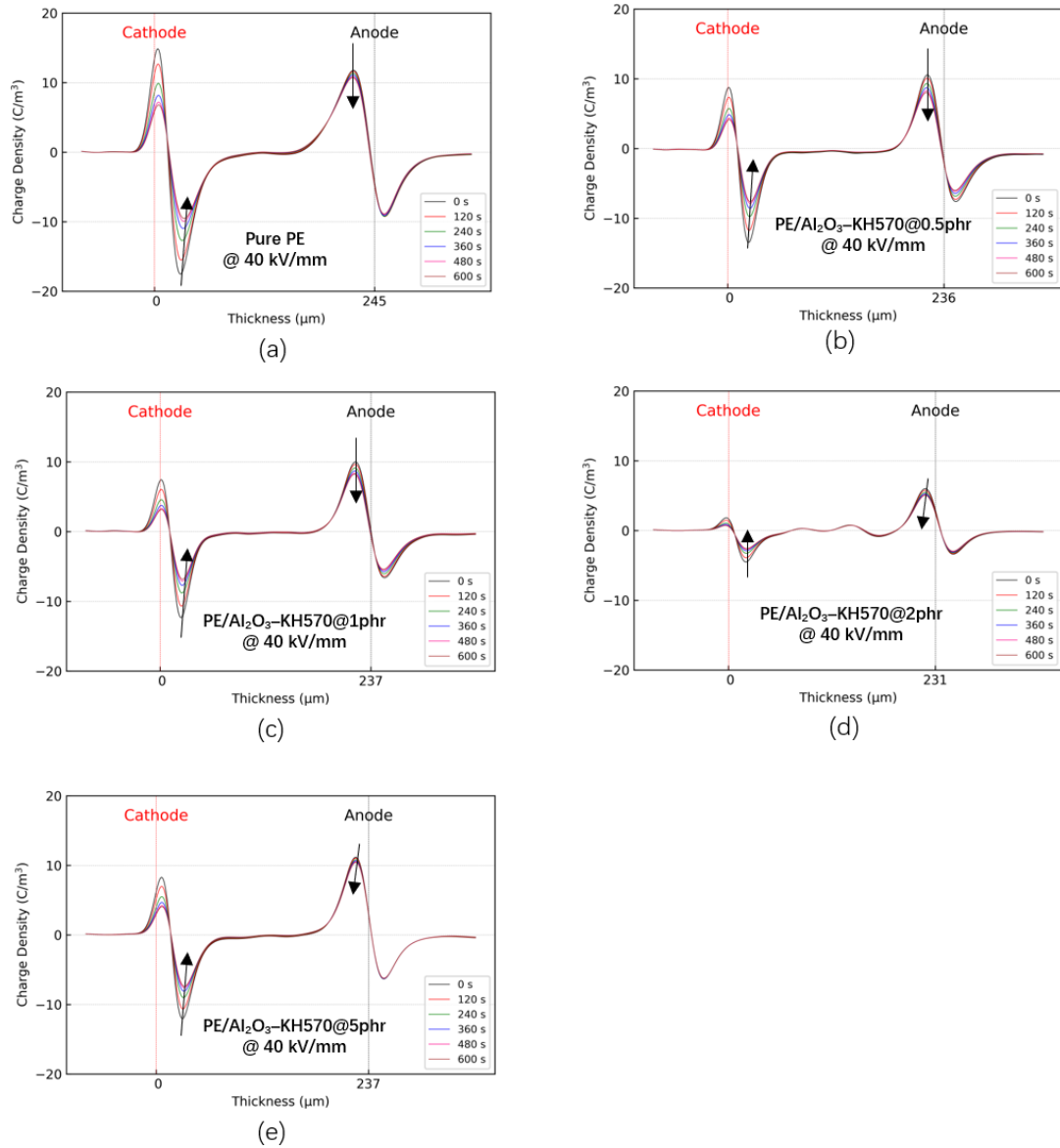


Figure 7.7 Space charge decay process of PE nanocomposites containing (a) 0 phr (b) 0.5 phr (c) 1 phr (d) 2 phr (e) 5 phr of KH570-treated nano-alumina stressed at 40 kV/mm DC electric field at 30 °C.

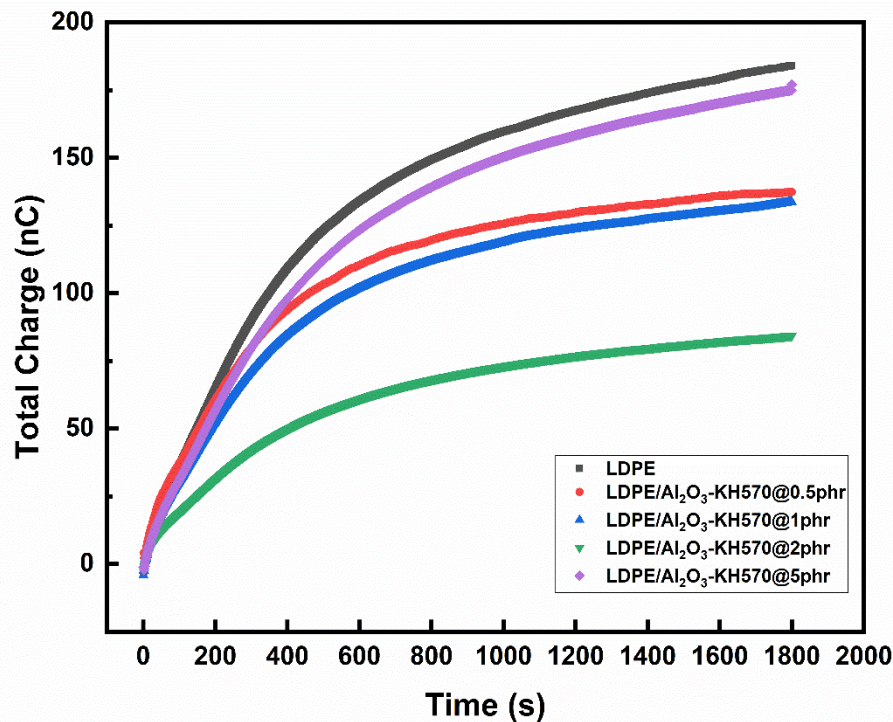


Figure 7.8 Total charge amount during the polarization process in the PE nanocomposites samples containing KH570-treated nano-alumina under the DC electric field of 40 kV/mm at 30 °C.

7.3.4 Discussion

The addition of nano-alumina particles with and without surface treatment has shown different results of the space charge accumulation of PE nanocomposites, as displayed by the above results. All samples have been affected by the homo space charge accumulation in varying degrees. In contrast to earlier findings [10], [11], [60], [147], however, no evidence of heterocharge was detected in this study. For unfilled PE, the electric field with different strengths was applied and the density of space charge increased when a higher electric field was applied. With the addition of nanoparticles,

most of the samples showed suppressed space charge accumulation and the amount of homocharge firstly decreased and then increased with the increasing of filling content for both untreated and KH570-treated nanoparticles. A similar migration process of homocharge was observed and it moved from the sample surface towards the inside of the sample with time.

The behaviour of space charge in nanocomposite is closely linked to carrier traps. T. Tanaka reported that the reduction of space charge accumulation in nanocomposites is caused by the increase of shallow traps and enhanced charge mobility [70]. But our results are in conflict with his model. The density of the deep trap level is profoundly increased in PE/ alumina nanocomposites based on TSDC results. In other word, the incorporation of nano-alumina introduces more deep traps in PE nanocomposite. With the addition of nano-alumina, the interphase between PE spherulites and the interfacial area between matrix PE and nanoparticles is increased, resulting in more traps are generated in the interface regions. When the homocharges are injected from the electrode, they are trapped by deep traps in the interface between electrode and specimen and forms a homo charge layer. This charge layer would block further charge injection by increasing the potential barrier and decreasing the electric field at the interface between electrode and specimen. Then, the space charge formation is suppressed. Furthermore, based on the results, the deep traps can also reduce the charge carrier mobility and then limits the ionization of impurity in the nanocomposites, which is in consistence with [149], [165].

Both filling content and surface chemistry of the nanoparticles have a significant suppression effect on the development of homocharge in PE nanocomposite. By comparing the total charge of samples with and without surface treatment at the same filling content, the addition of surface-treated nano-alumina has exhibited a better space charge suppression effect at the end of polarisation. Better dispersion of nanoparticles can increase the interfacial regions in nanocomposites, resulting in more deep traps. These results are consistent with [114]. PE/Al₂O₃-KH570@2 phr sample has shown the least total charge, which could be attributed to the highest density of deep trap level. It is in good agreement with the TSC results in Chapter 7 Section 5. Hence, it can be concluded that the space charge behaviour of nanocomposites is mainly affected by the addition of nanoparticles and the resulting changes to the interfaces between the polymer and nanoparticles.

7.4 Results and discussion for PP and PP nanocomposites

7.4.1 Measurements for Unfilled PP Sample

The space charge dynamics of unfilled PP stressed under a DC electric field of 20 kV/mm is showed in Figure 7.9. After 600 s, only a very small amount of homocharge is recorded near both electrodes. The development of space charge near the cathode is marginal with time. The development space charge near the anode is also negligible.

After increasing the DC electric field strength to 40 kV/mm, Figure 7.10 shows the space charge behavior of unfilled PP within 600 s. An increased homocharge

development was observed near both electrodes, compared with the previous results from the case of 20 kV/mm. The space charge packet in the vicinity of the cathode evidently moves towards the bulk sample. The peak of space charge density near anode becomes more significant with time, but its migration is minimal. The overall charge density is higher than that of unfilled PP stressed under a 20 kV/mm field.

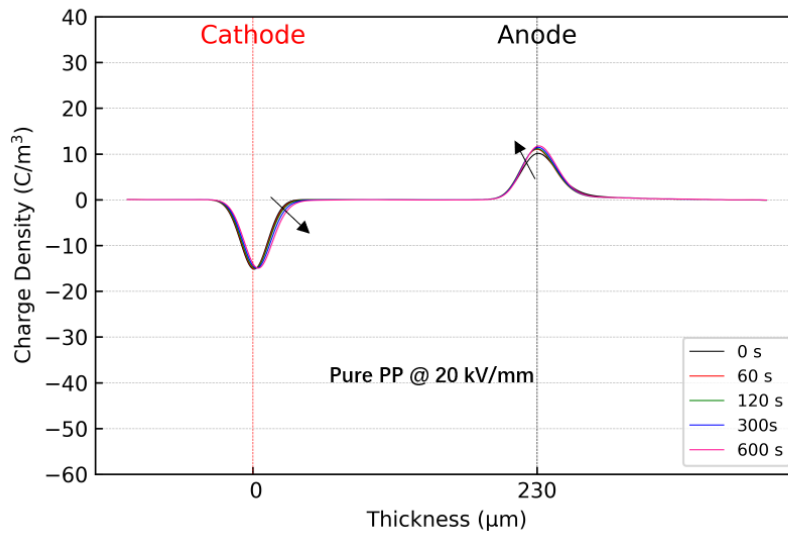


Figure 7.9 Space charge behavior of unfilled PP under a 20 kV/mm DC electric field at 30 °C.

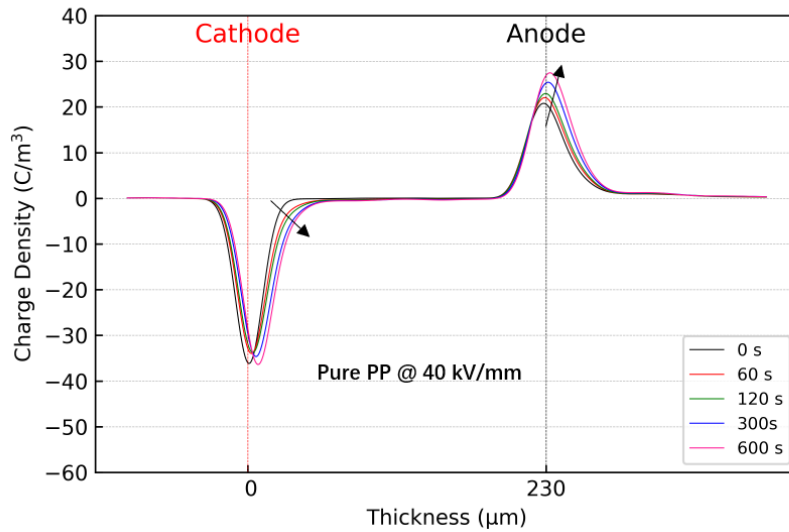
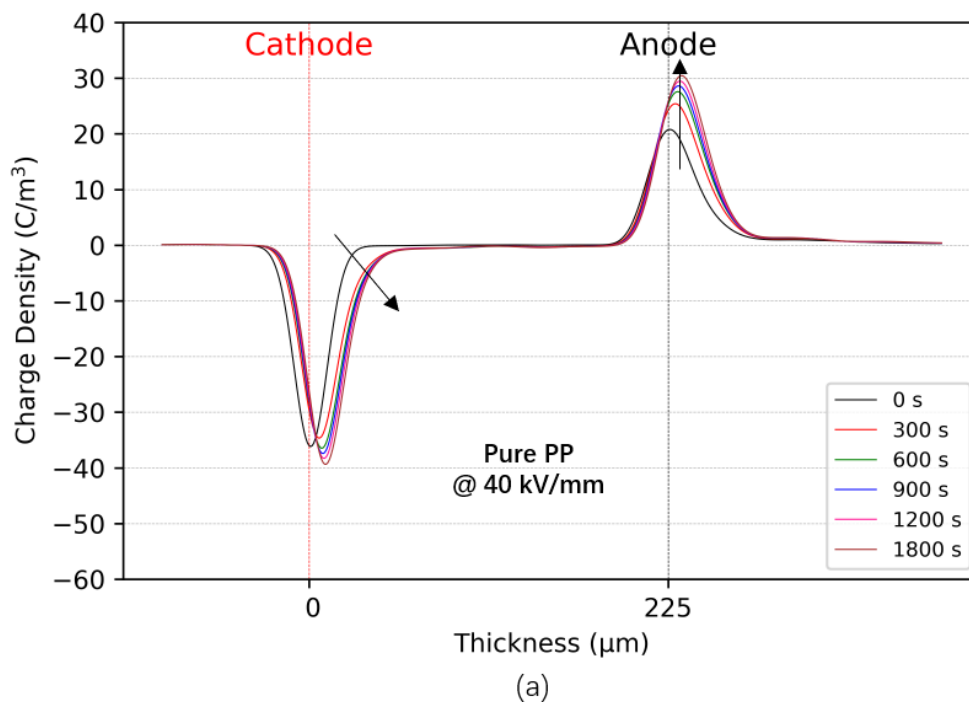


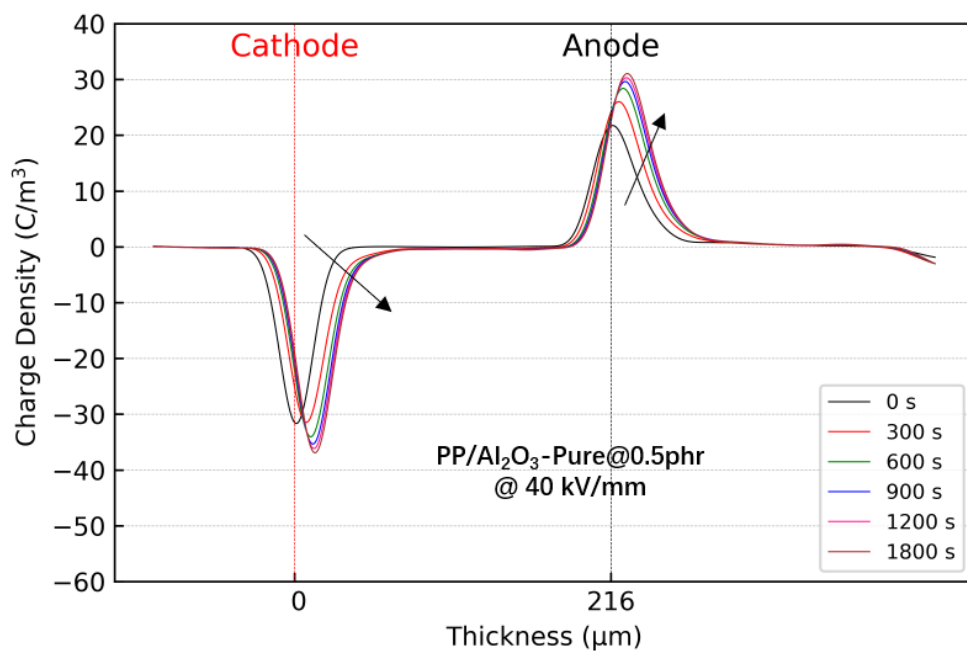
Figure 7.10 Space charge behavior of unfilled PP under a 40 kV/mm DC electric field at 30 °C.

7.4.2 Measurements for PP Nanocomposites containing Untreated Nano-alumina

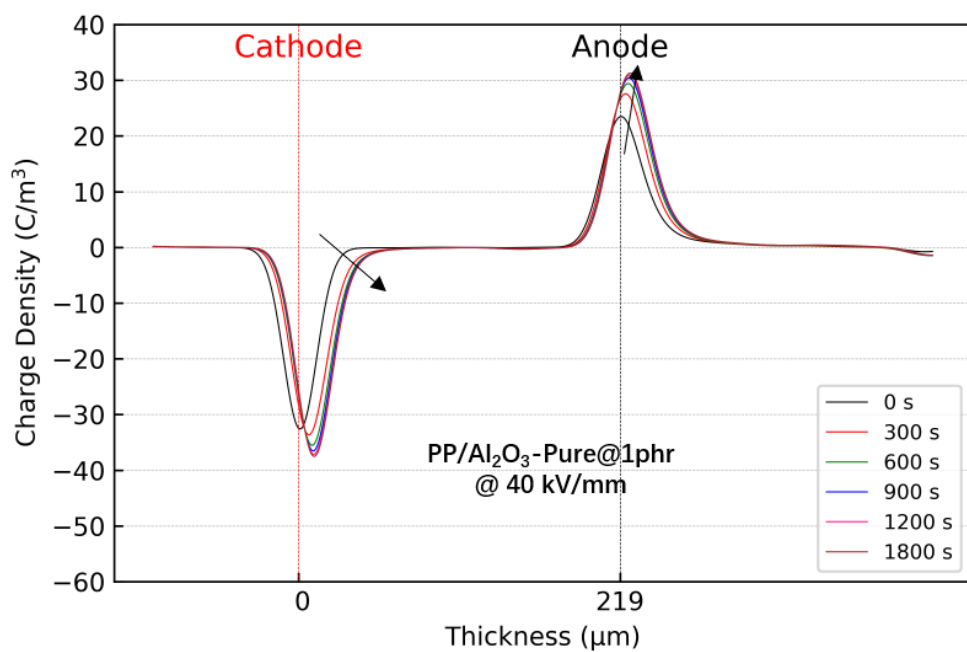
Figure 7.11 shows the space charge dynamics of PP nanocomposites containing 0 phr, 0.5 phr, 1 phr, 2 phr and 5 phr of untreated alumina nanoparticles stressed under a 40 kV/mm DC electric field for 30 min at 30 °C. Space charge accumulation is observed in the vicinity of both electrodes in PP nanocomposite and the amount of the injected charge is increasing over time. The migration of homocharge near the cathode is more obvious than that near anode. The injected electrons evidently move towards the bulk of the sample as polarizing time increases, but the injected electron holes hardly move. With the filling content increasing, the homo charge near both electrodes slightly decreases and the migration of injected electrons is reduced. The charge decay process

of PP nanocomposites, shown in Figure 7.12, further illustrates the existence of homo charge injection near both electrodes. The accumulated charges decay fast immediately after the electric field is removed for all PP/ untreated nano-alumina samples. The total charge of all tested samples is calculated and presented in Figure 7.13. The total charge for unfilled PP is 87.6 nC at the end of polarization. For each composite sample, the total injected charge increases with time and reduces as the filling content increases. The PP/ Al₂O₃-Pure@5phr shows the minimum total charge of 54.3 nC, which is reduced by 39 % compared with unfilled PP.





(b)



(c)

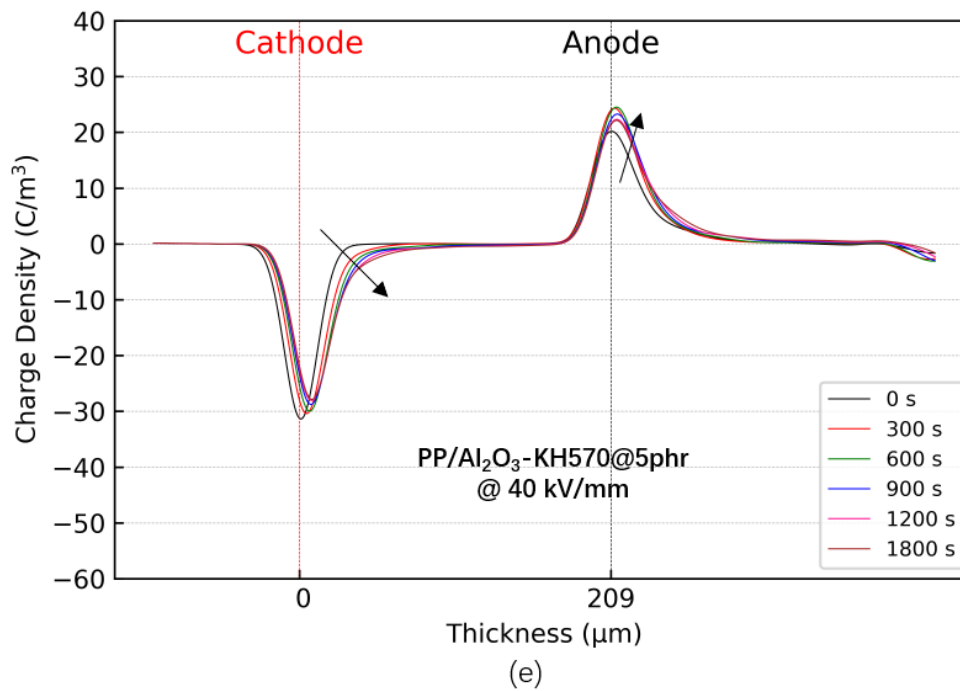
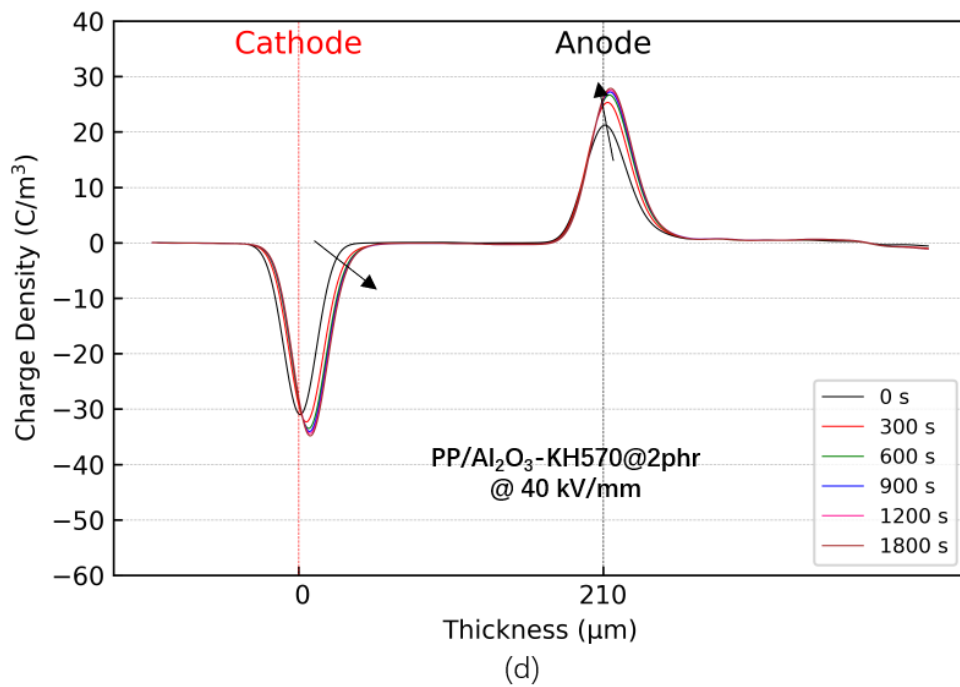


Figure 7.11 Space charge dynamics of PP nanocomposites containing (a) 0 phr (b) 0.5 phr (c) 1 phr (d) 2 phr (e) 5 phr of untreated nano-alumina stressed at 40 kV/mm DC electric field at 30 °C.

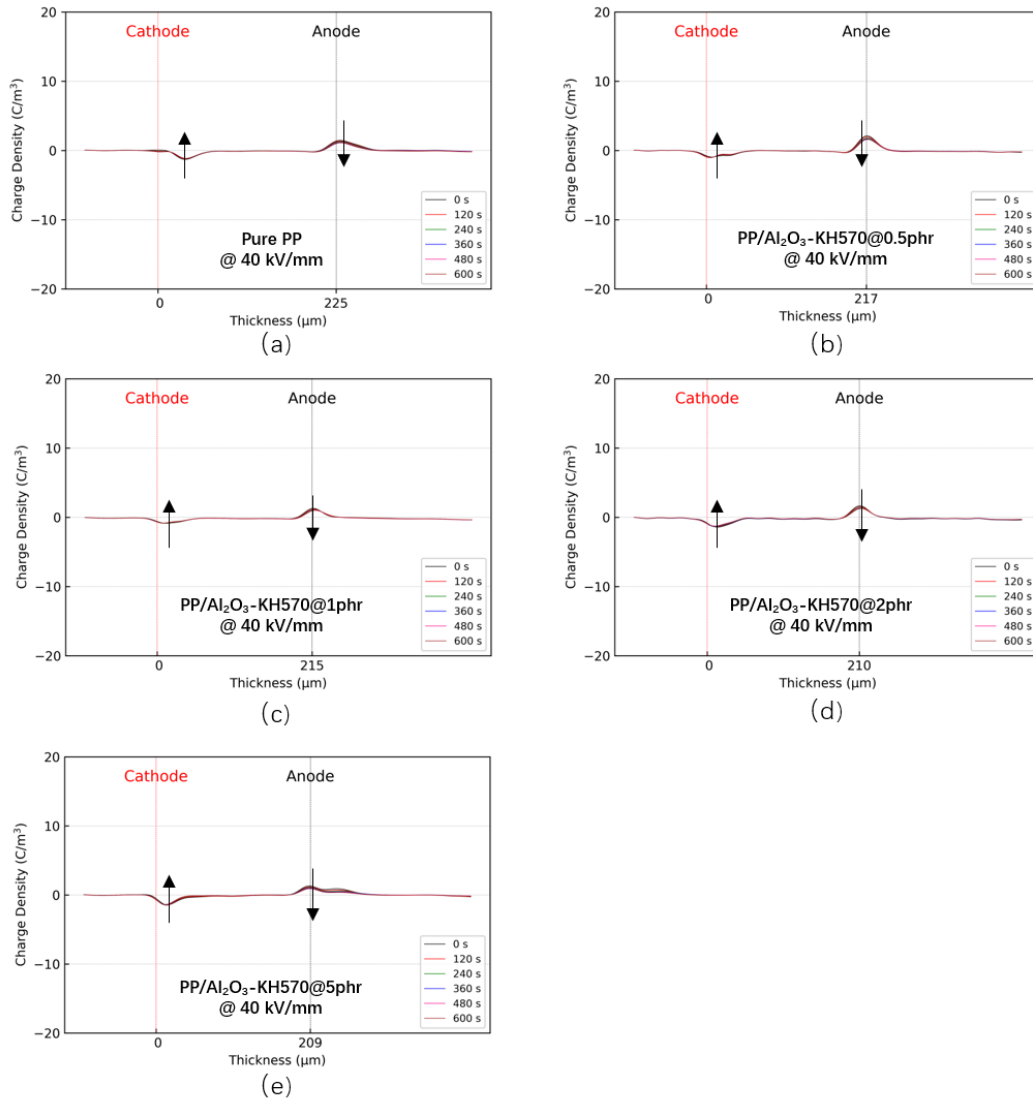


Figure 7.12 Space charge decay process of PP nanocomposites containing (a) 0 phr (b) 0.5 phr (c) 1 phr (d) 2 phr (e) 5 phr of untreated nano-alumina stressed at 40 kV/mm DC electric field at 30°C.

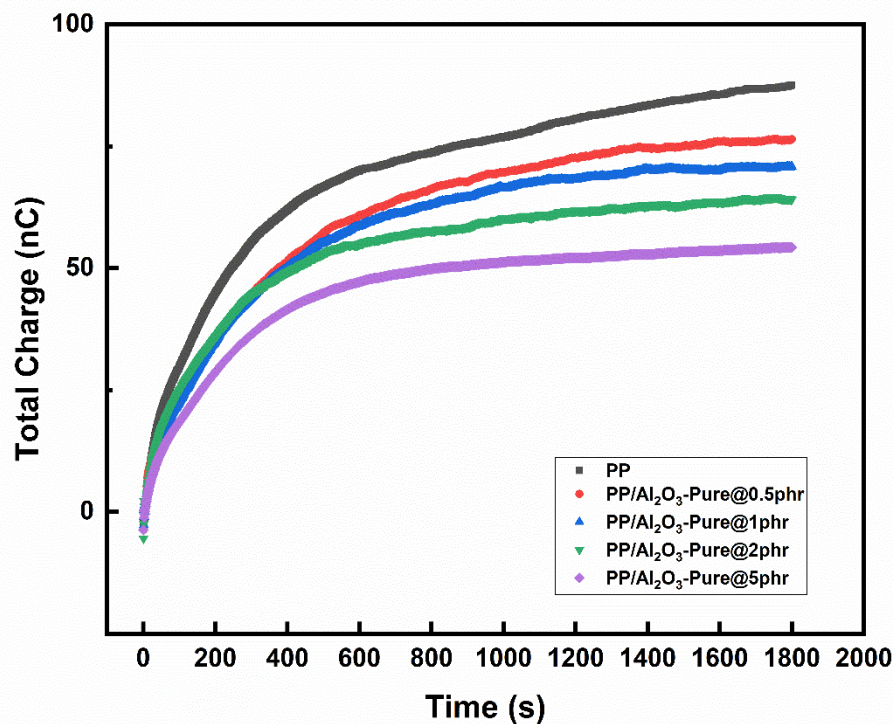
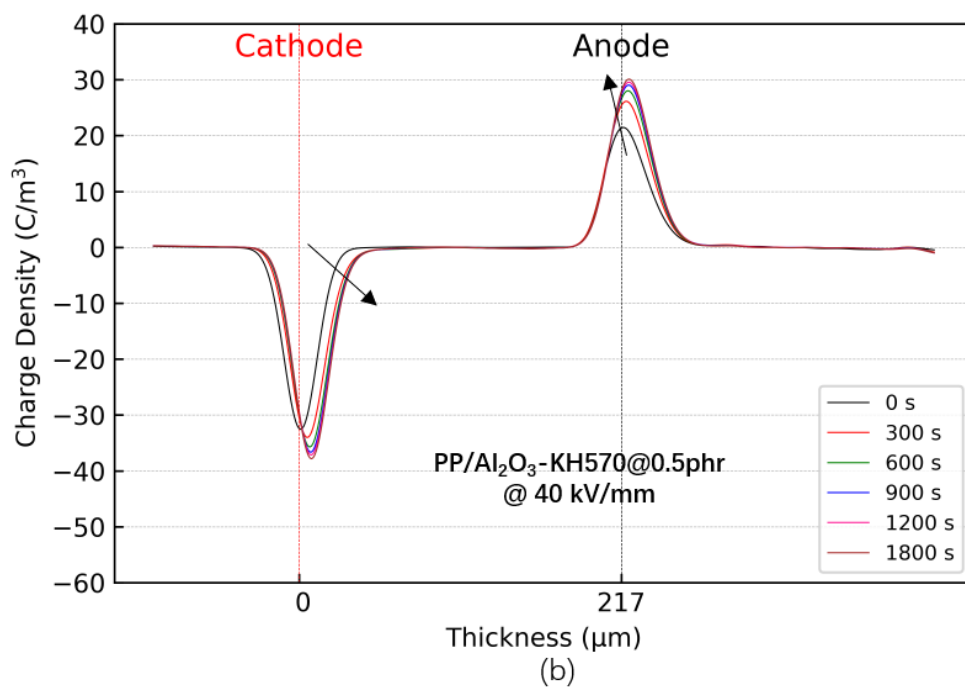
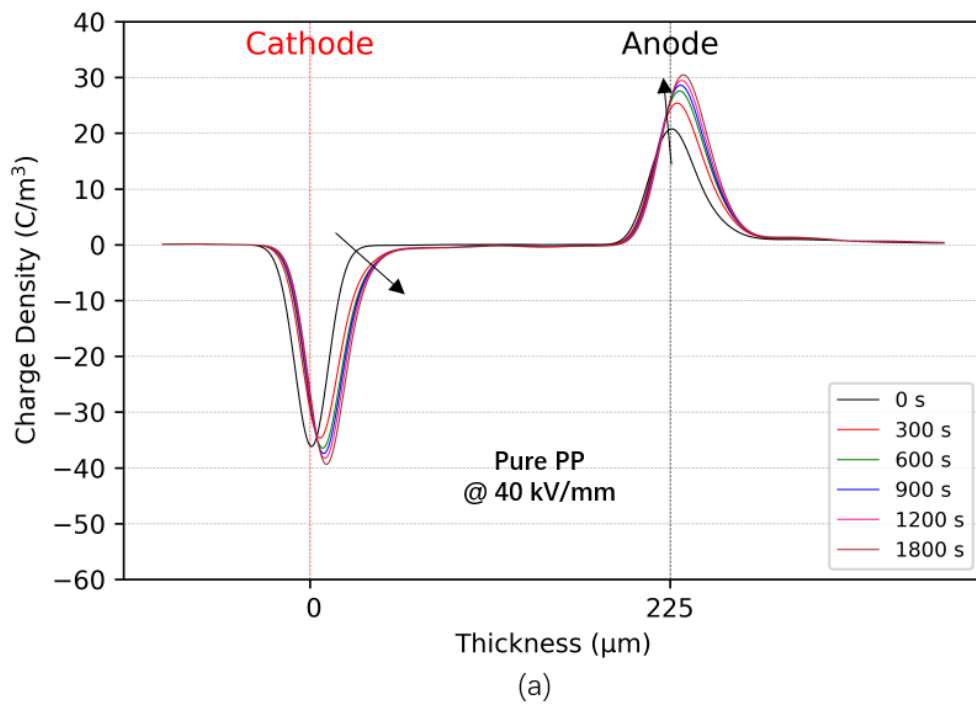


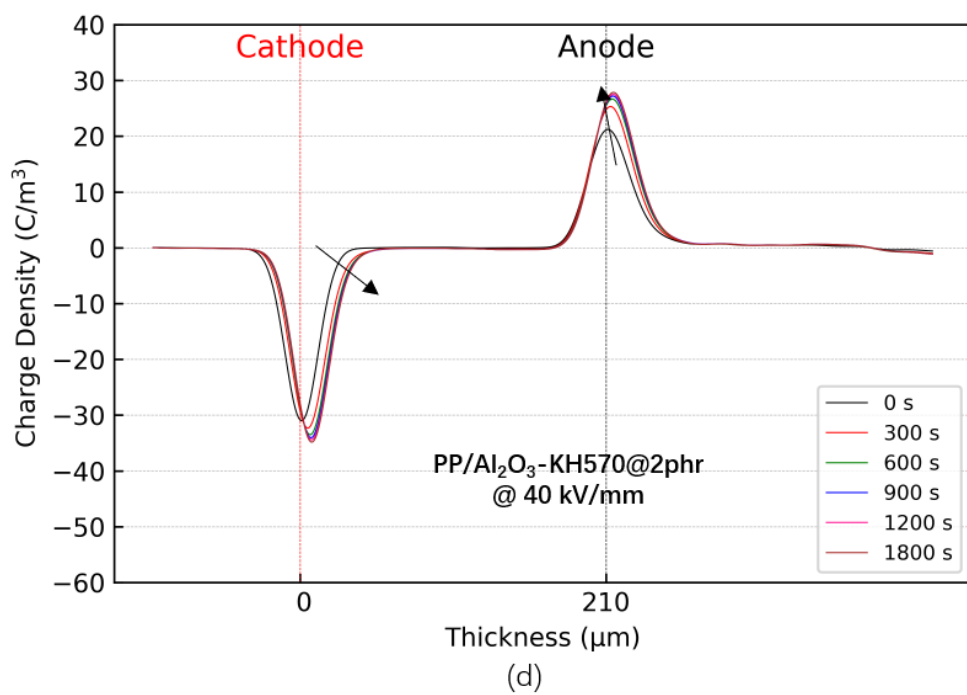
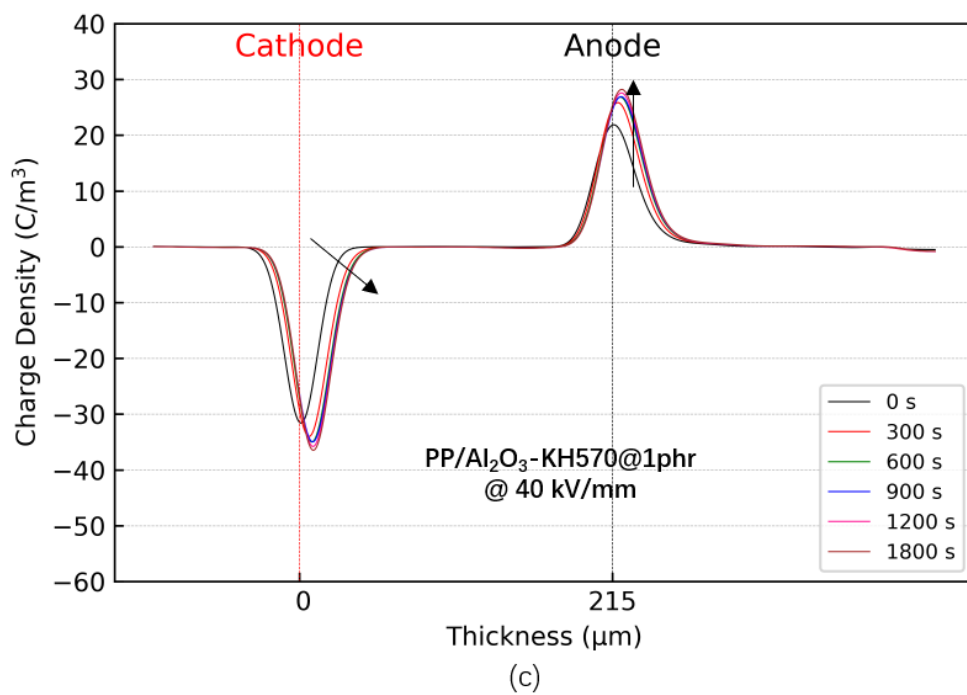
Figure 7.13 Total charge during the polarization process in the PP nanocomposites samples containing KH570-treated nano-alumina under the DC electric field of 40 kV/mm at 30 °C.

7.4.3 Measurements for PP Nanocomposites containing KH570-treated Nano-alumina

Figure 7.14 shows the space charge behavior of PP nanocomposites containing the KH570-treated nano-alumina with varying filling content. The space charge dynamics during the polarization process were recorded under a DC electric field of 40 kV/mm at 30 °C for 30 mins and then the charge decay during the depolarization process was measured for another 10 min. The development of homocharge is observed near both electrodes. The magnitude of space charge density is reduced with the introduction of

surface-treated nano-alumina. The injection depth of homo charges near the cathode is further suppressed with the increasing filling content. Especially for PP nanocomposite with 5 phr treated alumina, the magnitude of charge density in both electrodes is obviously reduced as compared with unfilled PP. All composites show a similar trend in the charge decay process as displayed in Figure 7.15. The injected space charges decay rapidly but there are still some remaining charges after 600s. Figure 7.16 describe the change of total charge for each nanocomposite during the polarization process. All the PP/ KH570-alumina nanocomposites demonstrate superior space charge suppression ability as compared with unfilled PP. The total charge for PP nanocomposites containing KH570-treated alumina is smaller than that of PP nanocomposites containing untreated alumina when the filling content is the same. The total charge of PP/ Al₂O₃-Pure@5phr samples is 47.2 nC, reduced by 46% compared with the total charge of unfilled PP.





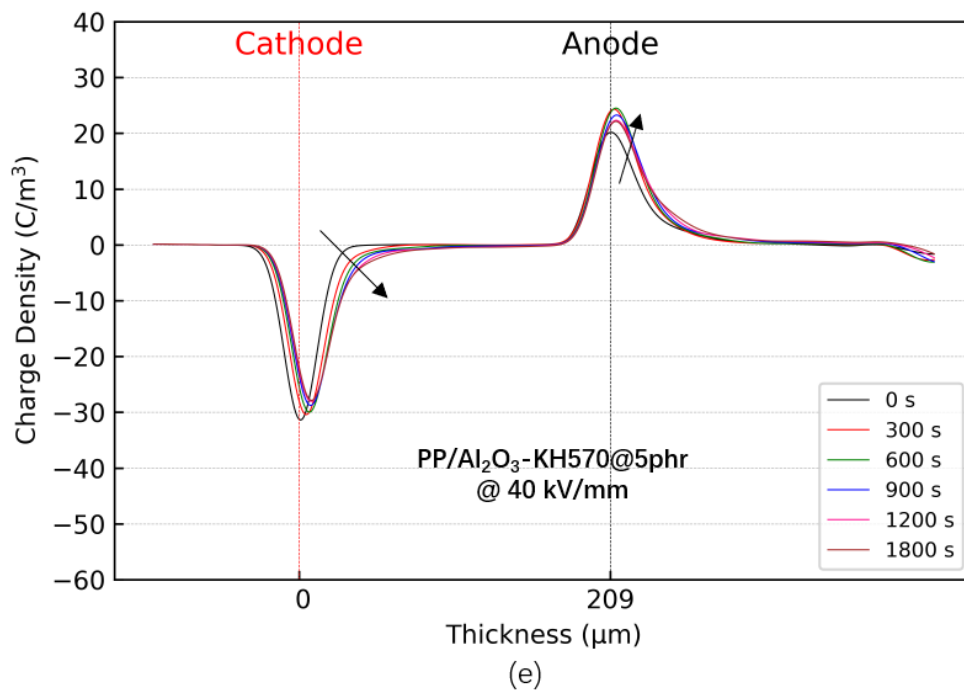


Figure 7.14 Space charge dynamics of PP nanocomposites containing (a) 0 phr (b) 0.5 phr (c) 1 phr (d) 2 phr (e) 5 phr of KH570-treated nano-alumina stressed at 40 kV/mm DC electric field at 30 °C.

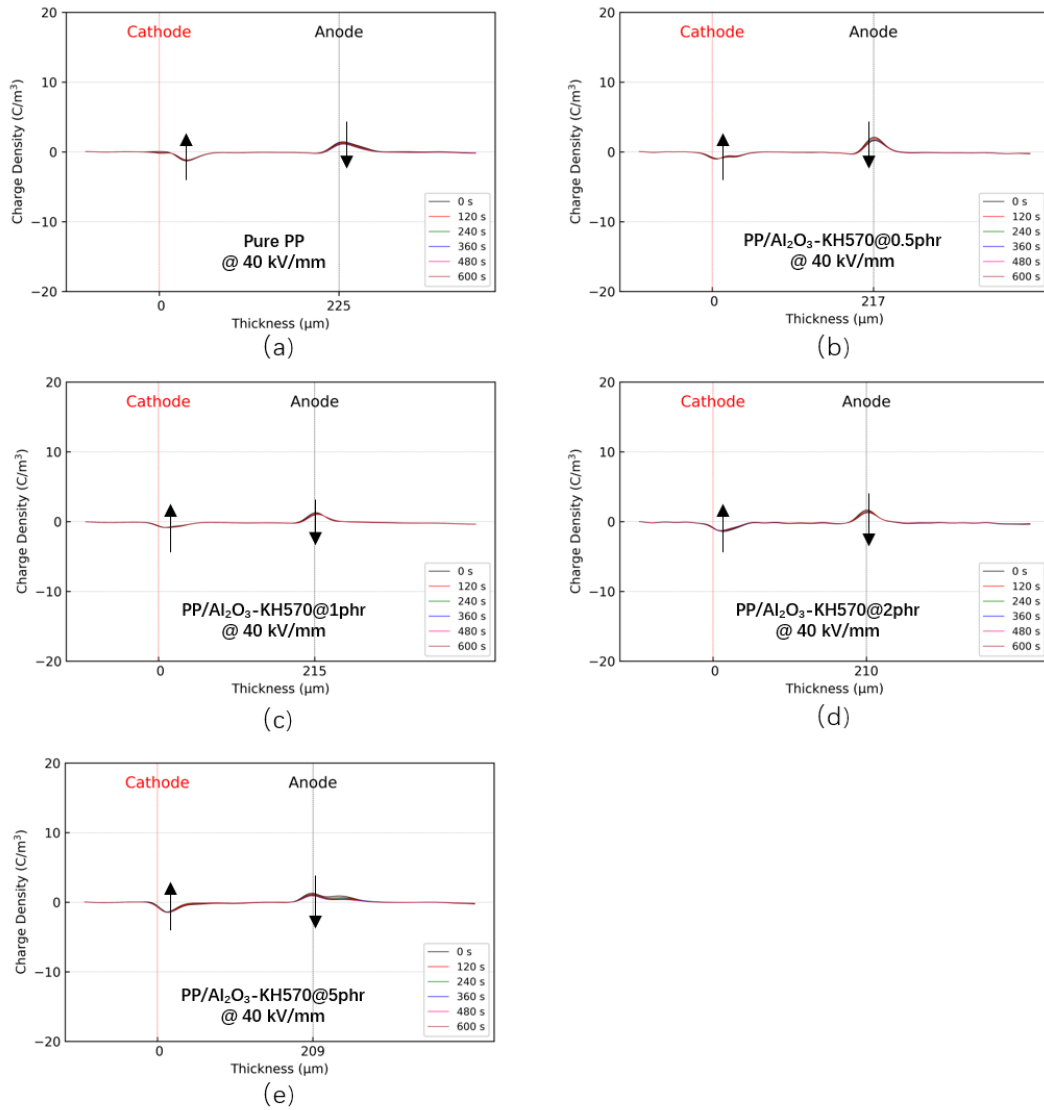


Figure 7.15 Space charge decay process of PP nanocomposites containing (a) 0 phr (b) 0.5 phr (c) 1 phr (d) 2 phr (e) 5 phr of untreated nano-alumina stressed at 40 kV/mm DC electric field at 30°C.

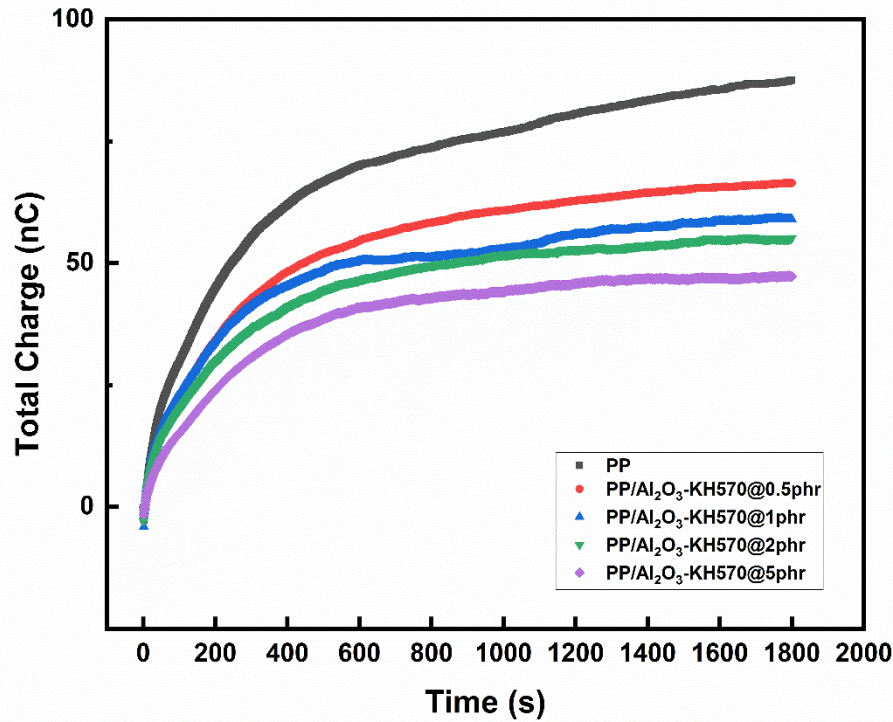


Figure 7.16 Total charge amount during the polarization process in the PP nanocomposites samples containing KH570-treated nano-alumina under the DC electric field of 40 kV/mm at 30 °C

7.4.4 Measurements for Unfilled PP and PP Nanocomposite under Temperature Gradient

After comparing the performance of PP/KH570-treated nano-alumina sample with different filling content, PP/nano-Al₂O₃-KH570@ 5 phr was selected to study the temperature dependent space charge dynamics. Unfilled PP was also tested as a reference. Figure 7.17 shows the time-dependent space charge behavior of unfilled PP and PP/nano-Al₂O₃-KH570@5 phr nanocomposite at different temperatures. The tests were conducted under a 40 kV/mm DC electric field 30 min. Figure 7.18 shows the

space charge decay process during the depolarization time for another 10 min. The tests were conducted at 30 °C, 50 °C, 70 °C and 90 °C.

At 30 °C, obvious homo space charge injection is found near the cathode of unfilled PP and it moves towards the interior of the sample over time. It can also be observed that a few homo charges is injected near the anode. The total charge is slowly increased during the polarization time. At 50 °C, a clear increase of homocharge is found near both electrodes. More injected homo charges move to the deeper interior of unfilled PP over time. Nevertheless, when the temperature reaches 70 °C, apparent homocharge injections from both electrodes are measured and there is a significant space charge accumulation in the first 600s. The space charge from both electrodes migrates further deeper into the bulk of the unfilled PP sample. The neutralization of the electron injected from the cathode and the holes injected from the anode might occur inside the sample. As the temperature continuously goes up to 90 °C, an obvious positive space charge accumulation is observed in the bulk of unfilled PP samples, suggesting the huge amount of space charge is accumulated in the sample. The injection of homocharge from both electrodes is enhanced during the voltage-on period.

Compared to the unfilled PP at the same temperature, PP/nano-Al₂O₃-KH570@5 phr exhibits a different space charge dynamic under the same electric field. Figure 7.23(b) shows only a small amount of homocharge injection from both electrodes during the polarization time at 30 °C. The injected space charge migrates slowly to the bulk of the

sample with time. Similar space charge development in PP/nano-Al₂O₃-KH570@5 phr at 50 °C is identified. However, when the temperature is rising up to 70 °C, more charges are injected from both electrodes and the injection depth is increasing with the stressing time. When it reaches 90 °C, a significant increase of homo space charge injection in the vicinity of both electrodes is recorded during the voltage-on time. A large number of positive charges move into the deeper interior position of the sample over time.

Figure 7.17 compares the depolarization space charger behavior of unfilled PP and PP/nano-Al₂O₃-KH570@5 phr nanocomposite after the 40 kV/mm electric field is removed at different temperatures. The existence of the homocharge peaks near both electrodes could evidentially prove the space charge injection. In terms of unfilled PP, the space charge decays rapidly with time at 30 °C. But with the increasing testing temperature, the decay process becomes slower than that at 30 °C. At 70 °C and 90 °C, the injected homocharge accumulation can be observed in the bulk of the sample rather than in the vicinity of electrodes. PP/nano-Al₂O₃-KH570@5 phr sample shows fast charge dissipation during depolarization at each temperature. However, the density of remaining charges is increasing as temperature goes up.

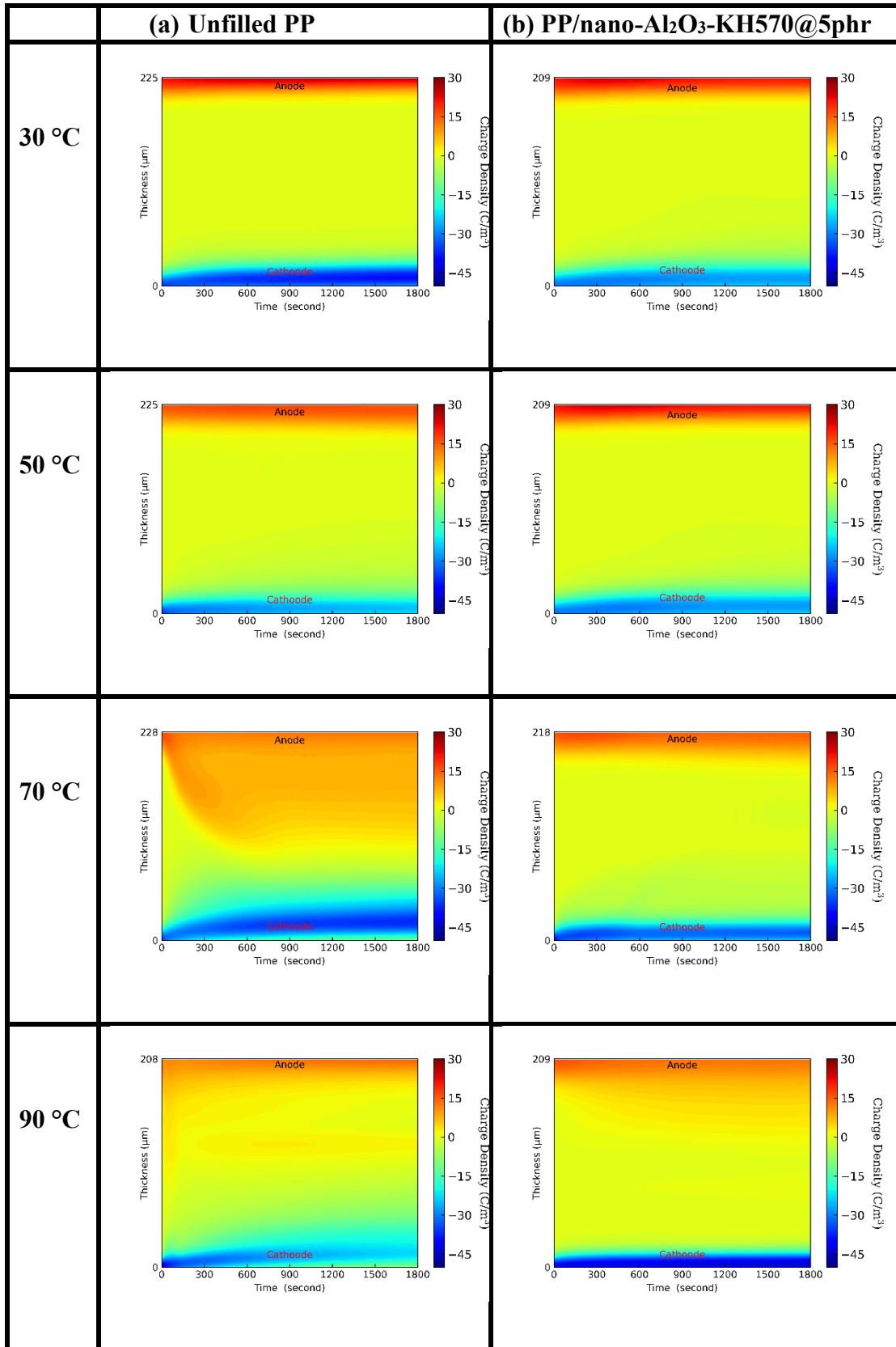


Figure 7.17 Temperature dependent space charge behavior of (a) unfilled PP, (b) PP/nano-Al₂O₃-KH570@5 phr nanocomposite.

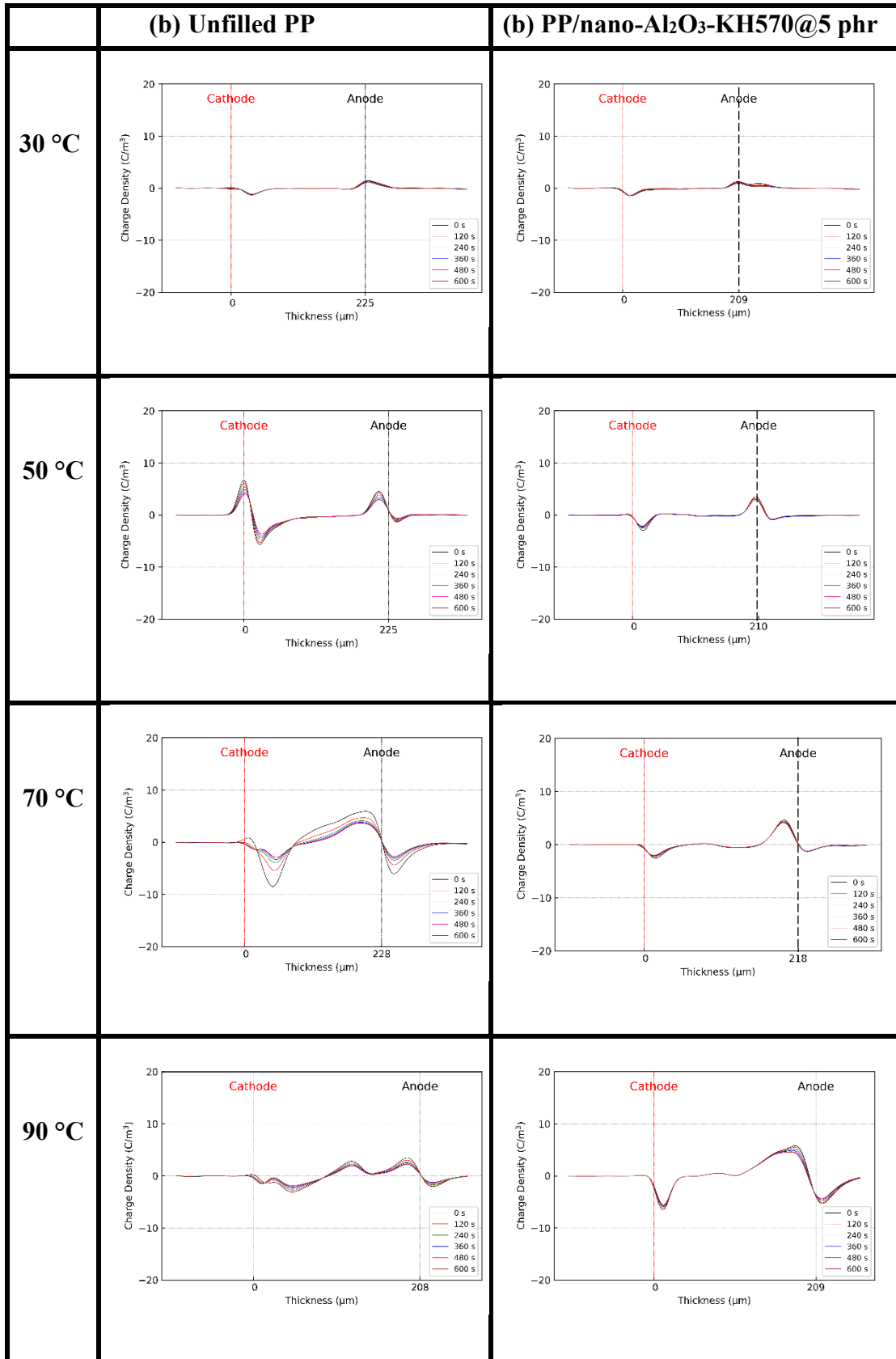


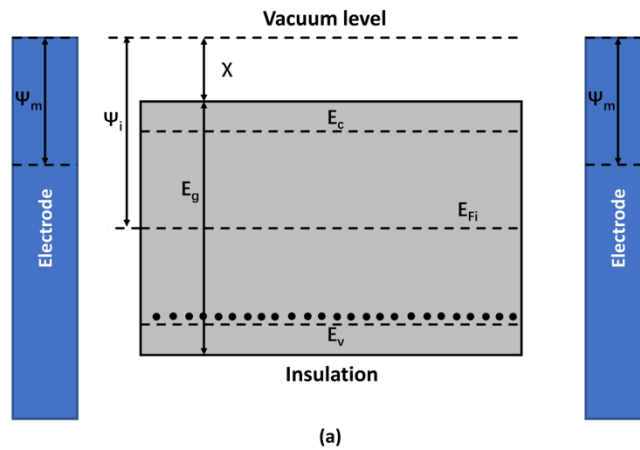
Figure 7.18 Temperature dependent charge decay behavior of (a) unfilled, (b) PP/nano-Al₂O₃-KH570@5 phr nanocomposite.

7.4.5 Discussion

Under DC electric field, the typical charge injection from electrodes is the carrier injection, which is realized by field assisted thermal-ionic emission (Schottky emission) [77], [166], [167]. The energy band structure for the polymer-electrode system is shown in Figure 7.19, where Ψ_m is the work function of the electrode material, χ is the electron affinity of polymer material, Ψ_i is the work function of the polymer, $\phi = \Psi_m - \chi$ is the potential barrier of charge injection, E_c is the conduction band of polymer, E_v is the valence band of polymer, E_{Fi} is the Fermi energy level, E_t is the trap energy level, E_g is the bandgap of polymer and E is the external electric field strength [168]. Under the electric field, the electrons from the cathode electrode would hop over the potential barrier at the interface between electrode and polymer through Schottky emission and reach the conduction band of the polymer. Some of the injected electrons are then trapped in the conduction band to form the space charge near the interface. In addition, the energy band in the polymer will tilt due to the bending of the conduction band under electric stress. Hence, the potential barrier for carrier injection near the anode is higher than that for negative charge injection from the cathode. Therefore, charges need more energy to hop into anode electrode than into cathode electrode. This is consistent with our findings in previous sections.

By comparing the space charge behavior between unfilled PE sample and unfilled PP sample at same electric field, it is found that homocharge was injected into both

materials, but the total charge of PE is more than that of PP under the same electric field and temperature. This difference could be explained based on the energy band theory of solid discussed above. When using the same electrodes, the potential barrier for charge injection, $\phi = \Psi_m - \chi$, is decided by the electron affinity of the polymer. The electron affinity of polyethylene material is 2.37 eV and the electron affinity of polypropylene material is 1.86 eV. Therefore, charge injection is more likely to happen in PE material.



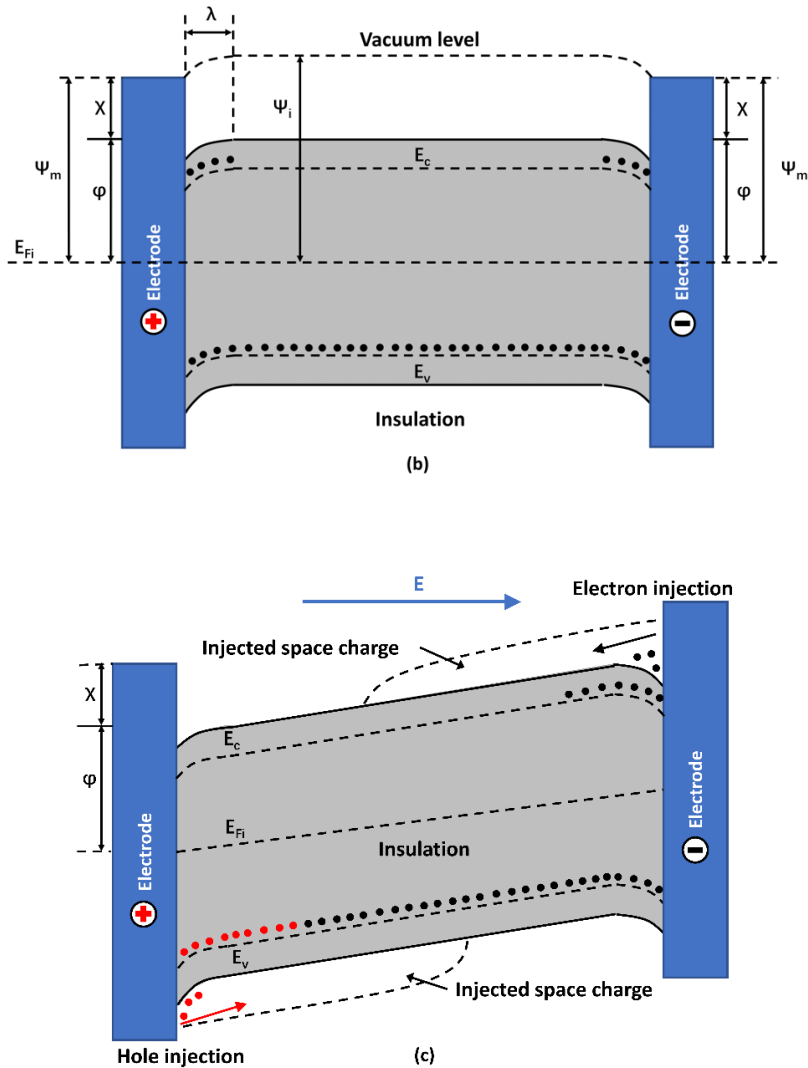


Figure 7.19 Energy band diagrams for the polymer-electrode system (a) before the polymer is in contact with the electrodes; (b) when the polymer is attached to the electrodes; (c) when an external electric field is applied.

The mobility of space charge is tightly relevant with the trap energy level and trap level density in the sample [169] and the relationship can be expressed as

$$\mu \approx \mu_0 \frac{N}{M} e^{-\frac{U}{KT}} \quad (7.4)$$

Where μ_0 is the mobility of free carrier, N is the number of energy level vacancy, M is

the total number of traps, U is the trap energy level, K is the Boltzmann constant and T is the temperature. Both PE and PP are semi-crystalline polymers, so there are amorphous and crystalline regions inside the material. From the TSDC results in this study, the trap level density of PP is about the same as for PE, but the trap energy level of PP is higher than that of PE. Hence, the charge mobility of PE is higher than that of PP under the same testing condition, which results in a higher injection depth in PE.

With the introduction of nanoparticles into PP, better space charge suppression has been observed in the nanocomposites. The total charge and injection depth decrease as the filling content increases. As discussed before, the addition of nano-alumina largely increases the interface area between nanoparticles and matrix PP and the interphase between PP spherulites, in which more deep traps are generated. The density of the deep trap is increasing with the increase of filling content as characterized by TSDC measurement. These deep traps can capture the homo space charges injected from the electrodes. The trapped charges can form the homo charge blocking layer around the interface between sample and electrodes and it can block the further injection of homocharge.

Upon the surface treatment, the total charge in the PP composite samples containing KH570-treated nano-alumina is further reduced compared with PP composite samples containing the same filling content of untreated nano-alumina. The surface treatment improved the compatibility between nanoparticles and PP, resulting in better

distribution of nanoparticles in composite systems and reduction of the size of PP spherulites. As a result, the interfaces are significantly increased, which leads to the increased density of deep traps.

When the temperature is low, the injected carriers can be easily captured by the traps and the space charge only accumulates around the electrodes. With the temperature increases, the trapped carriers are thermally excited and their mobility increases. The carriers then get out of the trap and start migrating again. Also, according to [12], [70], [170]–[172], the density of traps decreases due to the reduction of the interface between the phases at high temperature. Therefore, the charge injection for PP and its nanocomposites is increased when the temperature goes up.

7.5 Trap Characterization

7.5.1 Introduction

The defects and chemical impurities in solid dielectrics could result in the localized states within the energy band gap of the material which can capture or trap an electron or a hole. These localized states are also called traps for solid dielectrics. The traps electron and holes cannot move freely and contribute to the conduction or valence band of the dielectric, which results in decreased electrical conductivity. Therefore, the trap energy level and trap level density are important parameters in determining the electrical properties of nanocomposites. Generally, there are two kinds of traps, shallow

traps and deep traps. The shallow traps are generated due to different conformations of polymeric molecules. These conformations can cause physical disorders, resulting in the localized states in the bandgap. These states assist the charge transportation, named as shallow traps. The shallow trap energy level is usually between 10^{-2} eV to 1 eV [59].

The deep traps are formed due to chemical disorders. The chemical disorders are caused by the side chains, additives, reaction products and impurities. The physical disorder is also developed around the chemical disorders as the electronic properties of the foreign atoms are different from that of the original atoms in the polymer backbone. Thus, it leads to the formation of additional deeper energy levels in the bandgap, also known as deep traps. The deep traps suppress the space charge and charge transportation. The trap distribution in the energy band of the polymer is shown in Figure 7.20. The width of the bandgap is about 9 eV for polymeric insulation material [75]. The electron traps and hole traps are distributed on the different sides of the Fermi level. The shallow traps of electron trap exist near the bottom of the conduction band and the deep traps of the electron trap exist near the Fermi level. The hole traps have the similar distribution rule.

The electrical conductivity of a solid is related to the mobility and concentration of free charge carriers. The lower the mobility and the concentration of the free charge carriers, the lower the electrical conductivity of the solid. The detrapping of trapped electrons happens when electrons gain enough energy from the electric field. Then, the detrapped electrons start immigrating towards the opposite electrode. They might be trapped and detrapped for few times until they move to the opposite electrode.

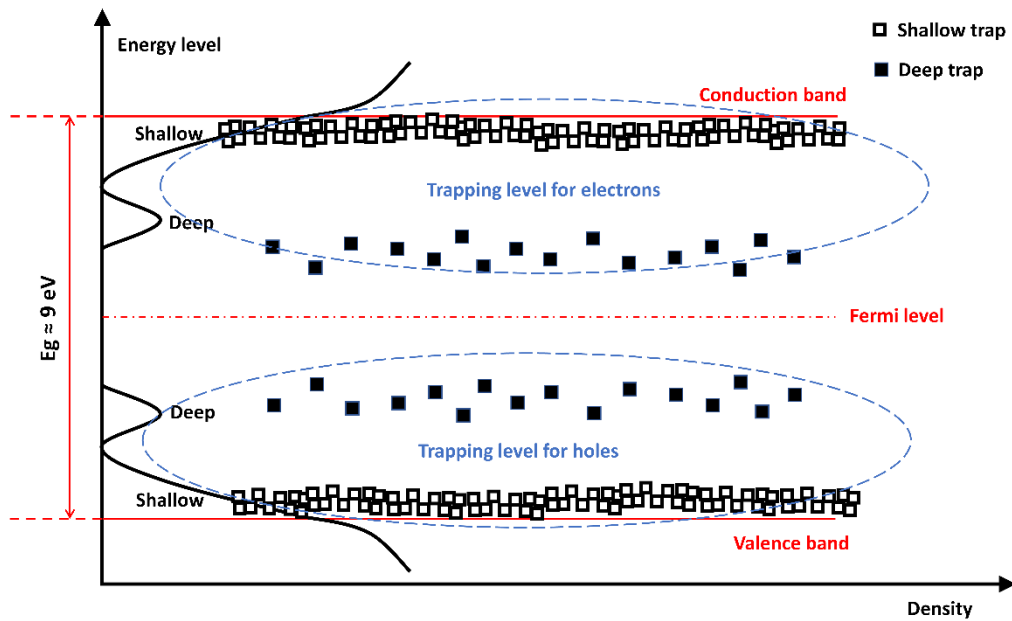


Figure 7.20 Schematic representation of trap distribution in the energy band of a polymer.

The detrapping of space charge in the polymeric dielectric is often achieved by thermal stimulation, electrical stimulation, or light stimulation. The distribution of the traps can be obtained by measuring the stimulated current and voltage during the detrapping process. Among these techniques, the thermally stimulated current method is the most widely used as it is fairly easy to conduct the test and obtain the trap energy level and trap density of insulation material. The TSC method includes the thermally stimulated polarization current (TSPC) method and thermally stimulated depolarization current (TSDC) method. TSDC is more commonly employed in the trap characterization of polymeric insulation material [173]–[175]. This method provides trap information of solid dielectric by measuring the depolarizing current caused by the depolarization and

charge detrapping during the heating process. Methods such as the initial rise method, peak temperature method and curve-fitting method for extracting the trap parameters from TSC curves have been reported in [119]. In this study, the modified thermally stimulated depolarization current is adapted as it can show the trap distribution in a continuous way. For the convenience of discussion about TSC theory, it is just the electron injection from the electrode that is considered. In other words, a electric field is applied across the sample and the anode electrode is in contact-blocking state [176]. The detected current in the measurement circuit of the conventional TSC method can be expressed as Equation (7.5):

$$\begin{aligned}
 J(T) &= \int_{E_v}^{E_c} \left[\int_0^l e f_0(E) N_t(E) \frac{x}{d} e_n(E, T) e^{-\frac{1}{\beta} \int_{T_0}^T e_n(E, T) dT} dx \right] dE \\
 &= \frac{el^2}{2d} \int_{E_v}^{E_c} f_0(E) N_t(E) e_n(E, T) e^{-\frac{1}{\beta} \int_{T_0}^T e_n(E, T) dT} dE
 \end{aligned} \tag{7.5}$$

where $N_t(E)$ is the distribution function of a continuous trap level distribution, l is the spatial depth that the trap level distribution exists in the sample, e is the electronic charge quantity, f_0 is a constant that shows the initial occupancy of a trap level, E is the energy level of trap, d is the thickness of the sample, β is the heating rate, ν is the frequency factor, $e_n(E, T)$ is the emission rate of electrons at trap level E and temperature T . The emission rate is calculated based on Equation (7.6):

$$e_n(E, T) = \nu e^{-\frac{E_t}{kT}} \tag{7.6}$$

where T is the temperature and k is the Boltzmann constant. The frequency is assumed

to be 10^{12} s^{-1} as discussed in [177]. Obviously, the calculation of trap level distribution would be very complex. F. Tian *et al.* developed a new function, $G1(E, T)$, to calculate the weighted contribution of an electron at trap level E to the current at temperature T ,

$$\begin{aligned} G1(E, T) &= e_n(E, T) e^{-\frac{1}{\beta} \int_{f_0}^T e_n(E, T) dT} \\ &= \nu e^{-\frac{E}{kT}} e^{-\frac{1}{\beta} \int_{f_0}^T e_n(E, T) dT} \end{aligned} \quad (7.7)$$

After using the integration approximation [176], the Equation (7.7) is then expressed as:

$$G2(E, T) = \nu e^{-\frac{E}{kT}} e^{-\frac{\nu k T^2}{\beta E} e^{-\frac{E}{kT}}} \quad (7.8)$$

It was proved that there might be a significant difference between results from Equation (7.7) and Equation (7.8), another approximation by using a delta function is raised in [119]:

$$G(E, T) = A(E_m) \delta(E - E_m) \quad (7.9)$$

where E_m is the demarcation energy above which the traps are free from electrons and A is a function of E_m . Assuming that all the traps are initially filled and $f_0 = 1$, the trap level distribution, $Nt(E_m)$, can be directly calculated by using Equation (7.5) and (7.9) as follow:

$$f_0(E_m) Nt(E_m) = \frac{2d}{e l^2} \frac{J(T)}{A(E_m)} \quad (7.10)$$

The approximal value of $A(E_m)$ is equal to the maximum value of $G1(E, T)$ according to [176]. Then the trap level distribution can be calculated in MATLAB based on the

TSC data. Figure 7.21 shows the measured current from TSC and the calculated density distribution of trap energy level of unfilled PE sample. A small peak of the thermally stimulated current can be firstly observed around the glass transition temperature of PE, -50 °C. The cause of this current peak is the movement of the molecular chain of PE. The corresponding peak of the trap energy level is about 0.65 eV. The traps near this peak are considered as shallow traps in PE. Another obvious current peak of 65 °C corresponds to the trap level of 0.96 eV. It can be identified as the deep traps due to the detrapping of the trapped charges [178]–[180]. The trap level density of deep traps in virgin PE is about $2.0 \times 10^{19} / \text{m}^3 \cdot \text{eV}$, which is consistent with the results in [59], [181]–[183]. T.Mizutani et al. also studied the trap energy level and trap level density of PE through X-ray-induced thermally-stimulated current technique and they have found there is always a trap energy level peak of PE around 50 °C. The trap depth was calculated to be 0.9 eV and the initial density of trapped carriers was $2.9 \times 10^{20} / \text{m}^3 \cdot \text{eV}$ [184]. The research reported by K.J. Kao et al. also supports the fact that PE has a trap peak around 0.97 eV [182]. The obtained trap information of PE nanocomposites and PP nanocomposites is presented and discussed in the next section.

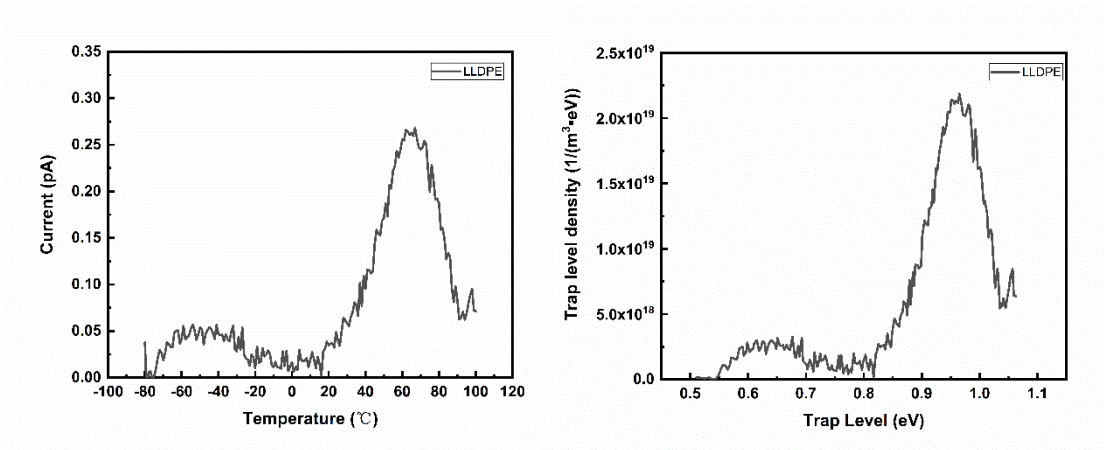


Figure 7.21 TSC current (left) and calculated trap distribution (right) of virgin PE.

7.5.2 Results and discussion for PE Nanocomposites

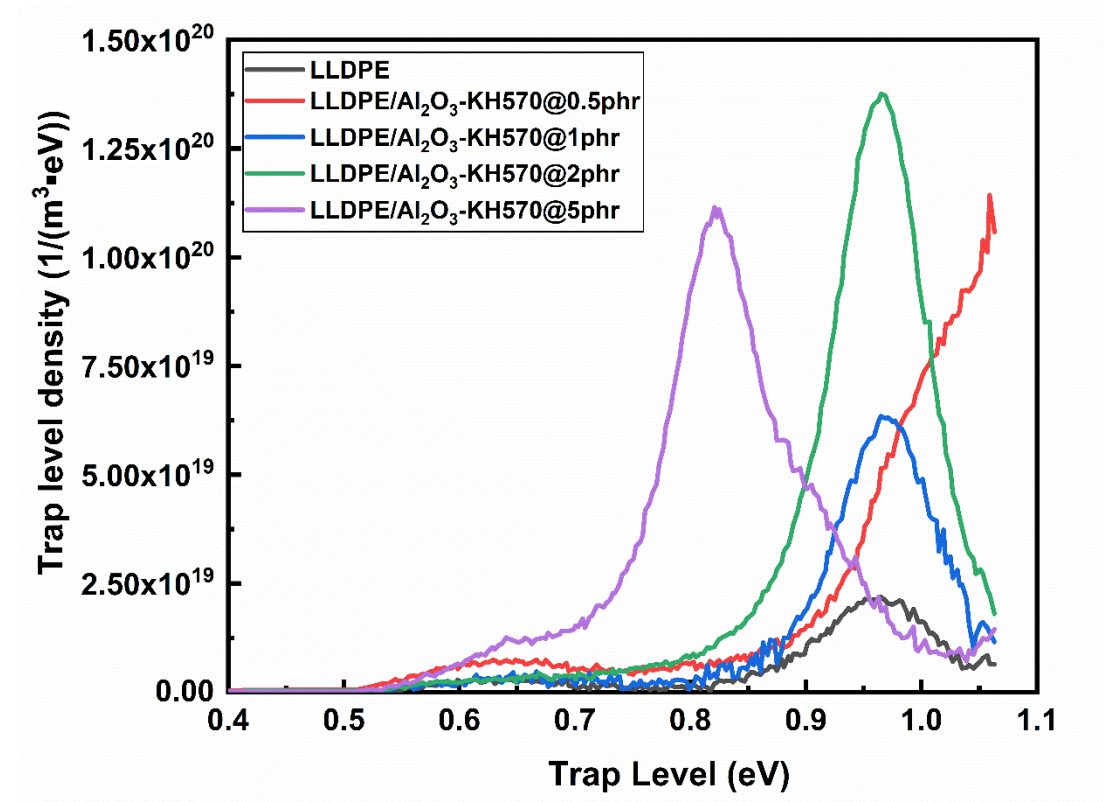


Figure 7.22 Trap distribution of PE nanocomposites containing KH570-alumina.

The density distribution of trap energy level of PE nanocomposites containing KH570-treated nano-alumina particles with varying content is shown in Figure 7.22. The most obvious is that the addition of nano-alumina increases the trap level density compared with unfilled PE, namely the increase of the depolarization current from the TSC test. Additionally, the peak position of the trap energy level moves towards the low trap energy level as the filling content of nanoparticles increases. The PE/ Al₂O₃-KH570@0.5 phr sample has shown the highest trap energy level of about 1.06 eV, suggesting more deep traps are produced in this nanocomposite. The trap level density of this sample is also increased to $1.0 \times 10^{20} / \text{m}^3 \cdot \text{eV}$. It is impossible to show the whole peak of this sample due to the limited energy provided by the thermally stimulated method. In addition, to release the charges trapped in traps of 1.05 eV, the stimulation temperature should be raised around 100 °C, which is out of the normal working temperature range of PE. The peak position of samples containing 1 phr and 2 phr of nano-alumina is similar to unfilled PE but with a wider range. The density of them, $6.3 \times 10^{19} / \text{m}^3 \cdot \text{eV}$ and $1.4 \times 10^{20} / \text{m}^3 \cdot \text{eV}$ respectively, are much higher than that of unfilled PE. The results indicate that more deep traps are formed in these samples. However, the peak trap level of PE/ Al₂O₃-KH570@5 phr reduces to 0.83 eV but with a high density of $1.1 \times 10^{20} / \text{m}^3 \cdot \text{eV}$. In other words, more shallow traps are generated in such nanocomposite samples.

Previous research has indicated that the origin of the traps in polymer nanocomposite consists of the traps induced by the chemical defects and the chemical bonds on the

surface of nanoparticles; the traps induced in the interphase region between the crystalline and amorphous regions and the interphase region between the spherulites; the traps induced in the interfacial region between the nanoparticles and the matrix. Moreover, according to previous studies [185]–[188], the discrete deep traps caused by chemical defects and chemical bonds are with energy levels between 1.0 and 5.0 eV and the continuous deep traps generated in the interface and interphase region of polymeric nanocomposites are about 1 eV. In this study, the detected traps of around 0.97 eV in PE nanocomposites are considered to be the cavity traps formed in the interphase region between the amorphous region and crystalline region and the interface between the nano-alumina and matrix polymer. In these cavity traps, the electrons are trapped by the polarized PE molecules. This is because the short-range repulsive force between polymeric molecules decreases as the distance between the molecules is increased in the cavities [185]–[188]. The shallow traps at around 0.7 eV in PE nanocomposites are mainly produced during the glass transition process in the amorphous region. From the results, the peak trap energy level density of PE nanocomposites is about 3 to 7 times larger than that of unfilled PE, indicating that a large number of traps have been introduced. The increase of the number of traps for nanocomposites is because the total area of interfacial region between nanoparticles and matrix polymer is increased with the increase of the filling content. It can also be observed in the SEM images. In addition, TGA and FRIR results in Chapter 4 show that the KH570 coupling agent is chemically grafted on the surface of nano-alumina

particles. Hence, more deep traps should be generated in the nanocomposite sample. However, the charges trapped in these deep traps (>1.5 eV) are hard to be released by thermal stimulation.

7.5.3 Results and discussion for PP Nanocomposites

The trap energy level distribution of the PP nanocomposites is shown in Figure 7.23. Two peaks of trap energy level are found for each kind of nanocomposite sample. For unfilled PP, the first peak, located at around 0.75 eV, represents the shallow trap peak. The peak of the shallow trap level density is about $1.1 \times 10^{19} / \text{m}^3 \cdot \text{eV}$. The corresponding temperature on the current curve of TSC is about -10 °C, which is the glass transition point of PP. Therefore, the shallow traps in PP/nano-alumina composite are formed due to the movement of the PP molecular chain. The second peak is the deep trap peak located at around 0.97 eV and the peak of deep trap level density is about $2.0 \times 10^{19} / \text{m}^3 \cdot \text{eV}$. These traps are generated by the relaxation of the charges trapped at the interphase region.

With the addition of KH570-treated nano-alumina particles, the small peaks of PP nanocomposites are still at about 0.75 eV and the density remains at the same level. This is to say that the addition of nanoparticles does not affect the glass transition process of PP. But the behavior of deep trap peak becomes more complex for PP nanocomposites. It is found that the deep trap peak shows at a similar trap level as

unfilled PP (about 0.97 eV), while the peak becomes wider and significantly higher as the filling content increases. The trap level density at 0.97 eV of samples incorporating 0.5 phr, 1 phr, 2 phr and 5 phr of KH570-treated nano-alumina is $3.9 \times 10^{19} / \text{m}^3 \cdot \text{eV}$, $5.5 \times 10^{19} / \text{m}^3 \cdot \text{eV}$, $7.4 \times 10^{19} / \text{m}^3 \cdot \text{eV}$ and $2.2 \times 10^{20} / \text{m}^3 \cdot \text{eV}$ respectively. The results indicate that the density of the deep traps is greatly increased for PP/alumina nanocomposites and the density increases with the increase of filling content. Another important finding is that an additional trap level peak is observed in the range of 1.1 to 1.2 eV for PP/Al₂O₃-KH570@0.5 phr and PP/Al₂O₃-KH570@1 phr, suggesting the deeper traps are generated in such composite systems. This should be attributed to chemical bonds in the interface area between the nanoparticles and matrix material is increased when the filling content is low (≤ 1 phr). When the filling content is high (> 1 phr), the agglomeration of nanoparticles becomes serious, resulting in the reduction of the effective interfacial area.

Similar to the previous discussion, the interphase between the crystalline region and amorphous region and the interfacial area between the matrix PP and nano-alumina play an important role in generating carrier traps of semicrystalline polymer nanocomposite. According to the POM results in Chapter 4, the nanoparticles act as heterogeneous nucleating agents, which reduces the PP spherulite size and increases the total number of PP spherulite. The interphase between crystalline and amorphous regions and the interphase between spherulites are then obviously increased compared with unfilled PP. Moreover, the interface area between the matrix PP and nano-alumina

increases compared with unfilled PP. Consequently, both the density and proportion of the deep traps of PP nanocomposite are increased.

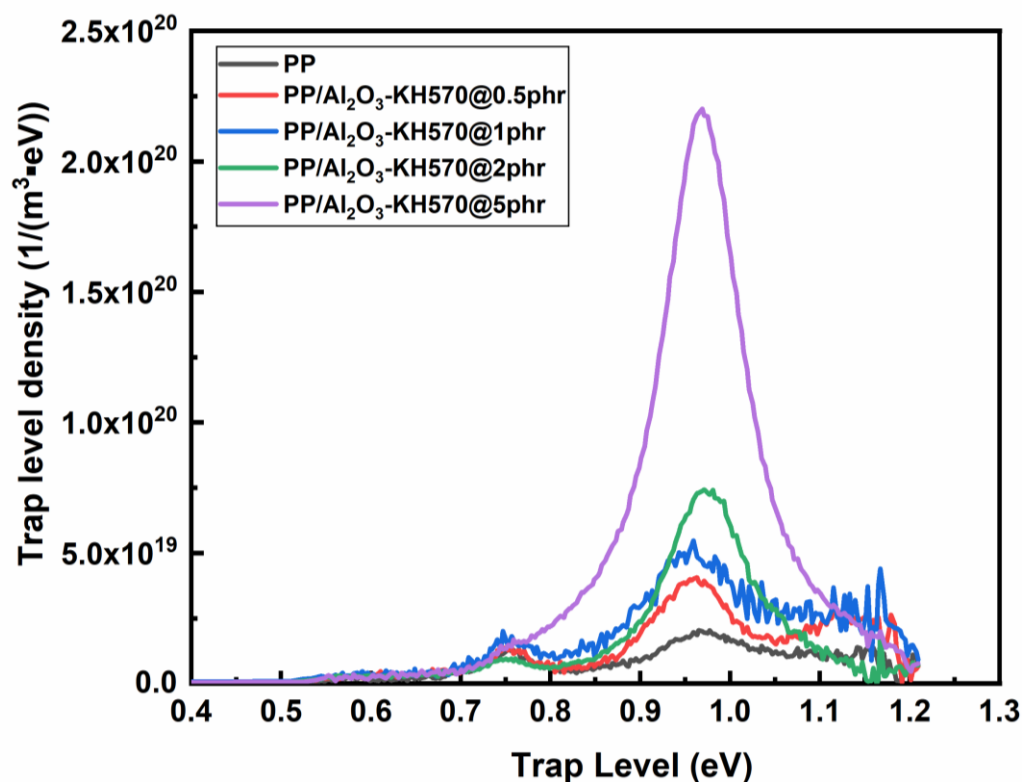


Figure 7.23 Trap distribution of PP nanocomposites containing KH570-alumina.

To further study the dominant factor in determining the trap distribution of PP nanocomposites, some chemical and morphological analysis for PP nanocomposites has been conducted in Chapter 4. The crystallinity was calculated based on the DSC results and characterize interphase between the crystalline region and the amorphous region. The SEM results can semi-quantitatively demonstrate the interfacial area between the polypropylene and the nano-alumina particles. The obtained spherulite data from POM images can semi-quantitatively shows the interphase between

spherulites. Compared with PP/Al₂O₃-KH570@2 phr sample, PP/Al₂O₃-KH570@5 phr has similar crystallinity, less effective interface area, but more interphase region between spherulites, resulting in more deep traps. It suggests that the interphase between spherulites seems to be the dominant factor for the increase of the traps in PP/nano-alumina composites.

7.6 Summary

In this chapter, space charge dynamics of PE nanocomposites and PP nanocomposites are presented and discussed. Homocharge accumulation was observed near both electrodes for all the nanocomposite samples. For unfilled PE, the space charge density increases with the increased electric field. The introduction of untreated nano-aluminum can slightly reduce the space charge accumulation. The space charge accumulation in nanocomposite samples containing KH570-treated alumina is obviously reduced as compared with unfilled PE. The total charge firstly decreases and then increases as the filling content increases. PE/KH570-treated alumina@2phr sample shows the minimum space charge, which could be attributed to the increased density of deep traps. Compared with unfilled PE, unfilled PP sample has less space charge accumulation at the same electric field and temperature. This phenomenon is explained based on the energy band theory. The PP nanocomposite samples containing both untreated and KH570-treated alumina show a reduced intake of space charge

during polarization. The total charge amount at the end of polarization decreases as the filling content increases. The addition of surface-treated nano-alumina also reduces electric distortion. Under temperature gradient, PP nanocomposite exhibits better space charge suppression compared with unfilled PP. The space charge behavior is tightly linked with traps in the sample. When nanoparticles are introduced, the TSC results reveal that more deep traps are introduced in nanocomposites. In general, deep traps can significantly suppress space charge accumulation, while shallow traps have little effect. This is because deep traps can capture and trap the charge carriers, reducing the number of free carriers available for space charge formation. The reduced space charge in nanocomposites is mainly attributed to the suppressed charge injection from the electrodes, which is resulted from the trapped injected charge in deep traps. Additionally, deep traps can also reduce the dielectric loss and increase the DC breakdown strength of material by capturing and trapping the charge carriers, reducing their mobility. In conclusion, designing and optimizing the trap level in nanocomposite dielectrics is important for suppressing space charge and improving dielectric properties.

Chapter 8 DC conductivity

8.1 Introduction

For good HVDC cable insulation, except for excellent space charge suppression ability and high DC electrical breakdown strength, a reasonable DC conductivity is another important parameter to evaluate. The electrical volume conductivity plays a vital role in determining the electric field distribution of polymeric insulation material. It strongly depends on the strength of the electric field and temperature. The value of DC volume conductivity determines the DC losses. A lower DC volume conductivity would lead to a lower DC loss. It is of great importance in limiting the temperature rise in cable insulation and increasing its lifetime. The measurement of DC conductivity could also be used to evaluate insulation ageing of high voltage electric applications. Additionally, the obtained DC conductivity information could contribute to the design of future polymeric nanocomposite insulation systems [61], [189], [190].

The measurement of conductivity of polymeric insulating material is usually conducted by measuring the leakage current under DC electric field. The leakage current, which is caused by the movement of charges under the DC electric field, exists in all non-ideal dielectric materials. The leakage current consists of three parts, the capacitive charging current (i_c), the absorption current (i_a), and the conduction current (i_g), as shown in Figure 8.1. The capacitive charging current is dramatically high at the very beginning of applying a voltage across the sample and then rapidly reduces to zero. The absorption

current is gradually decreasing to zero over time. The conduction current is a constant current flow in the dielectric, which is usually employed to calculate the conductivity of different insulating materials. Therefore, in the actual measurement, the current value is relatively high when the voltage is first applied and then decreases with time to reach a quasi-steady state. For each tested sample, we take the average current value recorded in the last 10 seconds as its conduction current value. The DC conductivity could be calculated based on

$$\sigma = \frac{I}{V} \cdot \frac{d}{A} = \frac{J}{E} \quad (8.1)$$

Where I is the leakage current, V is the voltage across the sample, d is the thickness of the sample, A is the area of measurements electrodes, J is the current density and E is the electric field strength applied across the sample.

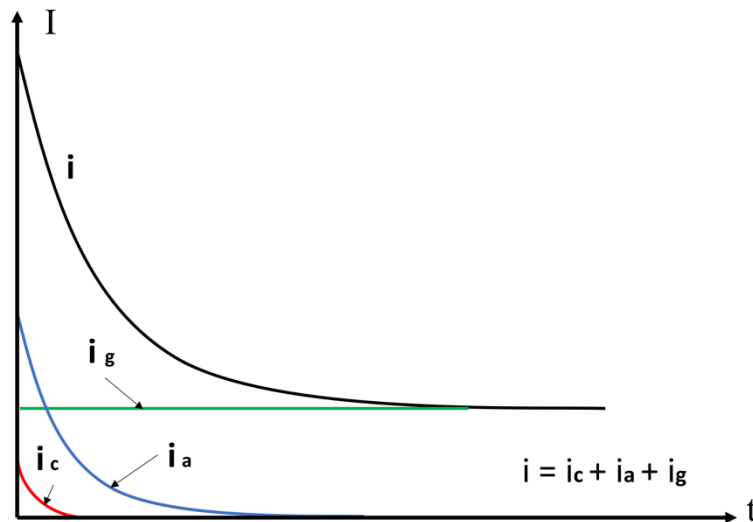


Figure 8.1 Typical time variation of the leakage current in a dielectric material.

In this chapter, the leakage current of PE nanocomposites and PP nanocomposites are measured by using the experimental setup introduced in Chapter 3 Section 3.3.8. The DC conductivity was calculated based on the data obtained under 30 kV/mm at 30 °C. In addition, to study the addition of nano-alumina on the threshold electric field of electrical ageing in nanocomposite systems, the chosen PE nanocomposite sample and PP composite sample were tested from 5 kV/mm to 70 kV/mm with a step of 5 kV/mm at 30 °C.

8.2 Results and Discussion

8.2.1 Measurements for PE nanocomposites

The leakage current of PE nanocomposites was monitored at 30 kV/mm and 30 °C for 600 s, as shown in Figure 8.2. The leakage current of the unfilled PE sample and PE composite samples containing untreated nano-alumina approaches a constant value after 250 s. The leakage current of PE composite samples containing KH570-treated nano-alumina shows a different behavior with a dramatic decrease in the first 30 s and becomes a constant value after that. It should be the consequence of the slow polarization process, as discussed by A.T. Hoang et al.[191]. Figure 8.3 compares the DC conductivity of unfilled PE sample and PE nanocomposite samples containing untreated and KH570-treated nano-alumina particles. The conductivity of unfilled PE is about 4.86×10^{-15} S/m. All the composite samples show reduced conductivity as

compared with unfilled LDPE. Upon the surface treatment, the PE/Al₂O₃-KH570 nanocomposite samples show smaller DC conductivity than the samples containing untreated nano-alumina with the same filling content. The DC conductivity of PE/Al₂O₃-KH570 nanocomposites firstly decreases and then increases with the increasing filling content. The PE/Al₂O₃-KH570@1 phr has the lowest DC conductivity among all the samples, which is about 7.12×10^{-16} S/m. The conductivity of unfilled PE is 4.86×10^{-15} S/m, which is about seven times greater than that of PE/Al₂O₃-KH570@1 phr.

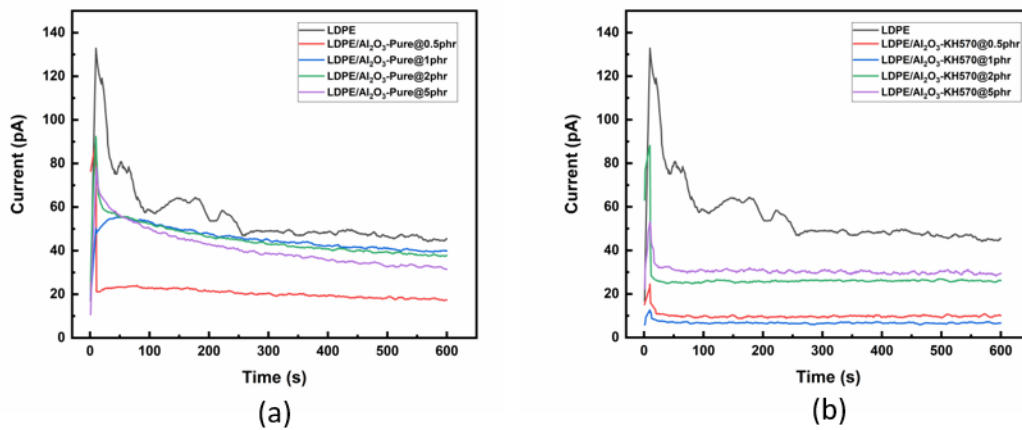


Figure 8.2 The measured leakage current curves of (a) PE/ untreated nano-alumina samples and (b) PE/KH570-treated nano-alumina samples at 30 kV/mm and 30 °C.

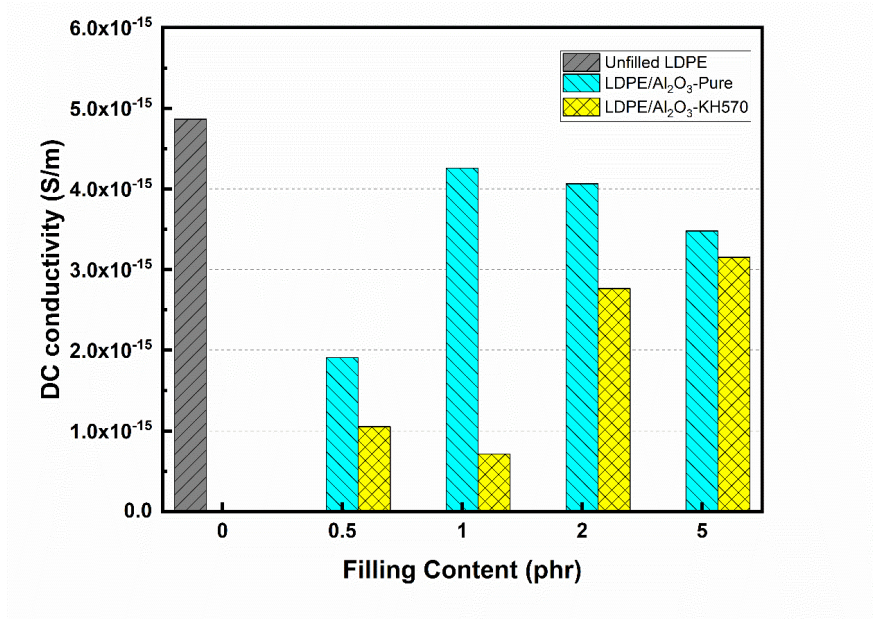


Figure 8.3 The DC conductivity of PE and its nanocomposites under a 30 kV/mm DC electric field at 30 °C.

8.2.2 Measurements for PP Nanocomposites

Figure 8.4 shows the leakage current of PP nanocomposites recorded at 30 kV/mm and 30 °C for 600 s. The leakage current of all samples reaches a quasi-steady state after 200 s. The current curves are quite noisy. It might be because the current values are approaching the sensitivity limit of the instrument. Figure 8.5 shows the DC volume conductivity of unfilled PP and PP nano-alumina composites as a function of filling content. The conductivity of unfilled PP is around 6.11×10^{-16} S/m. All PP composite samples show a reduction in DC conductivity compared with unfilled PP samples. For PP composites containing untreated nano-alumina particles, the DC conductivity decreases when the filling content is 0.5 phr and then increases when filling content is increasing from 1 to 5 phr. The conductivity of PP nanocomposites filled with KH570-

treated nano-alumina decreases with the increasing filling content until 1phr and increases with a further increase of filling content until 5phr. The magnitude of conductivity of PP nanocomposites containing KH570-treated alumina is similar to that of PP nanocomposites containing untreated alumina, suggesting the surface modification by KH570 has limited influence on the improvement of DC conductivity. The PP/Al₂O₃-KH570@1 phr has the lowest conductivity of 4.40×10^{-17} S/m, which is about 14 times smaller than that of unfilled PP.

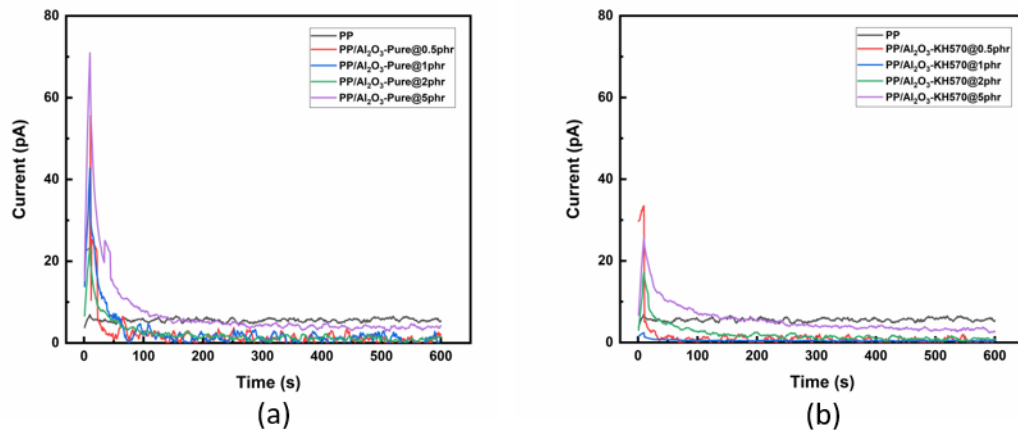


Figure 8.4 The measured leakage current curves of (a) PP/untreated nano-alumina samples and (b) PP/KH570-treated nano-alumina samples at 30 kV/mm and 30 °C.

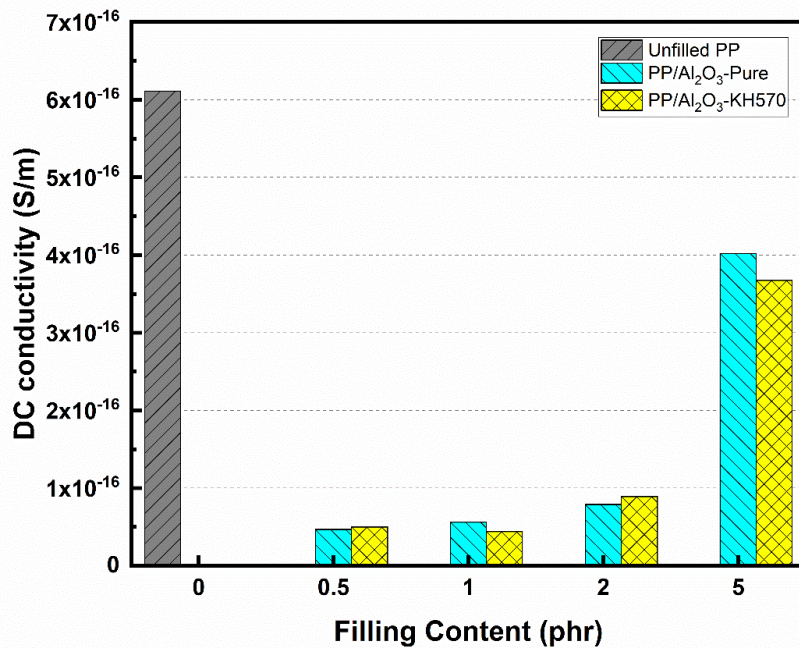


Figure 8.5 The DC conductivity of PP and its nanocomposites under a 30 kV/mm DC electric field at 30 °C.

8.2.3 Discussion

It is observed that the DC electrical conductivity of PE nanocomposites containing untreated and KH570-treated nano-alumina particles up to 5phr is lower than that of the unfilled PE sample. As for the PP nanocomposites, the samples filled with no more than 2phr nanoparticles have lower conductivity than unfilled PP. The reduction of conductivity is attributed to the increased interface between polymer and nanoparticles after introducing the nano-alumina particles. More traps are generated in the interfacial areas, which leads to the reduction of charge carrier mobility during the charge transportation [55], [64], [69], [149], [154], [192]. The increasing of conductivity at

high filling content is most likely due to the appearance of particle agglomeration.

From the results, the DC electrical conductivity of unfilled PP is more than one order of magnitude smaller than that of unfilled PE. Additionally, the conductivity of PP nanocomposites containing KH570-treated nano-alumina is also one order of magnitude smaller than that of PE nanocomposites containing KH570-treated nano-alumina when the filling content is the same. In other words, the PP nanocomposites own distinct advantage in reducing power losses when used as DC insulation material.

The complete mechanism of charge transport in the polymeric dielectric is still not clear yet. Researchers have proposed different charge transport models to explain the experimental results. The space-charge-limited conduction (SCLC) model [193], [194] is the most widely accepted one to describe the charge transportation behaviors in a solid dielectric material. To perform the theoretical analysis of conduction current in thin or thick film specimens of solid dielectric material, the following assumptions are made.

- 1) The characteristic of the carrier injection could be explained by using the energy band model.
- 2) Only the injected hole carriers are considered and an ohmic contact is made between the film sample and electrode (A similar treatment could be performed when only injected electron carriers are considered).
- 3) The current components due to carriers thermally generated and due to diffusion are neglected.
- 4) The density of free holes follows the Maxwell-Boltzmann distribution, and the

trapped holes are distributed as the Fermi–Dirac statistics.

- 5) The Pool-Frenkel effect, collision ionization and high field-effect mobility are neglected.

Figure 8.6 shows the typical J-E characteristic curve plotted in log-log scale for space-charge-limited current. The J-E curve can be divided into three bounded regions, the linear region, the trapped-SCLC region and the square region. The carrier distribution in the dielectric film under different situations is shown in Figure 8.7.

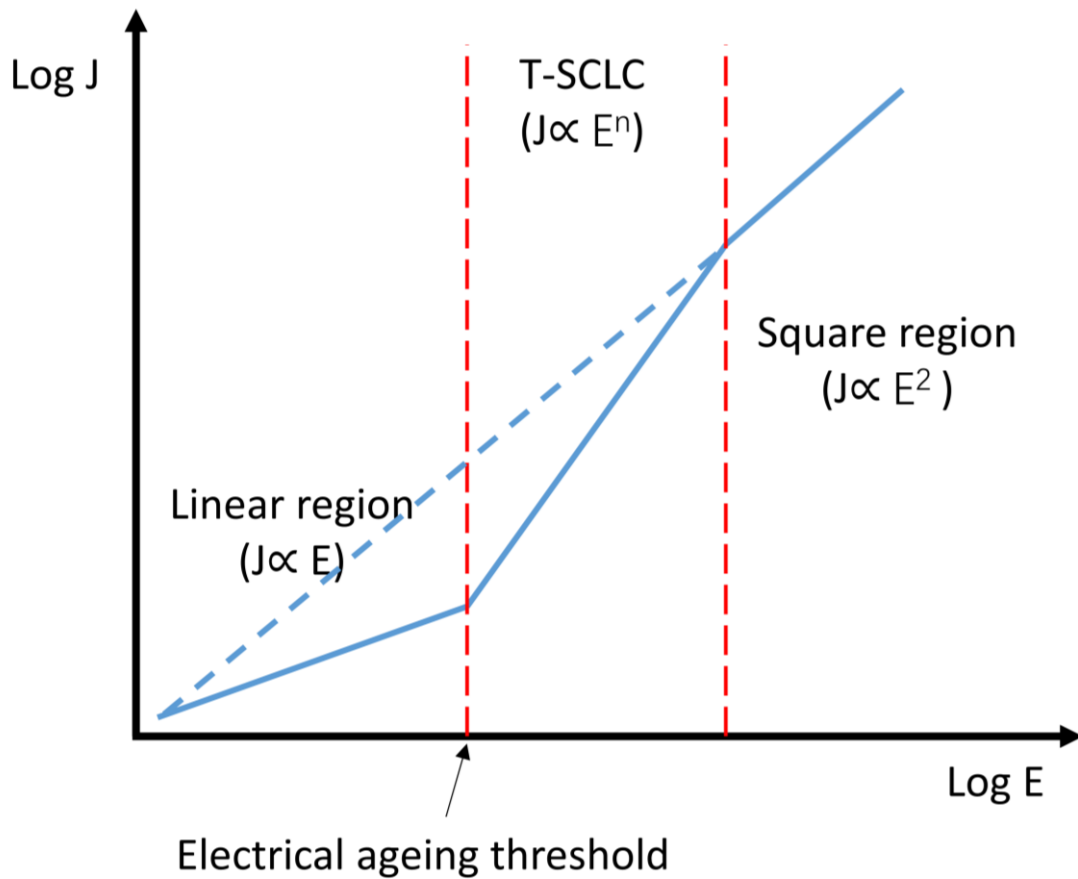


Figure 8.6 The J-E characteristic curve of space-charge-limited conduction current.

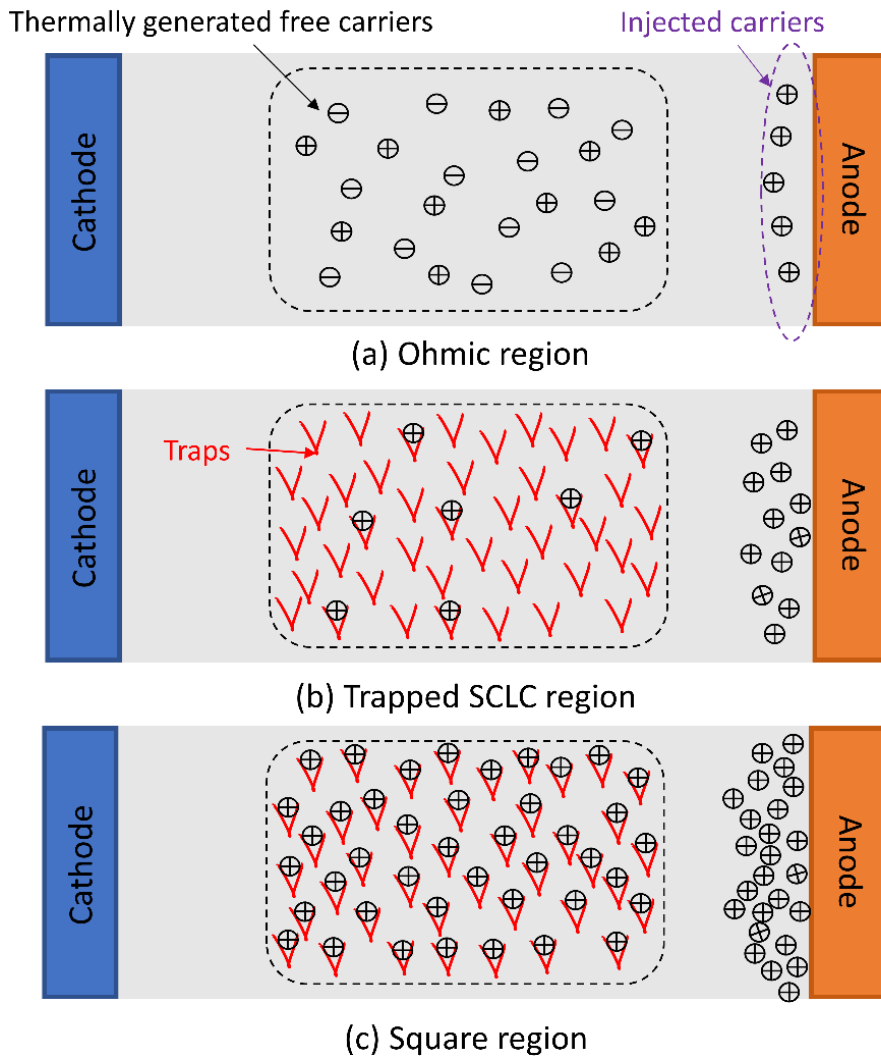


Figure 8.7 Carriers distribution in the dielectric film with space-charge-limited conduction theory.

Linear region

When the external electric field is low, the density of thermally generated free carriers in the film bulk is much larger than the density of injected carriers. The current follows ohm's law and the relationship between current density and electric field can be expressed as

$$J = qn_0\mu E \quad (8.2)$$

Where q is the electronic charge, n_0 is the concentration of the free charge carrier in thermal equilibrium, μ is the carrier mobility and E is the applied electric field strength. The slope of the J-E curve in the log-log scale should be equal to 1.

Trapped-SCLC region

When the applied electric field is increased, the density of injected carriers becomes larger than the density of thermally generated free carriers. The injected carriers at the electrodes start migrating towards the bulk of insulation and some of the injected carriers are trapped by the traps in the dielectric, which results in the space charge accumulation. The current caused by the transportation of other injected free carriers is determined by the trap energy level and trap level density of the dielectric. The conduction current at this time is also named the trapped space-charge-limited current. In most cases, the trap density is following the exponential distribution. The relationship between current density and electric field in this region can be expressed as [193]:

$$J = q^{1-l}\mu N_v \left(\frac{2l+1}{l+1} \right)^{l+1} \left(\frac{l}{l+1} \frac{\varepsilon}{H_0} \right)^l \times \frac{E^{l+1}}{d^l} \quad (8.3)$$

Where l is the ratio between the characteristic temperature (T_c) of trap distribution and the absolute temperature (T) of trap distribution, N_v is the effective density of states in the valence band, ε is the permittivity, H_0 is the function of the trap distribution and d

is the thickness of film sample. As T_c is usually larger than T , the index of the electric field ($l+1$) is always bigger than 2 [194]. Therefore, the slope of the J-E curve in the log-log scale is larger than 2 in the trap-filling region.

Square (SCLC) region

As the external electric field continuously increases, the traps are fully occupied by the injected carriers. The relationship between current density and electric field in this region follows the Child's Law [195]:

$$J = \frac{9\mu\epsilon E^2}{8d} \quad (8.4)$$

Thus, the slope of the J-E curve in the log-log scale at the square region is equal to 2.

The selected samples are tested under varying electric fields starting from 5 kV/mm until 70 kV/mm at 30°C. Figure 8.8 shows the J-E curves C of unfilled PE sample and PE/Al₂O₃-KH570@2 phr sample and Figure 8.9 displays the J-E curves of unfilled PP sample and PP/Al₂O₃-KH570@2 phr sample. At low field strength, the J-E characteristic follows the ohm's law. With the increase of electric field strength, the J-E curve is transferring from the ohmic region to the space-charge-limited region. In order to estimate the carrier mobility, the relationship between current density and electric field strength can be considered to follow the Child's Law when the electric field is high enough. Hence, the carrier mobility could be calculated from the slope (k) of the J-E curve according to Equation(8.4), expressed as

$$\mu = \frac{8d^3k}{9\epsilon} \quad (8.5)$$

where d is the sample thickness and it is 100 μm in this test; $\epsilon = \epsilon_0\epsilon_r$, ϵ_0 is the vacuum permittivity and ϵ_r is the relative permittivity of the sample. Table 8.1 represents the calculated carrier mobility of selected samples at 60 kV/mm. The carrier mobility of PP is about two orders of magnitude smaller than that of PE, indicating PP owns distinguished insulating properties when compares with PE. The carrier mobility of PE/Al₂O₃-KH570@2 phr sample is $2.37 \times 10^{-7} \text{ m}^2/(\text{V}\cdot\text{s})$, which is more than 5 times smaller than that of unfilled PE. The carrier mobility of PP/Al₂O₃-KH570@2 phr sample is $6.54 \times 10^{-9} \text{ m}^2/(\text{V}\cdot\text{s})$, which is about one order of magnitude smaller than that of unfilled PP. The results suggest that the addition of nano-alumina into matrix polymer can reduce the carrier mobility of nanocomposites. A large quantity of traps is generated in the interaction area between nanoparticles and matrix polymer and they can capture the carries. Thus, the carrier mobility is reduced.

Table 8.1 Carrier transport rate in PE nanocomposites and PP nanocomposites

Sample	k	$\mu \text{ (m}^2/(\text{V}\cdot\text{s}))$
PE	3.25×10^{-13}	1.30×10^{-6}
PE/Al ₂ O ₃ -KH570@2 phr	5.97×10^{-14}	2.37×10^{-7}
PP	1.71×10^{-14}	6.91×10^{-8}
PP/Al ₂ O ₃ -KH570@2 phr	1.62×10^{-15}	6.54×10^{-9}

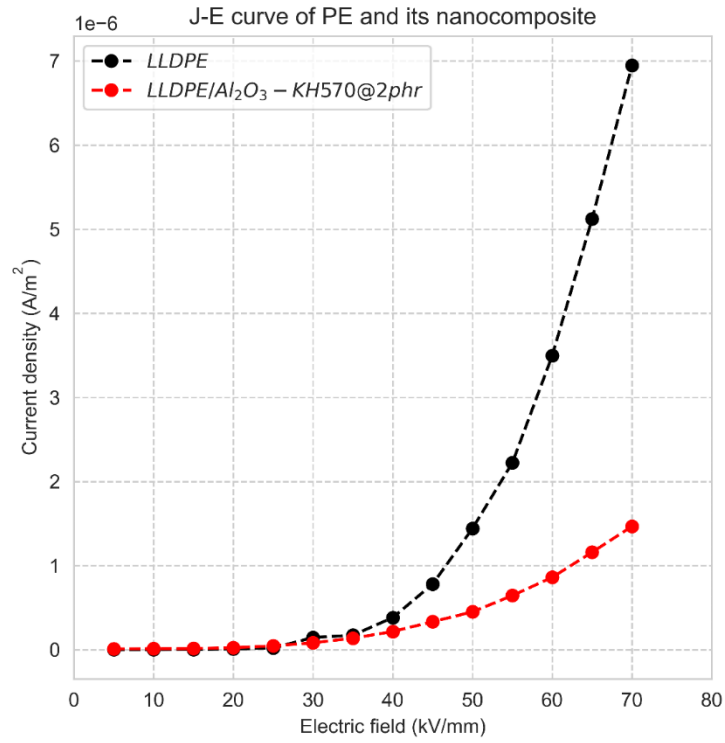


Figure 8.8 The J-E curve of PE/alumina nanocomposites.

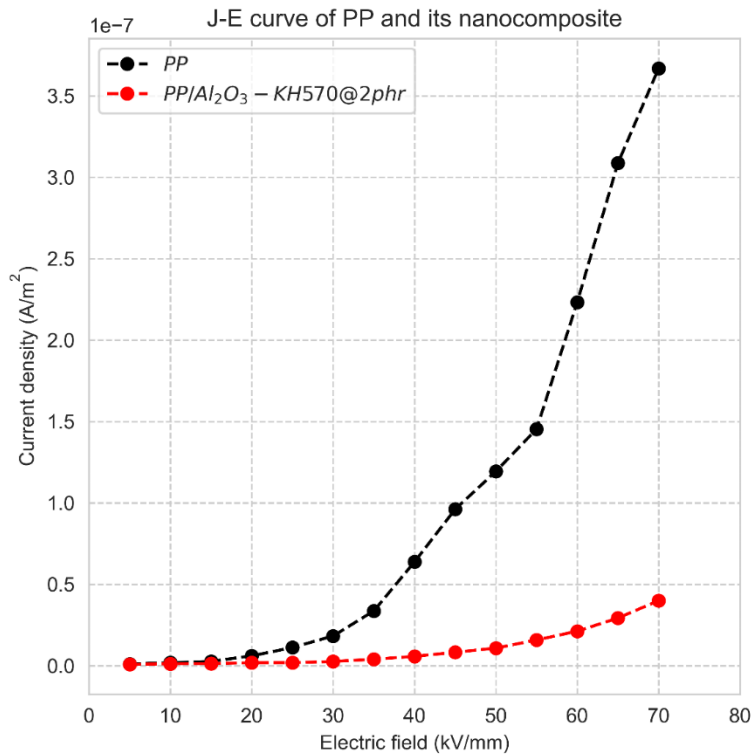


Figure 8.9 The J-E curve of PP/alumina nanocomposites.

The electric field strength at the intersection point between the ohmic region and the space charge limited current region is called the electrical ageing threshold, above which the degradation of insulation occurs. The current density versus electric field of PE and its composites is plotted in log-log scale, as shown in Figure 8.10. The electric field for which the slope of log J-log E plot exceeds unity, i.e., the threshold for electrical ageing is indicated by the arrow. The J-V curve for both samples consists of two parts, the ohmic region and the trapped SCLC region. After fitting with the least-squares method, the slopes for each part of the curve are recorded in Table 8.2. For both samples, the slopes in the ohmic area are near 1 and the slopes in the trapped SCLC region are larger than 2. The electrical ageing threshold at 30 °C for unfilled PE sample is 12.49 kV/mm. After adding 2 phr of KH570-treated nano-alumina into PE, the electrical ageing threshold is increased to 16.66 kV/mm.

Figure 8.11 shows the field-dependent current density of PP and its composites plotted in log-log scale. The same method is adapted to complete the curve fitting. The electrical ageing threshold of PP composite samples is summarized in Table 8.3. For each sample, the J-E curve is divided into the ohmic current and trapped SCLC current by the electric ageing threshold field. The slope of ohmic current is near 1 and the slope of trapped SCLC current is above 2, which is consistent with the theoretical analysis. The HVDC cables usually operate at 15 kV/mm. To realize the reliable long-term operation of HVDC cables, the electrical ageing threshold of cable insulation material must be higher than 15 kV/mm. From the results, the electrical ageing threshold at 30 °C

for unfilled PP and PP/Al₂O₃-KH570@2 phr is 15.91 kV/mm and 27.17 kV/mm, respectively, which is larger than that of unfilled PE material at the same temperature. Introducing the surface treated nano-alumina into PP material could obviously improve its electrical ageing threshold. The PP nano-alumina composite material is suitable to be used as HVDC cable insulation.

Additionally, as reported in [90], [196], the threshold value above which space charge accumulation occurs might be close to the threshold for electrical ageing under DC electric field. This is because the space charge and ohmic behavior of conduction current are mutually incompatible. The existence of space charge inescapable results in the distortion of the electric field and the non-linear behavior of current [194]. Hence, there is no space charge when the steady-state DC conduction current is in the ohmic region. The threshold for space charge accumulation defines the transition point of the electric field where a non-linear behavior of DC current occurs [90]. It is well-known that space charge accumulation is a challenging topic for HVDC cable insulation. From the J-E characteristic curves, the addition of nano-alumina particles could also increase the threshold of space charge accumulation.

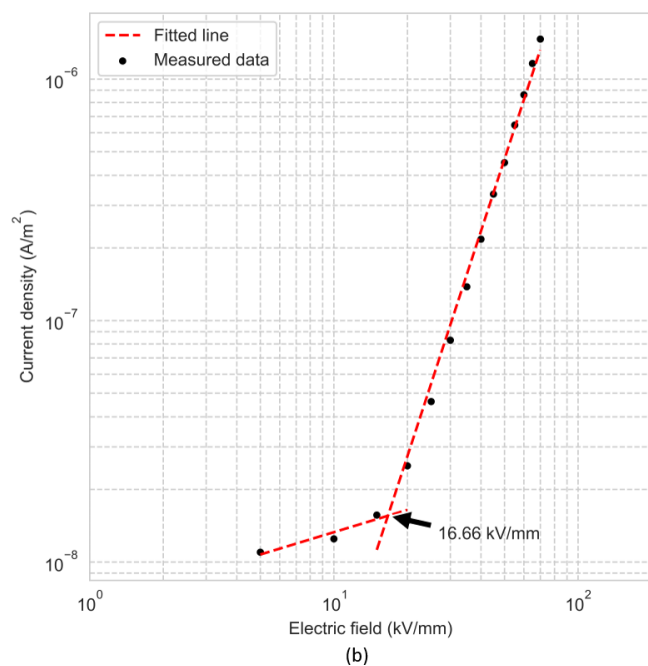
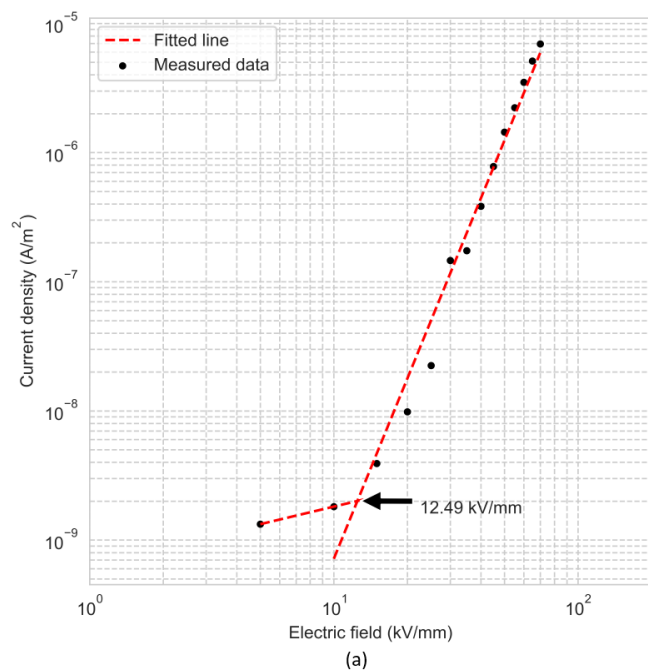


Figure 8.10 Current density versus electric field of (a) PE and (b) PE/Al₂O₃-KH570@2phr nanocomposite.

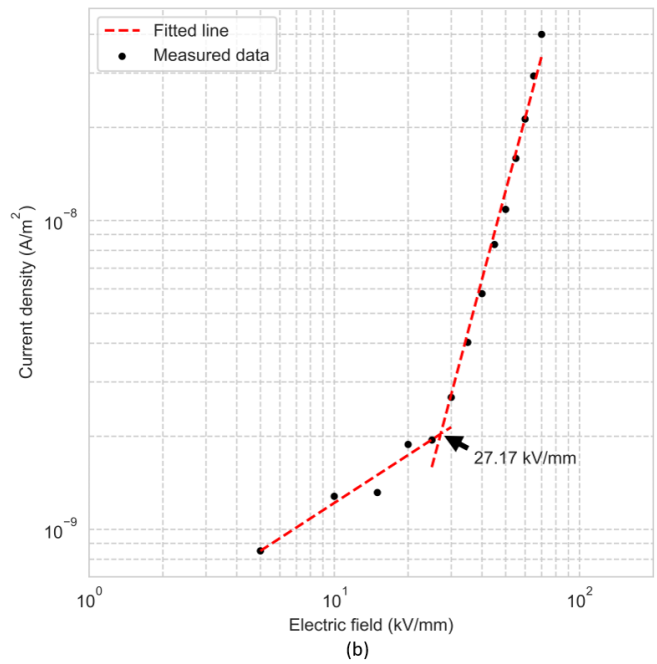
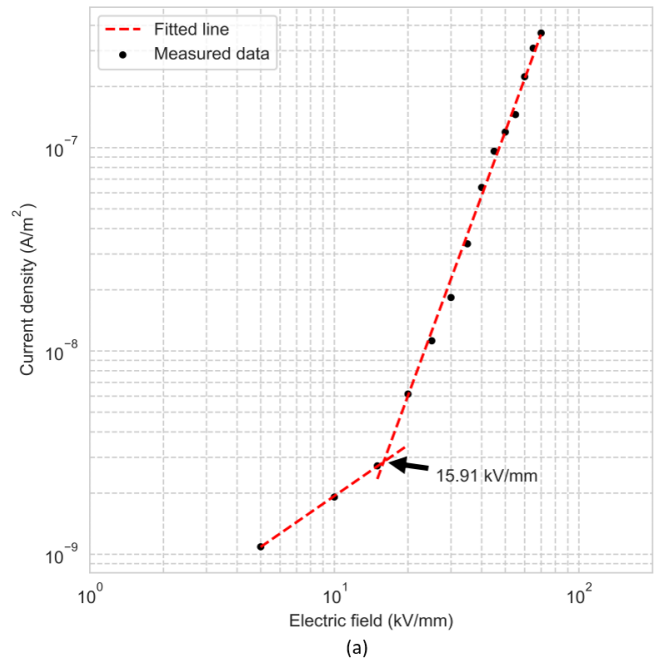


Figure 8.11 Current density versus electric field of (a) PP and (b) PP/Al₂O₃-KH570@2phr nanocomposite.

Table 8.2 The electrical ageing threshold for PE and its nanocomposite.

Sample	Slope of ohmic current	Slope of trapped SCLC current	Electrical ageing threshold (kV/mm)
PE	0.45	4.63	12.49
PE/Al ₂ O ₃ -KH570@2 phr	0.31	3.09	16.66

Table 8.3 The obtained electrical ageing threshold for PP and its nanocomposite.

Sample	Slope of ohmic current	Slope of trapped SCLC current	Electrical ageing threshold (kV/mm)
PP	0.83	3.27	15.91
PP/Al ₂ O ₃ -KH570@2 phr	0.51	2.97	27.17

8.3 Summary

In this chapter, the DC conductivity of PE nanocomposites and PP nanocomposites at 30 kV/mm and 30 °C are analyzed. Results show the addition of nano-alumina could decrease the DC conductivity of nanocomposites as compared with the virgin base polymer. But with the increasing filling content, DC conductivity increases. DC conductivity of PP nanocomposites is about one order of magnitude smaller than that of PE composites. In addition, the steady-state conduction current behavior in solid film samples is studied based on SCLC theory. The electric field-dependent current density of some selected nanocomposite samples is measured. The carrier mobility is reduced with the addition of nanoparticles.

Moreover, the electrical ageing thresholds of nanocomposites are calculated from the

J-E characteristic curves in the log-log scale. The results show that the inclusion of nano-alumina into the polymer can increase the electrical aging threshold. In conclusion, experimental results illustrate the improvement in DC conductivity and electrical ageing threshold after adding nano-alumina. However, more studies are still needed to explore the underlying charge transport mechanisms in nanocomposites.

Chapter 9 Conclusions and Future Work

9.1 Summary of Findings

The main aim of this project is to improve the understanding of the potential issues of using thermoplastic polymeric nanocomposites for recyclable HVDC cable insulation. Particularly, the electrical performance of nanocomposites under high DC voltage stress should be evaluated.

In this project, PE and PP were chosen as the matrix materials to synthesize polymer nanocomposites for potential HVDC cable insulation. Nano-alumina particles were selected as the target nano-filler. A successful and well-controlled surface modification method for nano-alumina by using KH570 silane coupling agent was developed and verified by using TGA and FTIR. Both PE nanocomposite thin film samples and PP nanocomposite thin film samples were successfully prepared in the form of varying surface treatment and filling contents. Overall, with regards to the recyclable HVDC cable insulation, a series of comprehensive studies on the physical, thermal, mechanical and electrical properties of four nanocomposite systems, i.e., PE/untreated-nano-alumina, PE/KH570-treated-nano-alumina, PP/untreated-nano-alumina and PP/KH570-treated-nano-alumina, were conducted.

The introduction of nanoparticles is found to affect the morphological structure of the matrix polymer. The morphological analysis was conducted by using POM and SEM in Chapter 4. Nanoparticle enhances the nucleation effect during the crystallization

process, resulting in the increased spherulite density and reduced spherulite size. Such effects become more apparent as the filling content is increased. With the surface treatment, this phenomenon is even more obvious. The surface treatment also improves the dispersion and distribution of nanoparticles in nanocomposites, which was observed through SEM images. The agglomeration of nanoparticles can still be observed with the high filling content. But the dimension of the agglomerations is largely reduced. From the DSC results, all the nanocomposite system shows stable thermal properties. The addition of untreated and KH570-treated nano-alumina did not have obvious influences on the melting traces and the melting temperature of PE nanocomposites and PP nanocomposites. Hence, the deduced lamellae thickness was similar for samples with the same matrix polymer. Together with POM results, introducing nano-alumina only had an impact on the nucleation but not on the crystallinity of polymer nanocomposites.

Dielectric response of all nanocomposite systems was investigated in Chapter 5. Permittivity and dielectric loss tangent of virgin PE and virgin PP maintained constant over the whole measuring frequency. For PE nanocomposites containing the untreated nano-alumina, the dielectric constant and loss were influenced by the surface chemistry and filling content. The dielectric loss tangent increases with the increase of the filling content of nano-alumina, especially in the low-frequency region. This is less obvious for PE nanocomposites containing surface-treated nanoparticles. A similar phenomenon was observed in PP nanocomposites.

The effect of the addition of nano-alumina on the DC breakdown performance was studied in Chapter 6. With the increasing filling content, DC breakdown strength of all composite systems firstly increases and then decreases. Surface treatment of nano-alumina can increase the DC breakdown strength when comparing to the samples containing the same amount of untreated nano-alumina. In general, the DC breakdown strength of PP nanocomposites is higher than that of PE nanocomposites when the nano-fillers and the filling content are the same. Possible explanations for the obtained breakdown behaviors were discussed, but the exact breakdown mechanism for nanocomposite is still not clear.

As for space charge dynamics presented in Chapter 7, homocharge accumulation was observed near both electrodes in all nanocomposite systems. The total charge amount for PE nanocomposites is reduced with the filling content no more than 2 phr. While for PP nanocomposites, the total charge amount continuously decreases as the filling content is increased. The total charge amount is further reduced in the nanocomposite samples containing KH570-treated alumina as compared with the samples containing the same amount of untreated alumina. In addition, the space charge injection for PP and its nanocomposites is enhanced when the temperature rises.

Measurements of leakage current of nanocomposites in Chapter 8 indicate that the introduction of nano-alumina can reduce the DC conductivity in all the nanocomposite systems compared with unfilled polymers. However, DC conductivity increases with

the increasing amount of nano-alumina. PP/ Al₂O₃-KH570@1 phr sample has the lowest DC conductivity, which is about 14 times smaller than that of unfilled PP. Moreover, the electrical ageing threshold for some selected samples was studied based on SCLC theory. Results show that adding nano-alumina can improve the threshold of electrical ageing field in nanocomposite systems.

By comparing the electrical properties of PE nanocomposites and those of PP nanocomposites, PP/KH570-treated nano-alumina composites at low filling content have shown higher DC breakdown strength, lower DC conductivity and less space charge accumulation.

9.2 Conclusions

The following conclusions are obtained for this research, which are also the main contributions of this research to knowledge:

- ◆ Successful and well-controlled surface modification method for nanoparticles and the nanocomposite manufacturing method were developed to guarantee the validity of obtained experimental results.
- ◆ Nanoparticles enhance the nucleating effect in nanocomposites and this phenomenon is more apparent when the filling content is increasing.
- ◆ Nanoparticles have limited influence on the melting trace and the crystallinity of nanocomposites.

- ◆ The introduction of nano-alumina has a negative evidential impact on the mechanical properties in the PP nanocomposite system and this needs further improvement.
- ◆ The inclusion of nano-alumina does not have significant influence on the dielectric spectroscopy both in the PE nanocomposite system and PP nanocomposite system.
- ◆ The DC electrical properties, such as DC breakdown strength, DC conductivity and space charge behaviors of polymer/nano-alumina nanocomposites, are strongly influenced by the surface chemistry and filling content of nanoparticles.
- ◆ Compared with unfilled PP, PP/ alumina nanocomposites show a better space charge suppression effect, in particular at high temperatures.
- ◆ Deep traps in nanocomposite appear to be mainly determined by the interphase between spherulites.
- ◆ A small amount of surface-treated nanoparticles can significantly reduce the DC conductivity in nanocomposites. The addition of nanoparticles increases the electrical ageing threshold.

9.3 Future Work

The experimental results and discussion presented in this project indicate that more work is required in the field of recyclable thermoplastic polymer nanocomposites. To

further understand the mechanisms of nanocomposite dielectrics and to quantify the influences of the addition of nanoparticles, the following work might be helpful:

- a) Space charge is one of the most important factors in constraining the development of HVDC polymeric power cables. How to effectively suppress the space charge has become a key issue in design the future polymeric HVDC cable. Hence, the space charge behavior of nanocomposites under a complex field should be further investigated. The complex field consists of the electric field, mechanical stress and temperature gradient. The obtained results will be invaluable in exploring the mechanisms of space charge formation, transport and dissipation.
- b) The poor mechanical properties of PP restrict its development as HVDC cable insulation. Therefore, it is necessary to improve the mechanical properties of the PP nanocomposite system. Published studies have shown that blending PP with other thermoplastic elastomers could improve its mechanical performance. Further improvement on the compatibility and reliability of the PP/elastomer/nanoparticles ternary system is still needed.
- c) The interfaces between the polymer and nanoparticles play significant roles in influencing the electrical properties of nanodielectrics, which is attributed to the special physical and chemical properties of the interfaces. Therefore, the characterization of the dielectric properties of interfaces should be investigated at the nanoscale. However, the required spatial resolution for the

characterization of such interfaces is far beyond the spatial resolution of most conventional methods. More advanced and accurate direct measurement methods should be developed to study the characteristics of the interfacial regions.

- d) This research evaluates the properties of polyethylene/nano-alumina and polypropylene/ nano-alumina as potential recyclable HVDC cable insulation. For polymeric nanocomposites, different fillers and matrix materials may have different interfaces, which results in distinct macroscopical properties. Hence, future research on different nanocomposite systems will be helpful to tailor the properties of nanocomposites and to design nanocomposite with specific purposes. Moreover, it can also provide some insights in revealing the underlying mechanisms of the nanocomposite.

References

- [1] K. Meah and S. Ula, "Comparative Evaluation of HVDC and HVAC Transmission Systems," in *2007 IEEE Power Engineering Society General Meeting*, 2007, pp. 1–5, doi: 10.1109/PES.2007.385993.
- [2] K. Meah and S. Ula, "Comparative evaluation of HVDC and HVAC transmission systems," *2007 IEEE Power Eng. Soc. Gen. Meet. PES*, pp. 11–15, 2007, doi: 10.1109/PES.2007.385993.
- [3] Y. Zhou, S. Peng, J. Hu, and J. He, "Polymeric insulation materials for HVDC cables: Development, challenges and future perspective," *IEEE Trans. Dielectr. Electr. Insul.*, vol. 24, no. 3, pp. 1308–1318, 2017, doi: 10.1109/TDEI.2017.006205.
- [4] T. L. Hanley, R. P. Burford, R. J. Fleming, and K. W. Barber, "A general review of polymeric insulation for use in HVDC cables," *IEEE Electr. Insul. Mag.*, vol. 19, no. 1, pp. 13–24, 2003, doi: 10.1109/MEI.2003.1178104.
- [5] G. Mazzanti *et al.*, "The insulation of HVDC extruded cable system joints. Part 1: Review of materials, design and testing procedures," *IEEE Trans. Dielectr. Electr. Insul.*, vol. 26, no. 3, pp. 964–972, 2019, doi: 10.1109/tdei.2019.007916.
- [6] G. Mazzanti and M. Marzinotto, *Extruded Cables For High-Voltage Direct-Current Transmission*. 2013.
- [7] Paul Dvorak, "Prysmian P-Laser 525 kV first recyclable HVDC cable," *Windpower Engineering and Development*. <https://www.windpowerengineering.com/prysmian-p-laser-525-kv-first-recyclable-hvdc-cable/>.
- [8] Y. Zhou, J. He, J. Hu, X. Huang, and P. Jiang, "Evaluation of polypropylene/polyolefin elastomer blends for potential recyclable HVDC cable insulation applications," *IEEE Trans. Dielectr. Electr. Insul.*, vol. 2, no. 2, pp. 673–681, 2015, doi: 10.1109/TDEI.2015.7076762.
- [9] S. Li, S. Yu, and Y. Feng, "Progress in and prospects for electrical insulating materials," *High Volt.*, vol. 1, no. 3, pp. 122–129, 2016, doi: 10.1049/hve.2016.0034.
- [10] N. Hussin and G. Chen, "Analysis of space charge formation in LDPE in the presence of crosslinking byproducts," *IEEE Trans. Dielectr. Electr. Insul.*, vol. 19, no. 1, pp. 126–133, 2012, doi: 10.1109/TDEI.2012.6148510.
- [11] Y. Zhou, J. Hu, B. Dang, and J. He, "Effect of different nanoparticles on tuning electrical properties of polypropylene nanocomposites," *IEEE Trans. Dielectr. Electr. Insul.*, vol. 24, no. 3, pp. 1380–1389, 2017, doi: 10.1109/TDEI.2017.006183.
- [12] B. X. Du, Z. H. Hou, Z. L. Li, and J. Li, "Temperature dependent space charge and breakdown strength of PP/ULDPE/graphene nanocomposites for HVDC extruded cable insulation," *IEEE Trans. Dielectr. Electr. Insul.*, vol. 26, no. 3,

- pp. 876–884, 2019, doi: 10.1109/TDEI.2019.007858.
- [13] C. L. M.F. Fréchette, A. Vjih, L. Utracki, M.L. Trudeau, A. Sami, “Nanodielectrics: A panacea for solving all electrical insulation problems?,” in *2010 10th IEEE International Conference on Solid Dielectrics*, 2010, pp. 1–29, doi: 10.1109/ICSD.2010.5568067.
- [14] N. H. Ismail and M. Mustapha, “A review of thermoplastic elastomeric nanocomposites for high voltage insulation applications,” *Polym. Eng. Sci.*, vol. 58, no. February, pp. E36–E63, 2018, doi: 10.1002/pen.24822.
- [15] I. Pleșa, P. V. Noțingher, C. Stancu, F. Wiesbrock, and S. Schlögl, “Polyethylene nanocomposites for power cable insulations,” *Polymers (Basel)*, vol. 11, no. 1, 2018, doi: 10.3390/polym11010024.
- [16] C. Kim, Z. Jin, P. Jiang, Z. Zhu, and G. Wang, “Investigation of dielectric behavior of thermally aged XLPE cable in the high-frequency range,” *Polym. Test.*, vol. 25, no. 4, pp. 553–561, 2006, doi: 10.1016/j.polymertesting.2006.03.009.
- [17] T. Andrews, R. N. Hampton, A. Smedberg, D. Wald, V. Waschke, and W. Weissenberg, “The role of degassing in XLPE power cable manufacture,” *IEEE Electr. Insul. Mag.*, vol. 22, no. 6, pp. 5–16, 2006, doi: 10.1109/MEI.2006.253416.
- [18] Y. M. Kim, Y. K. Cha, K. J. Lim, J. H. Nam, and G. J. Lee, “Electrical insulation evaluation of crosslinked polyethylene nanocomposite blended with ZnO,” *Proc. 2012 IEEE Int. Conf. Cond. Monit. Diagnosis, C. 2012*, no. September, pp. 1242–1245, 2012, doi: 10.1109/CMD.2012.6416386.
- [19] N. Hirai, R. Minami, T. Tanaka, Y. Ohki, M. Okashita, and T. Maeno, “Chemical group in crosslinking byproducts responsible for charge trapping in polyethylene,” *IEEE Trans. Dielectr. Electr. Insul.*, vol. 10, no. 2, pp. 320–330, 2003, doi: 10.1109/TDEI.2003.1194118.
- [20] N. Hirai, Y. Maeno, T. Tanaka, Y. Ohki, M. Okashita, and T. Maeno, “Roles of cumyl alcohol and crosslinked structure in homc-charge trapping in crosslinked polyethylene,” *2003 Annu. Rep. Conf. Electr. Insul. Dielectr. Phenom.*, pp. 213–216, 2003.
- [21] K. Yoshino, A. Ueda, T. Demura, Y. Miyashita, K. Kurahashi, and Y. Matsuda, “Property of syndiotactic polypropylene and its application to insulation of electric power cable -property, manufacturing and characteristics,” in *Proceedings of the 7th International Conference on Properties and Applications of Dielectric Materials (Cat. No.03CH37417)*, 2003, vol. 1, pp. 175–178 vol.1, doi: 10.1109/ICPADM.2003.1218381.
- [22] J.-W. Zha, M.-S. Zheng, W.-K. Li, G. Chen, and Z.-M. Dang, “Polypropylene Insulation Materials for HVDC Cables,” in *Polymer Insulation Applied for HVDC Transmission*, B. Du, Ed. Singapore: Springer Singapore, 2021, pp. 77–96.
- [23] K. Kurahashi, Y. Matsuda, Y. Miyashita, T. Demura, A. Ueda, and K. Yoshino,

- “The application of novel polypropylene to the insulation of electric power cable (3),” *Electr. Eng. Japan (English Transl. Denki Gakkai Ronbunshi)*, vol. 155, no. 3, pp. 1–8, 2006, doi: 10.1002/eej.20114.
- [24] I. L. Hosier, A. S. Vaughan, and S. G. Swingler, “An investigation of the potential of polypropylene and its blends for use in recyclable high voltage cable insulation systems,” *J. Mater. Sci.*, vol. 46, no. 11, pp. 4058–4070, 2011, doi: 10.1007/s10853-011-5335-9.
- [25] C. G. Ma, Y. L. Mai, M. Z. Rong, W. H. Ruan, and M. Q. Zhang, “Phase structure and mechanical properties of ternary polypropylene/elastomer/nano-CaCO₃ composites,” *Compos. Sci. Technol.*, vol. 67, no. 14, pp. 2997–3005, 2007, doi: <https://doi.org/10.1016/j.compscitech.2007.05.022>.
- [26] C. D. Green *et al.*, “Thermoplastic cable insulation comprising a blend of isotactic polypropylene and a propylene-ethylene copolymer,” *IEEE Trans. Dielectr. Electr. Insul.*, vol. 22, no. 2, pp. 639–648, 2015, doi: 10.1109/TDEI.2015.7076758.
- [27] Y. Zhou, J. He, J. Hu, X. Huang, and P. Jiang, “Evaluation of polypropylene/polyolefin elastomer blends for potential recyclable HVDC cable insulation applications,” *IEEE Trans. Dielectr. Electr. Insul.*, vol. 22, no. 2, pp. 673–681, 2015, doi: 10.1109/TDEI.2015.7076762.
- [28] Y. Zhou, B. Dang, J. Hu, X. Chen, F. Yu, and J. He, “Effect of magnesium oxide nanoparticles on tailoring the properties of polypropylene,” *Zhongguo Dianji Gongcheng Xuebao/Proceedings Chinese Soc. Electr. Eng.*, 2016, doi: 10.13334/j.0258-8013.pcsee.161814.
- [29] M. Johnston D.R.; Markovitz, “Corona resistant insulation,” 1988.
- [30] T. J. Lewis, “Nanometric Dielectrics,” *IEEE Trans. Dielectr. Electr. Insul.*, 1994, doi: 10.1109/94.326653.
- [31] P. O. Henk, T. W. Kortsen, and T. Kvarts, “Increasing the Electrical Discharge Endurance of Acid Anhydride Cured DGEBA Epoxy Resin by Dispersion of Nanoparticle Silica,” *High Perform. Polym.*, vol. 11, no. 3, pp. 281–296, 1999, doi: 10.1088/0954-0083/11/3/304.
- [32] J. K. Nelson, J. C. Fothergill, L. A. Dissado, and W. Peasgood, “Towards an understanding of nanometric dielectrics,” *Conf. Electr. Insul. Dielectr. Phenom. (CEIDP), Annu. Rep.*, pp. 295–298, 2002, doi: 10.1109/ceidp.2002.1048793.
- [33] Y. Kojima, A. Usuki, M. Kawasumi, A. Okada, T. Kurauchi, and O. Kamigaito, “One-pot synthesis of nylon 6–clay hybrid,” *J. Polym. Sci. Part A Polym. Chem.*, vol. 31, no. 7, pp. 1755–1758, 1993, doi: <https://doi.org/10.1002/pola.1993.080310714>.
- [34] S. Wu, Q. Yang, T. Shao, Z. Zhang, and L. Huang, “Effect of surface modification of electrodes on charge injection and dielectric characteristics of propylene carbonate,” *High Volt.*, vol. 5, no. 1, pp. 15–23, 2020, doi: 10.1049/hve.2019.0144.
- [35] Y. Zhou *et al.*, “Polypropylene-based ternary nanocomposites for recyclable

- high-voltage direct-current cable insulation,” *Compos. Sci. Technol.*, vol. 165, pp. 168–174, 2018, doi: 10.1016/j.compscitech.2018.06.022.
- [36] Y. Zhou, J. Hu, X. Chen, F. Yu, and J. He, “Thermoplastic polypropylene/aluminum nitride nanocomposites with enhanced thermal conductivity and low dielectric loss,” *IEEE Trans. Dielectr. Electr. Insul.*, 2016, doi: 10.1109/TDEI.2016.7736836.
- [37] A. Mazrouaa, “Chapter 14: polypropylene nanocompositestle,” in *Polypropylene*, InTech San Diego, Calif, USA, 2012, pp. 266--286.
- [38] Anh T. HOANG; Le WANG; Yuriy V. SERDYUK; Stanislaw M. GUBANSK, “DC electrical conductivity of LDPE-based nanocomposites,” 2015.
- [39] L. Zhang *et al.*, “Experiment and simulation of space charge suppression in LDPE/MgO nanocomposite under external DC electric field,” *J. Electrostat.*, vol. 72, no. 4, pp. 252–260, 2014, doi: <https://doi.org/10.1016/j.elstat.2014.03.005>.
- [40] C. Zhou and G. Chen, “Space charge and AC electrical breakdown strength in polyethylene,” *IEEE Trans. Dielectr. Electr. Insul.*, vol. 24, no. 1, pp. 559–566, 2017, doi: 10.1109/TDEI.2016.005811.
- [41] B. Dang, J. He, J. Hu, and Y. Zhou, “Tailored sPP/silica nanocomposite for ecofriendly insulation of extruded HVDC cable,” *J. Nanomater.*, vol. 2015, 2015, doi: 10.1155/2015/686248.
- [42] Y. Zhou *et al.*, “Temperature dependent electrical properties of thermoplastic polypropylene nanocomposites for HVDC cable insulation,” *IEEE Trans. Dielectr. Electr. Insul.*, vol. 26, no. 5, pp. 1596–1604, 2019, doi: 10.1109/TDEI.2019.008198.
- [43] S. Li *et al.*, “Short-term breakdown and long-term failure in nanodielectrics: A review,” *IEEE Trans. Dielectr. Electr. Insul.*, vol. 17, no. 5, pp. 1523–1535, 2010, doi: 10.1109/TDEI.2010.5595554.
- [44] M. Y. A. Fuad, H. Hanim, R. Zarina, Z. A. M. Ishak, and A. Hassan, “Polypropylene/calcium carbonate nanocomposites - effects of processing techniques and maleated polypropylene compatibiliser,” *Express Polym. Lett.*, vol. 4, no. 10, pp. 611–620, 2010, doi: 10.3144/expresspolymlett.2010.76.
- [45] M. F. Fréchette *et al.*, “Dielectric design of LDPE properties: With the help of double-core Si/SiO₂ and Carbon Black,” in *2016 IEEE Conference on Electrical Insulation and Dielectric Phenomena (CEIDP)*, 2016, pp. 52–57, doi: 10.1109/CEIDP.2016.7785471.
- [46] T. Andritsch, R. Kochetov, P. H. F. Morshuis, and J. J. Smit, “DC conduction in epoxy based nano- and mesocomposites,” in *2010 Annual Report Conference on Electrical Insulation and Dielectric Phenomena*, 2010, pp. 1–4, doi: 10.1109/CEIDP.2010.5723965.
- [47] Y. Zhou, J. He, J. Hu, and B. Dang, “Surface-modified MgO nanoparticle enhances the mechanical and direct-current electrical characteristics of polypropylene/polyolefin elastomer nanodielectrics,” *J. Appl. Polym. Sci.*, 2016, doi: 10.1002/app.42863.

- [48] X. Duan, W. H. Siew, M. Given, J. Liggat, and J. He, "Effect of different surface treatment agents on the physical chemistry and electrical properties of polyethylene nano-alumina nanocomposites," *High Volt.*, vol. 5, no. 4, pp. 397–402, 2020, doi: 10.1049/hve.2020.0081.
- [49] D. Liu *et al.*, "Influence of nanoparticle surface coating on electrical conductivity of LDPE/Al₂O₃ nanocomposites for HVDC cable insulations," *IEEE Trans. Dielectr. Electr. Insul.*, vol. 24, no. 3, pp. 1396–1404, 2017, doi: 10.1109/TDEI.2017.006310.
- [50] C. Calebrese, L. Hui, L. S. Schadler, and J. K. Nelson, "A review on the importance of nanocomposite processing to enhance electrical insulation," *IEEE Trans. Dielectr. Electr. Insul.*, vol. 18, no. 4, pp. 938–945, 2011, doi: 10.1109/TDEI.2011.5976079.
- [51] M. Roy, J. K. Nelson, R. K. MacCrone, and L. S. Schadler, "Candidate mechanisms controlling the electrical characteristics of silica/XLPE nanodielectrics," *J. Mater. Sci.*, vol. 42, pp. 3789–1799, 2007, doi: 10.1007/s10853-006-0413-0.
- [52] X. Wang, T. Andritsch, G. Chen, and S. Virtanen, "The role of the filler surface chemistry on the dielectric and thermal properties of polypropylene aluminium nitride nanocomposites," *IEEE Trans. Dielectr. Electr. Insul.*, vol. 26, no. 3, pp. 1009–1017, 2019, doi: 10.1109/tdei.2019.007773.
- [53] S. Peng, J. He, and J. Hu, "Influence of surface modification on electrical properties of polyethylene SiO₂ nanocomposites," *Proc. IEEE Int. Conf. Prop. Appl. Dielectr. Mater.*, vol. 2015-October, no. June, pp. 372–375, 2015, doi: 10.1109/ICPADM.2015.7295286.
- [54] K. M. Seven, J. M. Cogen, T. Person, J. R. Reffner, and J. F. Gilchrist, "The effect of inorganic and organic nucleating agents on the electrical breakdown strength of polyethylene," *J. Appl. Polym. Sci.*, vol. 135, no. 22, pp. 1–12, 2018, doi: 10.1002/app.46325.
- [55] K.Y. Lau, "Structure and electrical properties of silica-based polyethylene nanocomposites," University of Southampton, 2013.
- [56] X. Huang, Z. Ma, Y. Wang, P. Jiang, Y. Yin, and Z. Li, "Polyethylene/aluminum nanocomposites: Improvement of dielectric strength by nanoparticle surface modification," *J. Appl. Polym. Sci.*, vol. 113, no. 6, pp. 3577–3584, 2009, doi: 10.1002/app.30313.
- [57] W. Li, H. Hillborg, and U. W. Gedde, "Influence of process conditions and particle dispersion on the ac breakdown strength of polyethylene-aluminium oxide nanocomposites," *IEEE Trans. Dielectr. Electr. Insul.*, vol. 22, no. 6, pp. 3536–3542, 2015, doi: 10.1109/TDEI.2015.005366.
- [58] J. Liu, Y. Gao, D. Cao, L. Zhang, and Z. Guo, "Nanoparticle dispersion and aggregation in polymer nanocomposites: Insights from molecular dynamics simulation," *Langmuir*, vol. 27, no. 12, pp. 7926–7933, 2011, doi: 10.1021/la201073m.

- [59] S. Peng, B. Dang, Y. Zhou, J. Hu, and J. He, "Functionalized TiO₂ nanoparticles tune the aggregation structure and trapping property of polyethylene nanocomposites," *J. Phys. Chem. C*, vol. 120, no. 43, pp. 24754–14761, 2016, doi: 10.1021/acs.jpcc.6b07408.
- [60] S. Li, N. Zhao, Y. Nie, X. Wang, G. Chen, and G. Teyssedre, "Space charge characteristics of LDPE nanocomposite/LDPE insulation system," *IEEE Trans. Dielectr. Electr. Insul.*, 2015, doi: 10.1109/TDEI.2014.004524.
- [61] D. Liu *et al.*, "Influence of nanoparticle surface coating on electrical conductivity of LDPE/Al₂O₃ nanocomposites for HVDC cable insulations," *IEEE Trans. Dielectr. Electr. Insul.*, vol. 24, no. 3, pp. 1396–1404, 2017, doi: 10.1109/TDEI.2017.006310.
- [62] S. Hu *et al.*, "Surface-modification effect of MgO nanoparticles on the electrical properties of polypropylene nanocomposite," *High Volt.*, 2019, doi: 10.1049/hve.2019.0159.
- [63] K. Y. Lau, A. S. Vaughan, G. Chen, and I. L. Hosier, "Polyethylene nanodielectrics: The effect of nanosilica and its surface treatment on electrical breakdown strength," in *Annual Report - Conference on Electrical Insulation and Dielectric Phenomena, CEIDP*, 2012, pp. 21–24, doi: 10.1109/CEIDP.2012.6378712.
- [64] T. J. Lewis, "Interfaces are the dominant feature of dielectrics at the nanometric level," *IEEE Trans. Dielectr. Electr. Insul.*, vol. 11, no. 5, pp. 739–753, 2004, doi: 10.1109/TDEI.2004.1349779.
- [65] T. J. Lewis, "Interfaces: Nanometric dielectrics," *J. Phys. D. Appl. Phys.*, vol. 38, no. 2, pp. 202–212, 2005, doi: 10.1088/0022-3727/38/2/004.
- [66] T. Andritsch, *Epoxy Based Nanodielectrics for High Voltage DC Applications: Synthesis, Dielectric Properties and Space Charge Dynamics*, no. November. 2010.
- [67] S. Raetzke and J. Kindersberger, "Role of interphase on the resistance to high-voltage arcing, on tracking and erosion of silicone/SiO₂ nanocomposites," *IEEE Trans. Dielectr. Electr. Insul.*, vol. 17, no. 2, pp. 607–614, 2010, doi: 10.1109/TDEI.2010.5448118.
- [68] T. J. Lewis, "Interfaces: Nanometric dielectrics," 2005, doi: 10.1088/0022-3727/38/2/004.
- [69] T. Tanaka, M. Kozako, N. Fuse, and Y. Ohki, "Proposal of a multi-core model for polymer nanocomposite dielectrics," *IEEE Trans. Dielectr. Electr. Insul.*, vol. 12, no. 4, pp. 669–691, 2005, doi: 10.1109/TDEI.2005.1511092.
- [70] T. Tanaka, "Dielectric nanocomposites with insulating properties," *IEEE Trans. Dielectr. Electr. Insul.*, vol. 12, no. 5, pp. 914–928, 2005, doi: 10.1109/TDEI.2005.1522186.
- [71] R. H. Fowler and L. Nordheim, "Electron emission in intense electric fields," *Proc. R. Soc. London. Ser. A, Contain. Pap. a Math. Phys. Character*, vol. 119, no. 781, pp. 173–181, 1928, doi: 10.1098/rspa.1928.0091.

- [72] Schottky W, “Cold and Hot Electron Discharges (in German) 14, 63 (1923,” *Z. Phys.*, vol. 14, pp. 63–106, 1923.
- [73] D. L. Pulfrey, “The electrical breakdown of solid dielectrics in non-uniform fields,” *J. Phys. D. Appl. Phys.*, vol. 5, no. 3, pp. 647–655, 1972, doi: 10.1088/0022-3727/5/3/327.
- [74] M. P. Wilson, “Impulse breakdown of liquid-solid interfaces,” University of Strathclyde., 2011.
- [75] Kuffel E, W. S. Zaengl, and J. Kuffel, *High Voltage Engineering: Fundamentals*, 2nd Editio. Oxford, UK: Butterworth-Heinemann, 2000.
- [76] A. R. Blythe and D. Bloor, *Electrical properties of polymers*. Cambridge: Cambridge University Press, 2005.
- [77] L. A. Dissado and J. Fothergill, “Electrical degradation and breakdown in polymers,” 1992.
- [78] ASTM International, *ASTM D149-20, Standard Test Method for Dielectric Breakdown Voltage and Dielectric Strength of Solid Electrical Insulating Materials at Commercial Power Frequencies*. West Conshohocken, PA, 2020.
- [79] K. H. STARK and C. G. GARTON, “Electric Strength of Irradiated Polythene,” *Nature*, vol. 176, no. 4495, pp. 1225–1226, 1955, doi: 10.1038/1761225a0.
- [80] S. M. Gargari, P. A. A. F. Wouters, P. C. J. M. van der Wielen, and E. F. Steennis, “Practical experiences with on-line PD monitoring and interpretation for MV cable systems,” in *2010 10th IEEE International Conference on Solid Dielectrics*, 2010, pp. 1–4, doi: 10.1109/ICSD.2010.5567930.
- [81] Y. Yin, X. Dong, Z. Li, and X. Li, “The Effect of Electrically Prestressing on DC Breakdown Strength in the Nanocomposite of Low-density Polyethylene / nano-SiO_x,” in *2007 IEEE International Conference on Solid Dielectrics*, 2007, pp. 372–376, doi: 10.1109/ICSD.2007.4290830.
- [82] S. Okuzumi, Y. Murakami, M. Nagao, Y. Sekiguchi, C. C. Reddy, and Y. Murata, “DC Breakdown Strength and Conduction Current of MgO/LDPE Composite Influenced by Filler Size,” in *2008 Annual Report Conference on Electrical Insulation and Dielectric Phenomena*, 2008, pp. 722–725, doi: 10.1109/CEIDP.2008.4772933.
- [83] T. Okazaki *et al.*, “Electric characteristics of MgO/LDPE nanocomposite up to breakdown under DC ramp voltage,” in *2009 IEEE Conference on Electrical Insulation and Dielectric Phenomena*, 2009, pp. 654–657, doi: 10.1109/CEIDP.2009.5377863.
- [84] Y. Hu, R. C. Smith, J. K. Nelson, and L. S. Schadler, “Some mechanistic understanding of the impulse strength of nanocomposites,” in *2006 IEEE Conference on Electrical Insulation and Dielectric Phenomena*, 2006, pp. 31–34, doi: 10.1109/CEIDP.2006.312055.
- [85] Y. Zhou, J. Hu, B. Dang, and J. He, “Mechanism of highly improved electrical properties in polypropylene by chemical modification of grafting maleic anhydride,” *J. Phys. D. Appl. Phys.*, 2016, doi: 10.1088/0022-

- 3727/49/41/415301.
- [86] S. Ju, H. Zhang, M. Chen, C. Zhang, X. Chen, and Z. Zhang, “Improved electrical insulating properties of LDPE based nanocomposite: Effect of surface modification of magnesia nanoparticles,” *Compos. Part A Appl. Sci. Manuf.*, vol. 66, pp. 183–192, 2014, doi: <https://doi.org/10.1016/j.compositesa.2014.07.003>.
 - [87] J. M. Alison, “A high field pulsed electro-acoustic apparatus for space charge and external circuit current measurement within solid insulators,” *Meas. Sci. Technol.*, vol. 9, no. 10, pp. 1737–1750, 1998, doi: [10.1088/0957-0233/9/10/014](https://doi.org/10.1088/0957-0233/9/10/014).
 - [88] Yewen Zhang, J. Lewiner, C. Alquie, and N. Hampton, “Evidence of strong correlation between space-charge buildup and breakdown in cable insulation,” *IEEE Trans. Dielectr. Electr. Insul.*, vol. 3, no. 6, pp. 778–783, 1996, doi: [10.1109/94.556559](https://doi.org/10.1109/94.556559).
 - [89] G. C. Montanari, “The electrical degradation threshold of polyethylene investigated by space charge and conduction current measurements,” *IEEE Trans. Dielectr. Electr. Insul.*, vol. 7, no. 3, pp. 309–315, 2000, doi: [10.1109/94.848905](https://doi.org/10.1109/94.848905).
 - [90] L. A. Dissado, C. Laurent, G. C. Montanari, and P. H. F. Morshuis, “Demonstrating a threshold for trapped space charge accumulation in solid dielectrics under DC field,” *IEEE Trans. Dielectr. Electr. Insul.*, vol. 12, no. 3, pp. 612–620, 2005, doi: [10.1109/TDEI.2005.1453467](https://doi.org/10.1109/TDEI.2005.1453467).
 - [91] C. D. Child, “Discharge From Hot CaO,” *Phys. Rev. (Series I)*, vol. 32, no. 5, pp. 492–511, 1911, doi: [10.1103/PhysRevSeriesI.32.492](https://doi.org/10.1103/PhysRevSeriesI.32.492).
 - [92] I. Langmuir, “The Effect of Space Charge and Residual Gases on Thermionic Currents in High Vacuum,” *Phys. Rev.*, vol. 2, no. 6, pp. 450–486, 1913, doi: [10.1103/PhysRev.2.450](https://doi.org/10.1103/PhysRev.2.450).
 - [93] T. Mizutani, “Space charge measurement techniques and space charge in polyethylene,” *IEEE Trans. Dielectr. Electr. Insul.*, vol. 1, no. 5, pp. 923–933, 1994, doi: [10.1109/94.326659](https://doi.org/10.1109/94.326659).
 - [94] T. L. Hanley, R. P. Burford, R. J. Fleming, and K. W. Barber, “A general review of polymeric insulation for use in HVDC cables,” *IEEE Electr. Insul. Mag.*, vol. 19, no. 1, pp. 13–24, 2003, doi: [10.1109/MEI.2003.1178104](https://doi.org/10.1109/MEI.2003.1178104).
 - [95] Z. Li and B. Du, “Polymeric insulation for high-voltage dc extruded cables: Challenges and development directions,” *IEEE Electr. Insul. Mag.*, vol. 34, no. 6, pp. 30–43, 2018, doi: [10.1109/MEI.2018.8507715](https://doi.org/10.1109/MEI.2018.8507715).
 - [96] G. Chen, C. Zhou, S. Li, and L. Zhong, “Space charge and its role in electric breakdown of solid insulation,” in *2016 IEEE International Power Modulator and High Voltage Conference (IPMHVC)*, 2016, pp. 120–127, doi: [10.1109/IPMHVC.2016.8012888](https://doi.org/10.1109/IPMHVC.2016.8012888).
 - [97] N. Hozumi, H. Suzuki, T. Okamoto, K. Watanabe, and A. Watanabe, “Direct observation of time-dependent space charge profiles in XLPE cable under high electric fields,” *IEEE Trans. Dielectr. Electr. Insul.*, vol. 1, no. 6, pp. 1068–1076, 1994, doi: [10.1109/94.368656](https://doi.org/10.1109/94.368656).

- [98] J. He, L. Peng, and Y. Zhou, "Research progress of environment-friendly HVDC power cable insulation materials," *Gaodianya Jishu/High Voltage Engineering*, 2017, doi: 10.13336/j.1003-6520.hve.20170123001.
- [99] C. Zhou and G. Chen, "Space charge and AC electrical breakdown strength in polyethylene," *IEEE Trans. Dielectr. Electr. Insul.*, vol. 24, no. 1, pp. 559–566, 2017, doi: 10.1109/TDEI.2016.005811.
- [100] J. Xia, Y. Zhang, Z. An, and F. Zheng, "Blocking effect of PVF on space charge injection into low density polyethylene," in *2010 10th IEEE International Conference on Solid Dielectrics*, 2010, pp. 1–4, doi: 10.1109/ICSD.2010.5568005.
- [101] Chao Zhang and T. Mizutani, "Space charge behavior of LDPE with a blocking electrode," in *Annual Report Conference on Electrical Insulation and Dielectric Phenomena*, 2002, pp. 614–617, doi: 10.1109/CEIDP.2002.1048871.
- [102] T. Hori, K. Kaneko, T. Mizutani, and M. Ishioka, "Space charge distribution in low-density polyethylene with blocking layer," in *2003 Annual Report Conference on Electrical Insulation and Dielectric Phenomena*, 2003, pp. 197–200, doi: 10.1109/CEIDP.2003.1254827.
- [103] Y. Tanaka, G. Chen, Y. Zhao, A. E. Davies, A. S. Vaughan, and T. Takada, "Effect of additives on morphology and space charge accumulation in low density polyethylene," *IEEE Trans. Dielectr. Electr. Insul.*, vol. 10, no. 1, pp. 148–154, 2003, doi: 10.1109/TDEI.2003.1176580.
- [104] X. Wang, H. Q. He, D. M. Tu, C. Lei, and Q. G. Du, "Dielectric Properties and Crystalline Morphology of Low Density Polyethylene Blended with Metallocene Catalyzed Polyethylene," *IEEE Trans. Dielectr. Electr. Insul.*, vol. 15, no. 2, pp. 319–326, 2008, doi: 10.1109/TDEI.2008.4483448.
- [105] M. Salah Khalil, "International research and development trends and problems of HVDC cables with polymeric insulation," *IEEE Electr. Insul. Mag.*, vol. 13, no. 6, pp. 35–47, 1997, doi: 10.1109/57.637152.
- [106] M. S. Khalil and B. S. Hansen, "Investigation of space charge in low-density polyethylene using a field probe technique," *IEEE Trans. Electr. Insul.*, vol. 23, no. 3, pp. 441–445, 1988, doi: 10.1109/14.2385.
- [107] M. S. Khalil and A. A. Zaky, "The effect of cable structure on space charge formation," *IEEE Trans. Electr. Insul.*, vol. 23, no. 6, pp. 1043–1046, 1988, doi: 10.1109/14.16531.
- [108] N. H. Ahmed and N. N. Srinivas, "Review of space charge measurements in dielectrics," *IEEE Trans. Dielectr. Electr. Insul.*, vol. 4, no. 5, pp. 644–656, 1997, doi: 10.1109/94.625650.
- [109] M. Salah Khalil, "International research and development trends and problems of HVDC cables with polymeric insulation," *IEEE Electr. Insul. Mag.*, vol. 13, no. 6, pp. 35–47, 1997, doi: 10.1109/57.637152.
- [110] R. E. Collins, "Practical application of the thermal pulsing technique to the study of electrets," *J. Appl. Phys.*, vol. 51, no. 6, pp. 2973–2986, 1980, doi:

- 10.1063/1.328109.
- [111] R. A. Anderson and S. R. Kurtz, "Direct observation of field-injected space charge in a metal-insulator-metal structure," *J. Appl. Phys.*, vol. 56, no. 10, pp. 2856–2863, 1984, doi: 10.1063/1.333821.
- [112] T. Takada, "Acoustic and optical methods for measuring electric charge distributions in dielectrics," in *1999 Annual Report Conference on Electrical Insulation and Dielectric Phenomena (Cat. No.99CH36319)*, 1999, pp. 1–14 vol.1, doi: 10.1109/CEIDP.1999.804581.
- [113] E. Dörre and H. Hübner, *Alumina*, 1st ed. Berlin: Springer-Verlag Berlin Heidelberg, 1984.
- [114] S. J. Wang, J. W. Zha, Y. H. Wu, L. Ren, Z. M. Dang, and J. Wu, "Preparation, microstructure and properties of polyethylene/alumina nanocomposites for HVDC insulation," *IEEE Trans. Dielectr. Electr. Insul.*, 2015, doi: 10.1109/TDEI.2015.004903.
- [115] W. Wang and S. Li, "Correlation between trap parameters and breakdown strength of polyethylene/alumina nanocomposites," *Proc. Int. Symp. Electr. Insul. Mater.*, pp. 73–76, 2014, doi: 10.1109/ISEIM.2014.6870723.
- [116] W. Wang and S. Li, "Correlation between trap parameters and breakdown strength of polyethylene/alumina nanocomposites," 2014, doi: 10.1109/ISEIM.2014.6870723.
- [117] D. Liu *et al.*, "Interactions between a phenolic antioxidant, moisture, peroxide and crosslinking by-products with metal oxide nanoparticles in branched polyethylene," *Polym. Degrad. Stab.*, vol. 125, pp. 21–32, 2016, doi: 10.1016/j.polymdegradstab.2015.12.014.
- [118] B. Dang, J. He, J. Hu, and Y. Zhou, "Large improvement in trap level and space charge distribution of polypropylene by enhancing the crystalline-amorphous interface effect in blends," *Polym. Int.*, vol. 65, no. 4, pp. 371–379, 2016, doi: 10.1002/pi.5063.
- [119] F. Tian, W. Bu, L. Shi, C. Yang, Y. Wang, and Q. Lei, "Theory of modified thermally stimulated current and direct determination of trap level distribution," *J. Electrostat.*, vol. 69, no. 1, pp. 7–10, 2011, doi: 10.1016/j.elstat.2010.10.001.
- [120] T. Tanaka *et al.*, "Dielectric properties of XLPE/Sio₂ nanocomposites based on CIGRE WG D1.24 cooperative test results," *IEEE Trans. Dielectr. Electr. Insul.*, vol. 18, no. 5, pp. 1482–1517, 2011, doi: 10.1109/TDEI.2011.6032819.
- [121] J. K. Nelson and J. C. Fothergill, "Internal charge behaviour of nanocomposites," *Nanotechnology*, vol. 15, no. 5, pp. 586–595, 2004, doi: 10.1088/0957-4484/15/5/032.
- [122] Y. Zhou *et al.*, "Temperature dependent electrical properties of thermoplastic polypropylene nanocomposites for HVDC cable insulation," *IEEE Trans. Dielectr. Electr. Insul.*, vol. 26, no. 5, pp. 1596–1604, 2019, doi: 10.1109/TDEI.2019.008198.
- [123] F. M. Mirabella and A. Bafna, "Determination of the crystallinity of

- polyethylene/ α -olefin copolymers by thermal analysis: Relationship of the heat of fusion of 100% polyethylene crystal and the density,” *J. Polym. Sci. Part B Polym. Phys.*, vol. 40, no. 15, pp. 1637–1643, Aug. 2002, doi: <https://doi.org/10.1002/polb.10228>.
- [124] B. Wunderlich and G. Czornyj, “A Study of Equilibrium Melting of Polyethylene,” *Macromolecules*, vol. 10, no. 5, pp. 906–913, 1977, doi: 10.1021/ma60059a006.
- [125] D. W. van Krevelen and P. J. Hoftyzer, *Properties of polymers, their estimation and correlation with chemical structure*, 2nd ed. Amsterdam: New York:Elsevier Scientific Pub. Co., 1976.
- [126] A. L. N. Da Silva, M. I. B. Tavares, D. P. Politano, F. M. B. Coutinho, and M. C. G. Rocha, “Polymer blends based on polyolefin elastomer and polypropylene,” *J. Appl. Polym. Sci.*, vol. 66, no. 10, pp. 2005–2014, Dec. 1997, doi: [https://doi.org/10.1002/\(SICI\)1097-4628\(19971205\)66:10<2005::AID-APP17>3.0.CO;2-2](https://doi.org/10.1002/(SICI)1097-4628(19971205)66:10<2005::AID-APP17>3.0.CO;2-2).
- [127] J.-T. Xu, Q. Wang, and Z.-Q. Fan, “Non-isothermal crystallization kinetics of exfoliated and intercalated polyethylene/montmorillonite nanocomposites prepared by in situ polymerization,” *Eur. Polym. J.*, vol. 41, no. 12, pp. 3011–3017, 2005, doi: <https://doi.org/10.1016/j.eurpolymj.2005.04.042>.
- [128] Wikipedia, “Permittivity.” https://en.wikipedia.org/wiki/Permittivity#cite_note-9 (accessed Feb. 25, 2020).
- [129] T. W. Dakin, “Conduction and polarization mechanisms and trends in dielectric,” *IEEE Electr. Insul. Mag.*, vol. 22, no. 5, pp. 11–28, 2006, doi: 10.1109/MEI.2006.1705854.
- [130] X. Y. Huang, P. K. Jiang, and C. U. Kim, “Electrical properties of polyethylene/aluminum nanocomposites,” *J. Appl. Phys.*, vol. 102, no. 12, p. 124103, 2007, doi: 10.1063/1.2822336.
- [131] X. Huang, P. Jiang, C. Kim, Q. Ke, and G. Wang, “Preparation, microstructure and properties of polyethylene aluminum nanocomposite dielectrics,” *Compos. Sci. Technol.*, vol. 68, no. 9, pp. 2134–2140, 2008, doi: <https://doi.org/10.1016/j.compscitech.2008.03.009>.
- [132] X. Huang, “Study on the properties and oreoation of polyethylene aluminum nanocomposite dielectrics (in Chinese),” Shanghai Jiao Tong University, 2008.
- [133] C. Zhang and G. C. Stevens, “The Dielectric Response of Polar and Non-Polar Nanodielectrics,” *IEEE Trans. Dielectr. Electr. Insul.*, vol. 15, no. 2, pp. 606–617, 2008, doi: 10.1109/TDEI.2008.4483483.
- [134] W. Du, W. Zhong, Y. Lin, L. Shen, and Q. Du, “Space charge distribution and crystalline structure in polyethylene blended with EVOH,” *Eur. Polym. J.*, vol. 40, no. 8, pp. 1987–1995, 2004, doi: <https://doi.org/10.1016/j.eurpolymj.2004.04.003>.
- [135] K. Ishimoto, T. Tanaka, Y. Ohki, Y. Sekiguchi, Y. Murata, and M. Gosyowaki, “Comparison of dielectric properties of low-density polyethylene/MgO

- composites with different size fillers,” *Annu. Rep. - Conf. Electr. Insul. Dielectr. Phenomena, CEIDP*, pp. 208–211, 2008, doi: 10.1109/CEIDP.2008.4772819.
- [136] IEC-60243-2, “Electric strength of insulating materials,” 2001.
- [137] L. A. Dissado, J. C. Fothergill, S. V Wolfe, and R. M. Hill, “Weibull Statistics in Dielectric Breakdown; Theoretical Basis, Applications and Implications,” *IEEE Trans. Electr. Insul.*, vol. EI-19, no. 3, pp. 227–233, 1984, doi: 10.1109/TEI.1984.298753.
- [138] R. Ross, “Graphical methods for plotting and evaluating Weibull distributed data,” in *Proceedings of 1994 4th International Conference on Properties and Applications of Dielectric Materials (ICPADM)*, 1994, vol. 1, pp. 250–253 vol.1, doi: 10.1109/ICPADM.1994.413986.
- [139] W. Wang, S. Li, F. Tang, and J. Li, “Characteristics on breakdown performance of polyethylene/silica dioxide nanocomposites,” in *2012 Annual Report Conference on Electrical Insulation and Dielectric Phenomena*, 2012, pp. 521–524, doi: 10.1109/CEIDP.2012.6378834.
- [140] R. Sarathi, R. K. Sahu, and P. Rajeshkumar, “Understanding the thermal, mechanical and electrical properties of epoxy nanocomposites,” *Mater. Sci. Eng. A*, vol. 445–446, pp. 567–578, 2007, doi: <https://doi.org/10.1016/j.msea.2006.09.077>.
- [141] F. Guastavino, G. Coletti, A. Dardano, A. Fina, and A. S. Thelakkadan, “Thermo-mechanical and electrical characterization of epoxy/nanoclay composites,” in *2010 Annual Report Conference on Electrical Insulation and Dielectric Phenomena*, 2010, pp. 1–4, doi: 10.1109/CEIDP.2010.5723997.
- [142] T. Andritsch, R. Kochetov, Y. T. Gebrekiros, P. H. F. Morshuis, and J. J. Smit, “Short term DC breakdown strength in epoxy based BN nano- and microcomposites,” in *2010 10th IEEE International Conference on Solid Dielectrics*, 2010, pp. 1–4, doi: 10.1109/ICSD.2010.5568098.
- [143] T. Imai, F. Sawa, T. Ozaki, Y. Inoue, T. Shimizu, and T. Tanaka, “Roles of Fillers on Properties of Nano-TiO₂ and Micro-SiO₂ Filler Mixed Composites,” in *2007 IEEE International Conference on Solid Dielectrics*, 2007, pp. 407–410, doi: 10.1109/ICSD.2007.4290838.
- [144] J. K. Nelson, Y. Hu, and J. Thiticharoenpong, “Electrical properties of TiO₂/sub 2/ nanocomposites,” in *2003 Annual Report Conference on Electrical Insulation and Dielectric Phenomena*, 2003, pp. 719–722, doi: 10.1109/CEIDP.2003.1254955.
- [145] Qi Wang, P. Curtis, and G. Chen, “Effect of nano-fillers on electrical breakdown behavior of epoxy resin,” in *2010 Annual Report Conference on Electrical Insulation and Dielectric Phenomena*, 2010, pp. 1–4, doi: 10.1109/CEIDP.2010.5724024.
- [146] T. Andritsch, R. Kochetov, P. H. F. Morshuis, and J. J. Smit, “Short term DC breakdown and complex permittivity of Al₂O₃- and MgO-epoxy nanocomposites,” in *2010 Annual Report Conference on Electrical Insulation*

- and *Dielectric Phenomena*, 2010, pp. 1–4, doi: 10.1109/CEIDP.2010.5723960.
- [147] F. Tian, Q. Lei, X. Wang, and Y. Wang, “Investigation of electrical properties of LDPE/ZnO nanocomposite dielectrics,” *IEEE Trans. Dielectr. Electr. Insul.*, 2012, doi: 10.1109/TDEI.2012.6215078.
- [148] R. J. Fleming, A. Ammala, P. S. Casey, and S. B. Lang, “Conductivity and space charge in LDPE/BaSrTiO₃ nanocomposites,” *IEEE Trans. Dielectr. Electr. Insul.*, vol. 18, no. 1, pp. 15–23, 2011, doi: 10.1109/TDEI.2011.5704488.
- [149] T. Takada, Y. Hayase, Y. Tanaka, and T. Okamoto, “Space charge trapping in electrical potential well caused by permanent and induced dipoles for LDPE/MgO nanocomposite,” *IEEE Trans. Dielectr. Electr. Insul.*, vol. 15, no. 1, pp. 152–160, 2008, doi: 10.1109/T-DEI.2008.4446746.
- [150] R. C. Smith, C. Liang, M. Landry, J. K. Nelson, and L. S. Schadler, “The mechanisms leading to the useful electrical properties of polymer nanodielectrics,” *IEEE Trans. Dielectr. Electr. Insul.*, vol. 15, no. 1, pp. 187–196, 2008, doi: 10.1109/T-DEI.2008.4446750.
- [151] S. Li, W. Wang, S. Yu, and H. Sun, “Influence of hydrostatic pressure on dielectric properties of polyethylene/aluminum oxide nanocomposites,” *IEEE Trans. Dielectr. Electr. Insul.*, vol. 21, no. 2, pp. 519–528, 2014, doi: 10.1109/TDEI.2013.004131.
- [152] S. Li, G. Yin, S. Bai, and J. Li, “A new potential barrier model in epoxy resin nanodielectrics,” *IEEE Trans. Dielectr. Electr. Insul.*, vol. 18, no. 5, pp. 1535–1543, 2011, doi: 10.1109/TDEI.2011.6032822.
- [153] T. Tanaka, G. C. Montanari, and R. Mulhaupt, “Polymer nanocomposites as dielectrics and electrical insulation-perspectives for processing technologies, material characterization and future applications,” *IEEE Trans. Dielectr. Electr. Insul.*, vol. 11, no. 5, pp. 763–784, 2004, doi: 10.1109/TDEI.2004.1349782.
- [154] T. J. Lewis, “Nanometric Dielectrics,” *IEEE Trans. Dielectr. Electr. Insul.*, vol. 1, no. 5, pp. 812–825, 1994, doi: 10.1109/94.326653.
- [155] G. Chen, “Space Charge and Its Impact on Dc Breakdown of Polymeric Materials,” in *18th International Symposium on High Voltage Engineering*, 2013, pp. 686–691.
- [156] F. Rogti and M. Ferhat, “Effect of temperature on trap depth formation in multi-layer insulation: Low density polyethylene and fluorinated ethylene propylene,” *Appl. Phys. Lett.*, vol. 104, no. 3, 2014, doi: 10.1063/1.4862061.
- [157] S. Li, D. Min, W. Wang, and G. Chen, “Linking traps to dielectric breakdown through charge dynamics for polymer nanocomposites,” *IEEE Trans. Dielectr. Electr. Insul.*, vol. 23, no. 5, pp. 2777–2785, 2016, doi: 10.1109/TDEI.2016.7736837.
- [158] T. Tanaka and T. Imai, “Advances in nanodielectric materials over the past 50 years,” *IEEE Electr. Insul. Mag.*, vol. 29, no. 1, pp. 10–23, 2013, doi: 10.1109/MEI.2013.6410535.
- [159] F. Tian and C. Hou, “A trap regulated space charge suppression model for LDPE

- based nanocomposites by simulation and experiment,” *IEEE Trans. Dielectr. Electr. Insul.*, vol. 25, no. 6, pp. 2169–2177, 2018, doi: 10.1109/TDEI.2018.007282.
- [160] J. Lewiner, “Evolution of Experimental Techniques for the Study of the Electrical Properties of Insulating Materials,” *IEEE Trans. Electr. Insul.*, vol. EI-21, no. 3, pp. 351–360, 1986, doi: 10.1109/TEI.1986.349076.
- [161] S. J. Wang, J. W. Zha, Y. H. Wu, H. Da Yan, and Z. M. Dang, “Insulating properties of low density polyethylene/alumina nanocomposites,” *Am. J. Eng. Appl. Sci.*, 2015, doi: 10.3844/ajeassp.2015.405.409.
- [162] T. Takada and T. Sakai, “Measurement of Electric Fields at a Dielectric/Electrode Interface Using an Acoustic Transducer Technique,” *IEEE Trans. Electr. Insul.*, vol. EI-18, no. 6, pp. 619–628, 1983, doi: 10.1109/TEI.1983.298700.
- [163] IEC/TS 62758:2012, “Calibration of space charge measuring equipment based on the pulsed electroacoustic (PEA) measurement principle,” pp. 1–7, 2012.
- [164] N. Liu, C. Zhou, G. Chen, and L. Zhong, “Determination of threshold electric field for charge injection in polymeric materials,” *Appl. Phys. Lett.*, vol. 106, no. 19, p. 192901, 2015, doi: 10.1063/1.4921050.
- [165] F. Tian, Q. Lei, X. Wang, and Y. Wang, “Effect of deep trapping states on space charge suppression in polyethylene/ZnO nanocomposite,” *Appl. Phys. Lett.*, 2011, doi: 10.1063/1.3646909.
- [166] G. Teyssedre and C. Laurent, “Charge transport modeling in insulating polymers: from molecular to macroscopic scale,” *IEEE Trans. Dielectr. Electr. Insul.*, vol. 12, no. 5, pp. 857–875, 2005, doi: 10.1109/TDEI.2005.1522182.
- [167] R. C. Hughes, “The electronic properties of the metal-insulator contact: Space-charge induced switching,” *J. Appl. Phys.*, vol. 51, no. 11, pp. 5933–5944, 1980, doi: 10.1063/1.327511.
- [168] D.-M. Tu, X. Wang, Z.-P. Lu, K. Wu, and Z.-R. Peng, “Formation and inhibition mechanisms of space charges in direct current polyethylene insulation explained by energy band theory(in Chinese),” *Acta Phys. Sin.*, vol. 61, no. 1, pp. 17–24, 2012, [Online]. Available: <http://wulixb.iphy.ac.cn/en/article/id/51090>.
- [169] W. E. Spear, “Drift mobility techniques for the study of electrical transport properties in insulating solids,” *J. Non. Cryst. Solids*, vol. 1, no. 3, pp. 197–214, 1969, doi: [https://doi.org/10.1016/0022-3093\(69\)90001-5](https://doi.org/10.1016/0022-3093(69)90001-5).
- [170] D. Fabiani *et al.*, “HVDC Cable Design and Space Charge Accumulation. Part 3: Effect of Temperature Gradient [Feature article],” *IEEE Electr. Insul. Mag.*, vol. 24, no. 2, pp. 5–14, 2008, doi: 10.1109/MEI.2008.4473049.
- [171] Xinsheng Wang *et al.*, “Space charge in XLPE power cable under dc electrical stress and heat treatment,” *IEEE Trans. Dielectr. Electr. Insul.*, vol. 2, no. 3, pp. 467–474, 1995, doi: 10.1109/94.395415.
- [172] B. X. Du, C. Han, Z. Li, and J. Li, “Effect of graphene oxide particles on space charge accumulation in LDPE/GO nanocomposites,” *IEEE Trans. Dielectr.*

- Electr. Insul.*, vol. 25, no. 4, pp. 1479–1486, 2018, doi: 10.1109/TDEI.2018.006874.
- [173] C. Yang *et al.*, “Study on the trap distribution in polyimide thin film based on TSDC method,” in *2009 IEEE 9th International Conference on the Properties and Applications of Dielectric Materials*, 2009, pp. 911–913, doi: 10.1109/ICPADM.2009.5252244.
- [174] P. Yang, Y. Ohki, and F. Tian, “Analysis on thermally stimulated currents in polyethylene-terephthalate and polyethylene-naphthalate,” in *Proceedings of 2014 International Symposium on Electrical Insulating Materials*, 2014, pp. 401–404, doi: 10.1109/ISEIM.2014.6870804.
- [175] E. Logakis, L. Herrmann, and T. Christen, “Electric characterization of LDPE films with TSC and dielectric spectroscopy,” *IEEE Trans. Dielectr. Electr. Insul.*, vol. 23, no. 1, pp. 142–148, 2016, doi: 10.1109/TDEI.2015.004874.
- [176] Fuqiang Tian *et al.*, “A new method for direct determination of trap level distribution from TSC measurement,” in *2009 IEEE 9th International Conference on the Properties and Applications of Dielectric Materials*, 2009, pp. 980–983, doi: 10.1109/ICPADM.2009.5252276.
- [177] N. F. Mott and R. W. Gurney, *Electronic Processes in Ionic Crystals*. London: Oxford University Press, 1948.
- [178] F. Tian, J. Zhang, X. Peng, and C. Hou, “Interface trapping effects on the charge transport characteristics of LDPE/ZnO nanocomposites,” *IEEE Trans. Dielectr. Electr. Insul.*, vol. 24, no. 3, pp. 1888–1895, 2017, doi: 10.1109/TDEI.2017.006435.
- [179] M. Ieda, “Electrical Conduction and Carrier Traps in Polymeric Materials,” *IEEE Trans. Electr. Insul.*, vol. EI-19, no. 3, pp. 162–178, 1984, doi: 10.1109/TEI.1984.298741.
- [180] X. Wang, N. Yoshimura, Y. Tanaka, K. Murata, and T. Takada, “Space charge characteristics in cross-linking polyethylene under electrical stress from dc to power frequency,” *J. Phys. D. Appl. Phys.*, vol. 31, no. 16, pp. 2057–2064, 1998, doi: 10.1088/0022-3727/31/16/016.
- [181] F. Tian, W. Bu, L. Shi, C. Yang, Y. Wang, and Q. Lei, “Theory of modified thermally stimulated current and direct determination of trap level distribution,” *J. Electrostat.*, 2011, doi: 10.1016/j.elstat.2010.10.001.
- [182] K. J. Kao, S. S. Bamji, and M. M. Perlman, “Thermally stimulated discharge current study of surface charge release in polyethylene by corona-generated excited molecules, and the crossover phenomenon,” *J. Appl. Phys.*, vol. 50, no. 12, pp. 8181–8185, 1979, doi: 10.1063/1.325958.
- [183] Y. Yin, Z. Li, X. Li, and P. Jiang, “The thermally stimulated currents of SiO₂/low-density polyethylene micro- and nanocomposites,” in *2008 International Symposium on Electrical Insulating Materials (ISEIM 2008)*, 2008, pp. 495–498, doi: 10.1109/ISEIM.2008.4664466.
- [184] T. Mizutani, Y. Suzuoki, M. Hanai, and M. Ieda, “Determination of Trapping

- Parameters from TSC in Polyethylene,” *Jpn. J. Appl. Phys.*, vol. 21, no. Part 1, No. 11, pp. 1639–1641, 1982, doi: 10.1143/jjap.21.1639.
- [185] S. Serra, E. Tosatti, S. Iarlori, S. Scandolo, and G. Santoro, “Interchain electron states in polyethylene,” *Phys. Rev. B*, vol. 62, no. 7, pp. 4389–4393, 2000, doi: 10.1103/PhysRevB.62.4389.
- [186] V. A. Zakrevskii, N. T. Sudar, A. Zaopo, and Y. A. Dubitsky, “Mechanism of electrical degradation and breakdown of insulating polymers,” *J. Appl. Phys.*, vol. 93, no. 4, pp. 2135–2139, 2003, doi: 10.1063/1.1531820.
- [187] M. Meunier and N. Quirke, “Molecular modeling of electron trapping in polymer insulators,” *J. Chem. Phys.*, vol. 113, no. 1, pp. 369–376, 2000, doi: 10.1063/1.481802.
- [188] M. Meunier, N. Quirke, and A. Aslanides, “Molecular modeling of electron traps in polymer insulators: Chemical defects and impurities,” *J. Chem. Phys.*, vol. 115, no. 6, pp. 2876–2881, 2001, doi: 10.1063/1.1385160.
- [189] A. M. Pourrahimi *et al.*, “Highly Efficient Interfaces in Nanocomposites Based on Polyethylene and ZnO Nano/Hierarchical Particles: A Novel Approach toward Ultralow Electrical Conductivity Insulations,” *Adv. Mater.*, vol. 28, no. 39, pp. 8651–8657, 2016, doi: <https://doi.org/10.1002/adma.201603291>.
- [190] L. K. H. Pallon *et al.*, “The impact of MgO nanoparticle interface in ultra-insulating polyethylene nanocomposites for high voltage DC cables,” *J. Mater. Chem. A*, vol. 4, no. 22, pp. 8590–8601, 2016, doi: 10.1039/C6TA02041K.
- [191] A. T. Hoang, L. Pallon, D. Liu, Y. V Serdyuk, S. M. Gubanski, and U. W. Gedde, “Charge Transport in LDPE Nanocomposites Part I—Experimental Approach,” *Polymers (Basel)*, vol. 8, no. 3, 2016, doi: 10.3390/polym8030087.
- [192] T. Lewis, “Charge transport in polyethylene nano dielectrics,” *IEEE Trans. Dielectr. Electr. Insul.*, 2014, doi: 10.1109/TDEI.2013.004173.
- [193] P. Mark and W. Helfrich, “Space-Charge-Limited Currents in Organic Crystals,” *J. Appl. Phys.*, vol. 33, no. 1, pp. 205–215, 1962, doi: 10.1063/1.1728487.
- [194] A. Rose, “Space-Charge-Limited Currents in Solids,” *Phys. Rev.*, vol. 97, no. 6, pp. 1538–1544, 1955, doi: 10.1103/PhysRev.97.1538.
- [195] M. A. Lampert, “Simplified Theory of Space-Charge-Limited Currents in an Insulator with Traps,” *Phys. Rev.*, vol. 103, no. 6, pp. 1648–1656, 1956, doi: 10.1103/PhysRev.103.1648.
- [196] J. L. Auge, C. Laurent, D. Fabiani, and G. C. Montanari, “Investigating dc polyethylene threshold by space charge. Current and electroluminescence measurements,” *IEEE Trans. Dielectr. Electr. Insul.*, vol. 7, no. 6, pp. 797–803, 2000, doi: 10.1109/94.891991.